THE UNIVERSITY OF EDINBURGH

INSTITUTE OF ECOLOGY AND RESOURCE MANAGEMENT

THE MICROMETEOROLOGY OF A HIGH ARCTIC SITE

COLIN ROGER LLOYD

BA (Open Univ.)

A THESIS SUBMITTED FOR THE DEGREE OF DOCTOR OF PHILOSOPHY

May 2001

Declaration

This thesis has been composed by myself.

The work that this thesis describes is my own work, except where stated otherwise, and has not been submitted in application for any other degree.

Colin R. Lloyd

May 2001

Dedication

I dedicate this thesis to my wife, Tricia, who has during this endeavour, as so often over the past decades, stoically endured my long periods of fieldwork away from home and my obsession with science.

And to my parents, especially to the memory of my father who showed me the power and joy in observation.

Acknowledgements

I would like to thank my supervisor, Paul Jarvis for his enthusiastic support throughout the progress of this thesis. Without his belief in my ability to do this thesis, I would not have begun the journey. Equally, without John Moncrieff, my other supervisor, the journey would not have got this far. At every opportunity, his friendship, enthusiasm and "I don't give up on people" attitude were the spur to complete a journey that, at times, I regarded as having a bridge too far.

Brian Wilkinson, the Director of the Institute of Hydrology, supported me in applying to do this thesis. Jim Wallace, the current Director of the Centre of Ecology and Hydrology, Wallingford (CEH-Wallingford), continued that support.

At CEH-Wallingford, I wish to thank Richard Harding, Tim Kyte, and Mike Stroud for their help in the collection of the field data especially during my absences from the field, and I thank Richard especially as my Section Leader for his guidance and support in this work. I wish to also thank John Gash, who has provided advice and knowledge in so many ways. I wish to thank Alistair Culf and David McNeil for their work in preparing the software and hardware for the first deployment of the Solent/LI-COR 6262 flux measurement system. However, the 3 hour video that they prepared of how to set the system up and operate it that arrived with the system in Ny-Ålesund in June 1995 will not win any awards.

At Ny-Ålesund, I must thank Nick Cox, Manager of the NERC Arctic Research Station. Nick, with his renowned enthusiasm, provided the logistical backup that cleared the way for me to just concentrate on the science. During my field trips there, I had many useful conversations with experts in their field, often in bars, or saunas, but always in daylight. So I thank Ian Alexander, Bill Block, Pat Butler, Terry Callaghan, Andy Hodson and Clare Robinson. For those I have missed, I'm sorry but probably they aren't. I thank Kings Bay Kull Company, the administrators of the Ny-Ålesund Research Facility for their logistical support. I made many friends on Svalbard and I would encourage anyone to visit what is a most beautiful and serene part of the world.

Publications

Publications in refereed Journals

Lloyd, C.R., Harding, R.J., and Robinson, M., 1994. Preliminary results of energy and water balance from two tundra sites in Svalbard. (10 International Northern Research Basins Symposium and workshop), 609-630.

Lloyd, C.R., 1998. The application of an instrument for non-destructive measurements of soil temperature and resistance profiles at a high Arctic field site. *Hydrology and Earth System Sciences* **2(1),** 121-128.

Harding, R.J. and **Lloyd, C.R.,** 1997. Measurements of water and energy fluxes from a high latitude tundra site in Svalbard. 2(Eleventh International Northern Research Basins Symposium and Workshop), 73-93.

Harding, R.J. and **Lloyd, C.R.,** 1998. Fluxes of water and energy from three high latitude tundra sites in Svalbard. *Nordic Hydrol.* **29(4/5),** 267-284.

Lloyd, C.R., Harding, R.J., Friborg, T., and Aurela, M., 2001. Surface fluxes of heat and water vapour from sites in the European Arctic. *Theoretical and Applied Climatology* **70,** 19-33.

Lloyd, C.R., 2001. On the physical controls of the carbon dioxide balance at a high arctic site in Svalbard. *Theoretical and Applied Climatology* **70,** 167-182.

Laurila, T., Soegaard, H., **Lloyd, C.R.,** Aurela, M., Tuovinen, J.-P., and Nordstrøm, C., 2001. Seasonal variations of net CO_2 exchange in European Arctic ecosystems.. *Theoretical and Applied Climatology* **70,** 183-201.

Lloyd, C.R., 2001. The measurement and modelling of the carbon dioxide exchange at a high Arctic site in Svalbard. *Global Change Biology* **7,** 405-426.

Publications in non-refereed conference proceedings and symposia

Lloyd, C.R. and Harding, R.J., 1997. Water, Energy and carbon dioxide fluxes from a high latitude tundra site in Svalbard. (Roy. Met. Soc./Inst. of Physics "Physics of Climate" Conference), London.

Lloyd, C.R., Aurela, M., Hargreaves, K.J., and Nordstrøm, C., 1999. Trace Gas Fluxes in European Arctic regions. In R.Valentini and C.Bruning (Eds) *Greenhouse Gases and their role in climate change: the status of research in Europe*, International Workshop, Orvieto, Italy. pp 40-47.

Lloyd, C.R., Aurela, M., Bruland, O., Fowler, D., Friborg, T., Hansen, B.U., Harding, R.J., Hargreaves, K.J., Nordstrøm, C., Laurila, T., Tuovinen, J.-P., Sand, K., and Vehviläinen, B., 2000. Understanding land surface physical processes in the Arctic. In A.Ghazi, K.Hasselmann, D.Carson, R.Valentini, D.Lalas and I.Troen (Eds) *European Climate Science Conference,* Vienna

Lloyd, C.R., Aurela, M., Bruland, O., Friborg, T., Fowler, D., Hall, R.L., Hansen, B.U., Harding, R.J., Hargreaves, K.J., Laurila, T., Marechal, D., Nordstrøm, C., Sand, K., Soegaard, H., Tuovinen, J.-P., and Vehviläinen, B., 1999. Final Report to EC DGXII on the LAPP: Land Arctic Physical Processes. Project ENV4-CT95-0093, 1-128.

Abstract

The Arctic is expected to undergo major changes in climate in response to global warming, and is currently represented within predictive models by simple representations of vegetation structure. Polar semi-deserts, the subject for this thesis, are important sub-biomes within the Arctic and predictions regarding the possible additional greenhouse gas emission from the arctic need to take into account their contribution. This study addresses the role of polar semi-deserts in land-atmosphere exchange processes by characterising a typical high arctic polar semi-desert site in terms of the major micrometeorological parameters that control and interact with the exchange of energy and carbon dioxide between the soil, vegetation and atmosphere. During 1995 and 1996 at a field site near Ny-Ålesund, Svalbard, surface fluxes of radiation balance, evaporation, sensible heat, momentum and carbon dioxide were measured during the active period between spring snowmelt and late summer freeze-up. Eddy correlation systems were used to measure the fluxes of water vapour, sensible heat, momentum and carbon dioxide. Radiation and climate variable measurements augmented the flux measurements and provided longer term continuity and driving data for modelling purposes. The two active seasons were markedly different with a much shorter active season in 1996 due to a very late snowmelt onset. The season in 1996 was also cloudier.

The aerodynamic roughness length was 3.5mm and the average aerodynamic resistance was 70 sm^{-1}. Average surface resistance was calculated to be 97 sm^{-1} in 1995 and 45 sm^{-1} in 1996.

The energy budget showed different partitions of latent and sensible heat at different times of the active season. Sensible heat was small and occasionally negative during the snowmelt period with the majority of the net radiation being used to melt the snowpack. In the 1995 active season, latent heat flux of 229 MJ m^{-2} was 40 per cent of net radiation. Sensible heat flux was 35 per cent (194 MJ m^{-2}) leading to an evaporative ratio close to 0.5. In the shorter active season in 1996, latent heat flux

increased to 55 per cent (105 MJ m^{-2}) of net radiation with sensible heat flux reducing to 27 per cent (50 MJ m^{-2}), leading to the much higher evaporative ratio of 0.68.

Assessing the effect of climate change requires predictive models and this study adapted current established soil respiration and vascular plant photosynthetic models to simulate the bryophyte surfaces of the polar semi-desert. The combined model was extended to include a hydration strategy for the bryophyte community. The model was then calibrated against pivotal periods during the 1995 active season. The calibrated model predicted that the active season in 1995 was a net sink for carbon dioxide of -3.9 (±3.7) gC m^{-2} (i.e. photosynthetic uptake was larger than soil and plant respiration) The calibrated model was then run for the same period during the 1996 active season. The model output compared well with the measurements taken in 1996 but produced a net source of 5.0 (± 3.3) gC m^{-2}. Comparison of the two model runs indicated that the timing of snow disappearance was crucial to the carbon dioxide balance. There was evidence that in non light-limiting years, the overall carbon dioxide balance was controlled by soil respiration and that average plant assimilation during the middle part of the active season was very similar in both years.

This study provides both the necessary surface energy exchange parameters and modelling scheme to allow current Soil-Vegetation-Atmosphere Transfer (SVAT) schemes in Global Climate Models (GCMs) to be used to simulate a bryophyte-dominated polar semi-desert site.

Table of Contents

List of Symbols

For brevity in this section, symbols in the main text which have primes (e.g. w') alongside, are fluctuations of the entity about a mean value. The mean value can be signified by an over-bar (e.g. $\overline{w}$) when it is an average over time and by brackets (e.g. <w>) when it is a moving average calculated from a digital signal. The prefix for designating 10^{-6} (μ) has not been italised. Symbols without SI units are either dimensionless or dependent upon application.

Symbol	Description	SI Units
Roman Capital Letters		
A_{cr}	Incident photosyntheticallyactive radiation (PAR)	W m^{-2}
A_h	Specific flux of energy advected into layer	W m^{-2}
A_L	Net rate of photosynthesis	μmol m^{-2} s^{-1}
ALPHA	Quantum efficiency	mol_{co2} mol_{PAR}^{-1} photons
B	Bowen Ratio = *H/LE*	
BETA1	Gas constant coupling coefficient for co-limitation	
BETA2	Gas constant coupling coefficient for co-limitation	
CO2	CO_2 mixing ratio	kg_{co2} kg_{air}^{-1}
C_p	Specific heat of air at constant pressure	J kg^{-1} K^{-1}
Dew	Critical point for dew formation ($=T_c - T_a$)	°C
DUF	Rate at which cryptogams can absorb precipitation	mm hr^{-1}
E	Flux of water vapour per unit area, Evaporation rate	kg m^{-2} s^{-1}
ELF	Cryptogam evaporation resistance factor	
EpCO2	Mol.wt. CO_2 / Mol.wt. dry air	kg_{co2} kg_{air}^{-1}
EpO2	Mol.wt O_2 / Mol.wt dry air	kg_{co2} kg_{air}^{-1}
F_c	Flux of carbon dioxide	kg m^{-2} s^{-1} μmol m^2 s^{-1}
Fd	Dark respiration coefficient	
F_R	Flux density of radiation (flux per unit solid angle)	W $steradian^{-1}$
G	Flux of heat conduction per unit area	W m^{-2}
GF	Growth factor – at start of active season	
Glmin	Minimum leaf conductance for H_2O	m s^{-1}
H	Flux of heat per unit area by convection in air (=Sensible Heat)	W m^{-2}
$I_{n,u}$	Normal component of unit radiation intensity from surface	

K_c	Michaelis-Menten constant for CO_2	Pa
K_o	Michaelis-Menten constant for O_2	Pa
K_z	Soil thermal conductivity	W m^{-1} K^{-1}
L	Obukhov stability length	m
L_c	Heat of assimilation for fixation of carbon	J kg^{-1}
L_s	Latent heat of sublimation	J kg^{-1}
L_b	Long-wave radiation at mean surface temperature	W m^{-2}
L_d	Downward long-wave radiation from the atmosphere	W m^{-2}
L_e	Long-wave radiation from the environment	W m^{-2}
L	Latent heat of vapourisation of water (also λ)	J kg^{-1}
LAI	Leaf Area Index	
M	Model value – in statistical sense	
MaxE	Maximum evaporation rate from cryptogamic surfaces	mm hr^{-1}
M_w	Molecular weight of water vapour	g mol^{-1}
NAR	Net Assimilation Rate	g co_2 g^{-1} hr^{-1}
NEP	Net Ecosystem Productivity	µmol m^{-2} s^{-1}
O	Observation – in statistical sense	
O_a	Atmospheric partial pressure of Oxygen	Pa
Omega	Leaf scattering coefficient for PAR	
O2	Atmospheric Oxygen concentration	kg_{o2} kg_{air}^{-1}
PAR	Photosynthetically Active Radiation	W m^{-2}
Press,P	Atmospheric Pressure	Pa
Q	Source strength	
Q_0	Unit area source strength flux density	
Q_s	Rate of energy storage in a layer	W m^{-2}
Q_{10}	Ratio of a rate at temperature *T* to that rate at *T-10°C*	
R	Molar gas constant	J mol^{-1} K^{-1}
R_d	Carbon dioxide respiration rate from plants	µmol m^{-2} s^{-1}
R_{ext}	External hydraulic resistance	s m^{-1}
R_{int}	Internal hydraulic resistance	s m^{-1}
R_n	Net radiative flux density at upper surface of designated layer.	W m^{-2}
R_s	Carbon dioxide respiration rate from soil and roots	µmol m^{-2} s^{-1}
R_{soil}	Soil hydraulic resistance	s m^{-1}
R_{10}	Soil respiration rate at 10°C	µmol m^{-2} s^{-1}
S_d	Direct beam short-wave solar radiation	W m^{-2}
S_{diff}	Incoming Diffuse short-wave solar radiation	W m^{-2}
S_e	Incoming short-wave solar radiation reflected from the environment	W m^{-2}
S_{refl}	Reflected Short-wave radiation	W m^{-2}
S_t	Total incoming short-wave solar radiation	W m^{-2}
SF	Senescence Factor – applies at end of active season	
T	Temperature	°C, K
T_a	Air Temperature	°C, K

T_c	Leaf or canopy temperature	°C, K
T_l^{eff}	Effective Temperature of a composite vegetation/soil layer	°C, K
T_0	Surface Temperature of the Earth	°C, K
T_s	Soil temperature	°C, K
T^*	Standard Temperature	K
V_m	Temperature dependent capacity of substrate-saturated Rubisco	μmol $m^{-2} s^{-1}$
V_{max}	Maximum rate of carboxylation of Rubisco	μmol $m^{-2} s^{-1}$
W	photosynthetic rate	μmol $m^{-2} s^{-1}$
W_C	Rubisco dependent gross photosynthetic rate	μmol $m^{-2} s^{-1}$
W_E	Leaf product transport dependent gross photosynthetic rate	μmol $m^{-2} s^{-1}$
W_L	Light and CO_2 availability dependent gross photosynthetic rate	μmol $m^{-2} s^{-1}$
X_{max}	Distance upwind to the maximum relative flux density	m

Roman small letters

a	Shape factor in Growth and Senescence Factor models	
b	Shape factor in Growth and Senescence Factor models	
c	Carbon dioxide concentration	μmol mol^{-1} ppm
c_a	Speed of sound in air at sea level	m s^{-1}
c_c	leaf surface partial pressure	mmol m^{-3}
c_i	Internal CO_2 partial pressure	mmol m^{-3}
c_p	Specific heat of air at constant pressure	J kg^{-1} K^{-1}
d	Willmott degree of agreement statistic	
d	Zero plane displacement height	m
dF_R	Flux density of radiation striking a full radiator	W m^{-2}
$dqcrit$	Critical humidity deficit	kg_{H2O} kg_{air}^{-1}
e	Exponential	
e	Vapour pressure of water in air	Pa, mbar
$e_{sat}(T)$	Saturated vapour pressure at some temperature T	Pa, mbar
$e_s(T)$	Saturated vapour pressure at some temperature T	Pa, mbar
f_o	c_l / c_c for $dqcrit=0$ – calibrated parameter	mmol m^{-3}
$fsmc$	soil water factor for vascular plants	
g	acceleration due to gravity	m s^{-2}
k	von Kármáns constant	
m_a	Molecular mass for dry air	g mol^{-1}
m_v	Molecular mass for water vapour	g mol^{-1}
nf	Constant relating V_{max} and leaf nitrogen	
n_l	leaf nitrogen concentration	kg N kg^{-1} C
p	Absolute atmospheric pressure	Pa, mbar

q	specific humidity (mass of water vapour per unit mass of moist air)	kg kg^{-1}
q_*, q_s	saturated specific humidity	kg kg^{-1}
q_h	Soil thermal flux	W m^{-2}
r_a	Aerodynamic resistance	s m^{-1}
ratio	Leaf resistance for CO_2 / Leaf resistance for H_2O	
r_c	cuticle resistance	s m^{-1}
r	correlation coefficient	
r_s	Effective surface resistance for the tundra site surface	s m^{-1}
t	time	s
u	Horizontal component of the wind velocity in the direction of the mean wind	m s^{-1}
u_r	Windspeed at a reference height r	m s^{-1}
u_*	Friction velocity	m s^{-1}
v	Horizontal component of the wind velocity normal to the mean wind	m s^{-1}
w	Vertical component of the wind velocity normal to the mean wind	m s^{-1}
x	Distance upwind of measurement position	m
x_{max}	Distance upwind to maximum source strength position	m
z	Measurement height or depth	m
z_0	Roughness length	m
z_{0h}	Roughness length for heat	m
z_{0v}	Roughness length for water vapour	m

Greek Capital Letters

Γ	Photorespiration compensation point	Pa
Δ	gradient of Saturation Vapour Pressure curve with temperature	Pa K^{-1}
Ψ	Momentum stability correction function	

Greek small letters

α	Quantum efficiency for CO_2 uptake	mol CO_2 (mol PAR photons)$^{-1}$
α_b	reflection coefficient from the surface	
β_E	Evaporative loss (range –3 to 1)	
β_s	Soil moisture factor (range 0 to1)	
γ	psychrometric constant	Pa K^{-1}
ε	Surface emissivity (0.97 for snow-free tundra surfaces)	

ζ	Stability length scale (dimensionless)	
θ	Angle between direction of radiation and the normal to the surface	degree
λ	Latent heat of vapourisation of water	$J\ kg^{-1}$
λ	thermal conductivity of soil	$W\ m^{-1}\ K^{-1}$
σ	Stefan - Boltzmann constant (5.67×10^{-8})	$W\ m^{-2}\ K^{-4}$
σ	Ratio of mean densities (ρ_v / ρ_a)	
ϕ_μ	Momentum stability correction function	
σ	ratio of mean densities for water vapour and dry air	
τ	Rubisco specificity for CO_2 relative to O_2	
τ	Momentum flux	Pa
μ	Mixing ratio = m_a / m_v	
ρ	density of air	$kg\ m^{-3}$
$\rho_{a,}$	density of dry air	$kg\ m^{-3}$
ρ_v	density of water vapour	$kg\ m^{-3}$
ω	Solid angle = A/r^2 where A is the area of cone projected from centre of sphere of radius r onto surface of sphere	Steradians

Subscripts

a	dry air
b	body - e.g. soil or vegetated surface
c	carbon dioxide
d	direct beam
diff	diffuse
e	environment
h	heat
t	total
v	water vapour

Chapter 1
Introduction

1 Introduction

1.1 Background

The consensus of scientific opinion is that global warming due to increased greenhouse gas emissions will be most pronounced at high latitudes (IPCC, 1990). IPCC (1996) reiterated this as "model simulations...show the following feature(s) ....maximum warming in high northern latitudes in late autumn associated with reduced sea ice and snow cover". Warming in the Arctic will initially affect the surface hydrology. The change in the extent of snow cover due to atmospheric warming will have an important positive feedback on global warming through the radiation input (Harvey, 1988). The date of formation of winter snow cover and the timing and rate of melt will strongly influence the thermal regime within the soil for the rest of the year and determine the start of the *active season,* (Rouse, 1984). The extent of an *active season* is usually defined through such indicators as plant phenology, air temperature or radiation levels. Such indicators are difficult to apply at a high Arctic site where mosses and lichens, begin photosynthesising under the snowpack well before the vascular plants. The onset of activity is thus largely decoupled from air temperature and occurs when radiation amounts have generally passed their highest levels before snowmelt has completed. The cessation of plant activity is also problematic as the vascular plants will generally begin to senesce during mid-August, well before light levels and air temperature would indicate. Meanwhile the mosses and lichens continue activity until air temperatures freeze them or deep snowfall covers them. Snowpack depth is probably the best indicator of the start of the active season and surface temperature the best indicator of the end. Thus *active season* is here defined as the period during which the majority of carbon and moisture exchange occurs within and between the vegetation, soil and atmosphere, a period which begins partway into the spring snowmelt and continues until the soil is again frozen in the autumn. The melt also provides the major water source for subsequent vegetation use and is the major input to any river systems. The balance between runoff and infiltration is governed by the extent of frost depth (in the absence of continuous permafrost) and the rate of withdrawal of the permafrost

horizon (Repp, 1988). The permafrost horizon creates a general lower limit to soil water drainage above which saturated and unsaturated soil horizons form. Within these soil moisture regimes, the production of methane and carbon dioxide may occur to a greater or lesser extent and their release into the atmosphere provides another positive feedback to global warming (Christensen, 1991).
While the production of carbon dioxide and methane can be regarded as biochemical in origin, the rate of production of these greenhouse gases will be correlated with the thermal and moisture regimes within the soil horizons (Christensen, 1993). The exchange of available energy at the arctic land surface is dominated by evaporation and the production of sensible heat (Kane *et al.*, 1990). Evaporation of surface and soil water during a lengthening active summer period will also provide a positive feedback to global warming. The rate of loss of soil moisture through evaporation has important effects upon the production of carbon dioxide and methane. This thesis examines and explains the net carbon dioxide flux and evaporation of surface and soil water in terms of the micrometeorological and soil physical variables that provide both the energy and transport for these processes.

The Arctic encompasses many surface types; from the sparse birch forests at the edge of the boreal forest biome, through the more typical landscape of deep organic bogs, hummocks and open water of the middle Arctic of Finland, Siberia, Canada and Alaska, to the Polar semi-deserts of Svalbard and the northern Canadian islands (Bliss and Matveyeva, 1992). The rate of exchange of water vapour, carbon dioxide and methane will depend on particular vegetation and soil types. Fluxes of evaporation, carbon dioxide and methane are typically high over tussock and wet sedge (mire) tundra and low over Polar semi-deserts (Oechel and Billings, 1992). The overall effect of climate change in the Arctic on the global atmospheric carbon dioxide load will be somewhere between these extremes and will depend on the combination of emission rate and areal extent of that tundra type within the Arctic. While wet sedge tundra may have a much higher net photosynthetic and accumulation rate than polar semi-desert, the greater extent of the latter compared to wet sedge creates comparable carbon stores and accumulation amounts over the

entire Arctic region (Oechel and Billings, 1992). This study was based at a high Arctic polar semi-desert site characterised by a sparse vegetation cover comprised of bryophytes, lichens and dwarf vascular plants. Bryophytes and lichens are unable to control their moisture content (poikilohydric), frequently desiccate completely, and only resume their growth and the uptake of carbon dioxide through photosynthesis, when their surfaces and cell interiors are sufficiently moist to allow diffusion of carbon dioxide through the cell walls (During, 1992). Unlike vascular plants with access to soil moisture, the particular pattern of wetting and drying through the active season is crucial to both their growth rate and their contribution to the net carbon dioxide flux observed at the surface as the balance between plant uptake and soil and plant respiration.

The polar semi-desert is the northern limit of the tundra biome, which comprises a major part of the Arctic region. While the Arctic occupies only 10 per cent of the Earth's land area, it has been estimated that about one-third of the total pool of soil carbon is contained in the Arctic's permafrost and seasonally thawed soil layers (Post *et al.*, 1985). This amounts to between 250 and 455 x 10^{15}g of carbon (Miller *et al.*, 1983; Post *et al.*, 1985; Gorham, 1991) and in the Arctic accounts for more than 90 per cent of the ecosystem carbon total. This soil carbon has been accumulating over past millennia from the deposition of dead vegetation matter. Cold soils and perennial permafrost have limited the microbacterial decomposition of this accumulation of humic matter back into gaseous compounds of carbon. The Arctic, currently regarded as a slow but positive sink for carbon (Post, 1990; Gorham, 1991) may, with the expected warming, become a source of carbon dioxide and methane, providing a positive feedback to the current increasing level of greenhouse gases. Counteracting this effect is the possible increase in plant growth in a climate with increased carbon dioxide and temperature and a longer growing season. The currently sparsely vegetated regions of the northern tundra, including polar semi-deserts, would appear to be likely candidates to benefit from increased carbon dioxide levels and a warmer climate and to increase its vegetation growth and cover. However, these regions are known to be nutrient limited and there is evidence that

this nutrient limitation will restrict photosynthesis and growth in arctic plants more than the overall availability of photosynthate (Chapin and Shaver, 1985; Oberbauer *et al.*, 1986; Tissue and Oechel, 1987; Chapin, 1991). Combined with the possibility of lower summer rainfall and drying soils, this may limit the ability of the vegetation to increase its uptake of carbon dioxide by increased growth.

It is therefore extremely important, for an accurate assessment of the possible extra carbon dioxide loading to the atmosphere from the change in the Arctic climate, to understand and be able to simulate the physical processes linking the energy balance with the fluxes of carbon dioxide and evaporation from the surface. The Arctic may become warmer and wetter or it may become warmer and drier. If warmer and wetter, then this has major consequences on evaporation and carbon dioxide only if the extra precipitation occurs during the summer period, as increased winter snowfall will largely only contribute to increased runoff and river flow over frozen ground. The onset of the active season may be delayed through the extra time required to melt a deeper snowpack. In the warmer and wetter scenario, the active layer will be deeper. This will allow greater differentiation between the unsaturated and saturated soil layers as the warmer surface dries out through increased evaporation, and drainage of the increased precipitation will deepen the waterlogged layer over the retreating permafrost front. This will have repercussions not only on the sizes of the carbon dioxide and methane fluxes but may move the balance between the production of carbon dioxide and methane in the soil towards methane. A wetter summer, if characterised by more frequent storms rather than larger infrequent storms, will benefit the growth of bryophytes and lichens that are only actively growing when their cells are kept moist through surface water. Any increase in plant photosynthesis will help to balance the increased soil respiration. Increasing bryophyte and lichen cover may insulate the soil from further warming and may reverse the trend of retreating permafrost (Oechel and Van Cleve, 1986). A warmer and drier Arctic with largely unsaturated soil above the permafrost will limit methane production and maximise carbon dioxide production from the soil. The

vascular plants may be able to exploit the drier conditions at the expense of the mosses and lichens but this may be a slow process.

In summary, recent results from General Circulation Models (GCM's) have shown that in the event of global climate change, northern latitudes will be disproportionately affected. The initial effect is likely to raise the surface temperature of the Arctic by as much as 2.5^0C. This will have profound effects upon the depth and spatial distribution of any permafrost present. The northern latitudes have been accumulating, over many millennia, large stores of organic material in the soil horizon. The low temperatures slow chemical decomposition and prevent bacteriological and soil organism decomposition of this organic store. Any decomposition that does occur can only occur in the short period when the ground is unfrozen and over the depth to which the permafrost retreats. The increase in surface temperature which may occur with global warming will extend, in time, areal extent and depth, the unfrozen soil horizon and also provide the conditions for chemical decomposition and the colonisation of the soil horizon with bacteria and soil organisms capable of decomposing the organic material.

The likely future scenarios of warmer and wetter, or warmer and drier climates, has repercussions for the water and energy balance of the arctic. This will affect the current evaporation and carbon balance. Eventually this will probably lead to plant species changes that will have feedback effects on the climate and energy and carbon balances.

1.2 Thesis Aims and Structure

The results presented in this thesis were obtained initially as part of a NERC Institute of Hydrology project investigating the soil-vegetation-atmosphere interactions at an Arctic tundra site and latterly as part of an EC Climate and Environment funded project comparing carbon, water and energy balances at several European Arctic sites (see Lloyd *et al.*, (1999b)). This thesis presents both the first micrometeorological study of polar semi-desert on Svalbard and the first field-scale

carbon dioxide flux study in high arctic polar semi-deserts. Measurements of momentum, sensible and latent heat and carbon dioxide fluxes were made. To complement these measurements and to provide driving data for modelling, temperature and moisture profiles were measured continuously in the soil above the permafrost horizon and climate variables were measured using an automatic weather station (AWS). These flux measurements, taken during two seasons from before snowmelt, through the active season and into the early autumn freeze-up, were used to explain the partitioning of the energy balance and the observed net carbon dioxide balance. In the light of future climate change, an important part of this thesis was to investigate the combination of an established soil respiration model and an established and routinely used vascular plant photosynthesis model to the bryophyte-dominated polar semi-desert. The photosynthetic routine is routinely used within current Soil-Vegetation-Atmosphere Transfer (SVAT) schemes to simulate the surface exchange. In particular, it is used within the Meteorological Office Surface Exchange Scheme (MOSES) in the operational Hadley Centre Global Climate Model (GCM). It was therefore not appropriate to develop new models but to indicate where the current schemes could be "tuned" to simulate effectively this novel surface.

The aims and structure of this thesis are thus:

- To characterise, in a micrometeorological sense, a typical polar semi-desert site.
- To investigate the energy balance and the partitioning of available energy.
- To investigate the daily net carbon dioxide balance in terms of its controlling factors
- To tune current models of soil respiration and vascular plant photosynthesis to simulate the bryophytically dominated polar semi-desert site
- To test the resultant model with independent data from the same site.

The remainder of this study consists of 6 further chapters and two appendices.

Chapter 2: A literature review of energy and carbon dioxide balances in the Arctic. This has been done to illustrate the bias of arctic work towards the low and middle arctic regions and thus towards dwarf-shrub and tussock tundra – vascular plant dominated areas with nearly complete surface cover.

Chapter 3: A description of Svalbard climate and the measurement field site at Ny-Ålesund, Svalbard. An investigation of the micrometeorological parameters that characterise the vegetated surface and control its energy and carbon dioxide exchange processes.

Chapter 4: A description of the instrumentation used, in particular the flux measurement equipment and their calibration. The eddy correlation method is described. The problems of energy closure in heterogeneous terrain are explored.

Chapter 5: The high arctic radiation balance, being the driving force behind the energy and carbon dioxide balances is stated theoretically and illustrated with particular data. Theoretical aspects of the partitioning of the net energy flux are considered. The remainder of the chapter describes the daily partitioning of the energy fluxes at the site with regard to important active season periods, climate and soil factors, and net seasonal energy balances. Daily patterns of carbon dioxide flux are similarly described for the important active season periods.

Chapter 6: The description of established soil respiration and carbon dioxide assimilation models is presented as implemented in the current Soil-Vegetation-Atmosphere-Transfer (SVAT) model of the Hadley Centre GCM. In order for this combined Net Ecosystem Productivity (NEP) model (developed for temperate vascular vegetation surfaces) to adequately simulate Arctic cryptogam-dominated vegetation surfaces, the moisture control on assimilation is modified to deal with the peculiar cryptogamic water relations. The resultant NEP model was calibrated against active season measurement periods in 1995. The calibrated NEP model was

run for the same period in 1996 using climate variable forcing data and the results compared to measurements taken at the same time.

Chapter 7: General conclusions are drawn from the results gained in the previous chapters. In particular, given that climate change is likely to occur, the important climate factors leading to a change in the water and carbon dioxide balance of the high Arctic are highlighted. Some guidance for future work is included.

Appendices

- A MathCad (Mathsoft Inc., Massachusetts, USA) description of the Collatz C_3 carbon dioxide assimilation model is presented. This was used particularly to check the numerical validity of each stage within the full NEP model.

- Published Journal papers that have been written using the methods and results presented in this thesis.

Chapter 2
Literature Review

2 Literature Review

2.1 Introduction

This chapter reviews past research in energy balance and carbon dioxide flux measurements and carbon dioxide modelling in the Arctic. In micrometeorology, energy balance consists of income through radiation and metabolism, and expenditure through radiation, convection and evaporation (Monteith and Unsworth (1990). In this chapter, energy balance is, in general, concerned with combined radiation, convection and evaporation terms. The chapter indicates the scope of the work done and places this thesis within this general body of work. More focussed literature, dealing with particular aspects of the energy and carbon dioxide balance, are discussed in the appropriate chapter.

2.2 Previous Arctic Energy Balance Studies

Ohmura (1982) provided an historical review of energy balance studies in arctic tundra and has been a rich source for researching the historical work performed in the high Arctic. Surface radiation balance work in the Arctic began with the 1st International Polar Year (IPY-1) in 1882-83 when the necessary measurements for evaluating the surface radiation balance were recommended as optional observations (Heathcote and Armitage, 1959). This was the first attempt to measure global radiation simultaneously at many locations in the Arctic. Other field groups measured surface temperature of ground and snow cover to calculate the surface emission by Stefan's Law but combined radiation observations were insufficient to assess the total radiative budget. IPY 1 did not produce meaningful results of the arctic surface radiation balance, mainly because of bad planning and large workload rather than inadequate knowledge, instrumentation or formulation of the problem. While strictly not in the Arctic, Homén (1897) published the first description of a comprehensive experiment on energy balance in S. Finland although his estimate of sensible heat flux was as a residual of the energy balance equation and his scheme

required no knowledge of turbulence. Planck presented the theory of thermal radiation encompassing the classic theories of radiation in 1900. Ångström (1924) pointed out the importance of multiple reflection as a cause of large global radiation in the arctic. He also divided diffuse radiation into primary and secondary diffuse radiation for bare and snow covered surfaces.

Church (1941) who reported on the Greenland expedition of the University of Michigan in the late 1920's gave the first systematic measurement of evaporation from the surface of the arctic tundra. The expedition measured evaporation at many sites over a 150 km stretch of the tundra between Holsteinsborg and the Inland Ice and found a mean evaporation rate of 0.48mm d^{-1} for the period 11 August to 2 September. Closer to this study's field site, and fully aware of the work of Prandtl and von Kármán, Sverdrup (1935) conducted micrometeorological energy balance experiments on glaciers in Spitsbergen. Amongst other things, he demonstrated the validity and usefulness of fluid dynamics in the field. This work was done during the 2nd International Polar Year (IPY-2) which included as a major objective, the advancement of radiometry. With the increase of radiation stations installed during this time, an accurate understanding of the seasonal and annual distribution of global radiation was achieved by Ångström and Tryelius (1934) and Perl (1935) to such an extent that, according to Ohmura (1982), global radiation was still "probably the best known component within the energy balance equation for the Arctic" up to the early 1980's.

After the Second World War, geopolitical considerations provoked extra interest in the Arctic region. The United States of America, Canada and the former USSR constructed or reconstructed Arctic research stations and field experiments and results expanded in line with this extra interest. The following is a résumé of relevant arctic field measurements in these regions.

2.2.1 Alaska

The first long-term record of global radiation in North America started at Fairbanks, Alaska in 1936 (Hand, 1941). Energy balance measurements were first attempted at

Barrow in 1953 by Bryson (1956), who, based on only two clear days in June, succeeded in deducing the diurnal variation in the components of the surface energy balance, which appear in the light of present day knowledge to be realistic. At Barrow, Mather and Thornthwaite (1956) made an intensive and thorough energy balance measurement programme for tundra in the summer of 1956 as preparation for the International Geophysical Year and also in the years 1957 and 1958 as the US contribution to IGY (Mather and Thornthwaite, 1958). This work is still one of the few experiments which cover more than one years measurements and is a reliable source of information regarding the annual energy balance on arctic tundra (Ohmura, 1982). Further radiation measurements were made at Barrow by the Department of Atmospheric Sciences of the University of Washington during 1962 to 1966, the results being summarised by Maykut and Church (1973). Work at Fairbanks, Alaska by Wendler (1971), where the characteristics of the energy balance of a valley bottom and a hill-top were compared, showed that the winter energy balance differed significantly between the valley bottom and the hill-top with respect to net radiation and sensible heat flux - a result at variance with earlier belief that winter energy balance is homogeneous due to the lack of solar radiation and the existence of snow cover. Weller and Holmgren (1974) summarised the work by the University of Alaska during the International Biological Programme (IBP). Harper and Wiseman (1977) measured the variation of surface roughness (z_0) over a tundra surface as it progressed from snowcover (z_0 = 0.1 mm) to full summer vegetation canopy development (z_0 = 28 mm), an important parameter in the modelling of turbulent fluxes. Even though, by 1990, eddy correlation and aerodynamic methods representing mass transfer had been developed, "research related to evaporation in the arctic (was) limited for several reasons....remoteness....difficulty of continuous measurements even during the summer ....and the necessity to operate instrumentation from batteries or small generators" (Kane *et al.*, 1990) and evaporation was still classically estimated as the residual of the energy balance. The NASA Global Tropospheric Experiment/Arctic Boundary Layer Experiment (GTE/ABLE 3A) conducted during July - August 1988 in the Yukon-Kuskokwim region of western Alaska provided the platform for the direct measurements of

turbulent surface fluxes of heat, momentum and water vapour using the eddy correlation technique. Fitzjarrald and Moore (1992) reported an average evaporation rate during a dry period in July of 1.9mm d^{-1}, maximal values of sensible heat flux of 150W m^{-2}, observed Bowen ratios of 1 and a strong resistance to water vapour transfer from the upper soil layer through the ground cover of 200s m^{-1}.

2.2.2 Canada

The first continuous measurement of global radiation in the Canadian Arctic was reported by Latimer and Truhler (1967) for the area around Aklavik, North West Territories (N.W.T.) during 1948. Other work on the components of the radiation balance were reported for Tanquary Fjord, Ellesmere Island and for the Arctic Institute of North America Base camp on Devon Island (Dahlgren, 1974).

Brown (1965) measured radiation and evaporation for several vegetation covers at Norman Wells, N.W.T. and related the temperature and depth of the active layer to the vegetation in an attempt to show that the existence of permafrost and the depth of the active layer are the result of the surface energy balance, although the lack of a full energy balance measurement programme limited the validity of the results.

The first full energy balance study for tundra was made at Resolute by Vowinckel (1966) based on his synoptic heat balance method where sensible and latent heat fluxes are not separated. The first energy balance study for tundra where the surface fluxes were separately and directly measured was by Ahrnsbrak (1968) at Keewatin over 13 days. His large values for the Bowen ratio (β = 2.5 - 60) were at variance with the much smaller values proposed by Bryson and Kuhn (1962) but were regarded as being closer to correct values in a review by Ohmura (1982). Ohmura (1972) used the aerodynamic and Bowen ratio method to measure evaporation from field sites on Axel Heiberg Island, N.W.T during 1969. This work was extended during late April and August 1970 and reported by Ohmura and Müller (1976) and summarised by Ohmura (1981). This work highlighted the differences in the regional

climate of the Arctic during June, July and August due to surface differences and pointed out that the difference in heat balance between the sea, the tundra and the ablation area of glaciers is due to the latent heat of fusion and not to differences in net radiation. An energy balance approach was used by Addison and Bliss (1980) to describe the microclimate of a lichen-moss-rush tundra community near Cape Abernathy, King Christian Island (to the west of Axel Heiberg and Ellesmere Islands). Evaporation was measured using soil block lysimeters, soil heat flux using Middleton soil heat flux plates and sensible heat flux as a residual of the energy balance equation. Their results showed latent heat fluxes to vary from 17 per cent of net radiation for moss and cushion plants to 29 per cent for a bare surface - accounted for by high moisture content in the upper soil layers throughout the active season. Soil heat flux accounted for 4 per cent of R_n under the vascular plants to 14 per cent of R_n under bare soil and lichens. They concluded that high atmospheric humidity, low radiant heat load, and low ambient temperature predominated at the sites and resulted in a system that was dominated by these "free" air conditions.

To my knowledge, no direct measurements of the surface fluxes using the eddy correlation technique have been obtained from the Canadian high arctic region i.e. from the Queen Elizabeth Islands that include Axel Heiberg, Ellesmere, Devon and King Christian Islands. However, such measurements have been conducted extensively around the western shore of the Hudson Bay, especially close to Churchill and Lake Kinosheo (Fowler *et al.*, 1995; Hamilton *et al.*, 1994; Whiting *et al.*, 1992; Whiting, 1994)

2.2.3 Former USSR

The historical development of radiation studies in the former Soviet arctic was made by Gavrilova (1963) while Berlyand (1967) described the past studies on energy balance carried out by the Main Geophysical Observatory which included those over tundra. During the summers of 1952-1954, Balakov *et al.*, (1959) carried out a field study of the post-melt energy balance at a tundra site at Amderma. According to

Berlyand (1967), this was the only field experiment on the energy balance of the arctic tundra during the 1950's and 1960's. Comparing the monthly balance between grass-covered tundra and sand tundra for June-September, they noted that the higher albedo of the sand tundra produced less net radiation although heat conduction into the ground was almost identical for each site. Unfortunately, the sensible and latent heat fluxes were not separated.

During the 1960's, significant progress was made in measurements of radiation in the Arctic, including Gavrilova (1963), Chernigovskii and Marshunova (1965) and Marshunova and Chernigovskii (1966). However, the work by Marshunova (1961) is particularly important as it presents the features of radiative energy transfer in the most analytical form since the 1940's and is noted for its quantitative accuracy. The work showed the negative values of the annual net radiation in the central part of the Arctic Ocean in contrast to Gavrilova (1963) and Vowinckel and Orvig (1964) who obtained positive values. Marshunova and Chernigovskii (1971) presented the most accurate account up to that point of the distribution and main characteristics of radiation in the Arctic, and in this sense, replaces the work by Gavrilova (1963).
After this period, Soviet interest in the energy balance of the arctic was immense but mostly directed to the Polar Seas because of the strategic position of the Arctic and the importance of basic studies on radiation and energy balance for the planning and execution of the Northern Sea Route navigations. Short investigations were infrequently made on Arctic tundra where priority was given to the melt and refreeze processes in the active layer of permafrost (e.g. Bakalov *et al.*, 1959; Romanova (1971). Following the start of the Tundra Biome Programme within the International Biological Programme, the surface energy balance has predominantly been studied from the climatological viewpoint. Barry *et al.*, (1981) compared the July energy balance between the Soviet Arctic and the North American Arctic.
Since Ohmura's 1982 review, the emphasis has remained largely on the measurement and modelling of soil freezing (e.g. Gel'fan, 1989; Gusev and Yasitskiy, 1990; Demidov *et al.*, 1995; Polubesova *et al.*, 1996; Gusev *et al.*, 1997).

Tappeiner and Cemusca (1996) investigated the microclimate and energy fluxes but this concerned subalpine plant communities in the central Caucasus.

2.2.4 Svalbard

This thesis is the first micrometeorological study on Svalbard to combine energy and carbon dioxide balances. Individual aspects of the meteorology have been measured and Scherer (1992) measured net radiation, evaporation and soil heat flux at Liefdefjorden, on the north coast of Spitsbergen, but no concerted effort to characterise a Svalbard tundra surface in terms of its energy and carbon dioxide balance has previously been performed. Seven synoptic meteorological stations have operated on Svalbard since about 1920. Five out of these are still operated by the Norwegian Meteorological Institute (DNMI) including the station at Ny-Ålesund, which has operated since 1961. Similar meteorological stations are operated by the Polish and Russian authorities at Hornsund and Barentsburg respectively. Few direct measurements of permafrost thickness have been made although Liestøl (1977) quotes reports of temperature measurements in boreholes and in the coalmines and Gregersen and Eidsmoen (1988) report on permafrost investigations in the shore areas near Longyearbyen and Svea during 1987. The hydrology of the Bayelva basin was investigated during the years 1974-78 (Repp, 1979) but this study concentrated on glacial erosion, glacial hydrology and sediment transport. This work found that early runoff takes place on the surface with later meltwater drainage being englacial and subglacial. Following this work, the Norwegian National Committee for Hydrology restarted hydrological investigations in the Bayelva basin in 1988. Permanent devices for the measurements of water discharge and sediment transport were installed in the main river. Prior to the work reported by Repp (1979), very few hydrological investigations in Svalbard had been made (Sand *et al.*, 1991). An investigation of the heat balance at a site near Ny-Ålesund during short periods (late May to middle of June) in 1993 and 1994 was carried out and reported by Nakabayashi *et al.* (1996). This work was primarily concerned with the microclimate of a melting snowpack and did not extend appreciably into the active season. A

complete radiation balance was measured with sensible and latent heat fluxes derived using a bulk method approach. They observed evaporation from the snowpack prior to snowmelt with decreasing evaporation during the snowmelt period explained by the general increase in the atmospheric water vapour load. Air temperatures were always higher than snow surface temperature with sensible heat being transported to the snow pack. The main snowmelt heat source was net radiation in both years.

2.3 Carbon Dioxide Studies

The prospect of climate change and the effect of global warming have focused attention upon the future of the large carbon stocks present in northern soils. Whether these carbon stocks, which have gradually accumulated over thousands of years in these cold and often frozen soils, will become a net source of carbon dioxide and methane exacerbating greenhouse gas warming is still under debate.
Nearly all research into carbon dioxide exchange in the Arctic has concentrated on the low to middle regions of the Arctic. This has largely been due to logistical considerations in accessing and supporting field sites for measurements that have traditionally been power and personnel intensive, and to the fragility and temperamental nature of the flux equipment. Such considerations have meant that carbon dioxide work has largely concentrated near established facilities in Alaska. Greenland has recently established an arctic facility. The remoteness of arctic Canada has meant that, in terms of CO_2 measurements, researchers have concentrated on the subarctic and boreal sites around the Hudson Bay. There is little true Arctic tundra in northern Europe except for Svalbard and European researchers have tended to concentrate on the Boreal forest and subarctic zones in northern Fennoscandinavia.

2.3.1 Alaska

2.3.1.1 Measurements

Research in Alaska on CO_2 appears to have begun under the leadership of W.D.Billings at Barrow, on the north coast of Alaska in the 1970's. Barrow then became a focus for much of the Alaskan work over the next three decades. Peterson

and Billings (1975) measured soil CO_2 fluxes with chambers and found a positive linear correlation with soil temperature but also pointed out the disadvantages of laboratory experiments for this type of work. Coyne and Kelley (1975, 1978) used the aerodynamic method to measure CO_2 fluxes and despite reservations and difficulties with the method produced a 61 day total uptake of -772 g_{co2} m^{-2} during July-August 1971. Then began a large raft of work that revolved around chamber, cuvette and laboratory manipulations of moss ecosystems. Oechel and Collins (1976), Oechel (1976) and Sveinbjörnsson & Oechel (1981a, 1981b, 1983) studied the effects of light, surface temperature and water level and seasonal patterns on net photosynthesis and dark respiration.

The area around the Brooks Range in north central Alaska became a second focus for CO_2 research. Poole and Miller (1982) used soda-lime absorption techniques to estimate CO_2 flux from three arctic vegetation types including lichen heath where seasonal average CO_2 efflux was 1.7 g_{co2} m^{-2} d^{-1} during July-August 1981. The efflux also declined from July to August. Skre and Oechel (1981) nearby at Fairbanks found leaf water content in mosses to be an important limiting factor for photosynthesis.

Billings et al. (1982) and Peterson et al. (1984) performed controlled manipulations of soil cores and soil/vegetation microcosms, at Barrow with the emphasis on soil warming, water table influence and increased CO_2. They indicated that warming of the tundra climate could change the ecosystem from a current sink to a source.

At Toolik Lake and in the Brooks Range, growth chambers and small greenhouses *in situ* were used to manipulate and elevate CO_2 levels (Oberbauer *et al,* 1986; Tissue & Oechel, 1987; Grulke *et al,* 1990). They found that CO_2 enrichment had little effect as compensatory reductions in photosynthetic rate occurred. Oberbauer *et al.* (1991) using chambers for soil CO_2 efflux found a positive correlation with soil temperature with soil surface conditions being a better predictor of soil efflux than at 5-10cm.

The first eddy correlation measurements were taken by Fan *et al.* (1992) at Bethel on the north coast. They measured CO_2 and CH_4 and showed that solar irradiance was the primary control on the Net Ecosystem Exchange (NEE) of CO_2 with mean maximum uptake of -1.4 gC m^{-2} d^{-1} during the day and -0.73 gC m^{-2} d^{-1} respiration at night during July-August 1988. Whiting *et al* (1992), using eddy correlation and chambers at Bethel, measured -1.1 gC m^{-2} d^{-1} during the period 8 July- 8 August. At Fairbanks, Funk *et al.* (1994) controlled the variation of the water table within previously frozen soil cores and examined the effect this had on CO_2/CH_4/CO fluxes and concluded that drying of wetland soils may decrease CH_4 but the increased CO_2 would outbalance this sink and likely increase global warming. The importance of the hydration of mosses and lichens was emphasised by Oberbauer *et al.* (1996) who found mid-seasonal efflux limited by soil/moss/lichen hydration

The research effort changed direction as the importance of winter CO_2 fluxes came to be recognised. Cold season CO_2 fluxes were measured using eddy correlation, chambers and gas sampling probes. Oechel *et al* (1997) found winter fluxes to be highest in October and May and concluded that estimates of annual net CO_2 exchange, based on warm season measurements alone, were an underestimate. Fahnestock *et al.* (1998), in gas probe measurements through snow, found rates of CO2 increased from March to May while Oberbauer *et al.* (1998), by removing early and late season snow, showed that extended seasons increased both respiration and uptake. Jones *et al* (1998, 1999) at Toolik Lake increased early and late winter snow depths and found no direct relationship between snowdepth/temperature and CO_2 flux.

Long-term sequestration of carbon during the summer has recently been investigated by Oechel *et al.* (2000). Examination of CO_2 flux data from two Arctic ecosystems from 1960 to 1998 showed the ability of ecosystems to metabolically adjust to long-term changes in climate. In particular, despite substantial losses of terrestrial carbon during warm, dry climates in the early 1980's, a return to summer sink activity occurred during the 1990's – the warmest and driest period observed in the past four

decades. Despite this apparent acclimation, the two ecosystems investigated are currently still annual net sources of CO_2.

2.3.1.2 Models

The modelling of CO_2 exchange in arctic environments has been quite limited. Miller *et al.* (1978) used a mixed empirical and process-based model to simulate CO_2 uptake in mosses while Whiting *et al.* (1992) successfully compared eddy correlation and chamber measurements to a simple PAR based NEE. Waelbroeck & Louis (1995) in modelling net CO_2 exchange from wet sedge found the model more sensitive to litter chemical composition and decomposition parameters than to NPP parameters.

At the larger scale, Ostendorf (1996) used an established hydrological model and a canopy gas exchange model to model CO_2 and H_2O fluxes at the landscape scale and concluded that the hydrology is a major factor determining spatially integrated gas exchange rates.

2.3.2 Canada

An important and far ranging high Arctic study was conducted at Truelove Lowland, Devon Island (75^0 33'N, 84^0 40'W) during 1970 to 1974. This project, part of the International Biological Programme, investigated most aspects of a high arctic ecosystem (Bliss, 1977). Within the project, only Mayo *et al.* (1977) directly addressed carbon dioxide fluxes. They measured in the field carbon dioxide assimilation of vascular plants in enclosures using an InfraRed Gas Analyser. Samples were also sent to Edmonton for similar analysis in chambers. Besides identifying light compensation points, maximum fixation rates and net assimilation rates, they observed that *Dryas integrifolia* spontaneously entered dormancy without a cold temperature stimulus and suggested an internal control or degradation of the photosynthetic system.

More recently, Jones *et al.* (1999) have investigated CO_2 fluxes in snowpacks and identified the consequences of wind-induced advection in the snowpack and how this

is responsible for higher concentrations of CO_2 at the snow-atmosphere interface. The Canadian Land Surface Scheme, a Soil-Vegetation-Atmosphere Transfer (SVAT) model, has been used to model subarctic terrain (Bellisario *et al.*2000) but currently does not address the carbon balance of high arctic sites

2.3.3 Greenland

There was little, if any, CO_2 research carried out on Greenland before the establishment of the Zackenberg Ecological Research Station by the Danish Polar Center in the early 1990's. This high Arctic field station on the northeast coast of Greenland (74^0 28'N, 20^0 34'W) provided an accessible and large facility for research.

Some of the first results to emerge concerned CO_2. Soegaard and Nordstroem (1999) and Soegaard *et al.* (2000) used a similar eddy correlation system to that used in this thesis to measure net ecosystem exchange fluxes of CO_2. Over a three week period starting in mid-July, they found large differences in CO_2 flux between the surface types of vegetation (heath, grassland, fen and willow snowbed) with ranges from -0.7 gC m^{-2} d^{-1} over the dwarf shrub heath to -3.0 gC m^{-2} d^{-1} over the fen areas. They also successfully modelled these vascular plant dominated sites using photosynthetic and soil respiration models. Christensen *et al.* (2000) measured NEE of CO_2 and CH_4 in chambers and extrapolated their results from the different vegetation types to estimate that the entire valley bottom was a daytime sink of -96 mg_{co2} m^{-2} hr^{-1} from 15 samples taken throughout the thawed season.

2.3.4 Svalbard

Research on Svalbard has increasingly been concentrated at the Ny-Ålesund Research Base since its conversion from a coal-mining town to a scientific research base in the 1960's. In investigating the effects of heavy grazing by reindeer, Sendstad (1981) measured rates of soil respiration from vegetated and cleared lichen heath with an IRGA and found rates of 40-96 mg_{co2} m^{-2} hr^{-1} in vegetated plots and half this in the cleared plots, while Dziadowiec (1983), at a site 100 km further

south, used open chambers to measure soil CO_2 efflux and found 19-49 g_{co2} m^{-2} evolved over a period of 48 days and noted that the intensity of CO_2 evolution increased rapidly immediately after snowmelt. Wüthrich *et al.* (1994) used initially a gravimetric method and then soda-lime absorption in chambers to measure soil respiration. Wüthrich *et al.* (1999) subsequently in 1996 used chambers with an IRGA sampling system to repeat the soil respiration figures. He found the site to be a net source of CO_2 and attributed it to the cloudy conditions in the summer of 1996 limiting photosynthesis.

Chapter 3
Ny-Ålesund, Svalbard: A high Arctic site

3 Ny-Ålesund, Svalbard: A High Arctic Site

3.1 Location

Svalbard, which in old Norse means the Cold Coast, was mentioned for the first time in old Icelandic annals from the end of the 12th and the beginning of the 13th century. Svalbard comprises a set of islands of area 62,000 km^2 (the size of the Netherlands and Belgium combined) between longitudes 10^0 and 35^{0}E , and latitudes 74^0 and 81^{0}N (Figure 3-1). The archipelago is 650 km north of the Norwegian mainland, and surrounded by the Barents Sea to the south and east, the Greenland Sea to the west and the Arctic Sea ice pack to the north.

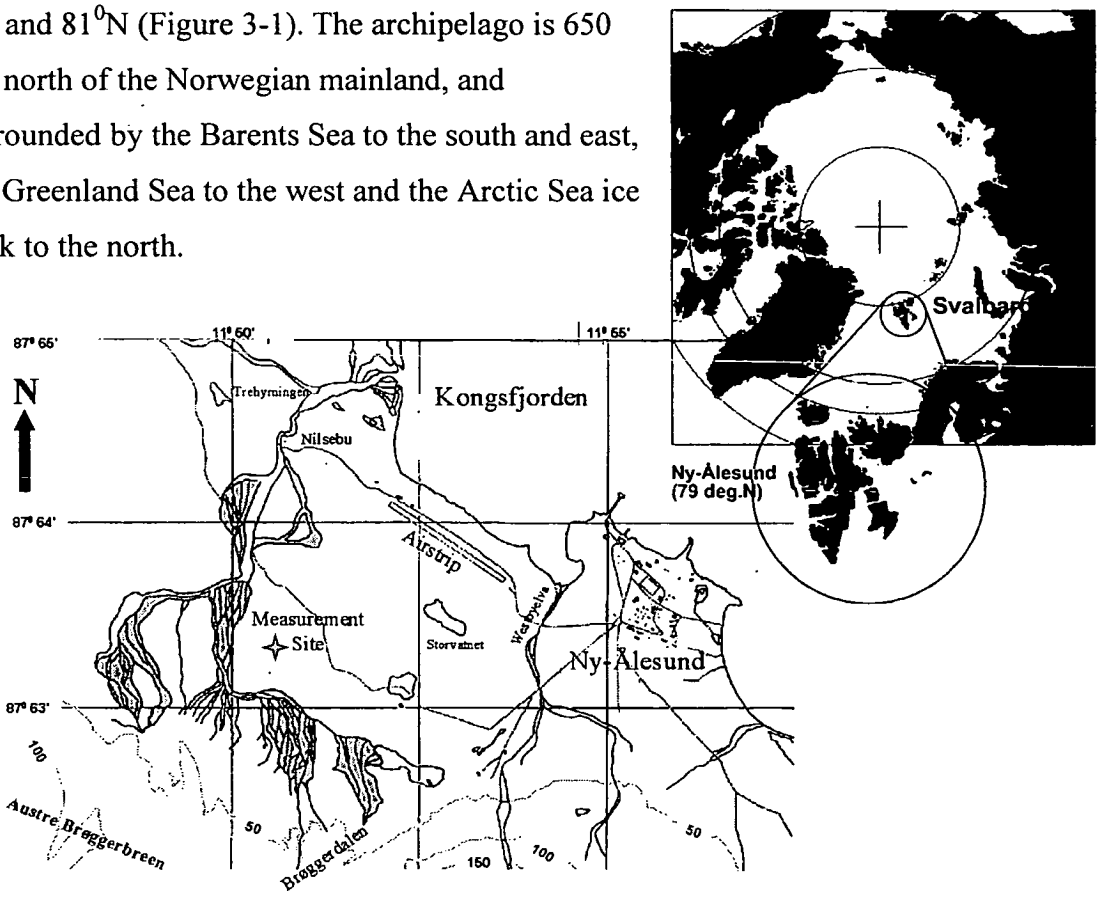

Figure 3-1 *Location of the measurement site near Ny-Ålesund, Svalbard and Svalbard's position within the circumpolar Arctic.*

Ny-Ålesund, the international research town close to the site for this study, is on the largest island of Spitsbergen (39,000 km^2). Ny-Ålesund is situated at 79^0 56' N, 11^0

55' E, on Brøggerhalvøya, a peninsula on the southern edge of Kongsfjorden (King's Fjord) on the site of a former coal mining community (Figure 3-1).

3.2 Geology and Soils

Fifty-four per cent of Spitsbergen remains covered by glaciers and permanent snowfields. The remainder, seasonally snowfree, has been placed by Tedrow (1977) in the Subpolar desert pedologic zone of the northern polar lands, a classification that equates to the tundra moss-lichen zonation of Korotkevich (1967). The area surrounding Ny-Ålesund is typical of the island of Spitsbergen with recent moraines, strandflats (a coastal lowland plain, partly covered with marine deposits) and postglacial terraces and raised beaches fronting steep flanked mountains which have intervening glaciers and permanent snowfields. The geology around Ny-Ålesund consists of metamorphic rocks of Caledonian age overlain by Carboniferous, Permian, Triassic and Tertiary sedimentary rocks (Challinor, 1967; Orvin, 1934). Only the uppermost decimetres of the ground thaw during the summer. Below this, the ground remains permanently frozen to depths of 100 to 400 m and this permafrost layer is almost continuous throughout Svalbard (Liestøl, 1977, 1980). The influence of the adjacent sea reduces the depth of permafrost closer to the coast although Liestøl (1977) measured a permafrost depth of 140 m in a borehole in the front of the Brøggerbreen glacier. The combined action of the heat from the earth's interior, the frictional heat from glacier motion, and glacial pressure is sufficient to maintain ground temperature beneath the glaciers at or slightly above freezing (Liestøl, 1977). Thus, even during winter, melt water may emerge from beneath glaciers even if unseen below the snow cover (Hagen *et al.*, 1991; Hagen and Lefauconnier, 1993).

The study site for this thesis is in the floodplain of the braided Bayelva river, which is the meltwater river from the Austre Brøggerbreen glacier. The braiding creates streams that are typically shallow with little energy to substantially alter the soil horizon. Although the soil has been created by glacier action and transported to the floodplain by the river, the settled soil has probably been more mixed by solifluction

action rather than by subsequent streamflow motion. The churning of the active layer soil by solifluction processes was reported by Smith (1956) who also showed that the pH values of Spitsbergen soils were within a range of 6.0 to 7.5 with a few extremes. The neutral character of Spitsbergen soils was also reported by Szerszén (1968) at Hornsund where marine deposits of loamy sand with fifty per cent cover of *Saxifraga* had pH values of 6.5,6.6 and 6.6 in soil layers from 0-25 mm, 150-200 mm and 280-300 mm respectively. In marine deposits of sand with thirty per cent cover of lichens, moss, willows and *Carex,* he reported pH values of 7.2 and 7.3 in the 25-100 mm and 300-405 mm layers respectively. The underlying rock at the study site is a red sandstone with a thickness of about 200 m overlain with glacial gravels and Carboniferous limestone boulders in a silty clay and sand gley soil. Grain size measurements from sediment transport experiments showed less than 10% as sand fraction and 90% as clay and silt fractions (Husebye, 1994). Husebye (1994) also indicated that in the period 1989-1993, approximately 90% of the suspended particles in the Bayelva were finer than 63 μm. These figures may reflect the current soil composition and grain size as the study site, at one time or another, was part of the braided river.

3.3 Svalbard's Climate

The climate of Svalbard in general is warmer than its northerly position would suggest. During the coldest months of the winter, January to March, the long term average temperature (1951-75) at Isfjord Radio (78.1^{0}N, 13.6^{0}E) is -11.9°C which is more than 20°C higher than at Isachsen, a station at the same latitude in the Canadian polar archipelago. However, the July mean at Isfjord Radio of 4.7°C is only a couple of degrees higher than at Isachsen. This relatively mild climate is a result of a complicated chain of oceanic and atmospheric influences. The major oceanic influence is the flow of warm Atlantic water via the Norwegian Current, a branch of the North Atlantic Current (a continuation of the Gulf Stream) which flows past the west coast of Spitsbergen. The atmospheric influence is the frequent transport of mild air from lower latitudes, usually in connection with passages of depressions over or near the Svalbard area. However, Svalbard also experiences great

temperature fluctuations due to the alternating influences of mild, southerly air streams and cold Arctic air from the north and east. These variations are much more pronounced in winter, when warm air from the south has, in recent years, melted the snow cover around Ny-Ålesund, which then refroze as a solid layer of ice some days later, when the cold Arctic air returned (Lloyd, unpublished data). The large variation of temperature with wind direction in winter is made greater by the frequent clear skies associated with northerly and easterly winds, combining net heat loss by radiation with the colder air mass. In contrast, southerly winds are often associated with overcast conditions, which reduce radiative heat loss and in combination with a warmer air mass, provide a considerable heat gain. In summer, the combined effect of wind direction and sky conditions leads to a much-reduced variation in temperature. Clear sky conditions now lead to heating of the lower air layers, while overcast skies reduce the heating effect of the sun.

On the west coast of Spitsbergen, the temperatures are similar to those experienced further south at Isfjord Radio. The mean monthly temperature for February-March, the coldest part of the year, is usually between -8° and -16°C with temperatures below -30°C being uncommon. During the summer, the same coastal area experiences mean July temperatures of 5°C with temperatures outside the range 1-10^{0}C being uncommon. The mixture of cold north and east winds with warm southerly winds often leads to stormy weather. Thus, in January, about 35% of wind observations at Isfjord Radio exceed Beaufort 5 (i.e. fresh breeze) whereas in summer, only 7% of wind speeds exceed this figure.

In Arctic regions, the water vapour content of the air masses is very often close to saturation. This is certainly true of the Ny-Ålesund area where, although the absolute humidity may be only 4 or 5 g m^{-3}, the associated relative humidity is above 85% (Lloyd, unpublished data). This leads to frequent advection fogs during the summer. The depth of the fog layer is a few hundred metres at most, and often not more than 20-30 metres. In general, the boundary layer in high latitudes is shallower than in regions to the south.

The west coast of Spitsbergen normally has less than 400mm of precipitation a year, with a maximum in the autumn. Rain can occur even in the middle of winter as can

snow during the summer. The climatic snow line (firn line) around Ny-Ålesund occurs between 200-300 m; above this height there is, on average, a net accumulation of snow; below this height, the snow melts away during the summer season.

At Ny-Ålesund, the period of the year when the entire solar disc remains above the horizon (the period of the "midnight sun") begins on 18 April and ends on 24 August, a period of 129 nights. The period of the polar night, when the entire solar disc remains below the horizon starts on 25 October and ends on 17 February, a period of 116 days.

3.4 Vegetation

The vegetation on the west coast of Spitsbergen is similar in some ways with that of eastern Greenland. However, the flora in the south of Svalbard shows Scandinavian similarities (Rönning, 1963). The vegetation around Ny-Ålesund, as in the rest of Svalbard, often has a mosaic character, where over a few square metres, it may alternate between communities of plant species typical of mounds and ridges and those typical of wetland depressions. The great differences in the distribution of plant communities are more a consequence of soil moisture and snow cover rather than the underlying geology. Despite the availability of 24-hour daylight from 18 April, the first spring plants do not flower before mid-June and the

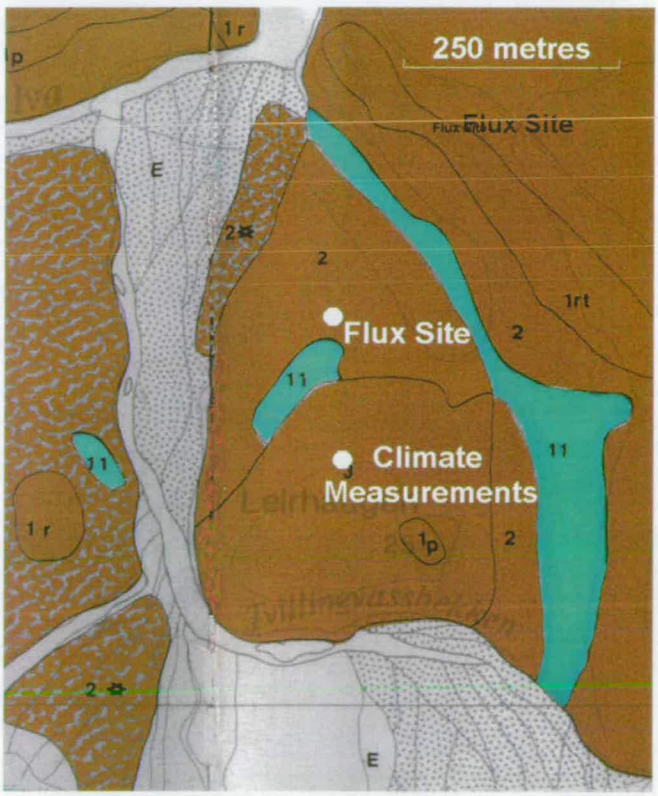

Figure 3-2 *Vegetation map of the measurement site (taken from Brattbakk, 1981). Brown areas 2,2* and 3 are 100-50%, <10% Saxifraga oppositifolia lichen heath and 100-50% Luzula confusa lichen heath respectively. Green areas 11 are 100-50% Deschampsia alpina snowbed community*

growing period is generally over around mid-August, coincident with the end of the midnight sun period. Cryptogams (mosses and lichens) however, will continue to photosynthesise from first emergence from the snowpack in the spring through the summer and autumn providing temperature, moisture and light levels allow it (Longton, pers comm).

The vegetation at the study site consists of three main plant communities. These are designated (Brattbakk, 1981) as 100-50% *Luzula confusa* lichen heath (Norw. Vardefrytle lavhei), 100-50% *Saxifraga oppositifolia* lichen heath (Norw. Rødsildre lavhei) and 100-50% *Deschampsia alpina* snow-bed community (Norw. Fjellbunke snøleie). There is also a small strip of <10% *Saxifraga* heath close to the Bayelva river (Figure 3-2).

The above definitions, although officially recognised, are confusing as they relate to

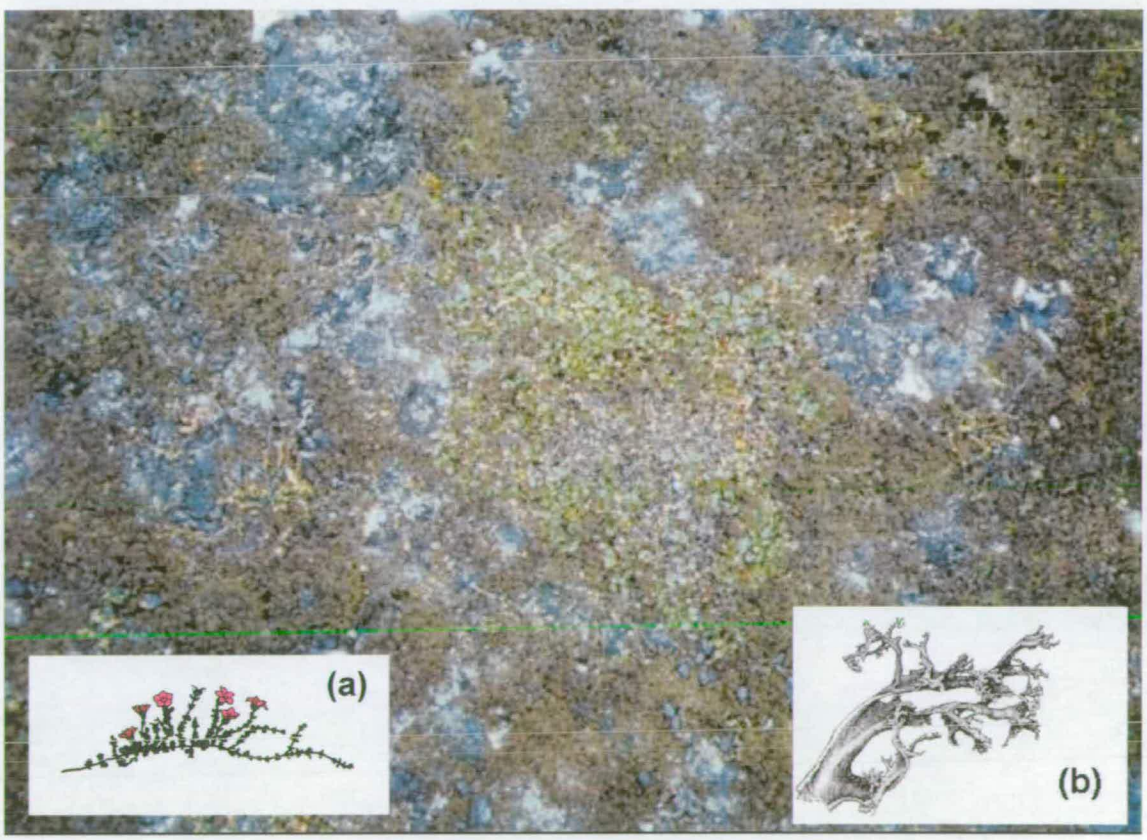

Figure 3-3 *An area of typical Saxifraga oppositifolia lichen heath at the flux measurement site. (a) is Saxifraga oppositifolia; (b) is Cetraria delisei. The area shown is approximately 50cm x 30cm.*

the total vegetation present, not the proportion of ground area that the individual vegetation type cover.. From an energy and carbon balance point of view, it is more pertinent to assess the percentage ground cover that individual plant communities, bare soil and stones occupy. A simple mapping of the flux measurement site indicated that 48 percent of the vegetation was lichen or moss, 20 per cent of the surface was vascular plants, 28 percent was bare soil and 4 percent was stone. The stones visible on the surface at the flux measurement site were generally flat, less than 0.1m diameter and did not protrude above the general vegetation height. The flux measurement site was level and flat – a result of its floodplain origins, while the immediate surroundings had shallow upward slopes. The major species at the site were *Saxifraga oppositifolia, Cetraria delisei, Drepanocladus* spp.and *Luzula confusa.* Figure 3-3 shows a typical surface area with a central area of prostrate *Saxifraga oppositifolia* surrounded by patches of dark brown lichen, *Cetraria delisei,* blue/black areas of detritus/bare soil and white stones. No *Drepanocladus* spp.or *Luzula confusa* is visible in this photograph.

3.5 General Site Micrometeorology

This section characterises the most important micrometeorological parameters of the site during the active season. These measurements provide the background for the subsequent description of the surface energy and carbon dioxide balances in later chapters. The instruments used to measure these characteristics are described in the next chapter.

Figures 3-4, 3-5 and 3-6 show minimum, maximum and average daily values for climate variables during 1995 and 1996 that are not explored in more detail within the relevant chapters of this thesis.

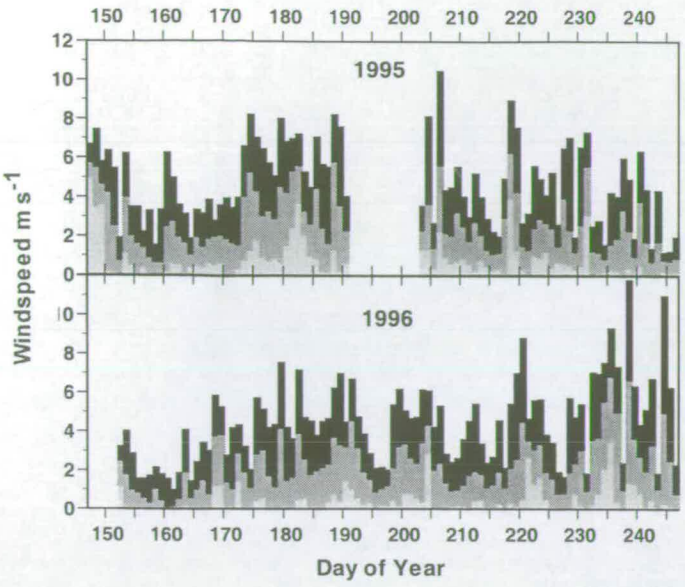

Figure 3-4 *Minimum(light grey), average (middle grey) and maximum (black) daily average windspeed for the active seasons in 1995 and 1996*

Figure 3-5 *Minimum(light grey), average (middle grey) and maximum (black) daily average relative humidity for the active seasons in 1995 and 1996*

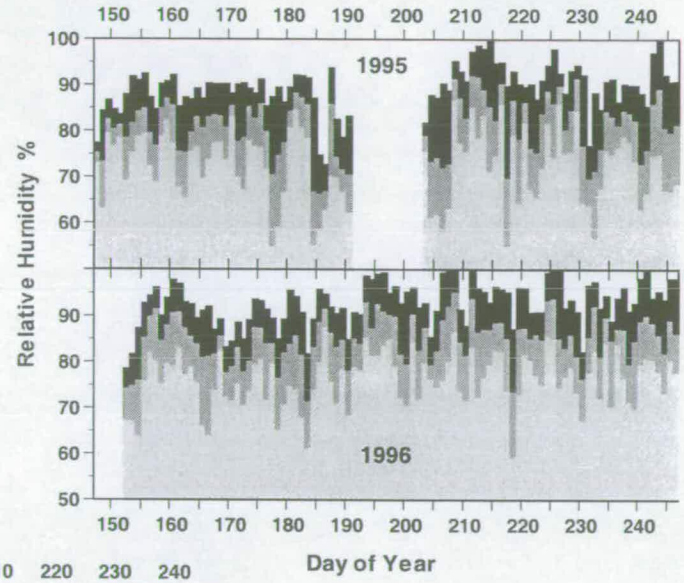

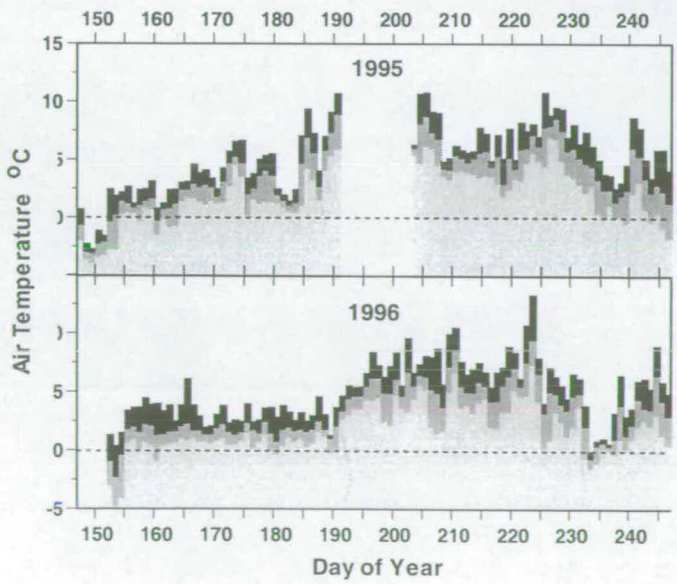

Figure 3-6 *Minimum(light grey), average (middle grey) and maximum (black) daily average air temperature for the active seasons in 1995 and 1996*

3.5.1 Surface Energy Parameters

3.5.1.1 Surface Layer Atmospheric Stability

The process of transporting the convective energy terms (sensible and latent heat) in the atmospheric surface layer via eddy motion is dependent upon the stability of the surface layer. An unstable surface atmospheric layer tends to promote convection processes leading to enhanced transport of sensible and latent heat away from the surface while a stable surface layer will tend to dampen these processes and may inhibit them entirely. A knowledge of the stability range of a site provides insight into its climate, its potential for increased convective fluxes and for defining the source area from which measured fluxes emanate.

A useful length scale for stability in the surface layer is the Monin-Obukhov surface layer scaling parameter (Monin and Obukhov, 1954):

$$\zeta = \frac{z-d}{L} \tag{3.1}$$

where L is the Obuhkov stability length (Obuhkov, 1946; Businger and Yaglom, 1971), z is measurement height and d is the zero plane displacement height, a hypothetical height where the distribution of shearing stress over the surface roughness elements is aerodynamically equivalent to the imposition of the entire stress (Monteith and Unsworth, 1990).

The Obuhkov stability length L *is* defined as:

$$L = \frac{-\rho_a c_p T_a u_*^3}{kgH(1+0.07/B)} \tag{3.2}$$

where ρ_a is density of air (kg m^{-3}), c_p is the specific heat of air at constant pressure (J kg^{-1} K^{-1}), T_a is the absolute air temperature (K), u_* is the friction velocity (m s^{-1}), k is von Kármán's constant (=0.41), g is the acceleration due to gravity (m s^{-2}), H is sensible heat flux (W m^{-2}) and B is the Bowen Ratio, the ratio between H and the latent heat flux. The Bowen Ratio correction term is often omitted. The Obuhkov length is typically positive during the night and negative during the day.

The zero plane displacement height d is often set to $0.67h$ where h is the height of the vegetation. Its interpretation is also questionable in heterogeneous vegetation canopies and can be difficult to determine (Lloyd *et al.*, 1992). Because of this, and the observation that at the Ny-Ålesund site, d was less than 3 per cent of the measurement height, it has been set to 0.67 of average vegetation height (d = 0.05m). Figure 3–7 shows the distribution of $\zeta=z/L$ between 30 May and 7 September in 1995 and 1996 as measured by both the Hydra and Solent/Licor systems when present. Values of z/L which were <-3 or >3 were set to –3 or +3 respectively. Such values usually occur during rain or when the sonic sensors are still wet, thus giving erroneous estimates of u_*. In 1995 the site was predominantly neutral (z/L close to zero) or unstable (z/L < -0.05) with few stable periods – a consequence of the 24-hour daylight.

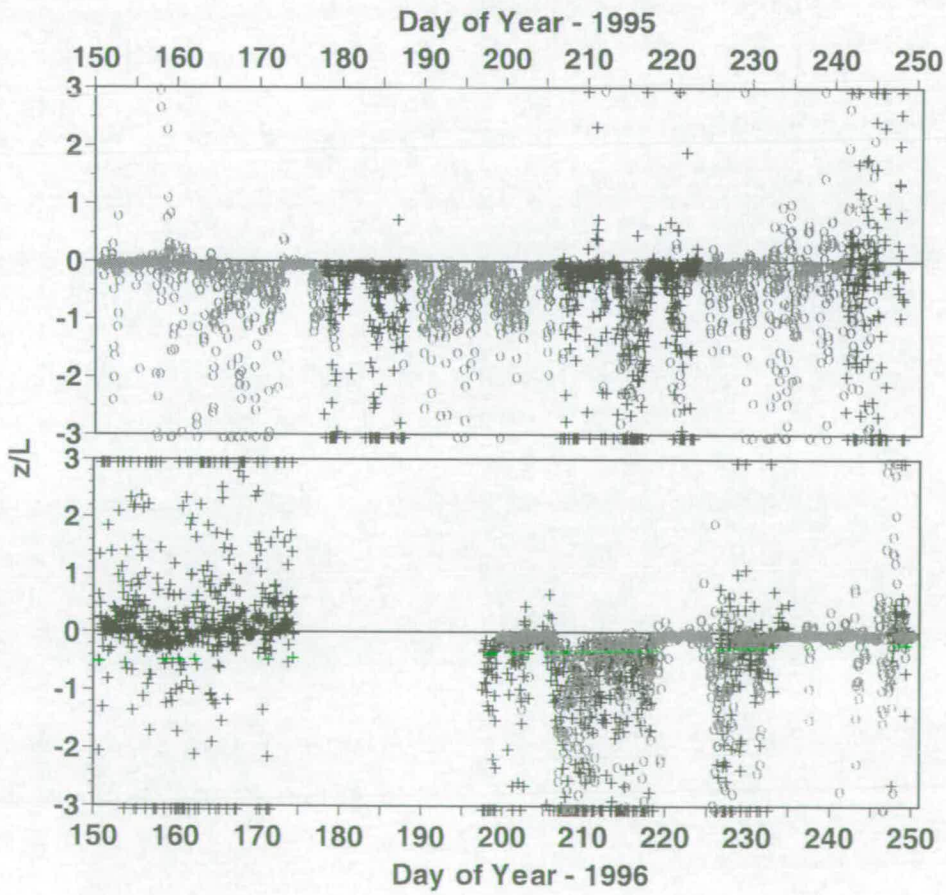

Figure 3-7 *Stability parameter values measured with the Hydra (○) and the Solent/Licor (+) systems during 1995 and 1996.*

In late summer, colder temperatures and the disappearance of the midnight sun allow stable situations to increasingly occur overnight. In 1996, the early period (days 150 – 170) are characterised by predominantly stable conditions over the snowpack. The summer period is again dominated by neutral to unstable conditions with a period around day 230 when snow showers allowed stable conditions to occur. Late summer again had both stable and unstable conditions.

The frequency of unstable/neutral and stable conditions during the two years is shown in Figure 3–8.Note that data from the snow-covered period in 1996 in Figure 3–7 are not included in this analysis.

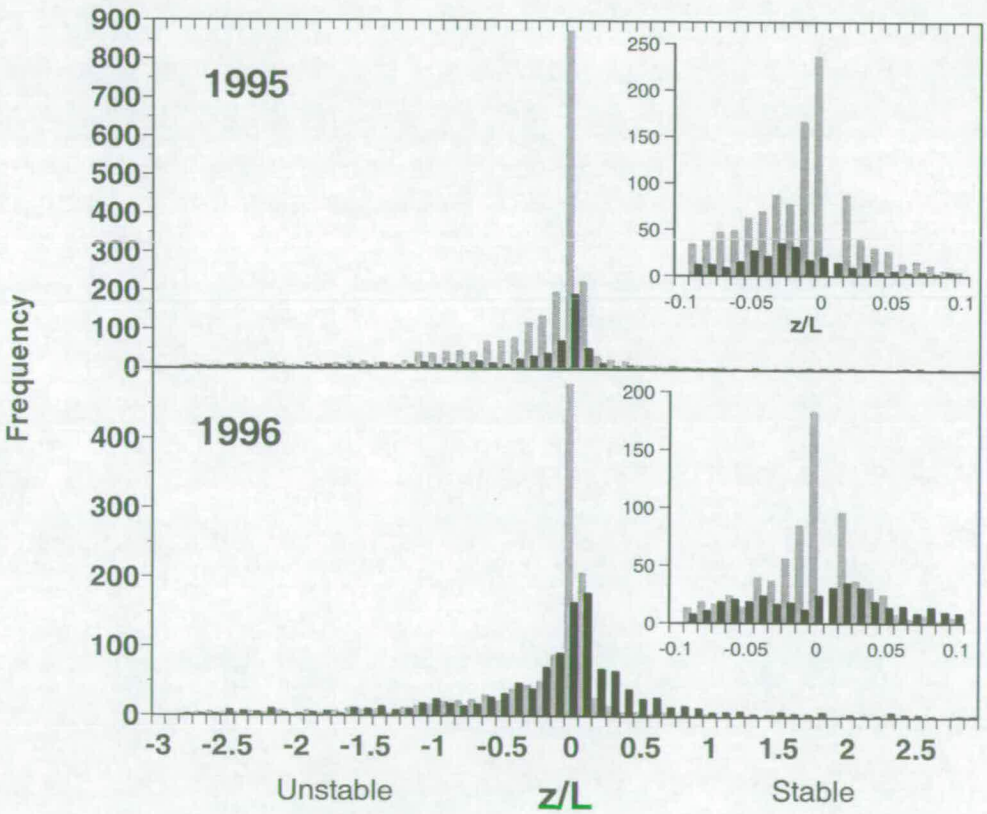

Figure 3-8 *Histogram of the stability parameter z/L during the active season in 1995 and 1996. Grey columns are from the Hydra and black columns from the Solent/Licor system.*

3.5.1.2 Roughness length

A fundamental parameter in the investigation of energy exchange at a vegetated site is the roughness length z_o and is a measure of the aerodynamic roughness of a

surface. It partly determines the efficiency with which momentum, water vapour and carbon dioxide are exchanged between the surface and the atmosphere. It is a function of the shape and density distribution of the canopy elements, and can often be estimated from the height and cross-sectional area of the vegetation (Lettau, 1969; Monteith and Unsworth, 1990). The roughness length is related, but not equal, to the height of the roughness elements and over homogeneous vegetated surfaces is commonly approximated as 0.1 of the mean vegetation height although a figure of 0.13 is better supported by the literature (Tanner and Pelton, 1960; Chamberlain, 1966,1968). For incomplete canopies and inhomogeneous surfaces the methods above are inadequate (Hatfield 1989). Over inhomogeneous surfaces of limited extent, roughness length is much more variable and its size is dependent upon measurement height and wind direction in relation to the particular spatial pattern of elements comprising the inhomogeneous surface. Dolman *et al.* (1992) found that roughness length was 0.4 m when measured at a height of 15.7 m over Sahelian natural open forest and that this value increased to 0.8m when measured from a tethered balloon at 300m due to local spatial inhomogeneity affecting the lower measurement. While this study's Arctic site does not have the large scale heterogeneity displayed in Sahelian open forest, possible differences in roughness length due to visually dissimilar surface cover in different wind directions are possible and require investigation.

The roughness length, z_0 is given by the well-known logarithmic wind profile equation for neutral conditions:

$$u = \frac{u_*}{k} \ln \frac{(z-d)}{z_0} \qquad (3.3)$$

where u is windspeed (m s^{-1}). Within the constant flux layer, this equation states that windspeed decreases with decreasing height until theoretically becoming zero at a height (z-d) which is equal to z_0. Logarithmic wind profile evaluation of z_0 can be used (see Thom 1975) but is not without criticism (Molion and Moore, 1983; De Bruin and Moore, 1985). Eddy correlation measurements provide a direct link between windspeed and friction velocity and allow Equation 3.3 to be solved for

either z_0 or d. Shuttleworth *et al.* (1984) and Gash *et al.* (1989) derived a parameterisation of the surface roughness by regressing u_* against u but had to assume a value for d. Lloyd *et al.* (1992) used eddy correlation measurements at several heights to simultaneously solve a set of logarithmic wind profile equations (Equation (3.3)) to obtain separate evaluations of z_0 and d. It was noted in that study that the displacement height is more sensitive to variability in the data than the roughness length. For this reason and the fact that the fetch was inadequate for measurements at several heights at this site (see below), this approach was not used. As stated above, the estimate of d would also be a very small percentage of z. Following Lloyd *et al.*, (1992), roughness length was therefore estimated from the slope of the regression of u_* against u (with the intercept forced through zero) from the following re-arrangement of the differential of Equation (3.3):

$$z_0 = \frac{z-d}{e^{(ku/u_*)}} \tag{3.4}$$

Data from both the Hydra and Solent systems in 1995 and 1996 were used to create estimates of roughness length for the individual systems within quadrant sectors of the field site for each year.

Figure 3–9 shows the wind directions obtained between 30 May - 5 September 1995 and between 29 May - 6 September 1996.Wind direction is separated into 22.5^0 sectors and the number of occurrences in each sector expressed as a percentage of the total number of hourly (1995) or half-hourly (1996) contributing data periods. In both years the sector from 180^0-202.5^0 was most prevalent and reflects the general

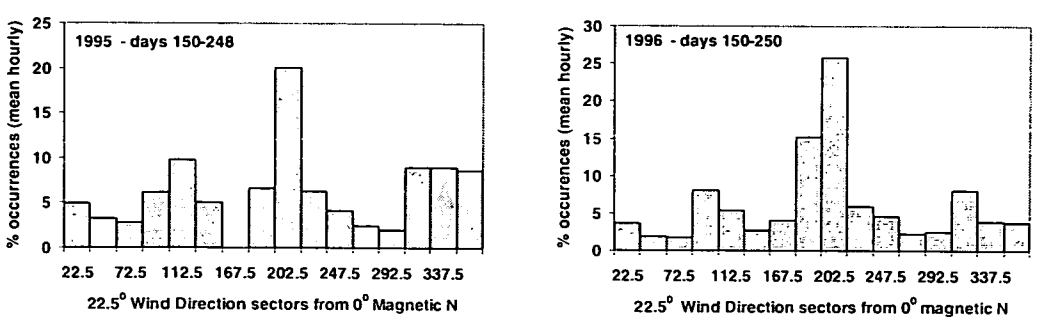

Figure 3-9 *Frequency of wind direction by 22.5^0 sectors during 1995 and 1996.*

atmospheric flow over Svalbard during the summer months. Otherwise, the wind directions are fairly equally spread.

Because of the difference in surface terrain, especially towards the northwest and the southeast, roughness lengths were calculated for the four quadrants of the compass. Both the Hydra and the Solent data were used. The Hydra has a cup anemometer for measuring horizontal windspeed and is subject to stalling at low windspeeds leading to erroneous estimates of u_*. Cup anemometers are also prone to overspeeding and a constant overspeeding error of 3 per cent was corrected for in the Hydra measurements. Although the Solent sonic anemometer does not have these deficiencies, it was thought prudent to have similar data sets for evaluation and comparison. Therefore all data pairs comprising u and u_* with u <1m s^{-1} or u_*<0.1 m s^{-1} were discarded from the Hydra and Solent datasets. Neutral conditions were specified initially to be within the range $-0.02<z/L<0.02$. Despite the extensive

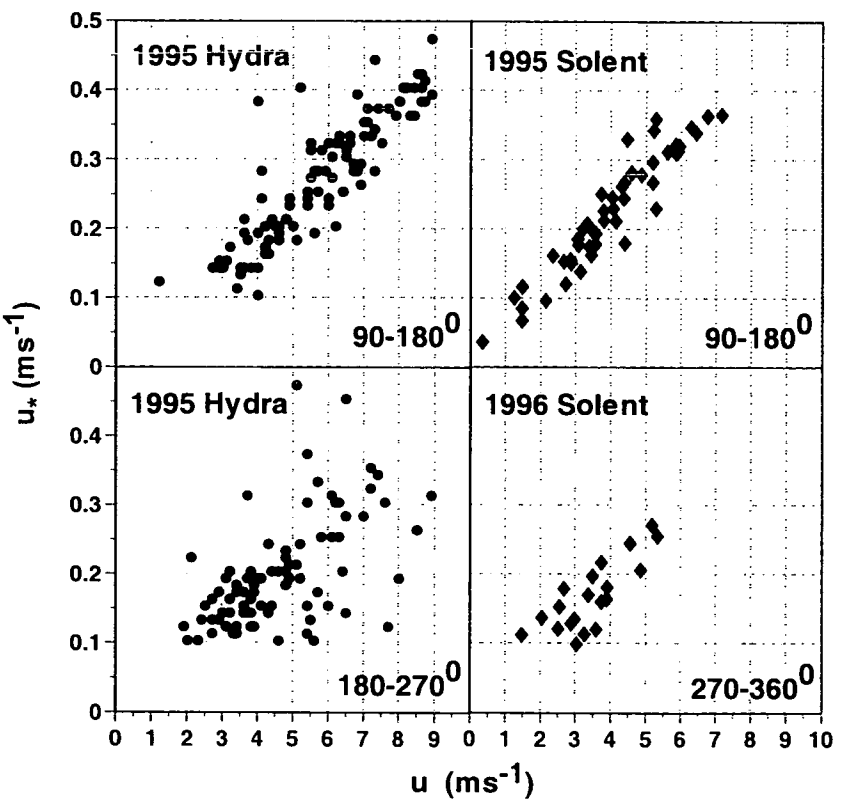

Figure 3-10 *Example Scatter plots of u_* against u. Upper pair illustrate the best relationships from the Hydra and Solent systems while the lower pair are the worst relationships. Also shown are the quadrant sectors and the year from which the data has been drawn.*

measurement set of 100 days in each year, the stability range often had to be widened to produce a sufficient number of values of u and u_* for a meaningful statistical regression to be produced. Figure 3–10 are four scatter diagrams of u_* against u illustrating extreme good and poor relationships for the Hydra and Solent systems.

In general, the regression relationships worsened as the neutral condition filter was widened. Hydra relationships were worse than the Solent because of the use of a cup anemometer for horizontal windspeed measurements. The stability range, number of data points in each regression and adjusted correlation coefficient r^2 for each wind sector in each year are shown in Table 3–1. The individual regression coefficients and their respective 95 per cent confidence intervals for the slope were used to solve Equation (3.4) for z_0 and to provide confidence intervals around this value. Figure 3–11 shows the estimates of the roughness lengths by year, sector and system. The error bars are the 95 per cent confidence interval around the estimated value.

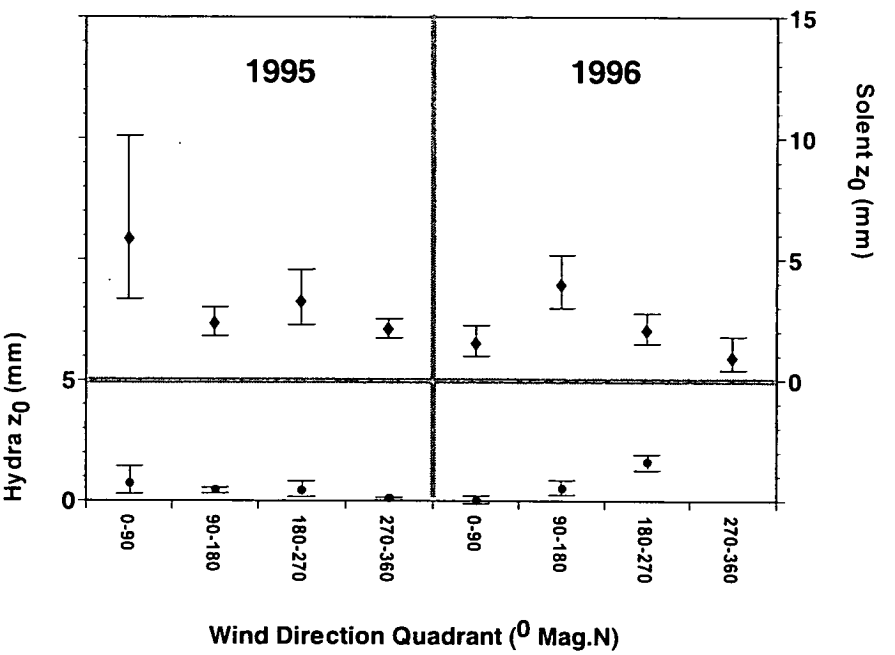

Figure 3-11 *Estimates of roughness length made by the Hydra (•) and Solent (♦) systems during 1995 and 1996 separated into wind direction quadrants together with error bars representing the 95% confidence limit about the mean*

		Hydra			Solent		
Year	Direction Quadrant	Stability Range $\pm z/L$	Sample size	r^2	Stability Range $\pm z/L$	Sample size	r^2
1995	0-90	0.5	28	0.69	0.5	40	0.66
	90-180	0.02	96	0.83	0.1	48	0.87
	180-270	0.02	85	0.15	0.1	56	0.76
	270-360	0.02	140	0.51	0.05	92	0.77
1996	0-90	0.5	27	0.69	0.5	23	0.82
	90-180	0.02	115	0.48	0.5	92	0.49
	180-270	0.02	137	0.72	0.02	43	0.74
	270-360	-	-	-	0.5	20	0.55

Table 3-1 *Statistics for evaluating roughness length from regression of u_* onto u.*

The Hydra values are much smaller, implying an underestimate of u_* or an overestimate of u, both of which are likely in a system using a cup anemometer (prone to overspeeding) which is situated some distance (0.5 m) from the vertical windspeed measurement. This lateral separation creates a loss of flux, in this case an underestimate of u_*, because the instantaneous measurements are slightly uncorrelated. This flux loss is most pronounced in the region of neutral to stable conditions, conditions that apply here. The Solent values are therefore regarded as the more accurate. Within these values, there is no significant difference between values (as judged by the overlapping of the 95 per cent prediction limits). The average roughness length value weighted by the prediction limits was 3.5 mm with a 95 per cent confidence range between 1.7 mm and 3.7 mm. This value can be compared to values of 3 ±1 mm for a harrowed field (Seginer (1974) and 21 ±7 mm found by Harper and Wiseman (1977) for a tussock tundra site at Peard Bay, Alaska. The study field site with low lichen and moss cover is closer in visual roughness to a harrowed field than to tussock tundra and approximates to the classification in Wieringa (1992) of a "featureless land surface without any noticeable obstacles and with negligible vegetation".

Roughness length is generally assumed to be equal to (and measured as) the roughness length for momentum transfer. There are analogous roughness lengths for the transfer of water vapour and heat. The difference is due to the different forces

acting in the transfer of the respective entities. While momentum is transferred by a combination of viscous shear and a drag effect formed by the roughness surface elements, heat and water vapour are primarily transferred through the action of molecular diffusion. Although the roughness lengths are similar for heat and water vapour, the difference between these two and z_0 becomes more important as z_0 increases in size with increasing roughness (Brutsaert, 1979) and can be important when identifying sources in gradient-based analyses. However, measuring roughness lengths for heat and water vapour (z_{0h} and z_{0v} respectively) is not easy. Garratt and Francey (1978) suggest that $z_{0h} = z_{0v} = z_0/7$ for general vegetated sites. However, the arctic polar site could be regarded as approaching a completely smooth surface like water, snow or sandflats where z_{0h} and z_{0v} can be comparable with or greater than z_0. In the absence of any measurements or clear precedence, and noting the very small effect that any difference would make, the scalar roughness lengths (z_{0h} and z_{0v}) are assumed equal to z_0 at this site.

3.5.1.3 Aerodynamic resistance

The rate at which turbulent diffusion transfers water vapour away from a surface is controlled by the aerodynamic resistance, r_a , most readily defined in this study of surface fluxes as

$$r_a = \frac{u_r}{u_*^2} \tag{3.5}$$

where u_r is windspeed at a reference height. The reciprocal of aerodynamic resistance, boundary layer conductance, is often used in models as it is effectively bounded and therefore numerically stable whereas aerodynamic resistance can become very large or infinite under low wind speed conditions. The reciprocal is also a non-linear form and tends to mask variability especially towards the upper limits and so, in this analysis, aerodynamic resistance is used to exemplify the variability in the measurements and between the two systems.

3.5.1.3.1 Aerodynamic Resistance as measured by the Hydra

Figure 3–12(a) shows hourly r_a values between days 150 and 246 during 1995, estimated from equation 3.5 using measurements of u and u_* from the Hydra. Data was again rejected if $u < 1.0$ m s^{-1}, $u_* < 0.1$ m s^{-1} and z/L was outside of the range $-0.1 > z/L > 0.1$. Aerodynamic resistance from this data was evaluated as 112 s m^{-1} with a standard deviation of 14.1 s m^{-1}.

However a histogram of this data (Figure 3–12(b)) shows the skewness of a Poisson distribution and the data was transformed using the natural logarithm of the r_a values (Figure 3–12(c)) before the mean and standard deviation was computed. The mean and standard deviation were then inversely transformed. The mean aerodynamic resistance for 1995 was 103 (±11.4) s m^{-1}.

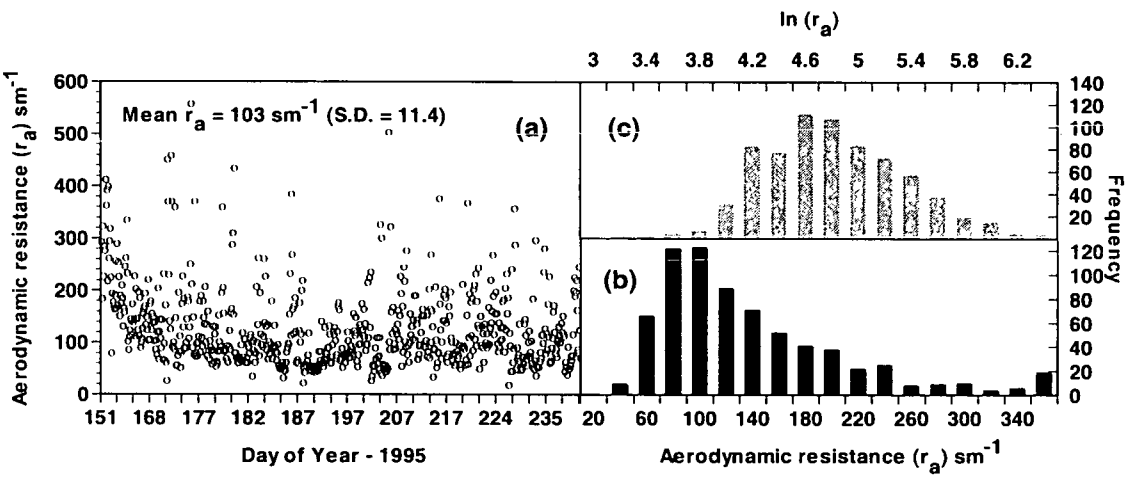

Figure 3-12 *Aerodynamic resistance results for the Hydra system in 1995. (a) Estimates of aerodynamic resistance (r_a) between 31 May and 31 August- this is not a full time series due to the data rejection procedure; (b) Frequency histogram of r_a; (c)Frequency histogram of the logarithmically transformed r_a estimates. The mean value of r_a is that of the transformed data.*

The same process was performed on the 1996 Hydra data and the results are shown in Figures 3–13 (a), (b) and (c)

The mean r_a for 1996 was 90 (±11.8) s m^{-1}. Snow was present in 1995 until day 156 and the stable conditions over the snow pack are apparent from the consistently higher values of r_a at that time (Figure 3–12). Similarly in 1996, the late summer snowfall in August (days 232-236) is also characterised by higher aerodynamic

resistance values. The general rise seen between 204-220 is not so readily explained nor is the apparent oscillatory pattern to the aerodynamic resistance values. However, the generally tighter distribution of values throughout 1996 may be due to the seasonal weather being overall more cloudy and duller – conditions that would have led to lower turbulence and thus reducing the effects of the deficiencies of the cup anemometer.

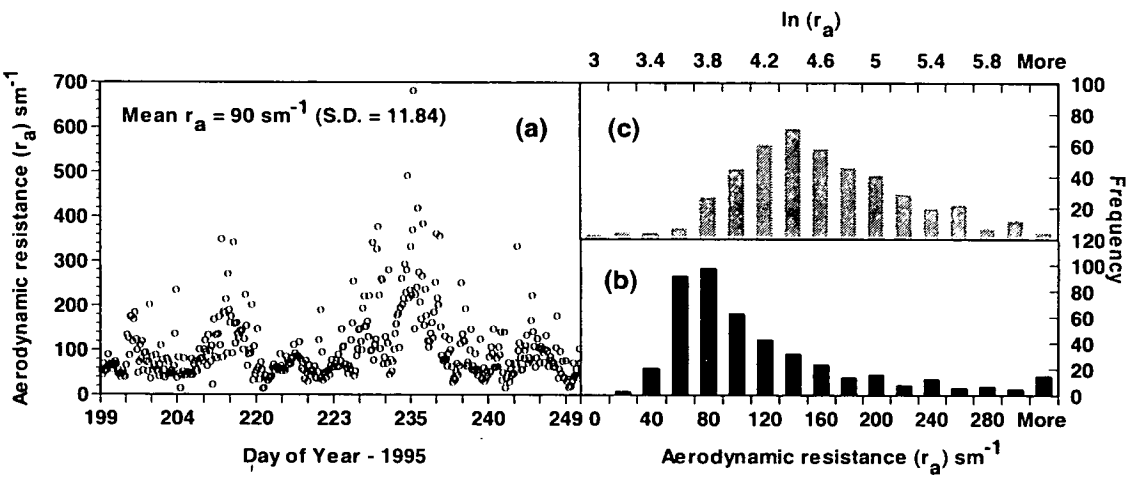

Figure 3-13 *Aerodynamic resistance results for the Hydra system in 1996. (a) Estimates of aerodynamic resistance (r_a) between 18 July and 6 September- this is not a full time series due to the data rejection procedure; (b) Frequency histogram of r_a; (c)Frequency histogram of the logarithmically transformed r_a estimates. Mean value of r_a is again for the transformed data*

3.5.1.3.2 Aerodynamic resistance as measured by the Solent

In the light of the differing roughness lengths (see 3.5.1.2) from the Hydra and Solent measurement system, the data from the Solent 3D sonic anemometer was analysed to identify if any systematic aerodynamic resistance difference was evident between the two systems. It was also necessary to establish which values would be used in subsequent analyses.

Figure 3-14 is analogous to Figure 3-12 but for the Solent data during 1995.

The Solent-Licor system was initially installed in June 1995 after snowmelt occurred and hence Figure 3-14 shows only aerodynamic resistance values after snowmelt. The aerodynamic resistance values for the Solent show less scatter due to the combined effects of (a) using sonic evaluation of both horizontal and vertical

windspeed and (b) measuring these at effectively the same point in space. These two factors will tend to increase the measurement precision and the correlation between the two measurements. The data is still skewed and a logarithmic transformation gave a mean (± standard deviation) of this data of 69.8 (± 6.5) s m^{-1}

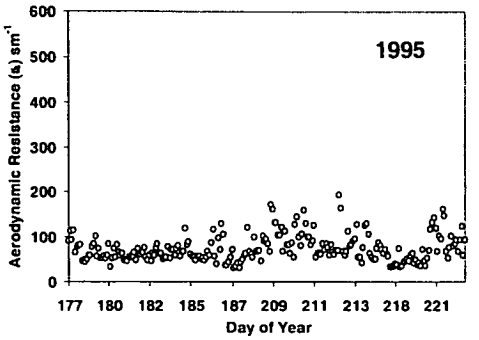

Figure 3-14 *Aerodynamic resistance estimated from Solent measurements for 1995. Data was subjected to the same low windspeed filter as the Hydra.*

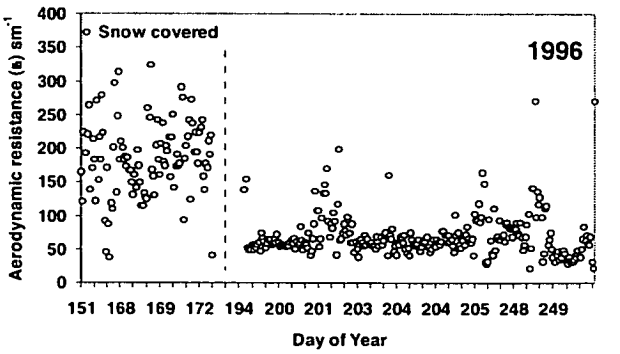

Figure 3-15 *Aerodynamic resistance estimated from Solent measurements for 1996. Data was subjected to the same low windspeed filter as the Hydra.*

In 1996 the Solent-Licor system was installed prior to snowmelt and Figure 3-15 does show values of aerodynamic resistance both prior to snowmelt and for the post-snowmelt period. The aerodynamic resistance prior to snowmelt is very scattered reflecting the variability introduced by the very smooth and stable snow surface. The log transform aerodynamic resistance during this snowmelt period had a mean (± S.D) of 175 (± 14) s m^{-1}. During the post snowmelt period, the log transform aerodynamic resistance was very similar to 1995 with mean (± S.D.) of 63.4 (± 6.1) s m^{-1}.

The combined results from both the Hydra and Solent-Licor systems are summarised in Table 3–2.

The unexplained rise in aerodynamic resistance around day 205 in 1996 measured by the Hydra was also measured by the independent Solent and can be regarded as real. The aerodynamic resistance values from the Solent anemometer were regarded as the more reliable and accurate because of the better measurement capability of the Solent compared to the Hydra. The 1995 summer climate was assessed as being

more typical of past summers and a value of 70 s m^{-1} was chosen for subsequent analysis (e.g. modelling) where windspeed flux data was not available.

	1995			1996		
	Mean s m^{-1}	S.D. s m^{-1}	Sample Size	Mean s m^{-1}	S.D. s m^{-1}	Sample Size
Hydra	103	11.4	696	90	11.8	443
Solent	69.8	6.5	233	63.4	6.1	265
Solent-snowmelt	-	-	-	175	14	100

Table 3-2 *Summary of Aerodynamic resistance as measured by the Hydra and Solent systems*

Table 3-3 shows the variation of aerodynamic resistance with stability. The stability was split into 3 classes from neutral to unstable. Data from both the Hydra and Solent systems for 1995 and 1996 are shown. The data periods are the same as for the above analysis and the data has been log-transformed. Aerodynamic resistance, in general increases with instability, except for the Hydra data in 1995 which decreases with instability. Wind at this site generally reduces in velocity with increasing instability which would explain the increase in aerodynamic resistance with increasing instability

Stability Class z/L	Hydra 1995 Mean ± S.D. s m^{-1}	Solent 1995 Mean ± S.D. s m^{-1}	Hydra 1996 Mean ± S.D. s m^{-1}	Solent 1996 Mean ± S.D. s m^{-1}
-0.01 to –0.5	114.0 ± 1.78	78.1 ± 1.49	89.5 ± 1.65	88.9 ± 1.54
-0.5 to –1.0	110.8 ± 1.38	106.9 ± 1.58	98.3 ± 1.92	118.6 ± 1.40
-1.0 to –1.5	106.6 ± 1.31	136.1 ± 1.36	109.3 ± 2.05	144.8 ± 1.39

Table 3-3 *Aerodynamic resistance within 3 stability classes for the Hydra and Solent systems in 1995 and 1996.*

3.5.1.4 Surface Resistance to the transfer of water vapour

Although surface resistance is a characteristic of any vegetated site representing the effective stomatal resistance to the transfer of water vapour from the vegetation, its estimation in this thesis is dependent upon sensible and latent heat fluxes. It is most appropriately dealt with after the investigation of the surface energy fluxes in that chapter.

3.5.2 Fetch and Source Footprints

The term *fetch* describes a fixed distance upwind that contains a surface whose turbulent and energy characteristics can be regarded as homogeneous . In micrometeorological work, there is therefore a need for research sites to have sufficient fetch if the measurements are not to be contaminated by areas with different turbulent or energy characteristics. At the interface of dissimilar surfaces, the air layer nearest the ground will rapidly acquire the turbulent characteristics induced by the different surface roughness of the new surface. Air layers further from the surface will still have turbulent characteristics generated by the previous surface. As the air mass travels over the new surface, the turbulent structure will gradually be propagated upward through successive air layers. Any entity being transported by the air flow, e.g. heat, moisture or carbon dioxide, will also gradually change in response to the new surface's energy and carbon balance. There are therefore three "indistinct" layers to the air flow. A layer of modified air which is fully in equilibrium with the surface characteristics, a layer of air which is in transition from the surface layer to the following - the third layer which has the characteristics of equilibrium flow from the previous surface. The air layer that is in equilibrium with the surface is termed the *constant flux layer* within which fluxes are effectively within 10 per cent of the surface value. The constant flux layer consists of two regions, the *roughness sublayer* closest to the surface where the turbulent structure is influenced by the spacing and structure of the individual roughness elements. And above this the *inertial sublayer* where the turbulent structure depends only on scales such as friction velocity and height. For a sensor to measure valid area-average characteristics of this new surface, it must be placed within the inertial

sublayer. This avoids both the unwanted variability caused by the heterogeneity of the new surface's individual roughness elements and the incorrect measurement of the new surface's characteristics caused by being in the layer of air largely characterizing the previous surface.

In past micrometeorological research over extensive homogeneous surfaces, for example prairie grasslands and forests, fetch for a particular measurement height was generally worked out using the knowledge that the equilibrium sub-layer grows with a slope of approximately 1 per cent downwind of a surface change and maximum fetch was thus 100 times the height of the measurement above the vegetation. As research moved into field scale homogeneous areas, e.g. agricultural crops, then a better estimate of fetch was required. Gash (1986), by considering the work of Calder (1949) produced a two-dimensional model that gave the effective fetch directly upwind from a measurement point based on measurement height, windspeed and roughness length. The model also provided distances from within which proportions or percentages of the entity being measured were occurring. This model was only applicable in neutral conditions, as was the model by Schuepp *et al.* (1990) which built on and extended the work of Gash (1986) to provide entity source strengths along the fetch length. The idea, implied but not implemented in Schuepp *et al.*, (1990), that their model could be modified to include atmospheric stability was taken up by Lloyd (1995) who produced a two-dimensional model that could produce fetches in unstable conditions given by:

$$\frac{1}{Q_0}\frac{dQ}{dx} = \frac{-2x_{\max}}{x^2}\phi_m \exp\left[\frac{-2x_{\max}}{x}\phi_m\right] \qquad (3.6)$$

where the left-hand side represents the relative source strength with Q_0 , a unit area flux density; x is distance upwind of the measurement position, x_{max} is the distance upwind at which the source strength is a maximum, and ϕ_m is a momentum stability correction function which following Dyer (1974) is given by:

$$\phi_m = \left[1 - 16\frac{(z-d)}{L}\right]^{-\frac{1}{4}} \qquad (3.7)$$

where L is the Obukhov stability length, z is measurement height and d is displacement height. The distance upwind to the maximum relative flux density, X_{max} given by Schuepp *et al.* (1990) as $X_{max} = U(z\text{-}d)/u_* k$ where U is defined as the average windspeed between the surface and the observation height, u_* is the friction velocity and k is the von Kármán constant was replaced, to implicitly incorporate stability, by a similar distance parameter described in the three-dimensional source area model of Schmid and Oke (1990) as:

$$X_{\max} = \frac{1.7 z^{1.03}\left[\ln\left(\frac{z}{z_0} - \psi\left(\frac{z}{L}\right)\right)\right]}{\left(1 - \frac{z}{L}\right)^{\frac{1}{2}}} \qquad (3.8)$$

where $\psi(z/L)$ is evaluated as:

$$\psi\left(\frac{z}{L}\right) = \left(1 - \frac{76z}{L}\right)^{-\frac{1}{4}} - 1 \qquad (3.9)$$

This model depends solely on measurement height, roughness length and stability and produces relative flux density at any upwind distance.

The above method is one of many based on turbulent diffusion theory that itself emanated from work carried out on the downwind dispersion of gas that arose after the First World War. This suite of methods are easy to use but require assumptions about the surface sources and also assume that atmospheric surface layer scaling applies. When these assumptions are not fully met, e.g. above tall forests, then stochastic trajectory footprint models (also called Lagrangian or Markovian footprint models) can be used (e.g. Rannik *et al.*, 2000, Leclerc and Thurtell, 1990). These

models start at the measurement point and by inverting the trajectory physics of the entities arrive at one of the sources that contribute to the final flux. The large number of modelled paths that have to be constructed to map out the source footprint have meant that only recently has the power of desktop computers been sufficient to render these methods useful for general micrometeorological research.

There is a lot of confusion about flux footprints and what they can and cannot do. What they cannot do is pinpoint exactly where measured fluxes are coming from. Not only is the method statistical but over a typical measurement period, both wind direction and stability change, often quite dramatically. Flux footprints are routinely calculated using mean values for stability, windspeed and wind direction (parameters required varies between models) and provide a statistically fuzzy area from which sources are thought to emanate. In reality, the areas are certainly much wider and probably either longer or shorter. The experimental and physical work underlying flux footprints progressed from studies of plume diffusion, either elevated (and therefore only slightly affected by the surface terrain) or over smooth grass. The validity of applying such models over more heterogeneous surfaces needs more research. Schmid and Lloyd (1999) investigated the effect that extreme heterogeneity had upon the spatial representativeness of flux measurements and the bias that can be introduced into the measurements depending on the sensor position within the heterogeneity. They showed that there is a measurement height at which the spatial inhomogeneity is ineffectual in biasing the measurements and that this height should be sought for inhomogeneous surfaces. The problem is then to decide a measurement height that is sufficiently high to be insensitive to local heterogeneity but sufficiently low to keep fetch within the larger scale homogeneity. This is what flux footprints can indicate: the overall validity of the measurements and as a tool for the placement of sensors in locations without large fetch.

Figure 3–16 shows 2 dimensional flux footprints (i.e. distance and source strength) using equation (3.6) for two typical stability ranges encountered at the Ny-Ålesund field site. One trace shows the relative source strength (proportion of total measured)

and the other trace the cumulative source strengths showing the distance of fetch contributing to the percentage total flux measured.

Figure 3–16(a) shows plots for an unstable condition (z/L= -1.0) and indicates that maximum relative source strength occurs at about 10 m upwind of the sensor position and that 90 per cent of the fluxes are emanating from within 90m upwind. Figure 3–16(b) shows plots for a neutral condition (z/L=-0.005) and indicates a maximum source strength at 30 m with 90 per cent of the measured flux emanating from within 320 m of the sensor. Note that Figures 3–16(a), (b) have different distance scales on the x-axis. The vertical dashed line indicates equal distance. Evidently, the fetch is adequate for unstable conditions but in neutral conditions, the

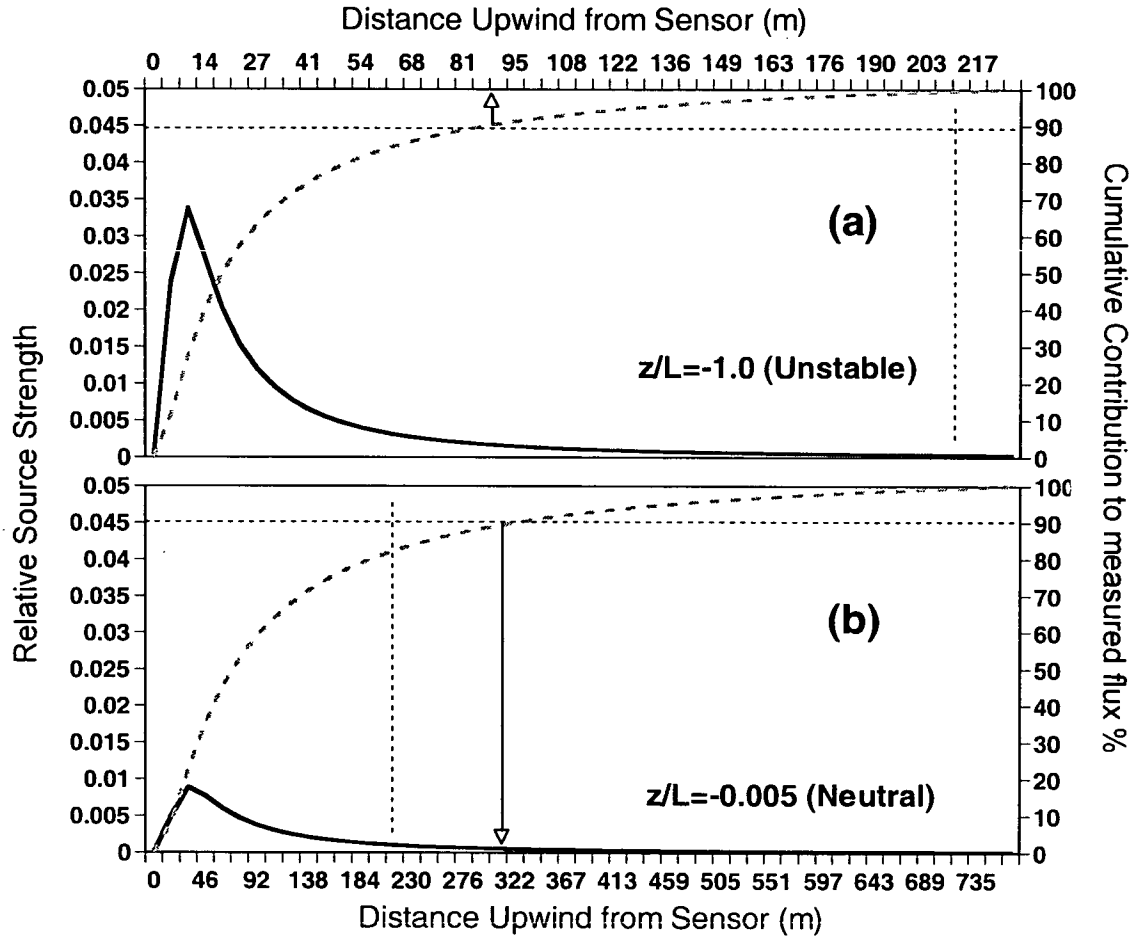

Figure 3-16 *Relative source strength (——) and cumulative source strength (- - - -) as percentage of total flux for (a) unstable conditions (z/L = -1.0) and (b) neutral conditions (Z/L=-0.005). Arrowed lines mark a distance upwind of sensor position from within which, 90% of the flux will emanate. Dashed vertical lines indicate equal distances for the different scaled abscissas.*

fetch extends beyond the immediate area of homogeneous surface (see Figure 3–2) especially towards the west where the Bayelva river forms braided streams. Such a fetch would be inadequate (within the strict 90 per cent limit), if beyond the immediate area, surfaces were of either a different roughness height or vegetation type. At this site, the same vegetation type (as far as roughness height and general energy exchange are concerned) existed in all directions. The problem west direction is towards the Austre Brøggerbreen glacier at 1km distance. When winds were from the west, they would be descending the glacier and provide very cold and stable airflows within which little energy or carbon dioxide exchange would occur. Within these restrictions, the site and measurement height were regarded as being adequate and measurements would not be significantly affected by more distant surface terrain.

3.5.3 Soil Temperatures

Soil temperatures and soil heat flux play an important part in both the energy and carbon dioxide balance of this site and as such need to be measured accurately. The level to which soil heat flux plates represented areal soil heat flux was questionable and soil heat flux was not included in this analysis and the reasons are given in Chapter 4. The soil surface temperature will be used in Chapter 6. In this site description chapter, the change with time and depth of soil temperature provides an appreciation of the change of energy within the soil during a typical season. Of particular importance at permafrost sites is the transition from frozen to unfrozen ground during the end-phase of snowmelt. The soils at the Ny-Ålesund site are predominantly glacial clay and gravel and are particularly difficult to excavate and return to a state that reflects the original thermal and hydraulic conditions. A temperature profile instrument was developed for this study to minimise the disturbance of the soil structure upon installation (Lloyd, 1998). Other development criteria for the instrument were to operate continuously through permafrost conditions and to locate the freezing front by appealing to the markedly different electrical resistances of frozen and unfrozen soil (Colman and Hendrix, 1949; Sartz, 1967). The freezing position in soil is not necessarily identified by the 0°C isotherm

(Bouyoucos, 1921) and more latterly Anderson and Tice (1970) who detected liquid water in soils at temperatures well below 0°C.

Figure 3–17(a) shows the progression of soil temperature at 8 soil depths as the freezing front moves down at the end of the snowmelt period. Figure 3–17(b) shows soil resistance measured through the soil matrix between adjacent measurement depths. It is evident that, as the temperature traces move through the 0°C isotherm, the highly correlated fall in soil resistance indicates little evidence of depressed freezing points in this soil. Despite being mid-summer during the polar day, there is marked variation in soil heating.

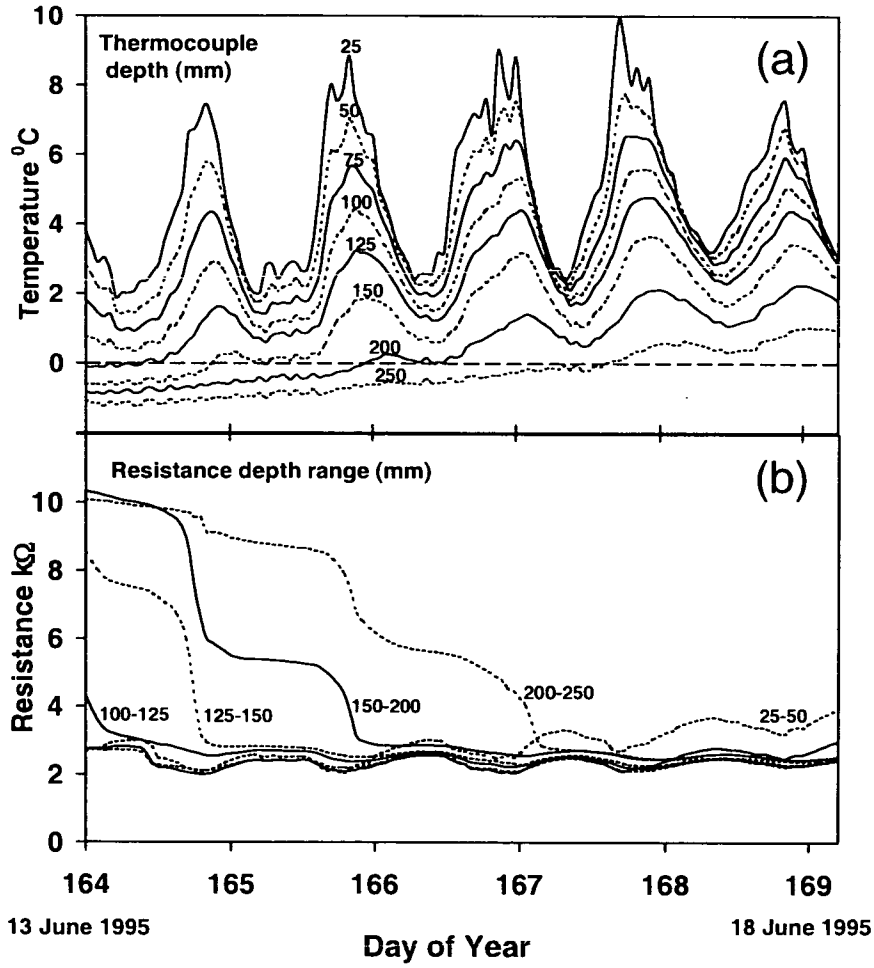

Figure 3-17 *Diurnal changes in soil temperature (a) and soil resistance (b) for the period 13-18 June 1995.*

The soil resistance measurements can also be used, after calibration for the particular soil, to monitor soil moisture providing the soil ionic content does not change with depth or over time (Lloyd, 1998). Figure 3–18(a) shows the progression of soil temperature at 25mm and 250mm depths for the active season in 1995. Figure 3–18(b) shows calibrated soil moisture content over the soil depths (25-50 mm, 100-125 mm and 200-250 mm).

The profile temperatures at 25 mm and 250 mm show both daily variation and a seasonal rise and fall. It is also apparent that rain provides heat to the soil as there is a marked correlation between rainfall and rising soil temperatures. Soil moisture at 200-250 mm is high at 25-30%. The measurements closer to the surface show it to remain moist, respond immediately to rainfall and show a drying out phase towards the autumn.

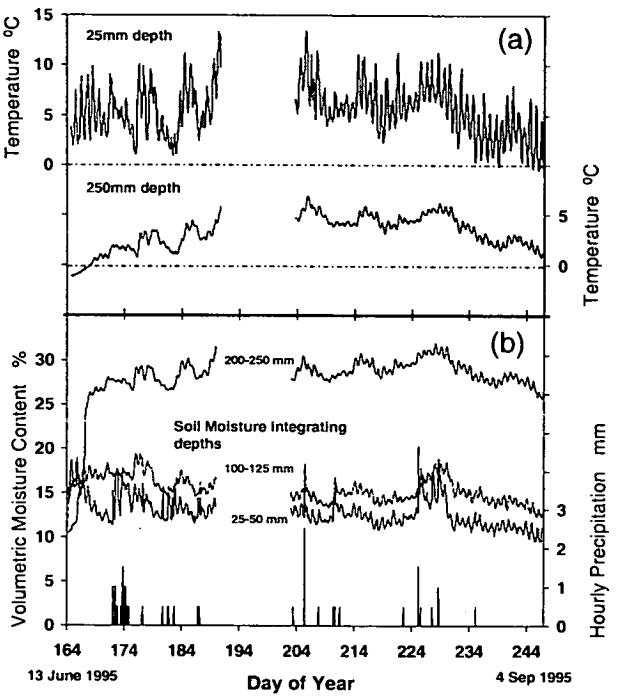

Figure 3-18 *Soil temperatures (a) and soil moisture values (b) for selected depths in the soil and rainfall during the active season in 1995*

3.6 Summary

This chapter places the Ny-Ålesund polar semi-desert field site within the context of Svalbard. The field site is characterised with regard to general micrometeorological parameters that are used, not only within the remaining thesis, but by field scientists and modellers who wish to have climate parameters which are fundamental to describing the exchange of energy and trace gases.

Chapter 4
Instrumentation Methodology

4 Instrumentation Methodology

4.1 Climate Measurement Site

An automatic weather station (AWS) was installed in June 1994 on a 5^0 north facing slope of approximately 200 m in length that terminated in the floodplain area where the flux measurements were made. The AWS conformed to the general pattern designed by the Institute of Hydrology and manufactured by Didcot Instruments (Abingdon, UK). It consists of a vertical mast with two horizontal cross–arms normal to each other that support and expose the sensors. The entire assemblage is kept vertical by guying from the extremities of one of the horizontal poles. The AWS operated continuously until August 1999. The AWS was initially fully exposed, but during 1995 was fenced in with a wooden fence 1m high to jointly protect local reindeer from being caught in the guywires and to protect the instruments from the attentions of the reindeer. The AWS measured incoming and reflected shortwave radiation (CM5, Kipp and Zonen, Delft, Netherlands), incoming hemispherical long-wave radiation (PIR, Eppley Laboratories, New Jersey, USA) and net allwave radiation (Didcot Instruments, Abingdon, UK), relative humidity and air temperature in an unaspirated radiation shield (MP100A, Rotronic AG, Switzerland), windspeed (DWR, Didcot Instruments, Abingdon, UK) and wind direction (DWD, Didcot Instruments, Abingdon, UK), ultrasonic distance to surface (for snowdepth) (SR50, Campbell Scientific, Shepshed, UK) and rainfall (0.5mm tipping bucket, Rimco, Australia). In adjacent fenced areas, soil temperature and electrical resistance profile units described by Lloyd (1998) were installed in August 1994 but were not fully operational until June 1995. They operated nearly continuously until August 1999.

4.2 Flux Measurement Site

The fluxes of carbon dioxide, water vapour, sensible heat and momentum were measured towards the middle of an area of the floodplain 200 m north of the AWS and soil physics sites. The floodplain extended 250 m to the north and 200 m to east and west. Two systems were operated during 1995 and 1996. A combined Solent R2 (Gill Instruments, Lymington, UK) 3-dimensional sonic anemometer and LI-COR

6262 (LI-COR Inc., Lincoln, NB, USA) H_2O/CO_2 infrared gas analyser (IRGA) was purchased in early 1995 and deployed for the first time at the Svalbard site. The novelty of the system, and concerns about its operational and measurement reliability in a harsh climate, prompted its deployment alongside a second independent system - a Hydra, developed and manufactured at the Institute of Hydrology. The Hydra consists of a single frame supporting a vertical sonic anemometer, an adjacent vertical open-path H_2O IRGA and a fine-bead thermocouple and a six-cup precision anemometer (Lloyd *et al.*, 1984, Shuttleworth *et al.*, 1988). Both flux measurement systems were mounted on top of thin masts at a height of 2.7 m above the surface. The Hydra provided continuous measurements of sensible and latent heat and momentum fluxes from before snowmelt, through the summer and into the beginning of the autumnal re-freeze for 1995. In 1996, the Hydra was deployed at another nearby field site until 17 July when it was repositioned alongside the Solent/LI-COR system for the rest of the active season. The Solent/LI-COR 6262 system was used to measure fluxes of momentum, sensible and latent heat fluxes and carbon dioxide flux. This system provided campaign-based period fluxes during 1995 and 1996.

4.3 Radiation Balance Measurements

4.3.1 Short-wave radiation measurements

The components of the short-wave radiation at this site were measured using Kipp and Zonen CM5 pyranometers or solarimeters (Kipp and Zonen, Delft, the Netherlands). Incoming short-wave was measured with one CM5 on top of the AWS Mast and another CM5 measured reflected short-wave radiation below one of the cross-arms of the AWS at a height of 1m. Incoming short-wave radiation can be considered spatially homogeneous over distances less than 1 km but reflected short-wave is modified by the inhomogeneity of the underlying surface. In order to quantify some of the spatial variability of the tundra surface, the reflected short-wave radiation measurement was replicated over typical but significantly different vegetation. The incoming and reflected solarimeters (manufactured in 1969, 1971 and 1986 respectively) were calibrated originally by the manufacturer and were

subsequently re-calibrated from time to time at the UK Meteorological Office calibration facility until it closed in 1988. Over that time the calibrations had drifted by less than 1 per cent.

4.3.2 Long-wave Radiation Measurements

Long-wave incoming radiation was measured using an Eppley Model PIR pyrgeometer (Eppley Laboratories, New Jersey, USA). The manufacturer's calibration value was used. Long-wave outgoing radiation was not measured directly but the surface temperature of typical surface types was measured using four Everest Model No.4000.4GL Infra-Red Thermometers (IRT) (Everest Interscience, Tucson, USA).

4.3.3 Net All-wave radiation measurements

The overall net radiation term, being the difference between the total incoming and outgoing radiation fluxes at all wavelengths was measured using two types of net radiometer. A Didcot Model 301 net radiometer (Didcot Instruments, Abingdon, UK) provided long-term measurements as part of the Automatic Weather Station (AWS) long-term monitoring station. Several other REBS Q*5 and Q*6 net radiometers (Radiation and Energy Balance Systems Inc., Seattle, USA) were deployed over different but typical surface types in order to measure the variability in net radiation.

4.4 Flux Measurements

4.4.1 Introduction

Net radiation is the radiation flux at the surface that is available for heating the air, vegetation and soil layers and for evaporation of water present in soil and vegetation - both from wet surfaces and from the loss of water vapour during photosynthesis. The remaining radiation flux once soil heating has occurred is termed *available energy* as this is the energy available to be used in the convective processes involved in the production of sensible and latent heat. There are several methods available to quantify sensible and latent heat in terms of the available energy including the

measurement of mean gradients, by aerodynamic and energy budget methods, and by eddy correlation. For this study, the first three methods, are suspect in their application for the following reasons. The measurement of mean gradients and the use of the aerodynamic method, while inexpensive and easy to operate, make assumptions in their use regarding turbulent transfer coefficients which render them inappropriate over heterogeneous terrain (Panofsky and Dutton, 1984). The energy budget method, through its use of measurements at two heights, is also suspect in heterogeneous terrain and in limited fetch conditions, because of the inability to define a source footprint (Horst, 1999). But the main concern is its reliance on net radiation to "fix" and quantify the sizes of the individual fluxes of sensible and latent heat explicitly measured as a ratio (the *Bowen Ratio*). Such a reliance is suspect in the light of current criticism regarding the accuracy of current net radiation instruments (see Energy Balance chapter). In heterogeneous terrain, it is also difficult to evaluate an available energy term that is representative of the source area contributing to the Bowen ratio measurement (Lloyd, 1995).

4.4.2 Flux Measurements – the Hydra

The Hydra, which is not commercially available, began development at the Institute of Hydrology in 1976 and this development has continued and is currently at the Mk.3 level. The Hydra used in this field study was the Mk.2 version. The physical redesign of the Mk.2 took account of the consequences of the analytical procedures described by Moore (1986) and improved the aerodynamic profile of the instrument and reduced the *volume of measurement* - the volume of air within which the eddy correlation measurements take place. The Mk.2 Hydra is shown in Figure 4–1. It

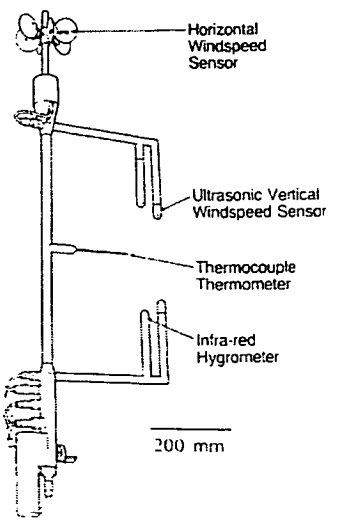

Figure 4-1 *A schematic of the Hydra Mk2 flux measurement system*

consists of a single ultrasonic anemometer (hereafter called the sonic for brevity), vertically aligned, with an open-path infra-red gas analyser (the hygrometer) operating around the 2.7 μm wavelength to measure H_2O in air. This is also vertically aligned just behind the sonic. A Chromel-Constantan thermocouple constructed from 38 μm wire protrudes 5mm from a supporting sheath, initially 0.25 mm in diameter and then 30mm from the junction, 1.5 mm in diameter which is attached to the rear support of the Hydra frame. The supporting sheath is of a length to place the thermocouple bead ~10 mm from the light path of the hygrometer. Horizontal windspeed is measured with a fast response 6-cup high resolution anemometer (Vector Instruments, Rhyl, UK) positioned vertically on top of the rear support of the Hydra frame.

The use of wind speed (rather than wind vector) and the distance between the ultrasonic anemometer and the cup anemometer reduces the accuracy of the momentum flux measurement. This was purposely done to enhance the accuracy of the more important (in most hydrological studies) surface energy flux measurements. The calibration of the infra-red hygrometer exhibits some dependence on absolute humidity, and the accurate measurement of evaporation therefore requires an approximate measurement of ambient humidity. The Hydra system incorporates a capacitance hygrometer Rotronic MP100A (Campbell Scientific, Shepshed, UK) housed in an unaspirated radiation shield to provide a measurement of relative humidity. A further input channel is routinely used to measure net radiation. Complete details of the principles, individual sensors, and calibrations are described by Shuttleworth *et al.* (1982, 1988), and Moore (1983).

The Hydra is controlled by an RCA CDP1802 CMOS microprocessor utilising ROM software written in Assembler code. The software is essentially an interrupt routine, which every 100 ms interrogates 8 sensor and status voltages which are converted to digital form, computations are performed to provide AutoRegressive Running Means (ARMA) of the instantaneous values of the fluxes, variances and mean values. This routine is interrupted at the end of each averaging period (1 hr) by further software which creates the time-average fluxes, variances and means which are then output to

a solid-state store. The ARMA procedure, which is a digital form of a low-pass electrical filter, provides real-time separation of fluctuations from the background mean trend and dispenses with the need to store raw data for flux calculation. This procedure has also been incorporated into the Solent/LICOR controlling software. The Hydra's eddy correlation software and original field trials are more fully described by Lloyd *et al.* (1984). Shuttleworth (1988) provides an integration of these results and improvements that contribute to the Mk.2 Hydra.

Because the Hydra employs a single vertical ultrasonic anemometer, the instrument has to be positioned normal to the local air streamlines. Failure to do this could result in larger or smaller flux measurements depending on whether time-averaged streamlines are perceived by the sonic to be away or towards the surface. The off-line software routinely compensates for any failure to meet this condition provided the instrument is reasonably normal to the streamlines.

4.4.2.1 The Hydra Calibration Procedure

The Hydra sonic anemometer is routinely calibrated using a calibrator circuit that acts as a plug-in substitute for the sonic transducers. The calibration of the electronics can be used to compute a theoretical calibration for the sonic anemometer as a whole. Shuttleworth *et al.* (1988) reported the rigorous testing of this procedure using a wind tunnel. The results showed that the theoretical calibration was within 1-2 per cent, for most field situations and certainly better than 5 per cent for all wind vector directions likely to occur in the field and for a horizontal acceptance angle of 330^0. Outside of this range, the proximity of the support frame causes the vertical windspeed measurements and, by implication, derived fluxes to be suspect.

The Hydra Thermocouple circuit is calibrated at several set temperatures over the expected range of field conditions.

The Hydra hygrometer was calibrated at the start of each of the field seasons in 1995 and 1996. The use of a temperature-stabilised detector in the hygrometer significantly reduces the extent and complexity of the temperature dependence in its calibration (Moore, 1983). This effectively removes the temperature sensitivity of the detector and infra-red filter leaving a small temperature sensitivity that is

particularly associated with the physics of infra-red absorption in the atmospheric light path. The calibration procedure requires that the detector and filter are stabilised at a particular temperature and the remaining temperature sensitivity is expressed as a linear regression about this temperature. This procedure is performed for several set temperatures covering the expected range of field temperatures.

During the calibration, the entire Hydra sensor head and electronics box are placed inside a temperature and moisture controlled environment chamber. The environment chamber is then maintained at each set temperature, while the humidity of air passing through an enclosure between the source and detector is changed to three different set levels and the hygrometer output is monitored and compared with that given with dry air in the enclosure. The three temperature sets of 3 humidities are then regressed simultaneously using a standard multi regression package to collapse the solutions onto a single calibration curve as detailed in Shuttleworth *et al.* (1988). Typically this results in a calibration curve with fitting correlation coefficient (R^2) of 0.999. Because the output of the hygrometer exhibits a response to atmospheric temperature fluctuations, there is a small contamination of the measured latent heat flux that is proportional to sensible heat flux. This correction is small, ~1 per cent of sensible heat.

The manufacturer's calibration value was used for the cup anemometer. All the calibrations, flux-loss corrections and other corrections are applied retrospectively to the raw data using an off-line program.

4.4.3 Flux Measurements – Solent/LI-COR 6262

The Solent/LI-COR 6262 system was newly acquired in 1995 and was deployed at this study field site on 26 June 1995. It was used in campaign mode to obtain fluxes until 5 September. In 1996, this instrument was deployed from late May (before snowmelt) and again acquired campaign-based period fluxes until 2 September.

The Solent/LI-COR 6262 flux system is shown in Figure 4–2 The IRGA was fitted with a pressure transducer to allow on-line pressure corrections to be made. A pump (Model CAPEX V2X, Charles Austin, Byfleet, UK) on the outlet side of the IRGA cell pumped sample air at 13 litres min^{-1} down a 2.5 m tube from an inlet at the same

height as the middle of the anemometer array but approximately 30mm to one side. The tube inlet was shielded to prevent rain from entering the tube and also to minimise flow distortion through the anemometer caused by the flow of air down the tube.

The tube, made of silicon rubber (Masterflex 6424-25, Masterflex, Illinois, USA), chosen for its impermeability to carbon dioxide and water vapour, had an internal diameter of 5mm. The time lag between the measurement of the vertical windspeed and the measurement of the gas concentration in the IRGA cell was determined in 1995 by calculating the flow time from the dimensions, distances and flow rate of the air through the tube and was set at 0.5 sec. In 1996, time lags were determined on-line by the data logging software by maximising the covariances between vertical windspeed and the two gases, CO_2 and water vapour.

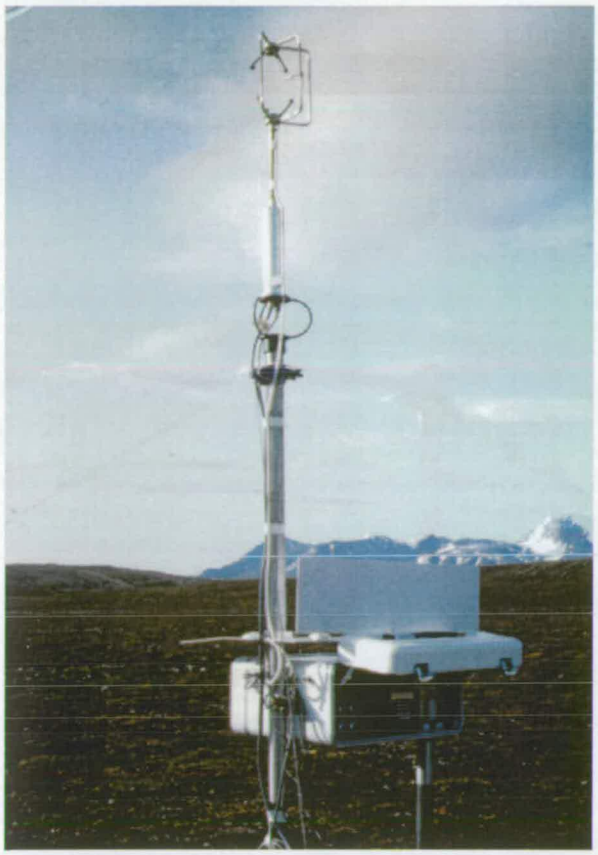

Figure 4-2 *The Solent R2 sonic anemometer on top of its support pole which also provides the support for the LI-COR 6262 which is installed in the waterproof white box.*

The analogue signals from the IRGA are processed through an analogue-to-digital converter within the *Solent* body that digitises the signals at a frequency of 10Hz. This is combined with the wind speed and speed of sound signals from the Solent which are being sampled at 21Hz and both sets of data are available for interrogation at the serial port of a laptop PC. Up to 5 analogue signals can digitised by the Solent and combined with the turbulent data. For this study, three were sampled; being the analogue outputs from the CO_2 and H_2O channels of the IRGA and the internal cell

temperature of the IRGA. Raw data output from the IRGA and Solent anemometer were logged continuously at 21 Hz on the laptop computer into 20 min period files (1995) or 30 min period files (1996). The laptop computer also calculated on-line period average fluxes. In 1995, the controlling software package was developed at the Institute of Hydrology; in 1996, the EdiSol software package (Moncrieff *et al.*, 1997) was used. In 1995 the inability to leave the system running unattended for more than 3 days meant that CO_2 and H_2O flux data from the LI-COR system was only taken during the short field expeditions during the summer. In 1996, field campaigns began well before snowmelt but a waterlogged laptop computer at the end of snowmelt again limited flux measurements from the IRGA system. An Institute of Hydrology Hydra eddy correlation system (Shuttleworth *et al.*, 1988) measuring sensible and latent heat fluxes and net radiation (Q*5, REBS, Seattle, USA) operated continuously at the same South Site during 1995 from the 30 May to the 3 September. In 1996, the Hydra operated continuously alongside the Solent-Licor system from 17 July to 6 September.

4.4.3.1 Solent-LI-COR 6262 Calibration

The Solent 3-dimensional sonic anemometer is calibrated by the manufacturer in a wind tunnel to provide 2-dimensional calibrations and it relies on 3-D calibrations of prototype sensors to compute the angle of attack cosine response. In this study those original manufacturer calibrations have been used.

The LI-COR Manual and laboratory procedure provokes the user of the LI-COR 6262 to calibrate the instrument as often as possible. In the following, the actual calibration procedure is outlined and then the reasons why, in this particular study, these procedures were not followed and the possible repercussions of such action.

The aims of the calibration procedure are to obtain the voltage output from the optical bench of the IRGA with zero concentration of CO_2 and H_2O and then to establish the gain (or span) of the voltage output for a known concentration of CO_2 and H_2O.

There does not seem to be a standard method of obtaining these zero and span calibration values. Zero values have been established either using dry Nitrogen from cylinders or using chemicals to scrub the air of both CO_2 and H_2O. Water vapour calibrations for the H_2O span have used either chemical methods or water vapour generators (LICOR Portable Dew Point Generator Model LI-610) while CO_2 spans are generally obtained using scale gases. Mixing pumps are probably the best way to calibrate these instruments.

There is nothing inherently difficult in the above procedures when performed in the laboratory. However, the situation is not so true in the field, especially at field sites that are either remote or experience harsh climates.

During the 1995 field season, calibrations were carried out in accordance with the manual but without any real feeling of certainty in the reliability of the process. In particular the following points became apparent during that field season and ought to be considered before even attempting a field calibration.

1. Zero calibrations are affected by changes in instrument temperature. It makes sense to calibrate on a "good" day as far as weather is concerned, which in the arctic tundra during the summer time may not be typical of general seasonal climate. Is it certain that any readjustment is improving the calibration?
2. The arctic summers are very short. Too much time spent on calibrations is time lost taking data.
3. Calibration of the span setting should be performed at the same flow rates as exist when the system is measuring surface fluxes to ensure that pressure differences within the optical bench between calibration mode and field mode do not invalidate the calibration. The portable water vapour generators used in the field (e.g. the LICOR LI-610) cannot supply consistent water vapour concentrations at a rate consistent with field flows (typically 12 litres min^{-1} down the inlet tube and 3.5 litres min^{-1} through the sample cell).

4. The arctic tundra site in this study had summer temperatures that rarely exceeded 10°C and more typically were below 5°C. In such conditions it is difficult to obtain reliable water vapour concentrations with portable water vapour generators when the dewpoint is close to or below 0°C.
5. At this study site, it was only possible to transport a bottle of scale gas for the CO_2 span calibration during the early spring when the surface was snow covered and snow-scooters could be used. Such a bottle left in the field all summer and subject to low temperatures will experience some "settling out" of the heavier CO_2. Consequently, the stated overall concentration of the bottle may not be what is delivered to the IRGA.

Taking all these factors into account, the following calibration procedure was adopted for 1996. Before the field season, the LICOR was sent back to the manufacturers for a re-calibration which included a complete dismantle and thorough cleaning of the optical bench. During the field season, the only calibration procedure that was performed at the field site was to regularly calibrate the CO_2 and H_2O zero settings. Because this could be done with little effort automatically through the use of chemicals, it could be done on any day - not just "good" days.
The LI-COR was sent back to LI-COR at the end of the field season with a request to establish the span drift before recalibration.
Span calibration in the field would only be done when drifts in the span became unacceptably large.
Confidence in this procedure was increased by the experience of other researchers who found the LI-COR 6262 to be relatively stable with regard to both zero and span (Moncrieff *et al.*, 1997) and the observation that the span is unlikely to have changed substantially if the zero has not changed substantially.

In comparing evaporation rates from the open-path Hydra and closed-path Solent/Licor systems, it was noted that with temperatures below 5°C and relative humidities above 80%, that the closed-path system suffered flux loss compared to the open-path. This could be due to reduced pressure in the metal inlet tube of the

closed-path system. Reduced pressure could have the effect of condennsing water vapour at these low temperatures and high relative humidities. Condensed water would be absorbed by drier air passing over it. Such an effect would lead to decreased variance in the water vapour signal leading to an evaporative flux loss. Another possibility is salt deposition on the inside of the tube providing nucleation points for water vapour absorption. The site is 2 km from the sea and the air could contain dissolved salts. It was not thought that the CO_2 concentration measured by the closed-path system was affected by this phenomena and evaporation fluxes from the Hydra were used in the analysis.

4.4.4 The Eddy Correlation Method

The eddy correlation method is a direct measurement with minimum theoretical assumptions. Recent rapid advances in both fast response sensors and low power computers with the processing power to both operate the sensors and gather data has meant that eddy correlation systems are now affordable and able to be operated in both extreme climates and over non-ideal surfaces.

The initial assumption of the eddy correlation method is that near the surface, the time-averaged mean horizontal wind is parallel to the ground and that therefore the time-averaged mean vertical wind velocity is zero. However, within this moving body of air, are turbulent eddies. Instantaneous values of wind velocity within these eddies may be in any direction and of varying velocity. These instantaneous values will have a vertical component that is either towards or away from the surface. The turbulent eddies are also transporting other atmospheric entities, which include heat, water vapour, carbon dioxide and momentum.

If evaporation is occurring, implying a time-average mean movement of moisture away from the surface, then eddies moving away from the surface as indicated by positive vertical velocity components will contain air that has, on average, a higher than average water vapour content.. At some future time, these eddies will be moving towards the surface characterised by a negative vertical velocity component and will contain air having a lower than average water vapour content. The technique

for combining the measurement of atmospheric entities with a measurement of vertical velocity to produce a flux measurement is called *eddy correlation* or *eddy covariance*. More formally, if the mean and fluctuating values for the water content of the air, measured as specific humidity (kg of water/kg of air) is denoted by $\bar{q}$ and q' respectively and the corresponding values for vertical velocity are $\bar{w}$ and w' (ms^{-1}) respectively, then the instantaneous measurements are given by:

$$q = \bar{q} + q' \quad and \quad w = \bar{w} + w' \tag{4.1}$$

In addition, the eddy also transports a mass of dry air, which within a unit volume, is given by a density ρ_a (kg m^{-3}) which also has mean and fluctuating components. The evaporation rate $\boldsymbol{E}$ is then given by:

$$\boldsymbol{E} = \overline{(\bar{\rho}_a + \rho_a')(\bar{w} + w')(\bar{q} + q')} \tag{4.2}$$

which can be expanded as:

$$\boldsymbol{E} = (\overline{\overline{\rho}_a \overline{w}\overline{q}} + \overline{\overline{\rho}_a \overline{w}q'} + \overline{\overline{\rho}_a w'\overline{q}} + \overline{\overline{\rho}_a w'q'} + \overline{\rho_a' \overline{w}\overline{q}} + \overline{\rho_a' \overline{w}q'} + \overline{\rho_a' w'\overline{q}} + \overline{\rho_a' w'q'}) \tag{4.3}$$

Because, by definition, all averages of *single* primed quantities are equal to zero, the second, third and fifth terms in equation (4-3) can be eliminated. If we allow that, at least within the air layer close to the surface, air density is constant, then the sixth, seventh and eighth terms involving the fluctuation of air density can be eliminated as they collapse to single prime terms. The first term can be eliminated if we restrict measurements to areas without preferred vertical motion and therefore neglect terms containing the mean vertical velocity. The reduced equation encompasses the eddy correlation method and is given by:

Latent heat flux: $$\boldsymbol{E} = \rho_a \overline{w'q'} \tag{4.4}$$

The averaging bar over ρ_a has been dropped as it is regarded as constant. Similar expressions can be constructed for fluctuations in the other entities and are summarised below:

Sensible Heat flux: $$H = \rho_a c_p \overline{w'T'} \quad (4.5)$$

Carbon dioxide flux: $$F_c = \overline{w'c'} \quad (4.6)$$

Momentum flux: $$\tau = -\rho_a \overline{w'u'} \quad (4.7)$$

A complicating factor, pointed out by Webb *et al.* (1980), arises because the assumption that underpins the eddy correlation method, namely that there is no net flux of air at the lower boundary of the atmosphere is not strictly true. Webb *et al.* (1980) pointed out that there is no net flux of *dry air* at the surface. The presence of moisture and heat in the air affects the overall density of this moist warm air creating an apparent mean non-zero vertical velocity, $\overline{w}$, which will cause contamination of mass fluxes deduced from devices measuring the density of constituents. This would not be a problem if the sensors measured the mass of constituent per unit mass of dry air i.e. the *mixing ratio*. The size of this mean non-zero vertical velocity, $\overline{w}$, is given by:

$$\overline{w} = \frac{\mu \overline{w'\rho_v'}}{\overline{\rho_a}} + \frac{(1+\mu\sigma)\overline{w'T'}}{\overline{T}} \quad (4.8)$$

where $\mu = m_a / m_v$ is the ratio of molecular masses for dry air and water respectively and $\sigma = \overline{\rho_v} / \overline{\rho_a}$ is the ratio of mean densities for water vapour and dry air; T is temperature (K). This non-zero vertical velocity has different ramifications for each of the fluxes being measured and whether these fluxes are being measured *in situ*. For open-path infrared gas analysers, the correction for flux loss due to this density can be quite large although typically the correction to water vapour fluxes is a few per cent (Webb *et al.* 1980). Such a correction is routinely made within the software

for the Hydra. Webb *et al.*, (1980) also state that the correction to CO_2 fluxes measured with open path IRGA's may be as large as the measured flux. By using the Li-COR 6262 closed path IRGA system and eliminating temperature fluctuations in the air stream before analysis of the gas is performed, the corrections for the density effects can be eliminated.

In order to use the eddy correlation method, fast response sensors have to be used in order to capture the information contained in the fluctuations. The required response time of the sensors depends on the range of eddy sizes that carry the flux and on the rate of change of the entity. Eddy sizes grow with increasing surface roughness over the surface so that measuring fluxes close to the surface of a snowpack requires much faster responses than over a very rough forest. An ideal eddy correlation instrument would measure the vertical velocity and atmospheric entity at a single point without interfering with the airflow past the instrument. In practice this is not currently possible - all measurements with the possible exception of temperature are measured over a distance and are often not collocated. All these instrumental limitations cause loss of information when eddies are smaller than the measuring path length and when sensor separation creates conditions where correlation between the measurements are not maximised. Moore (1986) has investigated the form and size of these flux-loss factors and how to compensate for them and these corrections are routinely applied by the software.

4.4.5 Energy Closure Problems in Heterogeneous Terrain

Testing the accuracy of micrometeorological measurements of the energy balance components is usually performed by attempting to close the energy budget equation

$$Rn - G = H + LE \tag{4.9}$$

by combining the individual measurements over some appropriate time period and examining any residual loss or gain. When both flux and radiative measurements are measured at appropriate heights over extensive areas of surface terrain exhibiting similar soil moisture and vegetation cover, e.g. grass or wheat fields, then this

closure often works in practice. During the early development of eddy correlation equipment, energy balance closure was used as a measure of the accuracy (or otherwise) of eddy correlation sensors by assuming that net radiation was correct and that soil heat flux could be minimised by setting the averaging time period to 24 hours. Most of this development was carried out over extensive grass or similar homogeneous crop with assumed homogeneous soil moisture. The success of the eddy correlation principle has caused it to be used in more heterogeneous terrain that by its very nature may not be extensive. The extent to which adjacent flux measurements could vary over heterogeneous terrain was examined by Lloyd *et al.*, (1997). They found that individual hourly estimates of fluxes could be, on average, 15 per cent different for sensible heat and 20 per cent different for latent heat. The heterogeneity of soil moisture was a principle factor for the discrepancy. However, summing the measured hourly fluxes over longer time periods eliminated a lot of the inherent and real variability. Three day flux totals were found to be within 3 per cent of each other. While energy closure problems are stated here for eddy correlation measurements, they are equally valid, if not more so, for measurements incorporating the gradient, aerodynamic or Bowen ratio (by definition utilising energy closure to partition the fluxes of sensible and latent heat) methods in non-ideal terrain.

4.4.5.1 Combining Flux and Static measurements

The crux of the energy closure problem is the dynamic and large spatial averaging of flux measurements compared to the static and generally small sample measurement of the radiation and soil energy terms. Fetch and flux footprints have already been examined and evaluated in Chapter 3.

4.4.5.2 Static radiation and soil heat flux measurements

Radiation and soil heat flux measurements in a micrometeorological experiment are usually obtained from static instruments. Incoming short- and long-wave radiation may be regarded as being homogeneous over the area encompassing a typical micrometeorological field site. However, the reflected and outgoing short- and long-wave radiation is rarely homogeneous over the same area because the surface will

have variable albedo and surface temperature caused by differing vegetation and soil properties. The radiation instrument measuring this outgoing radiation will integrate this heterogeneity according to its own flux source footprint. Radiation instruments have a radiative source area created by the receiving of radiation at angles other than normal to the thermopile plate. Such a radiation source area can be inferred from Lambert's Cosine Law, which describes the energy emitted by a full radiator at an angle other than normal to the radiator surface. A corollary of this law is that the flux density of radiation striking a full radiator at angles other than normal to the radiator's surface, $\mathbf{d}F_R$, is given by:

$$\mathrm{d}F_R = I_{n,u} \cos\theta \, \mathrm{d}\omega \qquad (4.10)$$

where $I_{n,u}$ is the normal component of the unit radiation intensity originating from the surface, dω is a differential solid angle, with its centre located θ away from the nadir.

Figure 4–3 is a re-analysed graph originally presented by Reifsnyder (1967) and shows, for various proportions of radiation emanating from a surface, "the view factor", the diameter of ground area contributing to the measured radiation at different measurement heights. The scales are such that any consistent units can be applied. For example, 80 per cent of radiation emanating from a surface directly beneath a radiometer will come from a circle of radius 10 m when the sensor is placed at a height of 5 m above the surface. It is a useful rule-of-thumb gained from this figure that 50 per cent of radiation incident upon a radiometer from the ground is coming from sources contained in a circle of radius equal to the height between the radiometer thermopile and the ground surface.

Increasing the height of radiation instruments reduces the effect of the surfaces' heterogeneity upon the overall measurement of net radiation by increasing the area sensed as implied in Figure 4–3. However, there are two complicating factors: it becomes difficult to prevent the instrument support structure from being "seen" by the instrument and flux divergence becomes important. Ideally, net radiation should be measured at the ground surface. As the instrument moves further away from the surface, the ground radiation is increasingly being scattered and absorbed by the

intervening atmospheric layer so that the radiation measured by the net radiometer is attenuated. Close to the surface, this flux divergence can be ignored but it can become a problem when measuring at heights greater than 10 metres above the radiating surface (Zdunkowski and Johnson, 1965).

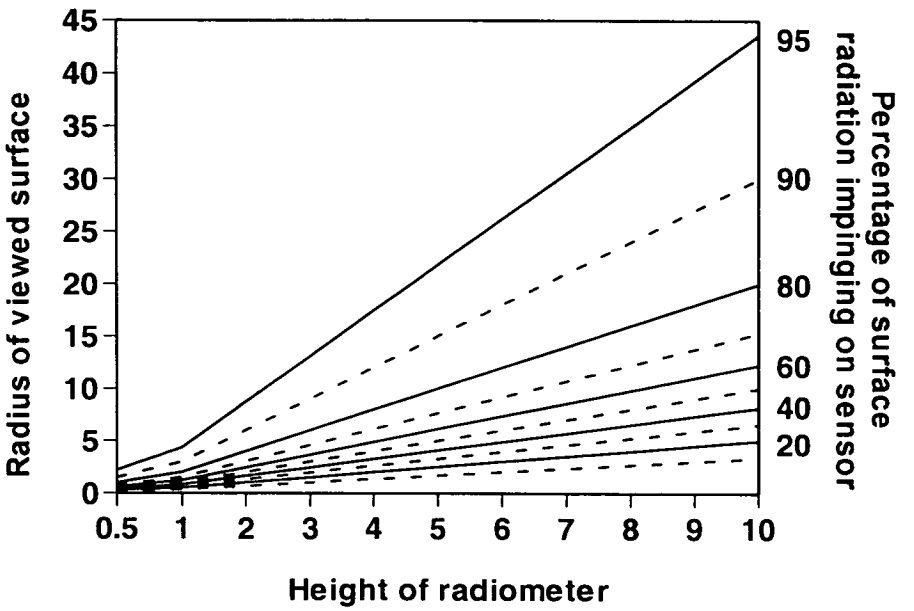

Figure 4-3 *Relationship between radiation sensor height and radius of surface contributing to the measurement for required percentage of surface contributing. Radius and height are in the same units*

The sensor for measuring soil heat flux could not be simpler consisting of a flat plate containing a thermopile which measures the differential temperature across the plate. The material of the plate has generally been chosen for typical soils. In untypical soils e.g. wet peat soils, the thermal properties of the soil do not match those of the sensor and the sensor will either experience more or less heat flux than the surrounding medium. This effect can cause a heat flux plate to experience relative changes in the surrounding medium of more than an order of magnitude (Schwerdtfeger, 1976). In terms of the energy closure problem, soil heat flux and soil heat storage is even more variable than net radiation from heterogeneous surfaces. In temperate biomes, providing energy closure is not required for periods of less than a period of 24 hours, soil heat flux can largely be ignored as heat gained during the

day is largely lost at night with the very gradual change in soil temperature with season being a small residual. However, in the Arctic, there is effectively one period of constant light (the polar day) followed by a period of darkness (the polar night). Heat is constantly being gained by the soil during the polar day and only when the polar night arrives does the soil begin to lose heat. Thus both heat flux, heat storage and their spatial variability cannot be ignored. However, the inherent variability and limited instrumentation for multiple sampling beneath the different soil, stone and vegetation types gave little confidence for correct measurement and they have been omitted from this analysis, preferring to rely on the larger sampling ability of flux measurements and radiometers to produce a reasonable estimate of soil heat flux.

An extreme example of the failure of measurements to close the energy balance equation in heterogeneous terrain is given by Lloyd (1995) where it is shown that even if the areal available energy (R_n - G) were to be correctly measured within the footprint of correctly measured surface fluxes the energy budget would still not close because of the disparity between the areal averaging processes of the fluxes as compared to that of the available energy.

4.5 Soil Temperature

Long term measurements of soil temperature in ground subject to permafrost can be difficult. The sensors must be robust enough to withstand ice pressure and yet still be able to maintain contact with the surrounding medium. The soils at the study site were glacial till clays which through the action of permafrost and flooding over time has created a well-packed soil. Disturbance of this matrix should be kept to a minimum if measurements are to be representative of the surrounding soil. An instrument was designed and constructed to provide both profile soil temperatures and soil resistances in a form that would withstand ice pressure and be installed with minimal disturbance to the soil structure. Soil resistance measurements were included because soil temperature does not necessarily indicate where the freezing front is – in certain soils liquid water has been detected at temperatures well below

freezing (Anderson and Tice, 1970). However, the soil resistance value for frozen soil is very different from that for unfrozen soil. An added advantage of the instrument is that it provides qualitative indications of soil moisture movement in soils and can provide quantitative values if the soil is calibrated. The instrument is constructed in such a way that different configurations of overall length and distance between measurement depths can be assembled. The instrument also maintains relative positions between measurement depths even if permafrost pressure succeeds in moving the instrument vertically in the soil. The instrument uses simple fine-wire thermocouples for temperature measurements. Measurement frequency and data storage is controlled by a CR10 logger via an AM416 multiplexer unit (both Campbell Scientific, Shepshed, UK). The multiplexer allows up to 16 measurement positions and the logger could accommodate 5 multiplexers. The design, calibration and performance of this instrument are detailed in the Appendices.

Chapter 5
Surface Energy and Carbon dioxide balance

5 Surface Energy and Carbon dioxide Balance

5.1 The Partitioning of Energy Incident upon the Earth

At the land-atmosphere interface, radiant, thermal and kinetic energy are inextricably linked by the climate processes of Earth. If the land-atmosphere system was in a steady state, then the total incoming energy gain would be balanced by the total outgoing energy loss. Climate change produces a situation whereby outgoing energy loss falls short of the incoming energy gain and therefore allows extra energy to remain in the surface layers of the Earth, and both passively and dynamically in the atmosphere.

5.1.1 The Terrestrial Radiation Balance

The overall radiation balance of any vegetated terrestrial surface is given by:

$$\overline{R}_n = (1-\alpha_b)(\overline{S}_d + \overline{S}_{diff}) + \varepsilon(\overline{L}_d + \overline{L}_e) - \overline{\sigma T_b^4} \qquad (5.1)$$

where R_n is net radiation, α_b is the reflection coefficient or albedo of the surface, S_d and S_{diff} are the direct beam and diffuse components of the incoming shortwave radiation, S_e is shortwave radiation reflected from the environment but contributing to the incoming shortwave radiation; ε is the surface emissivity, L_d and L_e are the longwave components from the atmosphere and the environment respectively and σT_b^4 is longwave emission from the surface, with σ, the Stefan-Boltzmann constant and T_b the surface temperature. The overbars imply period averaging. The individual balances and their provenance are explained below.

5.1.2 The Arctic Radiation balance

Most natural surfaces act as diffuse reflectors (as opposed to specular or mirror-like reflection) when the sun angle relative to the surface is greater than 30° or 40°. At angles below this, grazing incidence can occur, where the reflection from smooth surfaces and shiny or waxy leaves can become dominantly specular and reflectivity

increases. Ny-Ålesund is at 79^0 56' N and the sun reaches a maximum elevation of 32.5^o at local solar noon on 21 June. At all other times of the year the sun is below this elevation and specular reflection may be important in decreasing the absorption of incident solar radiation.

The *visible* waveband from 0.4 to 0.7μm contains energy that has a fundamental role in photosynthesis. Because the energy of solar radiation is often measured with instruments sensitive over the whole *visible and infrared* waveband from 0.4 to 3 μm, it is important to be able to estimate what proportion of this energy is available for photosynthesis. The general assumption is that this fraction is 45 per cent, a figure derived from the spectral distribution of solar radiation when the sun is more than 30^0 above the horizon (Moon, 1940). However, this figure refers to direct radiation only. Not only is diffuse sky radiation predominantly in the visible spectrum but diffuse radiation was found to be equal to or exceed direct radiation on a cloudless day at solar elevations less than 20^0 at Sutton Bonington, UK (Monteith, 1973). The visible fraction of total solar radiation during overcast conditions (a typical occurrence during the Spitsbergen active season) tends to be slightly greater than during cloudless conditions. Such considerations imply that the visible fraction of the total beam (and hence the photosynthetically active radiation (PAR)) at high arctic sites may exceed the 50 per cent derived by Monteith (1973).

5.1.3 The Surface Energy balance at the Arctic Site

The full energy balance equation of the land-atmosphere system at the surface interface in conditions of snow and ice is given by:

$$R_n - \lambda E - H - G + (L_c F_c + A_h) = Q_s \qquad (5.2)$$

where, in this case, energy fluxes towards the surface are positive and energy fluxes away from the surface are negative (Brutsaert, 1984). R_n is the net sum of the short and longwave radiation terms incident on the surface layer, λ is the latent heat of vapourisation, E is the rate of evaporation, H the flux of sensible heat into the

atmosphere and G the flux of heat conducted into the earth. The lesser terms inside the brackets in equation (5.2) are L_c the thermal conversion factor for fixation of carbon dioxide, F_c the specific flux of carbon dioxide and A_h the energy advection into the layer expressed as specific flux. The residual Q_s is the rate of energy storage per unit area in the layer. If an ice or snow layer is present then Q_s will include the energy used for fusion and λ may have to be replaced by L_s the latent heat of sublimation. The factors in the brackets in equation (5.2) are often neglected for the following reasons. The energy involved in plant fixation of carbon can be 5 per cent of incoming solar radiation under very favourable conditions but are more typically less than 1 per cent (Jones 1992). The slow growth rate of the mosses and lichens at the study site imply that this figure of 1 per cent is probably an upper limit. The energy advection term, A_h , could apply at this site if energy was being transported horizontally through the surface layer by water flow. Although horizontal flow of water cannot be ruled out, the temperature of the water entering and leaving any particular area would be very similar and heat advection would be minimal. While vertical advection of energy through rainfall into the surface layer is included in G, rainfall onto a snow cover will advect energy into that snowpack that will not be included in G. However, for this study, A_h will be neglected. Q_s for snow free periods at this site, is also negligible as the mass of vegetation is small. However, for the period of snowcover, this term can be important (e.g. McKay and Thurtell, 1978) as it then incorporates the energy utilised in fusion. In this study, this term will also be neglected as it is difficult to determine from the properties of snow and no attempt was made to do so. The energy balance equation (5.2) thus reduces to:

$$R_n = H + \lambda E + G \tag{5.3}$$

Although G, the specific flux of heat conducted into the surface layer, over an extended period of years must be equal to zero if the surface layers are not to experience long-term increase or decrease in temperature, this is not true for shorter periods of time. In climates experiencing normal day-night cycles, it is often assumed that the net daily balance of soil heat flux is numerically equal to zero

although the fact that summer soils warm and winter soils cool indicates that this daily balance is not strictly true even in these cases. When compiling energy balances over periods shorter than a day (hourly say) G is a significant energy term and cannot be ignored. At Ny-Ålesund, continuous daylight as defined by the period of the midnight sun is experienced from 18 April to 24 August (Hisdal 1985) and then cumulative daily balances of G are significantly different to zero and the assumption that G can be ignored when testing for energy closure is invalid.

5.2 The Measurement of the Surface Energy balance

5.2.1 Radiation measurement considerations

Of the components in the full radiative energy balance, as given in equation 5.1, direct beam (S_d) and diffuse (S_{diff}) shortwave radiation were not measured separately in this study but as combined total incoming short-wave radiation (S_t) . The short- and long-wave radiation components reflected from the environment (S_e and L_e) are consequences of local shading and shiny surfaces and cannot contribute any "extra" incoming shortwave radiation to properly placed instruments. The measurement of incoming shortwave radiation was above the height of the vegetation and shielded from reflections. The reflection coefficient was also not measured directly but was quantified from the ratio of reflected shortwave ($S_{refl} = \alpha_b(S_d + S_{diff} + S_e)$) to total incoming shortwave radiation. The value of ε for tundra surfaces is variously given in text books as 0.9-0.99, 0.97-0.98 (Oke, 1987; Brutsaert, 1984). Addison and Bliss (1980) assumed the surface to be a black body and used a value of 1.0 for ε while Szilder *et al.* (1996) used ε = 0.9. More recently, Young and Woo, (1997) used ε = 0.97 taken from Kondratyev (1969) as being a value falling within the range for snow-free tundra surfaces as reported by (Oke, 1987; Saunders and Bailey, 1994). This latter value has been used in this study.

With these considerations, the full radiation balance (equation 5.1) reduces to:

$$R_n = S_d - S_{refl} + \varepsilon L_d - \sigma T_b^4 \qquad (5.4)$$

It is pertinent to ask, if net radiation is the important component for surface energy partitioning, why is it necessary to measure the individual components of the radiation balance using several instruments, each with their own measurement errors, when a single instrument is available for the measurement of net radiation? When net radiometers first appeared in the 1950's, they were hailed as a major breakthrough but recent work by Oliver and Wright (1990), Halldin and Lindroth (1992) and Kustas *et al.* (1998) amongst others, have pointed to deficiencies in design and operation which places some doubt on the absolute accuracy of these instruments in the field. Net radiometers are relatively cheap and provide the means to replicate over heterogeneous surfaces. They were used at this field site extensively. However, until the possible deficiencies are addressed and answered, it remains prudent to maintain a check upon the performance of net radiometers through the measurement of the other components as far as possible. The introduction in 1997 by Zipp and Zonen of an integrated radiation system (Model CNR1, Kipp and Zonen, Delft, the Netherlands), that combines four instruments, measuring the individual short- and long-wave components effectively at one place supports the contention that net radiometers are not as accurate as once thought.

5.3 Results

5.3.1 Radiation Balance

5.3.1.1 The snowmelt period

The individual terms in the radiation balance at the end of the snowmelt phase are compared in Figure 5–1. These measurements over a period of 24 hours on 10 June 1995 were recorded by the Automatic Weather Station (AWS) over a snow-free patch, and by a Bowen Ratio System over a snow covered patch 10 metres away. Even though the summer solstice is only 11 days away and the 24 hour daylight appears to have little deviation in its brightness, there is a marked daily variation in all the terms of the radiation balance shown here. The total incoming solar short-wave energy over the 24 hour period is 27.08 MJ m^{-2}.

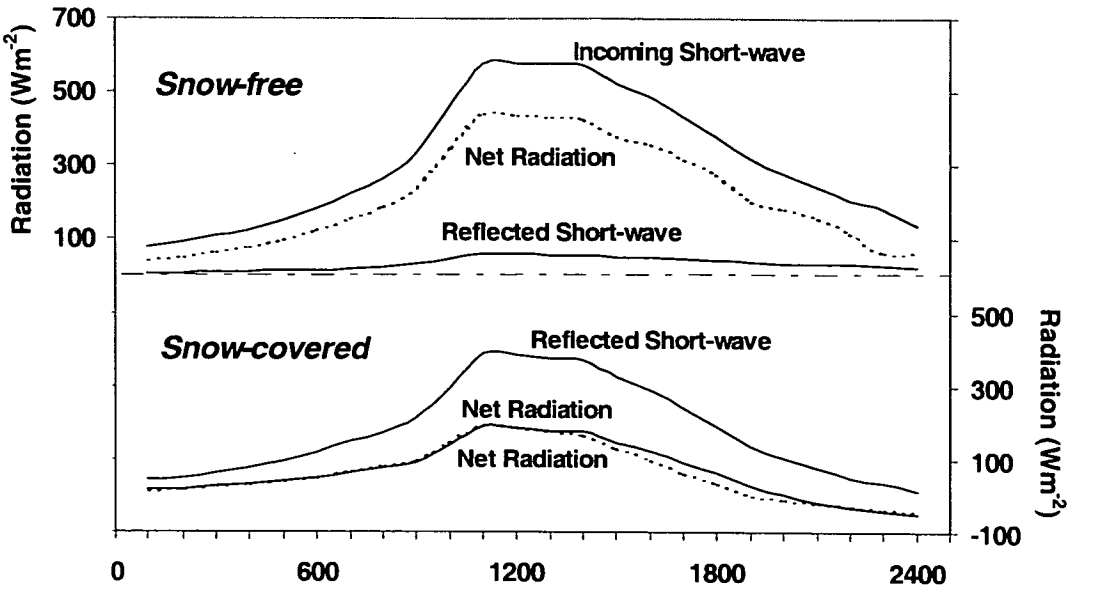

Figure 5-1 *Radiation balance terms for snow-free and snow covered surfaces during the 24 hour period of 10 June 1995.Two independent net radiation measurements over the snow-covered surface are shown.*

Over the snow-free patch, 11 per cent (2.98 MJ m^{-2}) of this is reflected back into the atmosphere and net radiation is 70 per cent (18.98 MJ m^{-2}) of the total incoming solar shortwave radiation. By contrast, the snow-covered patch is reflecting 56.6 per cent (15.32 MJ m^{-2}) of the incoming solar short-wave radiation. Net radiation (5.54 MJ m^{-2}) is only 20.5 per cent of incoming solar radiation. The snow-patch net radiation is also characterised by becoming negative during the "night-time" hours.

5.3.1.2 The effect of rainfall on the energy balance

The contrast between the surface radiation terms at the end of a rain-free period and measurements from the same instruments on the AWS the day after rain is shown in Figure 5–2.

A typical light drizzle rainfall occurred during the morning of the 10 August which was recorded by the AWS as 0.5 mm. Because the raingauge uses a tipping bucket, this event may have been more than 0.5 mm but less than 1 mm. Because of the different weather conditions before and after the rain (total incoming short-wave was 12.73 MJ m^{-2} on 9 August and 4.94 MJ m^{-2} on 11 August), the results have been

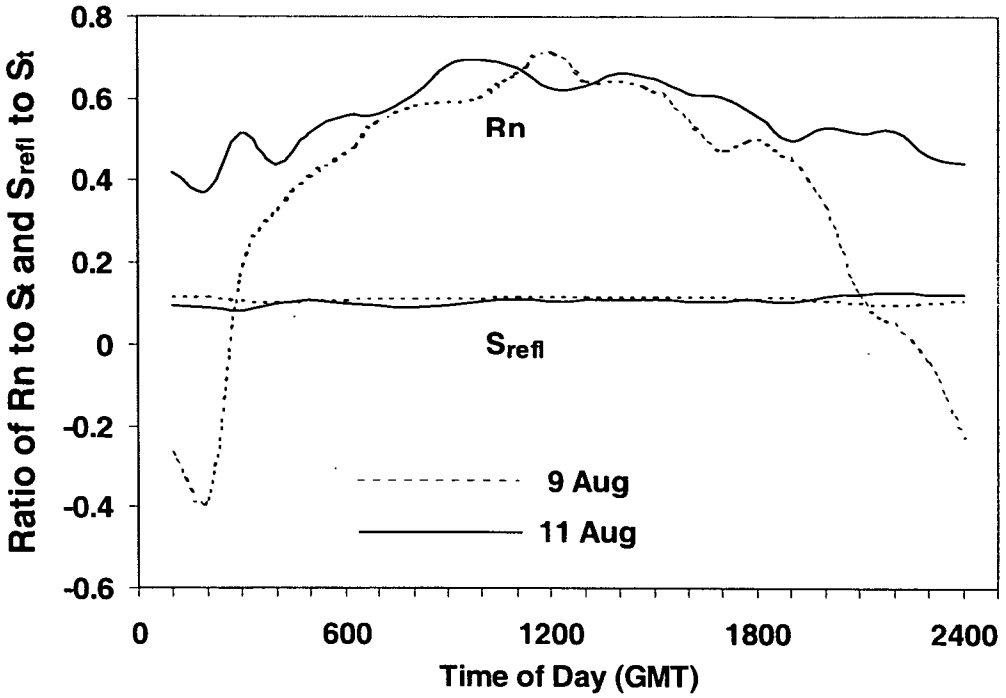

Figure 5-2 *Ratio's of Net radiation (R_n) and Reflected Shortwave (S_{refl})to incoming solar for a day prior to (9 Aug) and a day after (11 Aug) a rain event in 1995.*

normalised by the incoming total short-wave radiation (S_t). Reflected solar short-wave (S_{refl}) is very similar both before (9 August) and after (11 August). On the 9 August, reflected short-wave was 1.48 MJ m^{-2}, having an albedo of 11.6 per cent while on the 11 August, the albedo had dropped slightly to 10.8 per cent. Net radiation was also similar in relative terms, being 57.2 per cent of incoming total solar (7.28 MJ m^{-2}) on 9 August and 60.24 per cent of incoming total solar (2.98 MJ m^{-2}) on 11 August. However, the daily patterns are very dissimilar. While the post-rain net radiation on the 11 August has a flat daily response, the pre-rain net radiation values exhibit a marked daily trend with negative values during the "night-time". However, the values of both incoming total shortwave and net radiation are small.

5.3.1.3 Seasonal Patterns of solar and reflected radiation and albedo

Figure 5–3 and Figure 5–4 show the daily incoming shortwave radiation energy (Solar) incident on a horizontal surface and the cumulative seasonal shortwave energy for the two years 1995 and 1996 expressed as MJ $m^{-2}d^{-1}$ or MJ m^{-2} respectively.

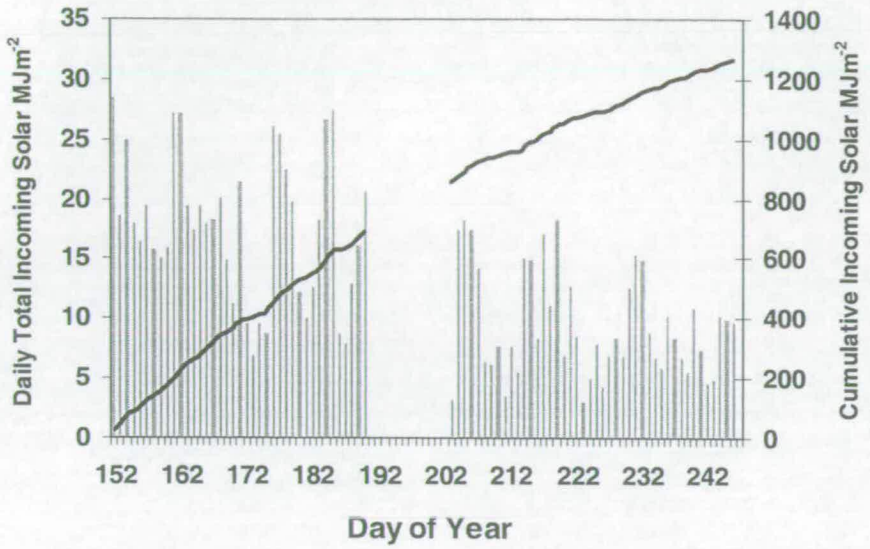

Figure 5-3 *Daily incoming solar radiation (columns) and cumulative solar radiation (line) for the year 1995.*

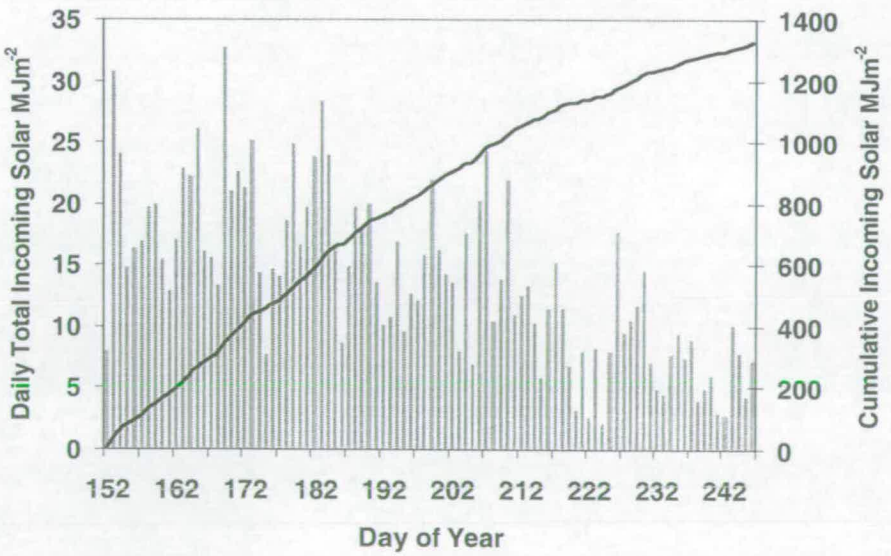

Figure 5-4 *Daily incoming solar radiation (columns) and cumulative solar radiation (line) for the year 1996.*

In 1995, data was lost between days 190 and 203. To compare the insolation in the two years, the cumulative energy for this period in 1995 has been interpolated by calculating a 10-day average value for daily solar energy before and after the data gap and scaling the missing days on a sliding scale between these two values. Both figures show the expected decline in daily energy input from midsummer on (day 172 (1995); day 173 (1996)) with 1995 having slightly higher daily insolation towards the end of the summer.

However, there is very little difference between the total incoming energy over the same periods in 1995 and 1996 (1269 and 1323 MJm^{-2} respectively). The average 24 hour solar influx to the surface during May-September in 1995 was 13.8 MJm^{-2}. It is worth noting that this is higher than the mean 24hr solar influx of 12.45 MJm^{-2} during May-Oct at Kew Observatory (51.5^0N) for the years 1956-1960 as reported by Monteith and Unsworth (1990).

The amount of shortwave energy that penetrates and warms the vegetation and the soil is controlled by the reflection coefficient or albedo of the composite surface. Figures 5–5 and 5–6 show the hourly values of albedo during the periods 27 May - 3 September 1995 and 31 May - 9 September 1996.

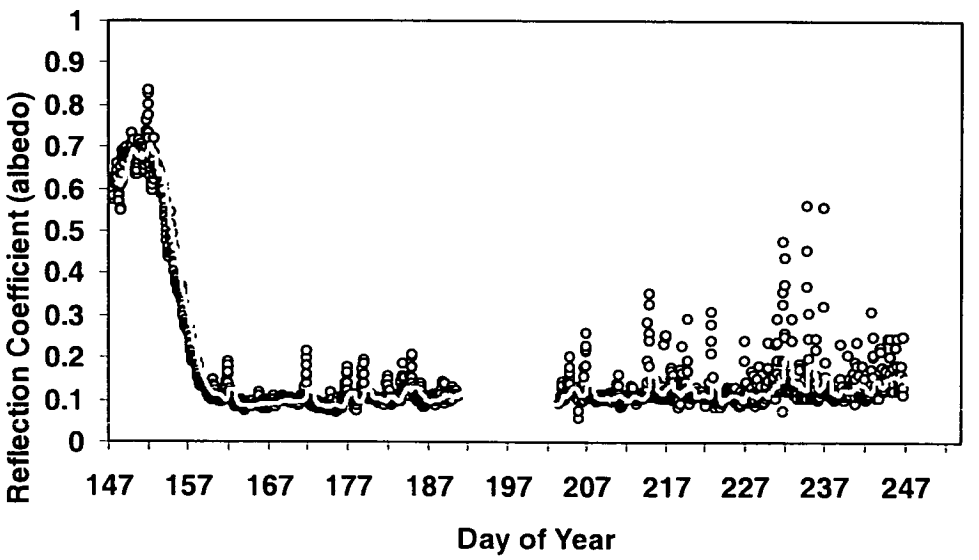

Figure 5-5 *Hourly values of albedo (o) between 27 May and 3 September 1995. A 24 hour moving average value of albedo (white line) is superimposed*

A trendline composed of a 24 point (i.e. 24 hour) moving average is also shown. Hourly data has been restricted to values of incoming solar greater than 5 Wm^{-2} to minimise the occurrence of high values of albedo due to instrumental measurement uncertainty at these low light levels.

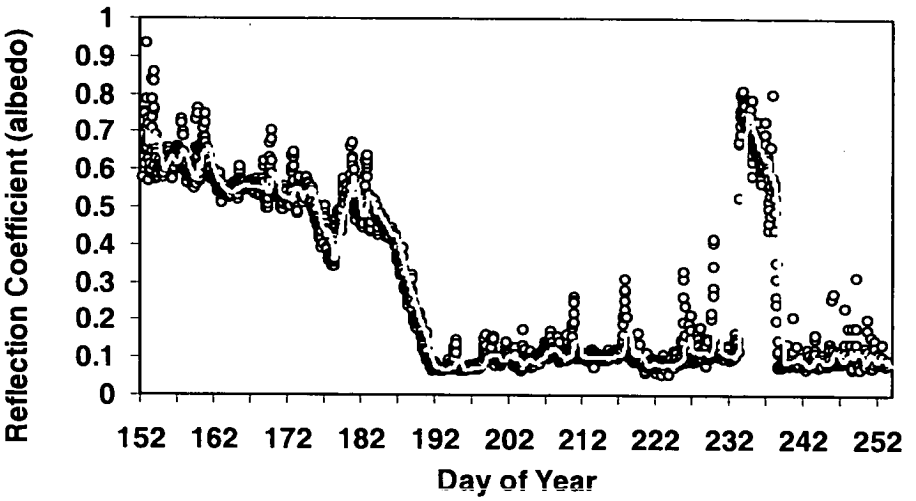

Figure 5-6 *Hourly values of albedo for the period 31 May – 9 September 1996. The 24 hour moving average trendline is shown in white*

However, high values of albedo do still occur, especially later in the season, and are likely to be caused by direct beam incursion into the reflected solarimeter at low sun elevations. An example of this is shown in Figure 5–7 The sinusoidal shape to the incoming solar radiation values indicates a largely cloud free day on 19 August. The period between 1800-1900 hrs appears to have cloud obscuring the solar disk as incoming solar radiation falls away sharply as does the albedo. Between 1900 and 2100 hrs, solar radiation increases again indicating a clearer solar beam. However, by this time the solar angle

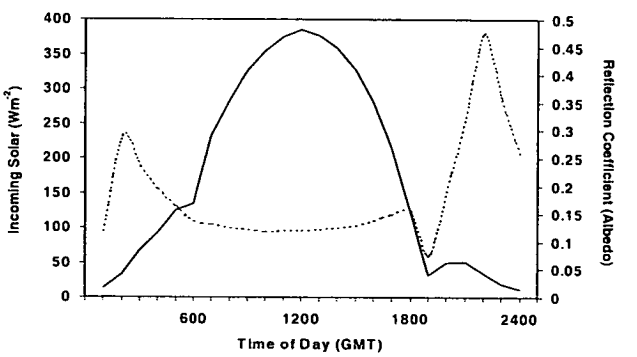

Figure 5-7 *Incoming solar radiation (——) and albedo (------) for 19 August 1995.*

is so low (6 deg at 2100 hrs) that direct radiation and specular radiation could be contaminating the reflected solarimeter and thus raising the apparent albedo. This phenomenon is also apparent to a lesser extent during the early hours of the same day. Figure 5–7 also shows the daily change in albedo with a minimum value around local solar noon when reflections from the soil and vegetation surfaces are also at a minimum.

The rapid but smooth transition from snow-covered albedo to snow-free albedo shown in Figures 5–5 and 5–6 is explained by three phenomena. Firstly, old and melting snow has a lower albedo than does fresh snow, typically in the range 0.4 (old snow) to 0.95 (fresh snow) (Oke, 1987). Secondly, as the snow surface becomes patchy, steadily increasing amounts of reflected radiation from these patches will impinge on the inverted thermopile, even though the patches may not be directly below the solarimeter as explained in the section on static radiation measurements in Chapter 4. Thirdly, soil particles and vegetation debris from the snow-free patches are transported by the wind onto the snow surface, not only lowering its albedo but also accelerating the snow-melt process.

The albedo of a surface is often sensitive to rainfall. Moisture usually tends to darken the soil and vegetation, the latter mostly by the washing of lighter coloured dust from the vegetation surface. Figure 5–8 shows the change in albedo for an extended period during 1996 prior to the snow event shown in Figure 5–6. During the initial 14 day period (day 205-219), there has been no recorded precipitation but the albedo has maintained a constant value, evaluated by linear regression, of 0.104. This period also has two occurences of contamination of reflected solar radiation by

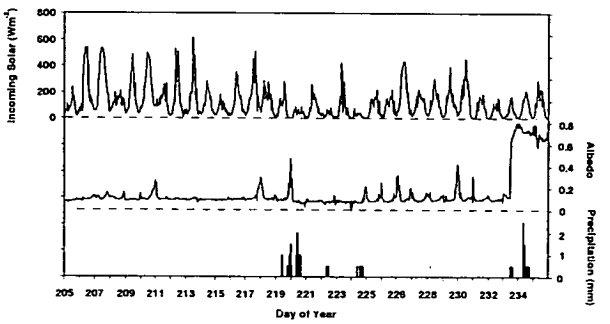

Figure 5-8 *Incoming solar radiation (top trace), albedo (middle trace) and precipitation (lower trace for the period 24 July – 23 August 1996.*

direct beam incursion. There was 23.5mm of rainfall during the period day 219-224, during which time the albedo reduced to 0.092. The average albedo after day 224 is difficult to determine because of the increasing occurrence of contamination of the reflected solar measurements.

However, it is apparent that in general rainfall is not a significant factor in the albedo variation at this site. Oke (1978) quotes albedo figures of 0.05-0.4 for dark,wet to light dry soils, and 0.18-0.25 for agricultural crops/tundra. Addison (1977) and Courtin and Labine (1977) measured summer albedo's at the Truelove high arctic site on Devon Island. Addison measured albedo's of 0.14 and 0.11 for a dry gravel surface and a wet, meadow site respectively while Courtin and Labine observed progressive drops in albedo to 0.08 and 0.07 at the same sites due to changes brought about by moisture changes. Courtin and Labine also quote Weller and Cubley (1972) who found that the albedo of a wet meadow increased from 0.15 to 0.20 when the site dried out.

5.3.1.4 Seasonal patterns of net radiation

Net radiation is the energy available for partitioning into evaporation and the heating of the air, vegetation and soil. In 1995, the Hydra, with a Q*5 net radiometer, was at the flux site for the entire period June 1 to 3 September. In 1996, the Hydra was not deployed at the site until 18 July. Net radiation values until then came from the AWS net radiometer. Comparison between the Hydra and AWS net radiometers during the 1995 post snowmelt season showed that the AWS net radiometer was 14 per cent higher than the Hydra net radiometer. Again in 1996, when the Hydra and AWS net radiometers were compared, the difference was 14 per cent. The measurement of net radiation by different instrument types is known to vary by up to 20 per cent (Halldin and Lindroth, 1992). In their analysis, the Didcot net radiometer employed at the AWS had a larger absolute error and an even larger error with low solar altitude than the REBS net radiometers when they were both compared to composite net radiation formed from the individual radiation components from reference standard instruments The vegetated surface beneath the AWS was populated with more moss species and less lichen than at the flux measurement site. The difference in albedo

and water content from these different surfaces may also have contributed to some or all of the 14 per cent difference. Net radiometer measurements at the flux site, by their position, were more representative of the energy available for partition into sensible and latent heat than the net radiation measurements at the AWS site. This, together with the implied higher accuracy of the REBS net radiometer, gave more confidence to the Hydra flux site net radiation measurements. The AWS net radiometer values for 1996 were therefore decreased by 14 per cent and then combined with the Hydra net radiometer data.

Figure 5–9 shows the daily and cumulative net radiation totals for both 1995 and 1996. It is apparent that 1995 had higher levels of Rn than 1996 during the early

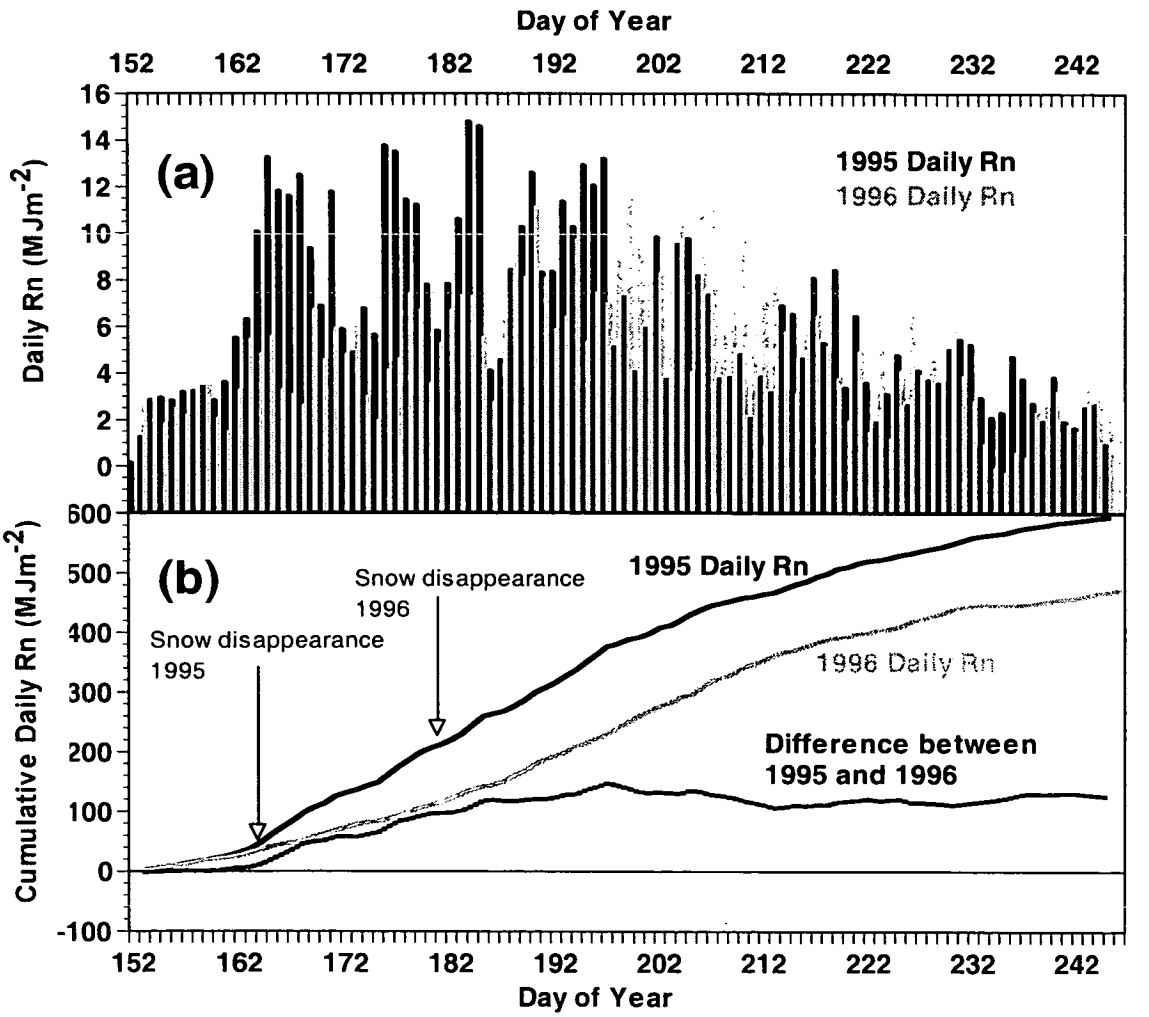

Figure 5-9 *(a)Daily net radiation totals for the period 1 June – 3 September in 1995 and 1996. (b) Cumulative daily net radiation for the same period in 1995 and 1996 and the cumulative total net radiation difference between the two years.*

season but lower from day 195 to 215 after which the totals were similar again. The cumulative totals show that the two years totals diverged, until the effect of snow had disappeared, and then the two seasons overall were very similar – as judged by the difference between the cumulative totals. The general characteristics of the two seasons are summarised in Table 5–1.

1995	Units	1995	1996
Maximum daily net radiation	MJ $m^{-2} d^{-1}$	14.79	11.93
Date of maximum net radiation		4 July	25 July
Total season net radiation budget	MJ m^{-2}	594	469
1996 as percentage of 1995			79

Table 5-1 *Summary of seasonal differences in net radiation*

5.3.2 Soil Heat Flux

Soil heat flux (SHF) was measured as part of a Bowen ratio system at the measurement site. Results from this system were disappointing, especially with regard to the SHF plate measurements and estimation of heat storage in the soil layer above the plates. Storage was estimated from a two-thermistor profile of soil temperatures above the SHF plate. The erratic nature, and estimates of soil heat flux that were evidently too large, placed little confidence in the measurements being useful in completing the energy closure. Soil profile temperatures were also measured and provide the estimate of soil surface temperature used in the carbon dioxide modelling in Chapter 6. These soil temperatures could have been used to estimate soil heat flux through application of Fourier's Law for soil given by:

$$q_h = -\mathrm{K}_z \frac{dT}{dz} \tag{5.5}$$

where q_h is the thermal flux, K_z is thermal conductivity, and dT/dz is the temperature gradient over a soil depth z. The surface measurement of the profile was in the organic section of the profile while the next temperature level down was in the

glacial clay. This would be problematic when assigning thermal conductivities and diffusivities to the soil layer between the two measurements and the thermal gradient between the two measurements could not be assumed to be linear. Using the next two measurements down the profile would have solved the thermal gradient problems and a soil heat flux value between these two measurements would have been possible. But a storage value for the overlying clay and organic soil would then have been difficult. The prospect of dubious soil heat flux values from a single position set of temperature profile measurements providing the means to assess energy closure would have clouded the issue. The error in assessing soil heat flux from this method was adjudged to be far higher than the errors in the other terms of the energy balance equation, energy closure was not investigated and soil heat flux was estimated as the residual of R_n-H-LE.

5.3.3 Surface Energy Partition

Net radiation provides the energy for evaporation, and warming of the air, vegetation and soil. The energy available for evaporation of soil and vegetation moisture and the sensible heating of surface air layers is the residual after heating of the soil has taken place. The partitioning of net radiation into evaporation (λE), sensible heat (H), and soil heat flux (G) is shown in equation 5.3 but restated here in terms of the available energy for λE and H production.

$$R_n - G = \lambda E + H \tag{5.6}$$

The investigation of the partitioning of available energy into latent and sensible heat amounts targets four pivotal periods within the active season in 1995: (i) Snowmelt, (ii) Post snowmelt, (iii) mid summer and (iv) late summer/early autumn. The last three periods will be revisited in relation to carbon fluxes in both this chapter and the next.

5.3.3.1 Snowmelt (5 June –11 June 1995)

Figure 5–10 shows the measurements of net radiation, evaporation and sensible heat fluxes from the Hydra system between 5 – 11 June 1995. It is apparent from Figure 5–10 that the majority of the available energy in the early part of this period is being used to melt the snow pack.

Approximately 4 MJ m^{-2} day^{-1} (enough to melt 12 mm water equivalent of snow per day) of net radiation is being used for this purpose. Evaporation from the snowpack surface is taking place but at a low level. These two processes are also occasionally extracting heat from the passing surface layer of air (e.g. sensible heat on day 160 is negative). By the 9th June (day 160), the snowpack was 120 mm deep (Harding and Lloyd, 1998) and patches were beginning to form. The evaporation from the snowpack increases and there is some heating of the air from the exposed vegetation patches. Although the rate of snowmelt is the same (Harding and Lloyd, 1998), the reduced snowdepth now requires less energy to maintain such a rate. The anomalous behaviour overnight between 10 and 11 June where net radiation dropped below zero is difficult to explain although the same phenomenon was measured by two net radiometers on a Bowen ratio system close by.

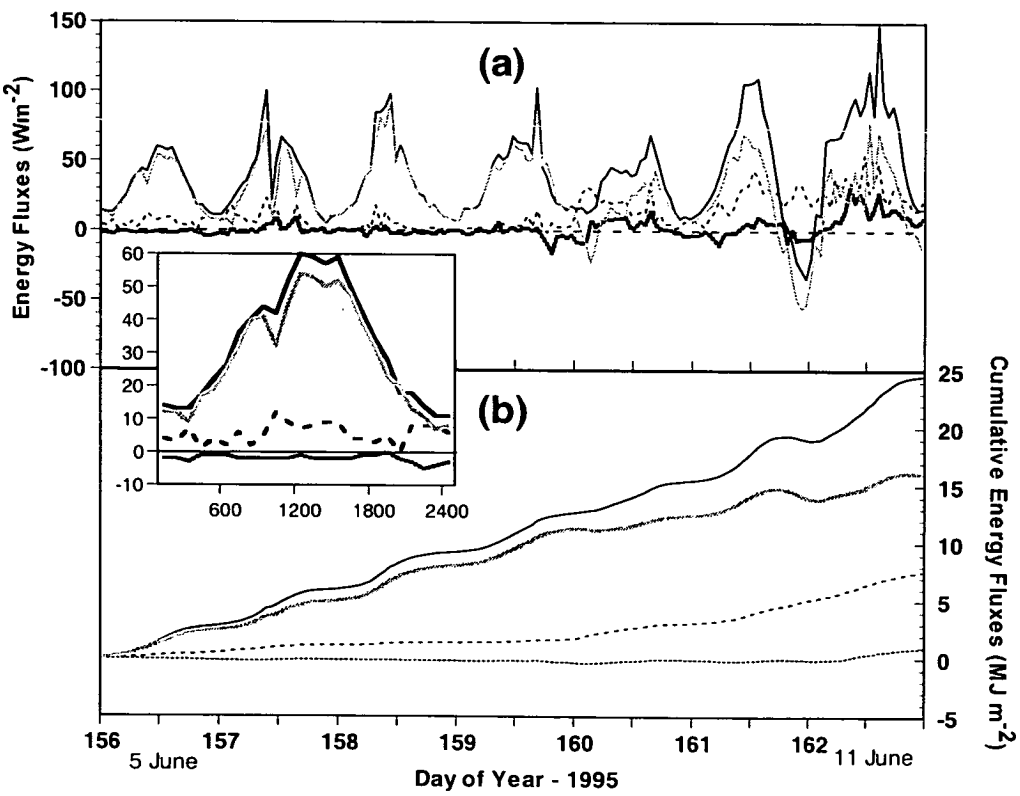

Figure 5-10 *(a) hourly values of Rn (black line), LE (dashed line), H (dotted line) and Rn-LE-H(residual into snowpack) (grey line). (b) cumulative R_n, LE, H, R_n-LE-H (same line types) for the period 5-11 June 1995. The insert graph is of 5 June to show typical daily behaviour.*

5.3.3.2 Post snowmelt (27-30 June 1995)

Figure 5–11 shows (a) the energy fluxes and (b) the cumulative energy fluxes over a period when the snow had finally disappeared. The period was marked by very cold and windy weather on 28 June (day179) followed by intermittent light snow showers during the afternoon of 29 June and again during the early hours of 30 June (day 181). Air temperatures dropped rapidly from 5°C to 1°C during the afternoon of 28 June and stayed at that temperature for the rest of the period. The snow showers explain the erratic nature of the evaporation values on 29 and 30 June as snow flakes settling on the lens of the hygrometer would send the instrument out of range. The cumulative energy fluxes in Figure 5–11(b) include the corrected latent heat flux values in Figure 5–11(a) obtained by replacing with linear interpolations formed from adjacent values.

During this period, latent and sensible heat fluxes are similar in size with the residual *soil heat flux* value now just less than the atmospheric fluxes.

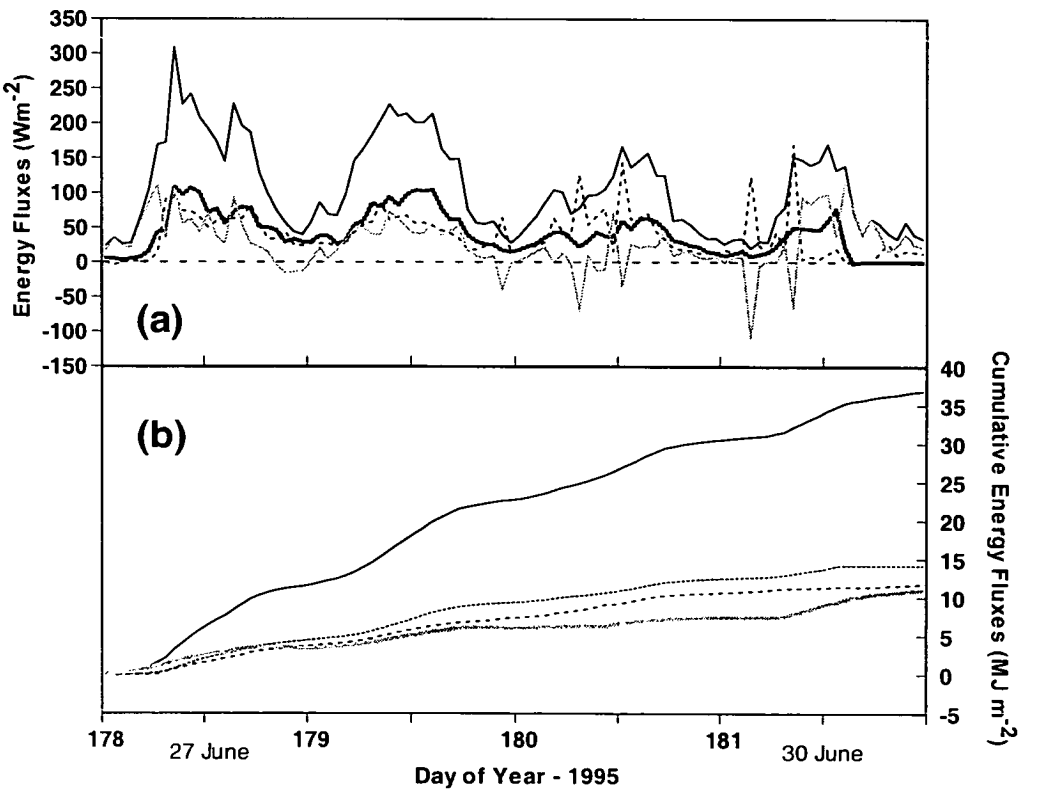

Figure 5-11 *(a)hourly values of Rn (black line), LE (dashed line), H (dotted line) and Rn-LE-H(residual into snowpack) (grey line). (b) cumulative Rn, LE, H, Rn-LE-H (same line types) for the period 27-30 June 1995.*

5.3.3.3 Summer period (30 July – 11 August 1995)

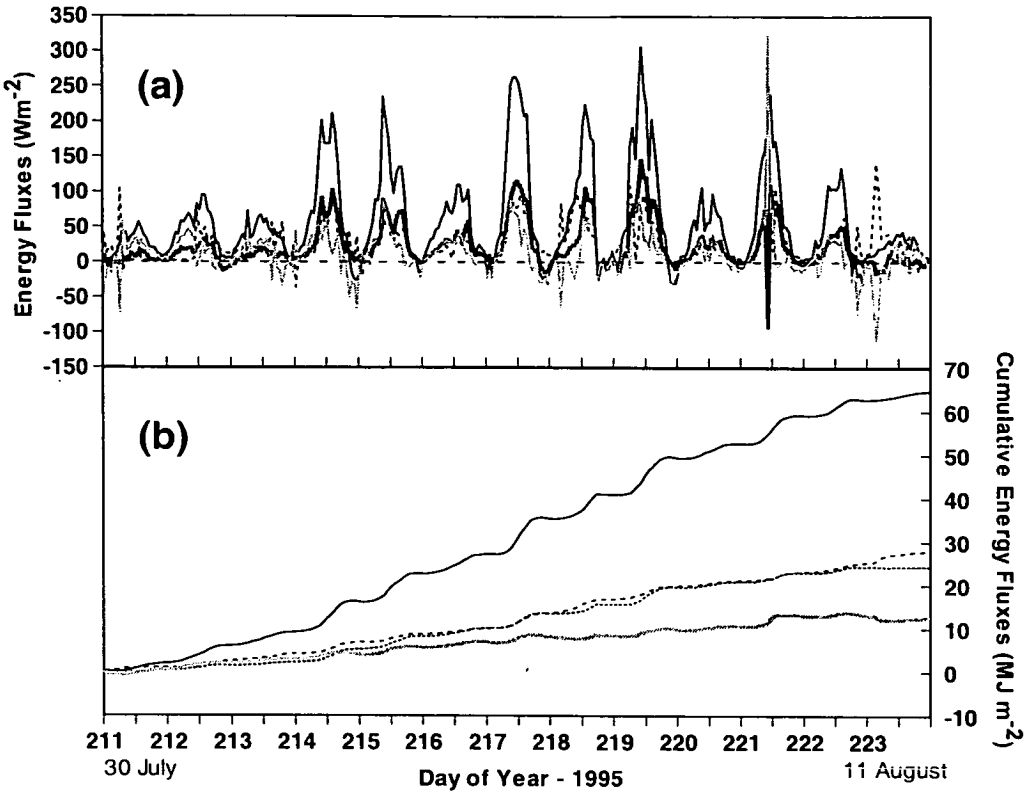

Figure 5-12 *(a) hourly values of Rn (black line), LE (dashed line), H (dotted line) and Rn-LE-H (residual into snowpack) (grey line). (b) cumulative Rn, LE, H, Rn-LE-H (same line types) for the period 30 July-11 August 1995.*

Figure 5–12 shows the energy fluxes during a thirteen day period in mid-season. Net radiation towards the end of this period shows negative values during the night for the first time during the summer as the sun's elevation becomes lower. At this time, the active layer depth in the soil would be approaching its maximum depth. In 1997, measurements

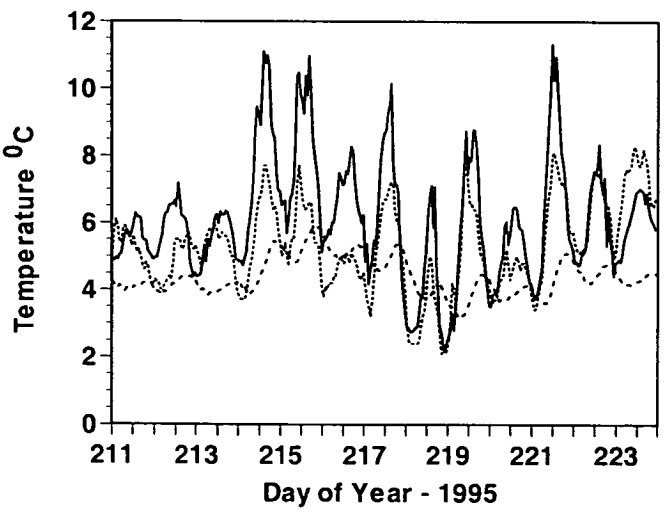

Figure 5-13 *Air temperature at 2.7m (Hydra thermocouple) (——) and soil temperatures at 25mm (.....) and 250mm (------) depths between 30 July and 13 August 1995.*

taken by Sand and Bruland (1999) at this site, indicated that between 14 June and 17 July, the soil active layer depth increased nearly linearly from zero (frozen surface) to 0.9m. Between 17 July and 18 August, the active layer would probably have deepened another 0.1m to 1m before a period of no change until 7 September when the permafrost front began to return to the surface (Sand and Bruland, 1999). Such a process can be seen in the cumulative traces (Figure 5–12(b)). While sensible and latent heat are still equal in size and positive, the residual term has become negative indicating that heat is now coming out of the soil. Such a conclusion is supported by soil surface temperatures now being always higher than air temperature (see Figure 5–13).

5.3.3.4 Early Autumn (29 August – 2 September 1995)

Figure 5–14 shows the energy balance for the early autumn phase. Net radiation is now regularly negative during the night. Evaporation is larger than sensible heat

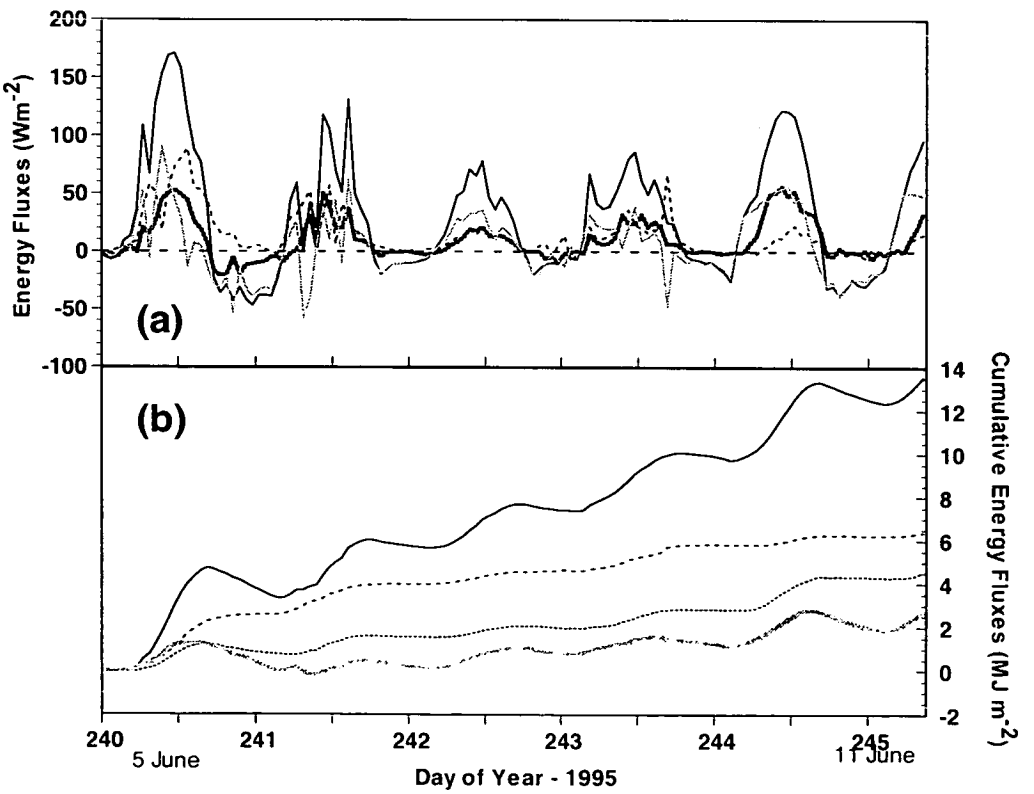

Figure 5-14 *(a) hourly values of Rn (black line), LE (dashed line), H (dotted line) and Rn-LE-H (residual into snowpack) (grey line). (b) cumulative Rn, LE, H, Rn-LE-H (same line types) for the period 29 August-3 September 1995*

which once again, as over the snow-covered surface at the start of the active season, goes negative at night as the ground is now colder than the air. From the residual of *Rn-H-LE*, it would appear as if heat into the soil was still occurring – again as a consequence of heat being taken out of the overlying air. This is probably a transient effect that will shortly stop as the radiation levels and and air temperatures decrease, speeding up the rate at which the permafrost front will return towards the surface.

The apparent flux of heat into the soil in the early autumn shown above and deduced from the residual of (Rn-H-LE) is at variance with the pattern of soil temperature during this time which both decreases overall, and decreases faster at the surface, during the same period (see Figure 3-15). This would certainly be difficult to explain in soils other than those affected by permafrost, where changes of state have to be taken into account. During the spring and summer, it is quite possible for soil heat flux to be positive into the soil with little change in soil temperature being observed as the energy is being used to melt permafrost – a process that consumes energy to convert from ice to water with no change in temperature. In the autumn, when the permafrost horizon is beginning to return towards the surface, this process is reversed. Then, converting water to ice releases heat that will both warm the adjacent soil layer and slow the rise of the permafrost front. However, the most likely cause is the cumulative effect of errors in the measurement of the net radiation at these very low solar elevations and the energy fluxes which will be collectively applied to the residual value designated as apparent soil heat flux.

5.3.4 Active season Energy Budgets for 1995 and 1996

The active season energy budgets for 1995 and 1996 as measured by the Hydra eddy correlation system are shown in Table 5–2. The 1996 season had half as many days for growth as 1995 and lower mean radiation levels per day. But the season started in mid July in 1996 when the sun was past its maximum elevation so the lower average daily levels may not indicate cloudier conditions. In 1995 evaporation exceeded rainfall by a factor of two – in contrast 1996 evaporation was less than the rainfall. This is reflected in the evaporative ratio figures with the wetter surface and vegetation in 1996 returning a higher ratio. Nevertheless the evaporative ratio in

1995 did not drop below 0.5, even during extended dry periods, indicating that the soil water storage is sufficient to maintain transpiration.

	Units	1995	1996
Number of post snowmelt days		81	44
Net radiation total (mean daily rate)	MJ m^{-2}	560.2 (6.92)	219.5 (4.99)
Evaporation total (mean daily rate)	MJ m^{-2}	228.6 (2.82)	122.5 (2.79)
Sensible Heat total (mean daily rate)	MJ m^{-2}	194.1 (2.40)	60.3 (1.37)
Rainfall	mm	43	53
Energy required to evaporate rainfall total	MJ m^{-2}	107	131.5
Evaporation as % of Net radiation		40	55
Sensible Heat as % of Net radiation		35	27
Residual (Rn-H-LE) as % of Rn		25	18
Median Evaporative ratio		0.53	0.63

Table 5-2 *The Energy budget for the snow-free active periods in 1995 (12 June – 31 August) and 1996 (17 July – 31 August).*

The progression of the evaporative ratio in 1995 and 1996 is shown in Figure 5–15. The median evaporative ratio of about 0.5 is a characteristic value which only rose to

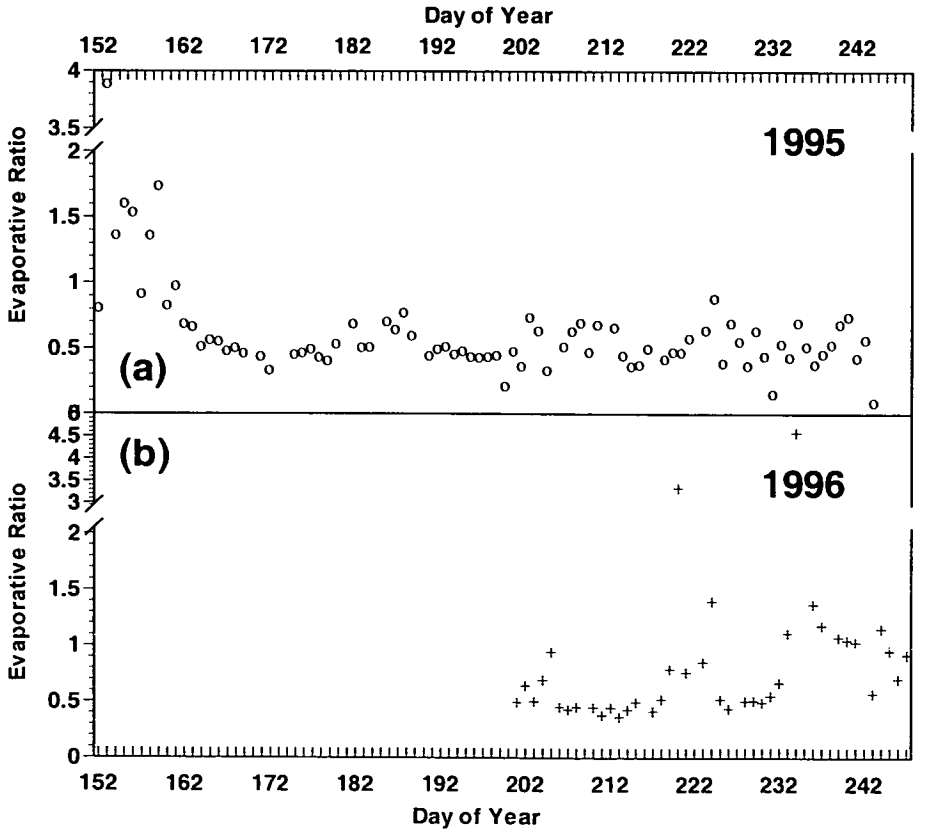

Figure 5-15 *Evaporative ratios (LE/(H+LE) during the snow free active periods in (a) 1995 and (b) 1996).*

nearly 1 during and following rain events when evaporation from bare soil and increased evaporation from wet mosses and lichens increased. The constancy of the evaporative ratio during the dry periods is probably a result of the fairly uniform temperature and humidity climate at this site. In 1996, evaporative ratios were over 1 during the isolated snow showers when sensible heat values became negative. A number of other studies have shown that the evaporative ratio in tundra areas is approximately 0.5 (e.g. Rott and Obleitner, 1992; Ohmura, 1982; Fitzjarrald and Moore, 1992) and this study appears to agree with that finding.

5.3.5 Surface Resistance to the transfer of water vapour

Although surface resistance could be regarded as a micrometeorological characteristic of a vegetated site, its evaluation in this thesis has been left until after the discussion of sensible and latent heat fluxes.

Transpiration from most vegetated surfaces is controlled by leaf stomata. In the high arctic, vegetation tends to be dominated by mosses and lichens, neither of which have stomates. However, the composite surface of mosses, lichens and dwarf vascular plants still has a resistance to the transfer of water vapour from the surface to the atmosphere which may be termed the surface resistance, r_s (s m^{-1}). Over the arctic surface, this surface resistance consists of the stomatal resistances of the vascular plant leaves in parallel with the diffusion resistances of the moss and lichen leaf surfaces and the diffusion of moisture from the bare soil surface. Figure 5-16 contrasts the

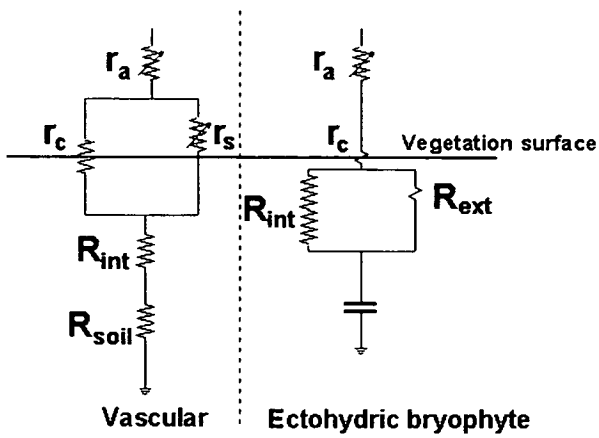

Figure 5-16 *The resistance network for water transport in vascular and ectohydric bryophytes.* R_{soil}, R_{int} *and* R_{ext} *are soil, internal and external hydraulic resistances respectively.* r_a, r_c, *and* r_s *are gaseous diffusion resistances respectively. The capacitor symbol implies an effective blockage to water from the soil for the bryophyte Redrawn from Proctor(1982).*

different resistance pathway for water trasnport in vascular and ectohydric bryophytes (those which gain and lose water over most of their surface but have no internal water transport system). The aerodynamic and surface resistances are the only variable resistances in this network that are affected by daily climate changes.

Over such a surface, it is difficult to define a surface resistance because of the difficulty is separating the boundary layer component from the vegetation component. Nevertheless, an estimate of a surface resistance for water vapour is important both for a complete description of the arctic surface and as a state parameter for modelling the evaporation from any vegetated surface . For a full or partly vegetated surface, an Ohm's Law analogue of surface resistance is given by (Garratt, 1994) as:

$$r_s = \frac{\rho\lambda\left\{q_s\left(T_l^{eff}\right) - q\right\}}{\lambda E} - r_a \qquad (5.7)$$

where $q_s(T_l^{eff})$ is the saturated specific humidity at the effective temperature of the vegetation-soil layer (which will be a temperature intermediate between that of the vegetation and the soil) and q is the specific humidity at a reference height. A problem with this approach for estimating an areal surface resistance is the measurement or estimation of the effective surface temperature especially over a surface that is very heterogeneous.

Alternatively, the difficulty of surface temperature can be avoided by obtaining the surface resistance through solving the Penman-Monteith equation (Monteith, 1965) for r_s using eddy correlation measurements of sensible and latent heat flux in place of the usual available energy term viz:

$$r_s = \frac{\Delta H r_a + \rho C_p\left(e_s(T) - e\right)}{\gamma\lambda E} - r_a \qquad (5.8)$$

where Δ is the gradient of the curve relating saturation vapour pressure to temperature, H is the sensible heat flux, $e_s(T)$ is the saturated vapour pressure (kPa)

at temperature T (°C) and e is the measured vapour pressure (kPa). In this thesis, the approximation for the saturated vapour pressure curve is the form of Tetens (1930), rearranged by Murray (1967) and used by Shuttleworth (1992) which is given by:

$$e_s(T) = 0.61078 \exp\left\{\frac{17.2694T}{237.3+T}\right\} \quad kPa \qquad (5.9)$$

The gradient of this expression, which approximates Δ is given by (Shuttleworth, 1992) as:

$$\Delta = \frac{4098 e_s}{(237.3+T)^2} \quad kPa\,{}^{o}C^{-1} \qquad (5.10)$$

Similarly, the latent heat of vapourisation λ is given by:

$$\lambda = 2.501 - 0.002361 T_a \quad MJ\,kg^{-1} \qquad (5.11)$$

and the psychrometric constant, γ is given by:

$$\gamma = \frac{C_p P}{0.622\lambda} \qquad (5.12)$$

where C_p is specific heat of air at constant pressure (J kg^{-1} K^{-1}) and P is atmospheric pressure (kPa).

The inversion of the Penman-Monteith equation provides a means of separating the ability of the surface to evaporate from the atmospheric demand. Figure 5–17 shows surface resistance values for the post snowmelt periods in 1995 and 1996. Data points were omitted from the analysis for hours with recorded rain together with the hour either side of the rainfall event. This filter increased the mean value by less than 2 per cent. In both 1995 and 1996, surface resistances greater than 500 s m^{-1} have been excluded (these accounted for less than 10 and 4 per cent of values in 1995 and 1996 respectively). The scatter in both sets of data is inevitable – the result of real variability and inevitable errors in the hourly flux measurements. Although the distribution of the values was skewed positive, the effect was not marked and a logarithmic transform did not improve the distribution. Median values of the measurements values gave a seasonal surface resistance mean (± S.E.) of 118 ± 3 s m^{-1} for 1995 and 58 ± 5 s m^{-1} for 1996. Although daily evaporation rates were similar in 1995 and 1996, sensible heat flux rates were nearly twice as high in 1995.

While aerodynamic resistances were higher in 1995, this difference in sensible heat values would produce surface resistance values in 1995 that are at least twice the size of those in 1996.

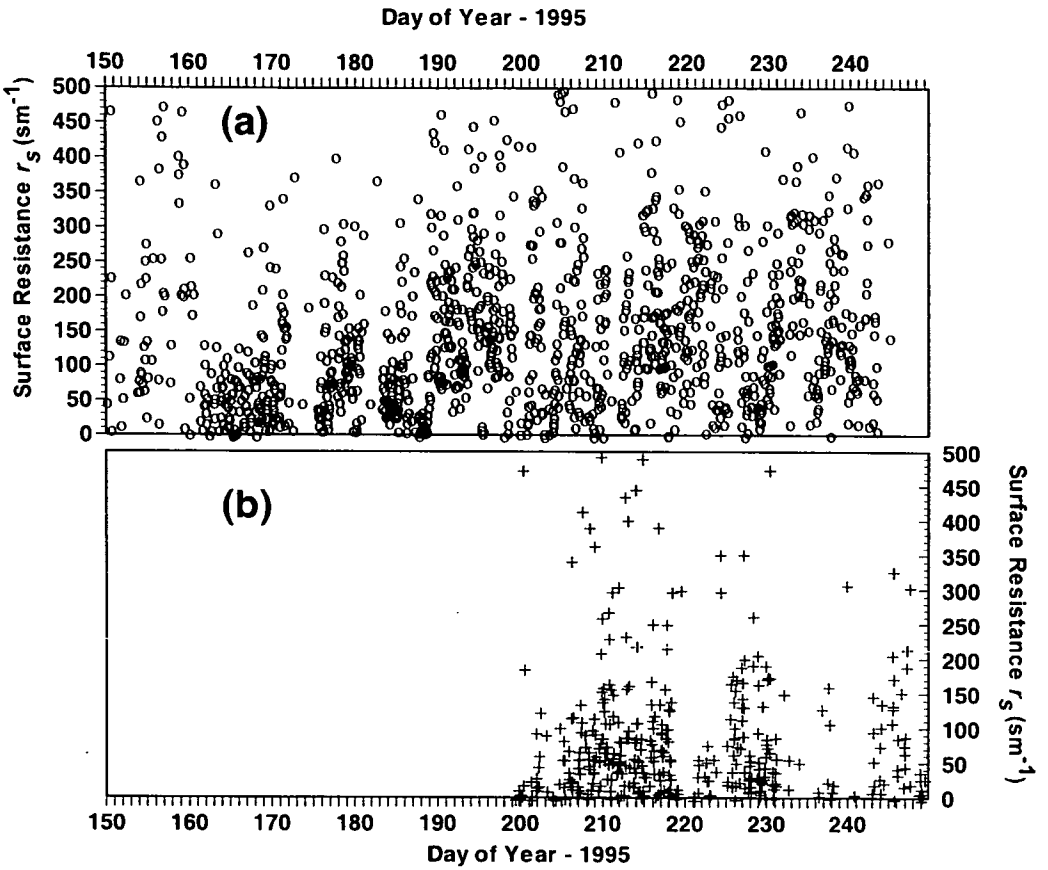

Figure 5-17 *Surface resistance values during the snowfree periods in (a) 1995 and (b) 1996. Values greater than 500 s m^{-1} have been excluded.*

The daily course of surface resistance is shown in Figure 5-18 for 1995. The data from Figure 5-17(a) has been square-root transformed to provide mean and standard error values. A curve in T^3 where T is the hour of the day was fitted to the data. Higher order terms did not substantially improve the fit. It can be seen that surface resistance is highest in the afternoon and lowest at night. In plants with stomates, this would imply some form of stomatal control limiting loss of moisture in the afternoon. Although possible, this is unlikely as the high soil moisture levels below the surface would not have been a limiting factor. A more likely explanation is the gradual drying out of the mosses, lichens and surface bare soil during the day from

relatively high moisture levels in the early morning through to recovery of moisture levels at night.

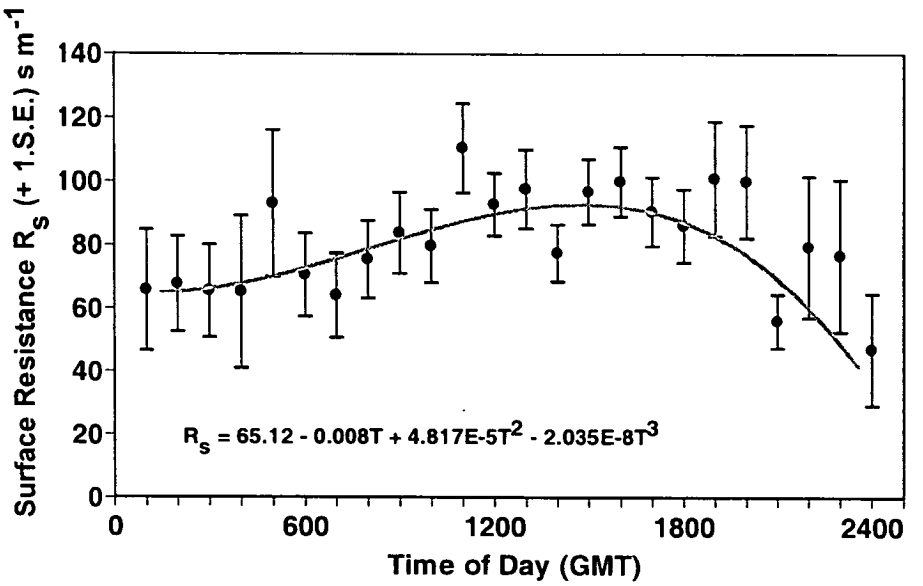

Figure 5-18 *The daily progression of surface resistance during 1995. The data points are mean ± 1 Standard Error and the fitted curve has been limited to a 3rd order polynomial fit to the data.*

5.3.6 Daily net carbon dioxide fluxes

The seasonal aspects of the net carbon dioxide flux from the site are more fully dealt with in Chapter 6 and there is no need to repeat them here. However, it is instructive to look at the daily course of net carbon dioxide balance during the four characteristic periods of the season chosen for energy balance investigation above. Figure 5–18 shows hourly average net carbon dioxide values for the (a) post snowmelt, (b) mid-season and (c) autumn periods. The micrometeorological convention is used throughout this study whereby assimilation is shown as negative (i.e. extracting carbon dioxide from the air) and respiration is positive. The traces are very noisy and show little of the ordered progression from overnight respiration to daytime assimilation seen in carbon dioxide measurements in temperate latitudes.

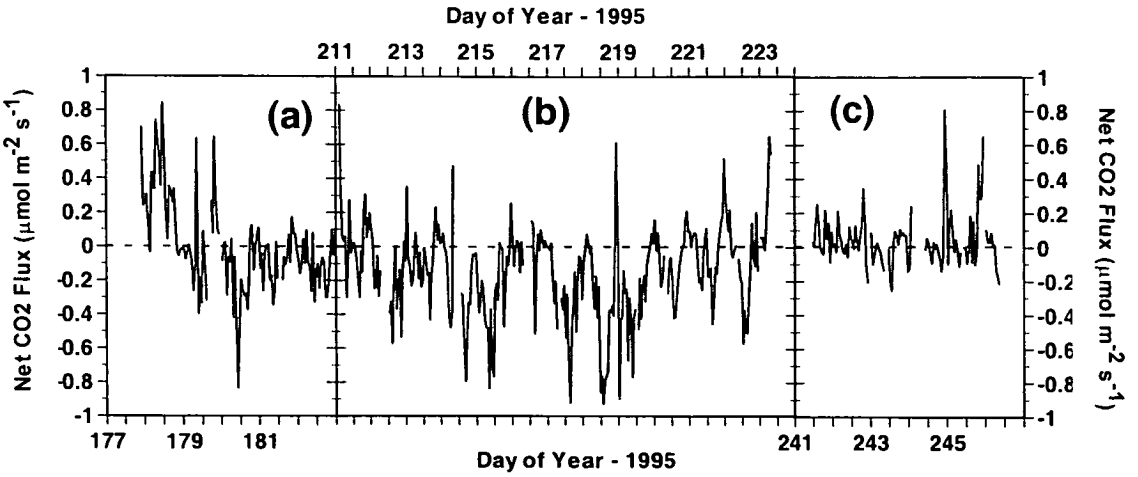

Figure 5-18 *Hourly average net carbon dioxide fluxes for the (a) post snowmelt, (b) mid-season and (c) autumn periods in 1995. The convention is that assimilation is shown as negative values.*

What can be seen is a change from general respiration dominated values to small assimilation in the post snowmelt period (a) to general assimilation dominated values in mid season (b) to a period where neither respiration or assimilation dominate in the autumn (c).In the autumn, the high respiration values on days 245 and 246 are the result of below freezing air temperatures (-1.5°C) which effectively switches off the photosynthesis of the plants while the soil is still above freezing (+3°C) allowing respiration to continue.

The variation of net carbon dioxide flux with time of day is shown in Figure 5–19. The post snowmelt period (a) has wide variation from hour to hour, probably explained by the heterogeneity of both unfreezing soil and plants emerging from dormancy. The mid season values do have a structure with assimilation dominating the CO_2 exchange process in the middle of the day and being equalled by soil and plant respiration during the night. During this period of the polar day, solar radiation had typical midday maximum values varying from below 100 W m^{-2} to over 500 W m^{-2}. Overnight values dropped to occasionally near zero but typically to 50 W m^{-2}. Soil temperatures at the top of the profile never dropped below 4°C and exceeded 13°C during one day. Soil respiration was therefore probably occurring throughout the day implying that assimilation must also have been occurring at night

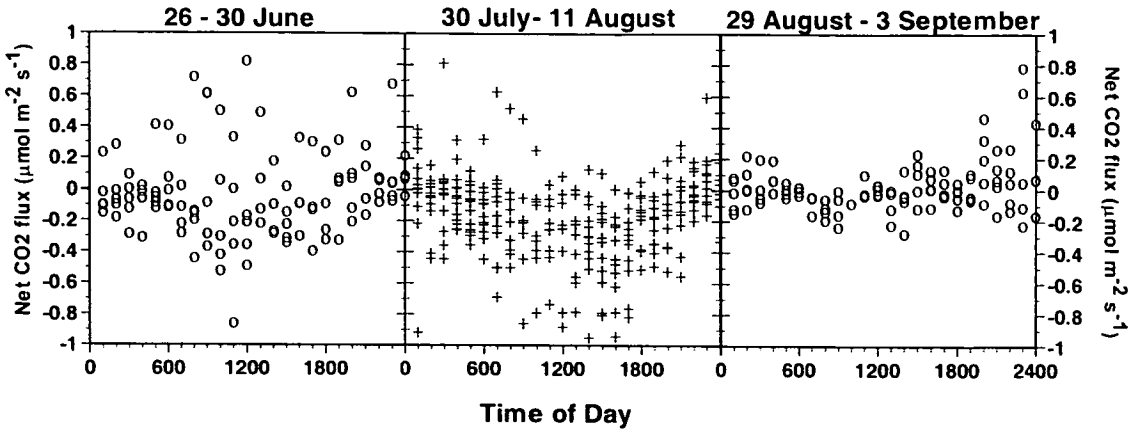

Figure 5-19 *Hourly average net CO_2 fluxes against time of day for (a) post snowmelt, (b) mid-season and (c) autumn periods during 1995.*

despite the low light levels. During the autumn period (c), the sun now dips below the horizon during the night and solar radiation never exceeds 300 W m^{-2} during the day, air temperatures are typically 1°C but can rise to 5°C, and soil surface temperatures drop below freezing during the last 2 days of the period. There is some assimilation occurring during the middle of the day, most probably from the moss and lichen community as the vascular plants have largely senesced by this time. Low light levels and soil that has been warmed during the day mean that soil respiration begins to dominate the exchange towards midnight. The large CO_2 values of 0.4, 0.7 and 0.8 µmol m^{-2} s^{-1} occurred on separate nights when air temperatures dropped below freezing effectively stopping plant photosynthesis.

Chapter 6
Modelling Surface fluxes of CO_2

6 Modelling Surface fluxes of CO_2

6.1 General Introduction

This chapter presents the first attempt to model the Net Ecosystem Productivity (NEP) of a high arctic polar semi-desert site. Measured carbon dioxide fluxes are used to create active season estimates of net carbon dioxide flux for the same active season time periods in 1995 and 1996. This is achieved by extending two established models (that describe the separate aspects of soil respiration and plant assimilation of carbon dioxide) to deal with the peculiar water relations of cryptogams. The plant assimilation model is routinely used within the Soil-Vegetation-Atmosphere Transfer (SVAT) Scheme that describes the land surface exchange within the UK Meteorological Office Hadley Centre GCM. The investigation therefore concentrated on a) assessing the performance of the current models in describing this high arctic site and b) providing a minimum set of necessary extensions to the model in order for the results to be used routinely within the current GCM configuration.

6.2 Previous model estimates of Arctic CO_2 balance

Oechel *et al.* (1993, 1997) show changes from carbon sink to carbon source at sites in Alaska but this and other studies have primarily been conducted in the low Arctic. This was pointed out by Soegaard and Nordstroem (1999) who hypothesised that this might not be typical of the high Arctic. Their measurements showed that their site at Zackenberg, Greenland (74^0 28'N, $20^0$34'W) was a carbon sink in 1996. However, they did point out that Shurpali *et al.* (1995) had found, at a peatland site in northern Minnesota, that a dry year producing a net carbon source was followed by a wet year producing a carbon sink. Soegaard and Nordstroem (1999), from their modelling exercise and recorded temperature changes over the past 30 years, predicted that their site had not yet changed from a net carbon sink to a net carbon source. At Eidembukta, 50 km to the south of Ny-Ålesund, Wüthrich *et al.*, (1998) also found 1996 to be a net source of carbon during 1996 and attributed this to the cold and cloudy summer in that year.

6.3 Theory and Methods

6.3.1 General Model considerations

The particular model of photosynthesis used in this paper is that developed by Cox *et al.* (1998, 1999) which is based upon the work of Collatz *et al.* (1991) for C_3 plants. Cox *et al.* (1998,1999) developed the model for inclusion in the Meteorological Office (UK) Surface Exchange Scheme (MOSES) which serves as the land surface scheme in the Hadley Centre Global Climate Model (GCM). The author chose not to use the full MOSES SVAT scheme because the current model is still undergoing development and testing of its freezing soil routines. However, in separating the NPP module from the overall MOSES model, the author has maintained the integrity of the MOSES model by using its defined state variables, model structure and C_3 parameter values.

6.3.1.1 Model Components

The carbon dioxide flux measured above a vegetated surface, often called the Net Ecosystem Productivity (NEP), is the balance between the uptake from the atmosphere of CO_2 by vegetation photosynthesis (W) minus the input of CO_2 into the atmosphere via plant respiration (R_d), and soil respiration (R_S) where soil respiration is the sum of heterotrophic microbial decomposition and root respiration viz.,

$$NEP = (W - R_d) - R_S \qquad (6.1)$$

The micrometeorological convention used in this thesis is that photosynthesis produces a negative CO_2 flux (extracting CO_2 from the atmosphere) and respiration a positive flux (adding CO_2 to the atmosphere).

Because the surface of the tundra site is characterised by a mixture of predominantly cryptogamic vegetation with isolated dwarf vascular plants and bare soil or stone patches, the model contains separate evaluations of bare soil/stony surface soil respiration, vascular net CO_2 uptake and its underlying soil respiration, and cryptogamic net CO_2 uptake and its underlying soil respiration.

6.3.1.1.1 Soil Respiration

Soil respiration is influenced by soil temperature and to a lesser extent by soil moisture. Soil moisture at this site was not regarded as limiting soil respiration rates thus enabling the soil respiration model of Lloyd and Taylor (1994) to be used. From a comprehensive survey of soil respiration results, they derived an empirical exponential equation relating soil respiration to soil temperature, which was an unbiased estimator over a wide range of temperatures, given by:

$$R_S = R_{10} e^{308.56\left(\frac{1}{56.02} - \frac{1}{T_s - 227.13}\right)} \qquad (6.2)$$

where R_S (μmol m^{-2} s^{-1}) is soil respiration, R_{10} is the soil respiration rate at 10°C and T_s (K) is soil temperature. Soegaard and Nordstroem (1999) have successfully applied this model at a high-arctic fen site in Greenland.

Each surface type within the model had a different R_{10} value and the models' area average soil respiration value was obtained from the individual soil respiration rates adjusted by their proportional cover. The soil respiration rates were measured during the summer and it is arguable whether these rates are consistent throughout the active season. The populations of soil organisms may fall in number, rather than just activity, with the return of the permafrost. Soil respiration rates would then upon unfreezing be a function of increasing populations of soil bacteria as well as increasing temperature. The evaluation of these rates are more fully described in section 6.4.1 and Table 6–3.

6.3.1.1.2 The Photosynthesis model

Several studies have indicated that cryptogams probably fix CO_2 by the C_3 pathway as in most temperate and polar flowering plants (Rastorfer, 1971; Valanne, 1984). The photosynthesis model used for both cryptogams and vascular plants in this study is the C_3 model of Collatz *et al.*, (1991) as used by Cox *et al.*, (1999). The main equations of the model are re-stated here – for a more detailed description see Cox *et al.*, (1999). Appendix 1 contains a MathCad version of the C_3 model as implemented in Cox *et al.*, (1999) as used to appreciate the operation of the model.

Using the nomenclature of Cox *et al.*, (1999), the gross leaf photosynthetic rate (W) approaches the minimum or most limiting of the three potentially limiting rates; W_C, the rate of gross photosynthesis dependent on the Rubisco capacity; W_L, the potential photosynthetic rate dependent upon light and CO_2 availability and W_E, the potential photosynthetic rate dependent upon the transport of photosynthetic products within the leaf. In practice, to allow a smooth transition from one limiting factor to another and some co-limitation between the three rates, the minimisation of these terms is performed by creating a continuous function through two nested quadratic transforms of the rates in combination (Collatz *et al.*, 1991).

V_m is the temperature dependent capacity of the substrate-saturated Rubisco given by:

$$V_m = \frac{V_{\max} Q_{10}^{0.1(T_c-25)}}{\left[1+e^{0.3(T_c-36)}\right]} \qquad (6.3)$$

where Vmax , (μmol m^{-2} s^{-1}) is the maximum rate of carboxylation of Rubisco assumed to be, following Schulze *et al.* (1994), linearly dependent on the leaf nitrogen concentration, n_l (kg N kg^{-1} C). T_c is leaf temperature (°C) and Q_{10}, the ratio of the rate at one temperature to that at a temperature ten degrees lower is set equal to 2.0,

The Rubisco dependent rate:

$$W_C = V_m \frac{c_i - \Gamma}{c_i + K_C\left(1+\frac{O_a}{K_0}\right)} \qquad (6.4)$$

where O_a (Pa) is the atmospheric partial pressure of oxygen, K_c and K_0 (Pa) are Michaelis-Menten constants for CO_2 and O_2 respectively, and Γ (Pa) is the photorespiration compensation point, defined for C_3 plants as $O_a/2\tau$ where τ is the Rubisco specificity for CO_2 relative to O_2 given as:

$$\tau = 2600 Q_{10}^{0.1(T_c-25)} \qquad (6.5)$$

with $Q_{10} = 0.57$.

The light and CO_2 availability dependence:

$$W_L = \alpha A_{cr} \frac{c_i - \Gamma}{c_i + 2\Gamma} \tag{6.6}$$

where α is the quantum efficiency for CO_2 uptake (mol CO_2 (mol PAR photons)$^{-1}$) and A_{cr} is the incident photosynthetically active radiation (PAR) in mol PAR photons m^{-2} s^{-1}.

The photosynthetic leaf product transport rate:

$$W_E = 0.5V_m \tag{6.7}$$

The rate of dark respiration in C_3 plants is assumed to be a constant fraction of the maximum rate of carboxylation of Rubisco:

$$R_d = 0.015V_m \tag{6.8}$$

6.3.1.1.3 Moisture control on photosynthesis

Cryptogamic plants differ from vascular plants in their response to soil and atmospheric moisture. Mosses and lichens typically are uncoupled from soil moisture, having no water-carrying root system. Soil moisture can however, diffuse through the cryptogamic mat as water vapour and under suitable conditions, condense on the outer surfaces.

There is therefore a need to differentiate the photosynthetic responses of cryptogams and vascular plants to changes in their moisture status. In vascular plants, this was achieved in the model of Cox *et al.*, (1998) through direct dependence of the net photosynthetic rate on the soil moisture status which had a functional form described by Stewart and Verma (1992) for the "Jarvis" model (Jarvis, 1976). The resultant soil moisture adjusted net rate of photosynthesis in that model is described by:

$$A_L = (W - R_d)\beta_S \tag{6.9}$$

where A_L is net rate of photosynthesis and β_S is the soil moisture factor which ranges between 0 (soil moisture concentration below the "wilting point" – when

transpiration ceases) and 1 (soil moisture concentration above the "critical point" – above which plants are not water limited). Muc (1977) recorded 67 per cent of live roots below 0.1m at the high arctic site at Truelove Lowland, Devon Island. At the Ny-Ålesund site, the volumetric soil moisture concentration at this level was always above 15 per cent volumetric water content (see Chapter 3). It was assumed that this was above the critical wilting point for these plants (Lloyd, 1998) and β_S would normally be set to 1.

However, for the cryptogamic community, transpiration and photosynthesis are not limited by variation in the soil moisture concentration. Photosynthesis in cryptogams reduces as moisture is lost by diffusion through the cell walls. There is also evidence of reduced photosynthetic rates above a certain water content (Oechel and Collins, 1976). The exact response curve and rate varies from species to species and with temperature and latitude and no account of these differences were made in the model. Instead an evaporative loss factor, operating in place of β_S in equation (6–9) above was used to limit transpiration and hence photosynthesis at the cryptogamic leaf level. This evaporative loss factor, β_E , was composed of a surface evaporation rate and an initial cryptogam moisture content value. The surface evaporation rate was evaluated from the Penman-Monteith equation (Monteith, 1965) using data from the AWS and with the saturation vapour pressure e_{sat} and vapour pressure e calculated at the leaf temperature. Hourly mean values of surface resistance, r_s , were evaluated by inverting and solving the Penman-Monteith equation for r_s using measurements of sensible and latent heat, air temperature and aerodynamic resistance from the eddy correlation sensors between 25 July and 10 August 1995. The frequency histogram of the hourly mean values of r_s was skewed and a square-root transform was applied before the seasonal mean was estimated as 80 s m^{-1} with a standard deviation of 20 s m^{-1}.

Lange *et al.* (1985) showed decreases of water content in two lichen species in Alaska from 200% of Dry Weight (DW) to 25% of DW in 12 hours. During that period, after an initial respiration burst, net photosynthesis reached a peak after 9 hours and then rapidly fell away and ceased after 12 hours. Gimingham and Smith

(1971) showed in *Calliergon sarmentosum* (a similar moss species to *Drepanocladus* at Ny-Ålesund) progressing from 100% water content to 15% water content in 10 hours. While laboratory measurements of water absorption by mosses may show uptake of >1000% of DW, water content under field conditions seldom exceed 300% of DW (Hicklenton and Oechel, 1976). In the model, the initial cryptogam moisture content value was used as a free variable to characterise the simulation output but was adjusted within limits providing desiccation times comparable to the above observations.

There is little evidence of cryptogams being able to extract water vapour from the air to replenish cell water concentrations. Although some mosses have specialised root-like structures for transport of moisture from the soil, the mosses at this site do not, and the only way that moisture levels within the cryptogamic cells can increase is through precipitation events, i.e. rain, fog, dew or snow (Longton, 1980). The photosynthetic process within cryptogams is thus controlled by the opposing actions of evaporation leading to desiccation and halting the photosynthetic process and wetting through precipitation leading to resumption of the photosynthetic process. The process of refilling the moisture store within the cryptogamic community is achieved by allowing the evaporative loss factor, β_E , to increase after a precipitation event. For periods during precipitation and for some hours afterwards the surfaces of the cryptogamic leaves would have been covered with a liquid water layer and incapable of photosynthesis. There does not appear to be any published results describing the amount of liquid water that cryptogamic canopies can support or how long this water takes to drain or evaporate away allowing photosynthesis to resume. The model therefore includes a variable time delay, which was optimised during the formation of the model's parameter set.

During this study it was observed that there appeared to be instances during the period 30 July – 11 August when possible dew formation was effectively allowing the cryptogams to resume photosynthetic activity (as observed in the measured net CO_2 flux) many days after the last precipitation event (see Figure 6–1). As Monteith and Unsworth (1990) point out, any negative differences between the soil and

dewpoint temperature over surfaces whose water content contains dissolved salts or water is held by capillary forces in a porous medium (i.e. both soil and bryophytes at this site) implies a strong possibility of dew formation at the surface. There are several occasions shown by the arrowed lines on Figure 6–1 where the measured CO_2 trace turns from a carbon source to a carbon sink following a time of implied dew formation. Further examination of the measured CO_2 values proceeds in Section 6.4.2.2.

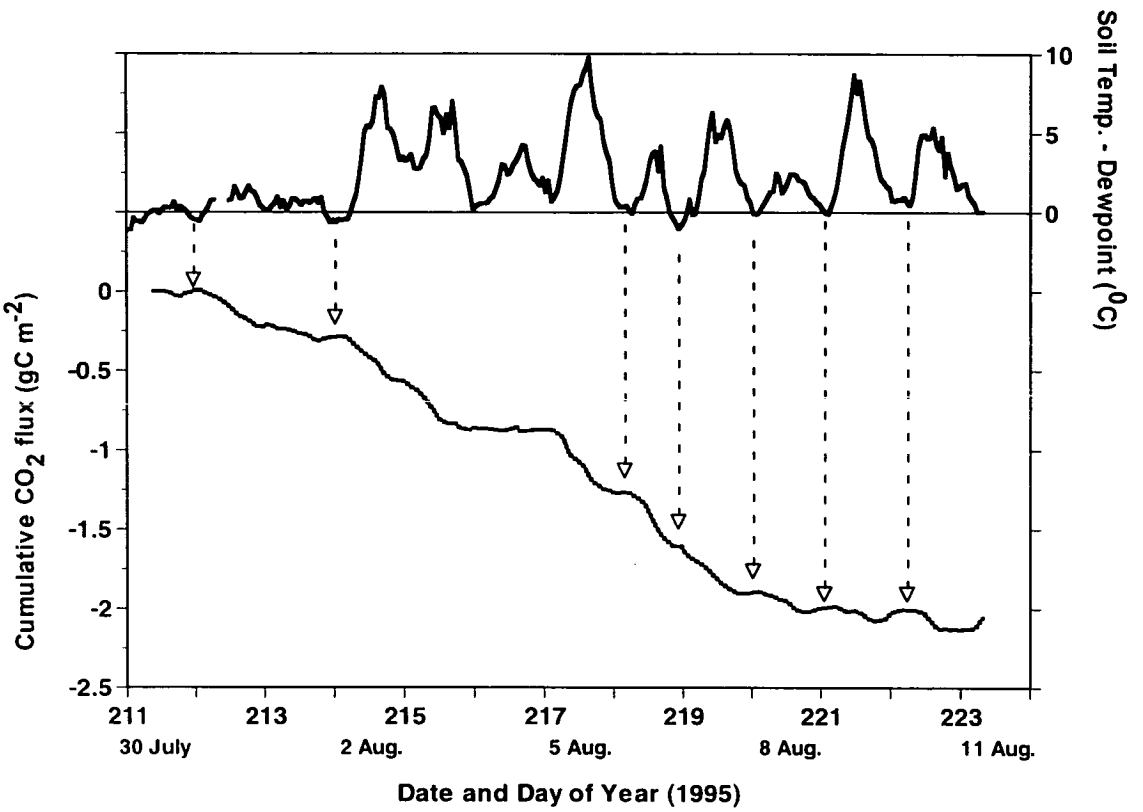

Figure 6-1 *Hourly average values of the difference between temperature at the soil surface and dewpoint at 2.7m (——) and the cumulative net CO_2 flux (·····)*

Lange *et al.* (1985) showed that dew formation raised water content from desiccation to 50% water content by Dry Weight and led to a burst of photosynthetic activity which had a rate and duration similar in extent to that occurring after rainfall. Dew formation was adjudged to have occurred if soil temperature was less than the dew-point of the overlying air i.e. (see Monteith and Unsworth, 1990) if:

$$T_c - \frac{T_a}{\left(\frac{1-\ln\left(\frac{e}{e_{sat}(T_a)}\right)}{B}\right)} < 0 \qquad (6.10)$$

where T_c is an assumed leaf temperature given by the soil temperature at the soil-vegetation interface, T_a is air temperature as measured at 2.7 m by the sonic anemometer and e and e_{sat} are the vapour pressure and saturated vapour pressure at air temperature as estimated from measurements of relative humidity recorded by the AWS. The factor $B = \lambda M_w/RT^*$, (where λ is the latent heat of vapourisation, M_w is the molecular weight of water, R is the gas constant and T^* is a standard temperature = 293 K), is however set to 19.65 which according to Monteith and Unsworth (1990), provides more exact estimates of e_{sat} over the smaller temperature range 273 – 293 K.

Where dew was assumed to have occurred, β_E was allowed to increase but at a slower rate than that following a rainfall precipitation event. Figure 6–2 shows the flowchart for deciding the size, rate and direction of β_E in response to wetting and

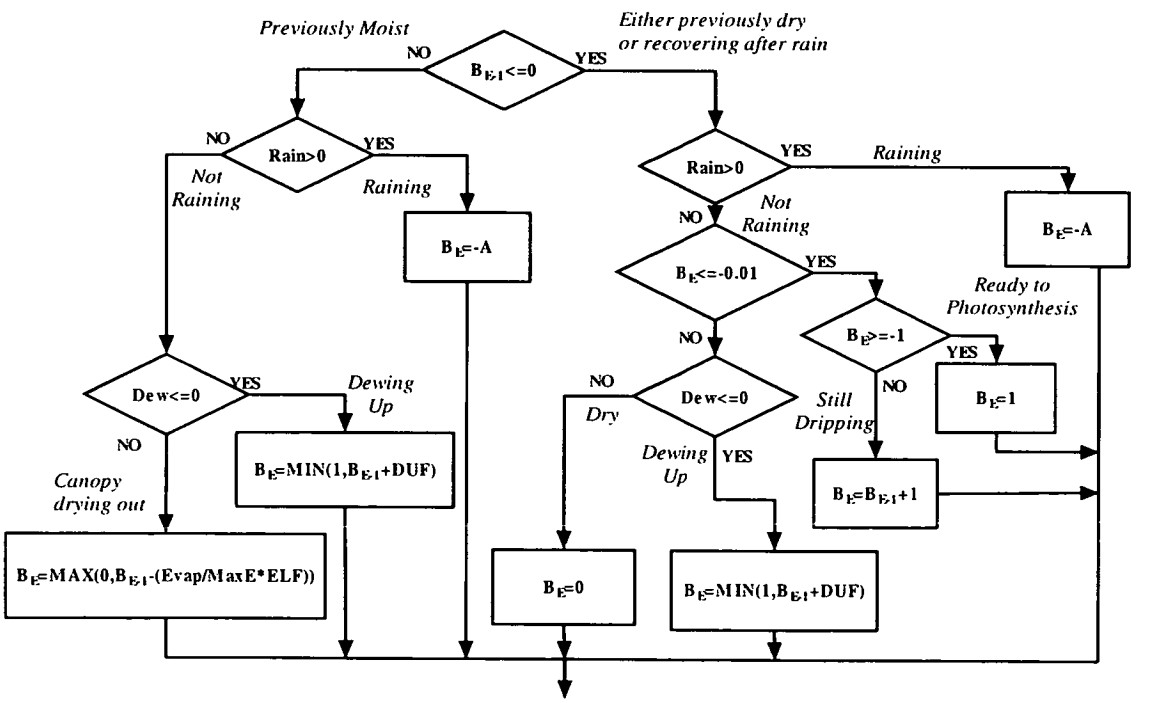

Figure 6-2 *Decision flowchart for water content status of cryptogams. DUF, maxE, Dew and A are described in Table 6-1.*

drying periods. During rain, β_E was set to an optimised value that indicated the time required for the cryptogamic surfaces to dry out sufficiently for photosynthesis to resume.

6.3.1.1.4 Growth and Senescence factors

Leaf Area Index (LAI) is used in many models of plant growth (including MOSES) to regulate the seasonal increase or decrease in photosynthetic activity. Soegaard and Nordstroem (1999), at Zackenberg, N.E.Greenland found a linear rise of LAI from 0 to 1.2 during 20 days in spring and a similar decrease from 1.2 to 0 in 24 days during the late summer. However, their site was predominantly sedges and grasses, which initiate new growth each year. The change in LAI that accompanies the increasing utilisation of CO_2 in emerging deciduous plants is not appropriate at the Ny-Ålesund site where little change is observed in LAI despite increasing photosynthetic activity. Leaf Area Index (LAI) of the predominantly evergreen vascular plant and cryptogam community was not measured at the Ny-Ålesund site. However, the maximum LAI was estimated to be much lower than at the Zackenberg site (Soegaard, pers. com.). Nevertheless, the plant community at Ny-Ålesund does increase its photosynthetic activity after snowmelt and decrease its photosynthetic activity at the end of summer. A surrogate replacement for LAI (termed a Growth Factor –GF) was used to model the change from zero to full photosynthetic activity and was applied to the separate vascular and cryptogamic surfaces using individual percentage surface cover. It is recognised that the two plant communities have different photosynthetic activity strategies not only in the spring but also in the autumn when cryptogams will continue to photosynthese through late summer and autumn providing temperature, moisture and light levels allow it (Hicklenton and Oechel, 1976; Oechel and Sveinbjörnsson, 1978). However, in the absence of data on this aspect and a desire to keep the model as simple as possible, the same GF rates were applied to both the vascular and cryptogamic plant communities. After the spring increase in activity, full potential photosynthetic activity was assumed to occur until late summer. A symmetrical growth equation, identified by Landsberg (1977) was used for the GF (and the SF) model. This is given by:

$$GF = SF = \frac{1}{1+e^{-(b+at)}} \qquad (6.11)$$

where a and b are shape factors for the model and t is an hourly time step. The rate at which GF increased (in spring) or SF decreased (in the autumn) were, in the absence of any defining work, given a free parameter status in a simple optimisation scheme which explored the total parameter space for the shape factors a and b.

6.3.1.1.5 Assimilation rates

Maximum net assimilation rates (NAR) in cryptogams is considerably lower on a dry weight basis than in angiosperm leaves (Longton, 1988). Wielgolaski (1975) found that maxima in the foliage of tundra angiosperms were 7-33 mg CO_2 g^{-1} h^{-1} compared to less than 5 mg CO_2 g^{-1} h^{-1} in the green parts of associated mosses and lichens. Similarly, Oechel and Svienbjörnsson (1978) at a site near Barrow, Alaska considered that Net Assimilation Rates (NAR) in mosses was only 8-9 per cent of that of vascular plant leaves. Kallio and Kärenlampi (1975) indicate C_3 plants having maximum net photosynthetic rates of 20-45 mg CO_2 dm^{-2} h^{-1} compared to lichens at 0.5-2.0 mg CO_2 dm^{-2} h^{-1} and mosses at less than 3.0 mg CO_2 dm^{-2} h^{-1}.
The cryptogamic NAR was found to simulate the measured flux when set to 15 per cent of the vascular rate (comparable to the maximum difference between rates in Wielgolaski, 1975) –see Table 6-1.

6.3.1.1.6 Light intensity limits in Cryptogams

Cryptogams have light compensation points and light saturation limits in a similar way to vascular plants. The light compensation point is where photosynthetic uptake is exactly balanced by plant respiration. The light saturation point is where further increases in light intensity has no effect up[on the rate of photosynthesis.
Miller *et al.* (1978) show that all four of their investigated moss species at Barrow were radiant energy saturated at 300 W m^{-2} PAR. Longton (1988) states that in polar species, light compensation points for both mosses and vascular plants in open tundra at Barrow, Alaska are commonly 5 - 12 W m^{-2} PAR but that mosses saturate at 80 - 120 W m^{-2} PAR – approximately 30 per cent of the level typical for local

angiosperms. During the period 30 July – 11 August 1995, 15% of the measured hourly average incoming solar radiation values were above 266 W m^{-2} (equivalent to 120 W m^{-2} PAR) but that including the radiation values above this cut-off point increased overall light availability by 14%. Nevertheless, a light saturation limit of 266 W m^{-2} (see Table 6-1) was applied to the cryptogamic photosynthetic process. No such limitation was applied to the vascular plant photosynthetic process.

Parameters	Units	Value
General		
Soil Heat Flux as percentage of Net Radiation	%	5
Bare Soil cover	%	20
Cryptogamic plant cover	%	67
Vascular plant cover	%	13
Number of hours after rain before plant photosynthesis can (A)	hr	3
Cryptogamic		
Light Saturation point for cryptogams	W m^{-2}	266
Critical factor for dew formation:Dew=($T_c - T_a$)	°C	-0.1
Evaporation-limiting factor for cryptogams (ELF)		0.35
Cryptogamic growth rate as proportion of vascular plant growth		0.15
Maximum evaporation rate from cryptogamic surfaces (maxE)	mm hr^{-1}	0.5
Rate at which cryptogams can absorb precipitation (DUF)	mm hr^{-1}	0.2

Table 6-1 *General and Cryptogamic-specific parameter values used in the combined soil respiration and photosynthetic model.*

6.3.1.2 Sensitivity Analysis

No deviation from the parameter set routinely used within MOSES (and the Hadley Centre GCM) for the C_3 photosynthetic module have been applied in the modelling aspects of this paper (see Table 6-2). Sensitivity analyses of this part of the model have been performed previously in Harding *et al.* (2000) and Huntingford *et al.* (2000). However, the additional parameters required to create the NEP model, i.e. the integration of the moss/lichen community into the MOSES C_3 photosynthetic routine and the addition of the soil respiration model, were subjected to a sensitivity analysis. Each parameter in turn was varied by ± 50% around its estimated or optimized value and the resultant estimates of NEP were compared to the NEP estimate given by the default parameter set for the 1995 modelling period.

6.3.1.3 Evaluation of the model's performance

The method recommended by Willmott (1984) was used to assess the performance of the model. He reported that his degree of agreement statistic *d* was a better measure of the quantitative correlation between observations (*O*) and modelled values (*M*) than the usual Pearson product-moment correlation coefficient (*r*) or coefficient of determination (r^2) which are insensitive to a wide range of additive and proportional differences that can exist between *O* and *M*.

Parameter	Name	Units	Value	MOSES Default value
Pressure	Press	Pa	101300	101300
Surface resistance	rs	$s\ m^{-1}$	80	-
Aerodynamic resistance	ra	$s\ m^{-1}$	70†	-
Critical humidity deficit	dqcrit	$kg_{H2O}\ kg_{air}^{-1}$	0.15	0.15
Atmospheric Oxygen pressure	Oa	Pa	20900	20900
C_i/c_a for dqcrit=0	fo	-	0.92	0.92
Dark respiration coefficient	Fd	-	0.015	0.015
Canopy CO_2 concentration		$kg_{CO2}\ kg_{air}^{-1}$	4.90E-04	4.90E-04
Mol.wt. O_2 / Mol.wt. dry air	Epo2		1.106	1.106
Mol.wt. CO_2 / Mol.wt. dry air	EpCO2		1.5196	1.5196
Atmospheric O_2 concentration	O2	$kg_{O2}\ kg_{air}^{-1}$	0.23	0.23
CO_2 mixing ratio	CO2	$Kg_{CO2}\ kg_{air}^{-1}$	0.00049	0.00049
Leaf scattering coefficient for PAR	Omega	-	0.15	0.15
Const. relating V_{max} and leaf nitrogen	nf	-	0.0008	0.0008
Default value for V_{max}	Vmax	$Mol_{CO2}\ m^{-2}\ s^{-1}$	4.69E-05	4.69E-05
Quantum efficiency	ALPHA	$Mol_{CO2}\ mol_{PAR}^{-1}$	0.04	0.04
Leaf nitrogen concentration	nl	$kg_N\ kg_C^{-1}$	0.05	0.05
Leaf resistance for CO_2 /Leaf resistance for H_2O	ratio	-	1.6	1.6
Minimum leaf resistance for H_2O	Glmin	-	1.00E-06	1.00E-06
Gas constant	R	$J\ K^{-1}\ mol^{-1}$	8.3144	8.3144
Coupling coeffs. for co-limitation	BETA1	-	0.83	0.83
Coupling coeffs. for co-limitation	BETA2	-	0.93	0.93
Soil water factor for vascular plants	fsmc	-	1	0-1

Table 6-2. *Parameter values for the C_3 photosynthetic model – these are the same as the default values within the standard MOSES model. † There is a typographic error in the published version of this table.*

In other words, it is quite possible to obtain extremely high values of *r* or r^2 when *O* and *M* are quite dissimilar in size but "track" each other well, leading to a good fit but poor model prediction values. On the other hand, *O* and *M* may not "track" one

another but their mean values are nevertheless much closer but with "noise" in one or both sets of data. The predicted final outcome will be close to the measurement result but the r^2 value could be very low. Such is the case with modelling surface fluxes. The flux values are inherently noisy compared to the modelled values. The statistic d varies between 0 (complete disagreement) and 1 (complete agreement) and is given by:

$$d = 1 - \frac{N.RMSE^2}{\sum_{i=1}^{n}\left[\left(M_i - \overline{O}\right) + \left(O_i - \overline{O}\right)\right]^2} \qquad (6.12)$$

where N is the number of observations, $\overline{O}$ is the mean observed value and $RMSE$ is the standard root mean square error given by:

$$RMSE = \left[N^{-1}\sum_{i=1}^{N}\left(M_i - O_i\right)^2\right]^{\frac{1}{2}} \qquad (6.13)$$

To gain further insight into the model's performance, Willmott (1981) separates $RMSE$ into systematic ($RMSE_s$) and unsystematic ($RMSE_u$) parts where :

$$RMSE_u = \left[N^{-1}\sum_{i=1}^{N}\left(M_i - \hat{M}_i\right)^2\right]^{\frac{1}{2}} \qquad (6.14)$$

and $\hat{M} = a + bO_i$, and a and b are the regression coefficients associated with an ordinary least squares simple linear regression between O and M. $RMSE_s$ is then given by:

$$RMSE_s = \left(RMSE^2 - RMSE_u^{\ 2}\right)^{\frac{1}{2}} \qquad (6.15)$$

. An acceptable model would not only have a high d, but the $RMSE$ should be low with relatively small $RMSE_s$ (i.e. the model explains most of the systematic variation) and with $RMSE_u$ approaching $RMSE$. In assessing the degree to which solar radiation and soil temperature control CO_2 flux, Lloyd (2001) used this method to optimise (and to evaluate the performance of) a simple model by minimising the

differences between measured hourly average values of CO_2 flux and modelled hourly values of NEP. In this study, where the aim is to model the active season CO_2 balance, the model's performance (and optimisation of its free parameters) were assessed by minimising the differences between the cumulative values of measured CO_2 flux and modelled values of NEP at hourly intervals. There is also evidence of increased confidence in period totals when estimating fluxes in heterogeneous terrain (Lloyd *et al.*, 1997). Evaluations of constants defined above and their units are shown in the results section below.

6.4 Results

The measurements during three periods in 1995 were chosen to optimise the free parameters within the model. These periods: 26-30 June, 30 July – 11 August and 29 August – 3 September represented three pivotal phases of the active season in 1995; the post snowmelt initial growth, full summer growth and late summer senescence respectively.

Post snowmelt growth periods are characterised by patchy snow cover, waterlogged areas and increasing but variable growth factors that lead to heterogeneity in both the soil respiration and the photosynthetic activity within the emerging vegetation. Similarly, late summer and early autumn are characterised by heterogeneous plant senescence coupled with frosts. In conditions like these, it can be difficult to interpret model results based on point measurements of radiation and soil temperature with flux measurements, which are integrations over a considerable area.

These heterogeneities, although not absent, are minimised during the main summer period. Therefore the full summer growth period (31 July – 11 August) was used to investigate the performance and reaction of the model to variation in the free parameters. Despite the inherent difficulty, the early and late periods were then used to parameterise the GF factor in order to incorporate plant growth and plant senescence into the model. Soil respiration was assumed to be without seasonal variability other than that provided by temperature.

6.4.1 Soil respiration

Nakatsubo *et al.* (1998) in their study of soil respiration rates at Ny-Ålesund had a site (Site III) at the top of the slope where the AWS was situated. Their results are shown verbatim in Table 6–3. The soil respiration model of Lloyd and Taylor (1994) requires values for R_{10} in μmol CO_2 m^{-2} s^{-1}. Equation (6.2) was therefore solved for R_{10} using the results of Nakatsubo and converted to the required units. These values (linearly averaged where there are two solutions) are also shown in Table 6–3.

Surface	Soil Temperature °C	Total respiration rate (mg $_{CO2}$ m^{-2} h^{-1})	Calculated R_{10} (μmol $_{CO2}$ m^{-2} s^{-1})
Bare Ground	7.6	12.8	0.103
Crust: cyanobacteria and lichens	7.3	54.8	0.389
	7.6	39.5	
Mixed: bryophytes and vascular plants	6.2	81.2	0.806
	6.9	96.4	

Table 6-3 *Soil respiration results (after Nakatsubo et al. 1998) and calculated R_{10} values based on these results as used initially in the model.*

Soegaard and Nordstroem (1999) set R_{10} = 1.6 μmol CO_2 m^{-2} s^{-1} for their Zackenberg, Greenland site – a figure based on a study in a boreal part of Sweden by Soegaard and Thorgeirsson (1998). The author's own observation of the site used by Nakatsubo *et al.* (1998) and their Figure 2 showing the surface at Site III indicates that while the bare ground and mixed bryophyte and vascular plant surfaces are very similar to those referred to in this paper, the crust surface of cyanobacteria and lichens was much sparser and closer to bare ground cover when compared to the more highly vegetated moss/lichen surface at the flux site. The lichen cover value for R_{10} was left free to assume some value between 0.389 and 0.806 (see Table 6-) during the creation of the model parameter set and was subsequently set to 0.6.

The difference in respiration rates is a compound effect of the difference in carbon amount in the soil underlying the vegetation, the difference in soil temperature caused by the effect of overlying vegetation and also any uptake of CO_2 by the vegetation as the CO_2 diffuses through it. Figure 6–3 shows the resultant modelled soil respiration values for the individual surfaces (per unit area) and the overall

average soil respiration, R_S equal to the linear sum of the individual respiration rates scaled by their percentage surface cover for the period 30 July - 11 August 1995.

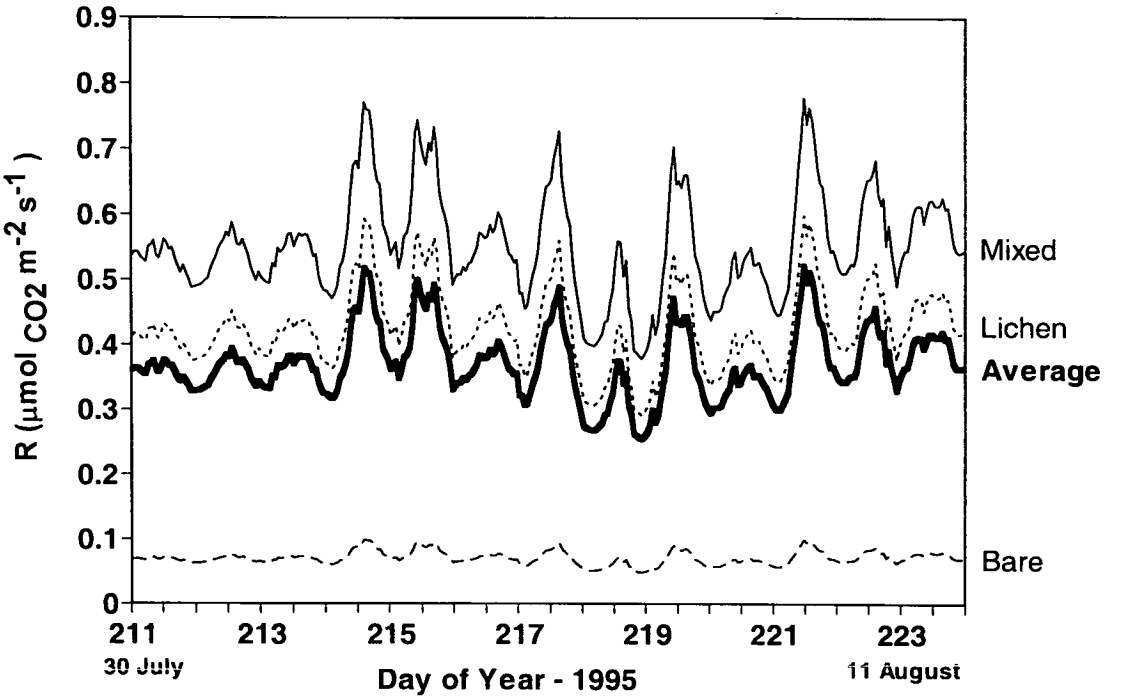

Figure 6-3 *Modeled soil respiration from bare soil, lichen covered soil, mixed vascular/bryophyte soil and area cover average soil respiration for the period 30 July – 11 August 1995*

Wüthrich *et al.* (1994), using soda-lime absorption techniques at undefined sites around Ny-Ålesund, found respiration rates that were 3 times higher (up to 6g CO_2 m^{-2} d^{-1}) than those of Nakatsubo *et al.* (1998). In a later study, Wüthrich *et al.* (1999) using a Li-Cor 6252 infrared gas analyser to take *in-situ* measurements at a field site 50km south of Ny-Ålesund, found soil respiration rates in *Cetraria delisei* sites that were approx. 1 g CO_2 m^{-2} d^{-1} and 4 g CO_2 m^{-2} d^{-1} at a mixed *Cetraria – Salix* site. Both these sites were ungrazed by reindeer (Wüthrich, pers. comm.), unlike the site in this study, and no data on soil temperature was given.

6.4.2 Net Ecosystem Production: 30 July - 11 August 1995

6.4.2.1 Cryptogamic water relations

Rainfall, amounting to 3.5mm during the early hours of 30 July followed by an isolated 0.5mm during the early morning of 31 July was the only recorded precipitation during this period (see Figure 6–4 (b)). However, there were instances during the whole period when calculated leaf temperatures dropped below the dewpoint leading to the likely deposition of dew onto the cryptogamic leaf surfaces.

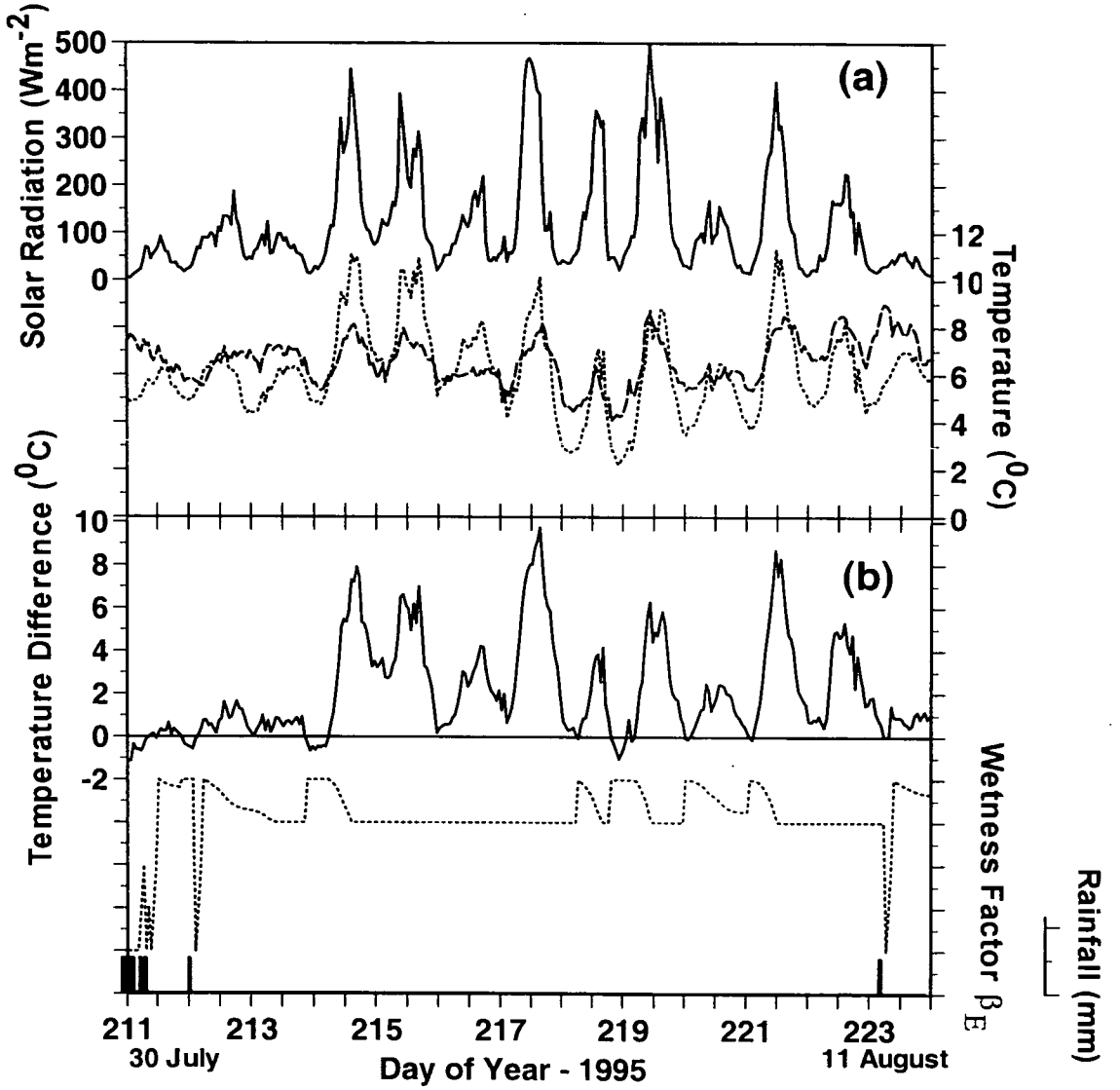

Figure 6-4 *(a) Solar radiation (solid line), air temperature (dashed line), soil temperature at 25mm (dotted line) for the period 30 July to 11 August 1995. (b) The expected occurrence of dew as indicated by the difference between leaf and dewpoint temperature (upper line); the rainfall (lower columns) and the effect these two conditions have upon the wetness factor (dotted line) controlling the photosynthesis of the cryptogams for the same period.*

While the vascular plants were assumed not to be significantly affected by either rainfall or dewfall, both situations would tend to affect the photosynthetic rate of the cryptogams by initially inhibiting photosynthesis through the deposition of a liquid film onto the leaf surfaces and then increased photosynthetic rates as the moisture is absorbed and the liquid water film disappears through absorption, drainage and evaporation. The dewfall rate and amount was assumed not to cause significant surface liquid water. Figure 6–4(b) shows the progression of the β_E factor (controlling the occurrence of cryptogamic photosynthesis) in the model as it responds initially to rainfall and then to dewfall. The cryptogamic leaf surfaces in the model can only photosynthese when $\beta_E > 0$ with maximum rates achieved when $\beta_E = 1$. β_E becomes negative during rain and begins to approach zero after cessation of rainfall as the surface liquid water disappears. Rainfall is assumed to fully replenish the water concentration in the leaves allowing the full photosynthetic rate to be achieved.

6.4.2.2 Gross Primary Production (GPP)

Figure 6–5(a) shows the modelled progression of unit area GPP during the period for the individual cryptogamic and vascular plant communities and the overall GPP produced by combining area-cover weighted values. It can be seen that during this period that the model simulates only seven periods of cryptogamic photosynthetic activity in response to the rain and dew events but that these are still significant in the overall GPP values, despite the lower photosynthetic rate of cryptogams, because of the large surface area covered by such vegetation. The model also shows that, despite the continuous daylight, there is a marked diurnal variation in the photosynthetic rate.

The summation of net GPP and net soil respiration produces the net carbon dioxide flux into the atmosphere i.e. NEP as defined in Equation (6.1). Comparison between the hourly measured and modelled NEP and the cumulative measured and modelled NEP is shown in Figure 6–5(b).

The model generally follows the hourly measurements but without the measurement variability. This is because the measurements are subject to spatial heterogeneity as the wind direction and atmospheric stability changes – heterogeneity that is not built into the model. Lloyd *et al.* (1997) showed that the effects of heterogeneity are smoothed out when fluxes are summed over periods and the cumulative plots shown in Figure 6–5(b) provide a better gauge of the performance of the model. It can be

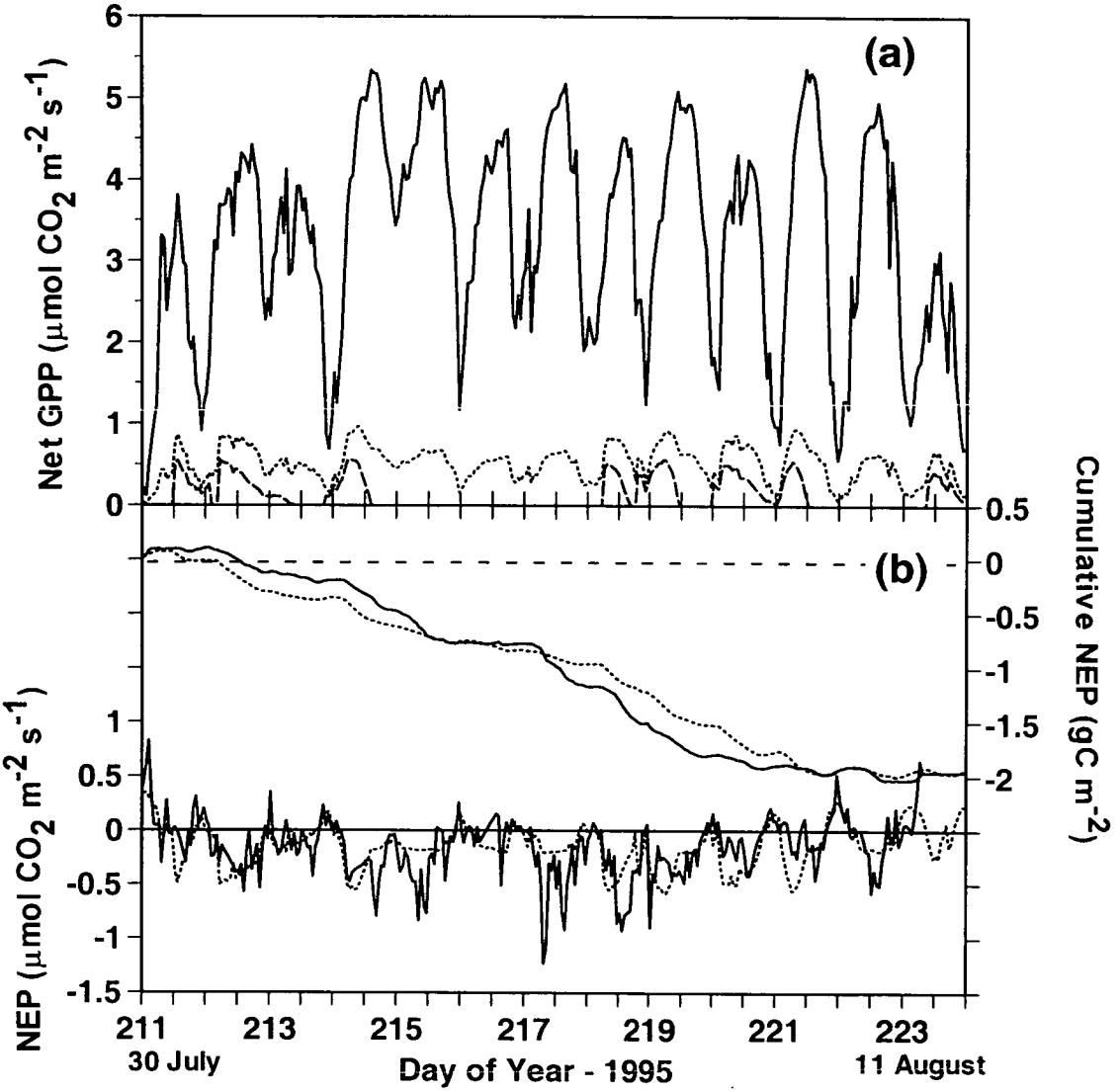

Figure 6-5 *(a) Gross Primary Production (GPP) per unit area for vascular plants (solid line), cryptogams (dashed line) and overall area weighted GPP for the surface (dotted Line) for the period 30 July – 11 August 1995. (b) Comparison between measured (solid lines) and modeled (dotted lines) Net Ecosystem Production (NEP) for the same period: Lower plots are individual hourly average NEP and upper plots are cumulative NEP.*

seen that the fit between model and measurements is generally good although the model misses the large photosynthetic uptake on days 215 and 217. Day 215 was characterised by high air temperature but relatively low soil temperature, while day 217 was characterised by clear skies, high solar radiation and high air and soil temperatures. Statistically, as shown in Table 6-4, the model performed well overall, with a high Willmott *d* statistic of 0.989. However, RMSE was relatively high and $RMSE_s$ and $RMSE_u$ were comparable in size, indicating a systematic error in the difference between the measurements and the model. Examination of Figure 6–5 indicates that the pivotal point was the large measured assimilation rates on Day 217, which the model failed to simulate.

6.4.3 Net Ecosystem Production: 27 – 30 June 1995

Harding and Lloyd (1998) showed that snow cover had virtually disappeared by 15 June in 1995. Figure 6-6(a) shows the solar radiation, air and soil temperature at the soil-vegetation interface for the period 27-30 June together with the isolated precipitation events which bracket this period.

While soil temperature at the soil-vegetation interface is closely coupled to solar radiation, air temperature is probably influenced by the disappearance of the last snow patches and eventually begins to exceed the soil temperature. This post snow melt period of 4 days was characterised by very cold and windy weather on 28 June followed by intermittent light snow showers during the early hours and afternoon of the 29th (Day 180) and again during the early hours of the 30th June (day 181) and with intermittent but strong snow showers during the afternoon of the 30th June. These snow showers were mostly light but did settle and may have inhibited photosynthetic activity through partial shading of the vegetation.

The comparison between individual hourly average modelled and measured NEP and their cumulative totals during 27-30 June 1995 (day 178-181) is shown in Figure 6–6(b) in an analogous way to Figure 6–5(b). Also shown is the optimised Growth Factor (GF) used to simulate vegetation emerging from dormancy. The defining shape factors, *b* and *a* for GF are shown in Table 6–4.

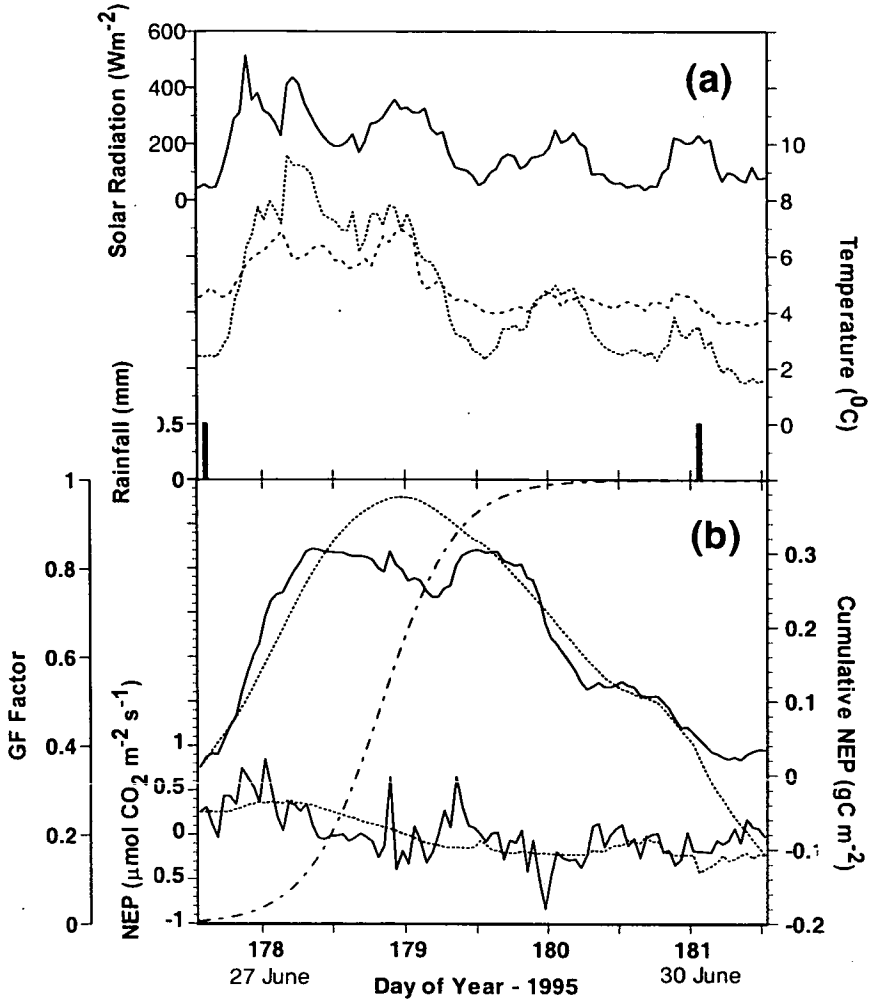

Figure 6-6 *(a) Solar radiation (solid line), air temperature (dashed line), soil temperature at 25mm (dotted line) and rainfall (columns) for the post snowmelt period 27 June to 30 June 1995. (b) Comparison between measured and modeled NEP for the same period. Legend is the same as for Figure 6–5. The post snowmelt increase in vegetation photosynthetic activity is shown by the model Growth Factor (GF) – (dot and dash line).*

Parameter	Period	26-30 June	30 Jul – 11 Aug	29 Aug – 3 Sep
GF (or SF) factor b		-5.1	N/A	(-0.4)
GF (or SF) factor a		0.16	N/A	(-0.01)
Willmott d statistic		0.947	0.989	0.973
RMSE		0.055	0.1483	0.022
$RMSE_u$		0.048	0.1078	0.020
$RMSE_s$		0.026	0.1018	0.008
r^2		0.877	0.974	0.92

Table 6-4 *Growth Emergence Factor (GF) and Senescence Factor (SF) parameter values and statistical measures of model performance for the three model calibration periods in 1995.*

The model fails to simulate the spiky nature of the measurements, which are probably due to the heterogeneity caused by patchy snow cover and soil moisture, and the different rates of photosynthetic activity from the emergent vegetation - effects lacking in the model. The cumulative modelled NEP follows the cumulative measured CO_2 flux in general with the early period indicating a net source of CO_2 followed by the period of net uptake of CO_2.

The model however fails to simulate the net uptake during the early part of 28th June (day 179) or the net source periods during the latter hours of the same day. The divergence between model and measurements during the latter half of 30 June (day 181) is easier to explain, as intermittent but strong snow showers would have inhibited plant assimilation as evident from the measurements - a factor that the model is unable to simulate at present.

6.4.4 Net Ecosystem Production: 29 August – 3 September 1995

Figure 6–7 shows a similar comparison to previous periods (Figure 6–5 and Figure 6–6) of the major driving factors of solar radiation and soil temperature and air temperature (Figure 6–7(a)) and the measured CO_2 fluxes and modelled hourly and cumulative NEP (Figure 6–7(b)).

Figure 6–7(a) shows that this period, (days 241-246), at the beginning of the autumn, began with overcast skies and low maximum radiation levels of less than 150 W m^{-2}, but had clear skies on 1 and 2 September (days 244,245) with maximum solar radiation levels of 290 W m^{-2} at solar noon on both days. Overnight soil temperatures at 25 mm dropped below zero from Day 244 to the end of the period (Day 246). There was no rainfall during this period - the last rainfall occurring on Day 235 (23 August). The vascular vegetation was assumed to be into a senescent state while the cryptogamic vegetation would be expected to continue to photosynthese providing moisture, temperature and light levels allowed it. The senescence factor, SF, used to reduce the overall effective area of active vegetation is plotted in Figure 6–7(b) and the shape factors, b, and a, for SF are tabulated in Table 6–4. In contrast to the trend

from dormancy to full activity seen during the post snowmelt period, the optimisation of the SF factor (see Figure 6–7(b)) produced a very gradual descent into vegetative dormancy during the late summer and autumn.

The general trend in both measurement and modelled outputs, shown in Figure 6–7(b), is for the period to be an overall source of CO_2 as soil respiration, although

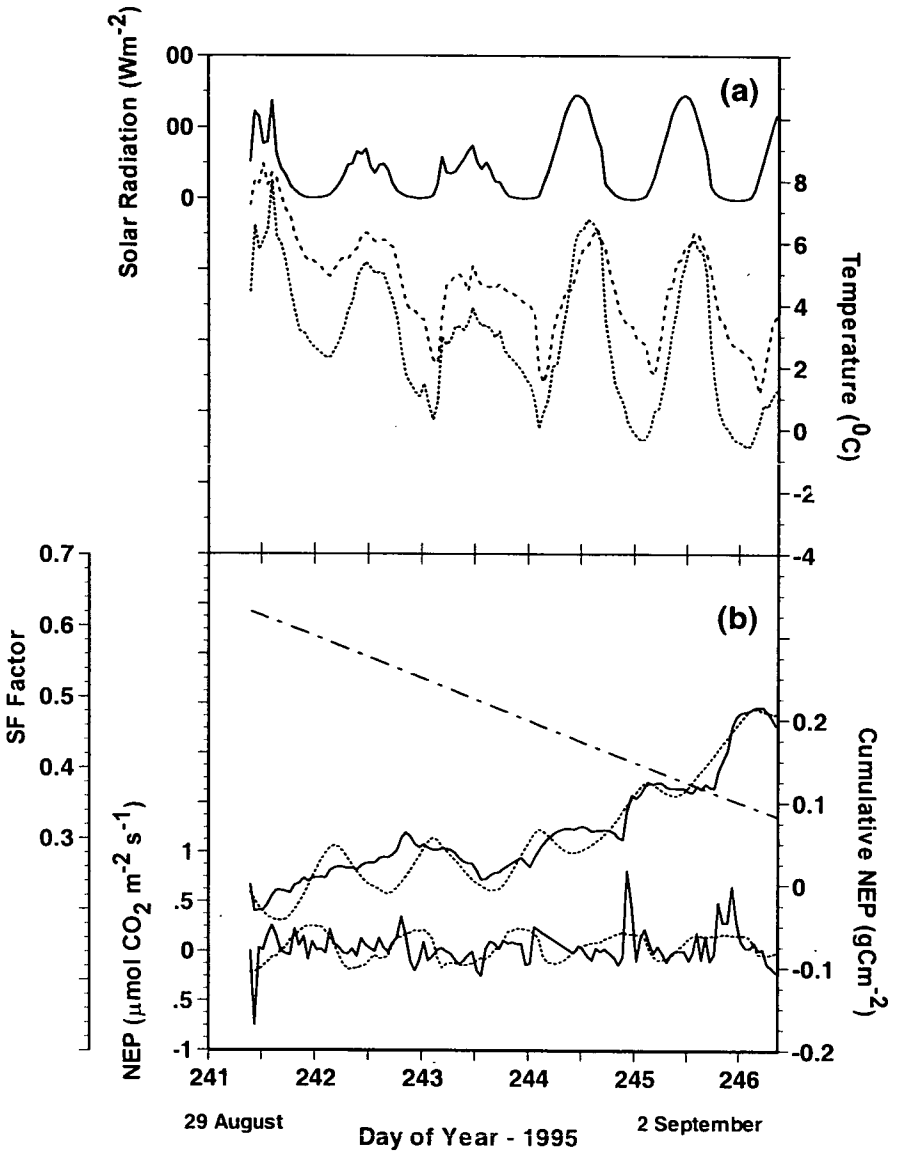

Figure 6-7 *(a) Solar radiation (solid line), air temperature (dashed line), soil temperature at 25mm (dotted line) and rainfall (columns) for the early autumn period 29 August – 3 September 1995. (b) Comparison between measured and modelled NEP for the same period. Legend is the same as for Figure 6–6 except that the change in the vegetation activity is now modelled by the Senescence Factor (SF) (dot and dash line).*

diminishing, is reducing at a slower rate than the photosynthetic uptake from the senescing vegetation. The model however shows much larger diurnal cycles than is seen in the measurements and there is evidence of a photosynthetic lag in the measurements with peak photosynthetic uptake occurring later in the diurnal cycle than the model predicts.

The model performs well, with a Willmott *d* statistic of 0.973, and with very low RMSE of 0.022, most of which again, is accounted for by unsystematic error indicating good model parameter estimation (see Table 6–4).

6.4.5 Flux measurement variability in 1995

Table 6–5 shows the mean daily value of NEP and the Standard Error of the mean for complete days during the three periods examined above. Two-thirds of the individual standard errors are less than or equal to 15% of the mean and those measurement errors above this figure are for very small overall daily NEP values.

Date (1995)	Day Number	Mean daily NEP ($gC\ m^{-2}$)	Unbiased daily SE	
			($gC\ m^{-2}$)	(% of mean)
27 June	178	0.300	0.017	6
28 June	179	0.004	0.013	361
29 June	180	-0.177	0.014	8
30 June	181	-0.093	0.010	11
30 July	211	0.102	0.015	15
31 July	212	-0.228	0.014	6
1 August	213	-0.065	0.011	17
2 August	214	-0.276	0.024	9
3 August	215	-0.295	0.016	5
4 August	216	-0.012	0.009	75
5 August	217	-0.392	0.019	5
6 August	218	-0.338	0.021	6
7 August	219	-0.298	0.017	6
8 August	220	-0.097	0.017	18
9 August	221	-0.038	0.017	44
10 August	222	-0.097	0.015	15
30 August	242	-0.037	0.009	24
31 August	243	-0.018	0.008	46
1 September	244	0.082	0.012	15
2 September	245	0.095	0.012	13

Table 6-5 *Mean and SE of the mean for each of the complete measurement days in 1995.*

The size of standard errors found at this site are comparable to those evaluated by Soegaard et al. (2000) at their Greenland site. They estimated daily standard errors to be of the order of ±15%

6.4.6 Active Season modelled NEP budget – 1995

Hourly measurements of the driving variables of the model - incoming solar radiation, air temperature, soil temperature and rainfall, were measured from 11 June to 3 September (days 162 – 246). Incoming solar radiation and rainfall measurements were missing from 10 –24 July. Auxiliary hourly measurements of net radiation, relative humidity, wind direction and replicates of air and soil temperature were also measured over this period and used to evaluate evaporation rates for the cryptogamic vegetation and for in-filling of missing data in the driving variables. The date for the final disappearance of snow was prescribed so that the growth factor value at the beginning of the first intensive CO_2 measurement (model calibration) period (i.e. 27-30 June) and in the full summer season model run were identical in value. Similarly the Senescence Factor during the late summer and autumn was prescribed to be identical in both the calibration period (29 August – 3 September) and the same period in the full summer model run. The Senescence Factor was also extrapolated backwards in time until SF equalled 1 (i.e. full activity) in the full summer season model run. The model thus suggested that the transition from full growth into senescence began around 21 August, close to the end of the period of the midnight sun.

Figure 6–8 shows the modelled estimates of individual and cumulative daily NEP from 11 June to 3 September 1995 with the measured daily CO_2 flux superimposed together with the daily rainfall. The end of snowmelt is set to occur on 27 June (day 178). Before that date, GF is zero for both vascular and cryptogamic vegetation, the outcome of the calibration of GF for the period 27 –30 June. A consequence of this is a rapid and large switch from CO_2 source to CO_2 sink as the vegetation is "switched on" at the start of the first intensive measurement period. Rapid transition from a CO_2 source to a CO_2 sink is a characteristic of the high arctic summer (Soegaard and

Nordstroem, 1999). However, the size of the switch is probably not realistic as there is evidence that cryptogamic vegetation can begin to photosynthese under snow providing light levels are sufficiently high (Kershaw, 1975; Larson and Kershaw, 1975): a process missing from the model that would have reduced the size of the overall CO_2 source. The possibility that 27 June had an anomalously high CO_2 source also cannot be discounted.

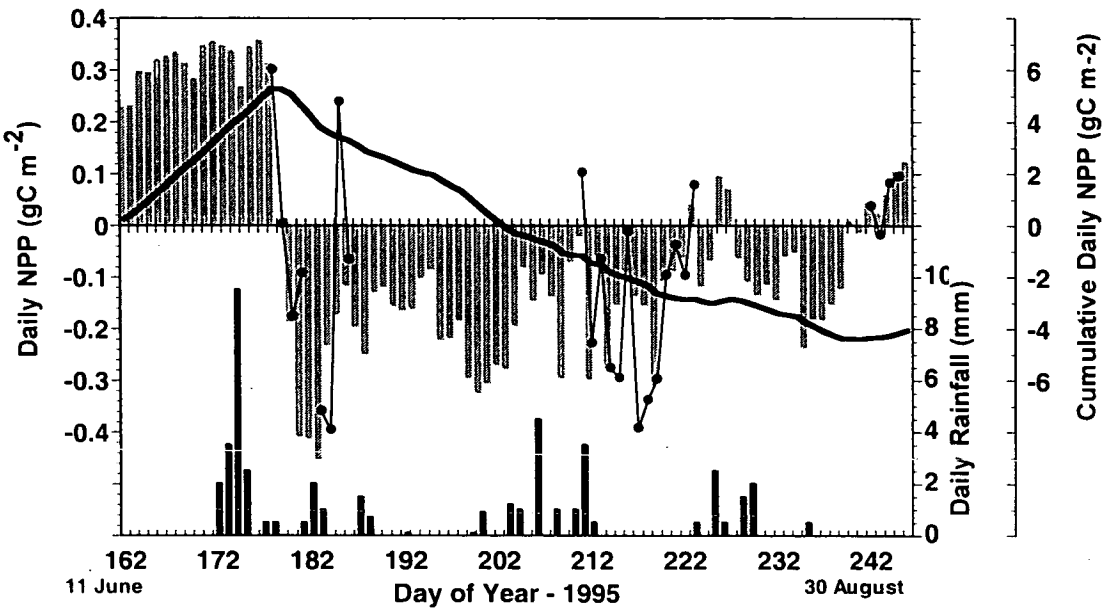

Figure 6-8 *Measured daily NEP (closed circles), modelled daily NEP (grey columns), daily rainfall (black columns) and cumulative modelled NEP (——) for the period 11 June – 3 September 1995.*

The model shows little evidence of a steady increase to a summer maximum in gross daily NEP in contrast to the results of Soegaard and Nordstroem (1999) which displayed a sinusoidal summer pattern with an evident maximum around 21 July in 1996. This is shown more clearly in Figure 6-9, where the modelled daily NEP values have been separated into the constituent NPP and soil respiration values. Soil respiration is relatively constant with NPP showing a slight seasonal pattern with the late summer senescence being apparent. Average soil respiration is 0.39 gC m^{-2} d^{-1} and NPP is 0.41 gC m^{-2} d^{-1} during this period.

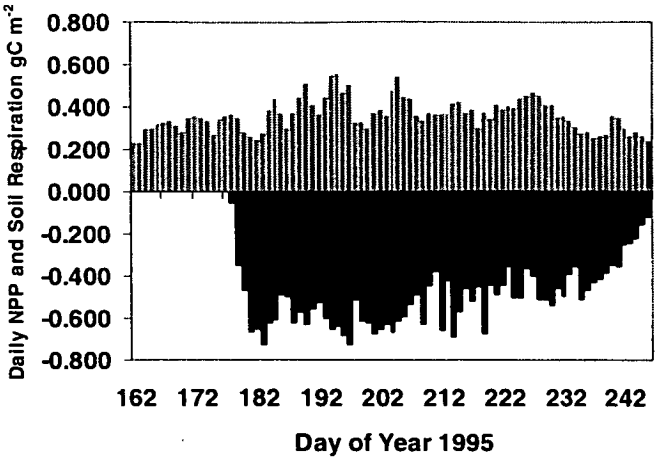

Figure 6-9 *Separation of the modelled daily NEP values into constituent NPP and soil respiration values for 1995*

For NEP, the model indicates that, while the overall daily carbon dioxide balance is a sink, the day-to-day variation is high and the model effectively predicts the response of the vegetation to periods with and without rainfall. For the period 9-24 July, when rainfall measurements were missing at the site, measurements of rainfall at Ny-Ålesund (Bruland and Marechal, 1999) of 0.7, 0.1, 0.1 and 0.9mm on 7, 11, 18 and 19 July respectively were substituted.

Overall, as shown by the modelled cumulative daily NEP curve, the 1995 active summer period had an NEP of 3.9 gC m^{-2} and was characterised by a period of carbon dioxide release to the atmosphere up to 28 June (day 179), followed by carbon dioxide uptake throughout the summer with the autumn returning to a carbon dioxide source. The active season in 1995 (28 June – 29 August), arbitrarily defined as the start and finish of prolonged daily CO_2 assimilation, produced a CO_2 assimilation of –9.7 gC m^{-2}. Confidence in these figures is examined in the sensitivity and confidence analysis in the next section.

The importance of soil respiration to the overall carbon balance of this high arctic site can be seen in Figure 6–10 where daily average soil temperature at 25mm and daily total solar radiation are overlaid on the daily NEP amounts. It is evident that the NEP balance follows closely the soil temperature that is itself dependent, in these

relatively bare soils, upon solar radiation. Such a result implies that during this period, plant assimilation was near optimal with soil respiration providing the control on the overall carbon dioxide balance.

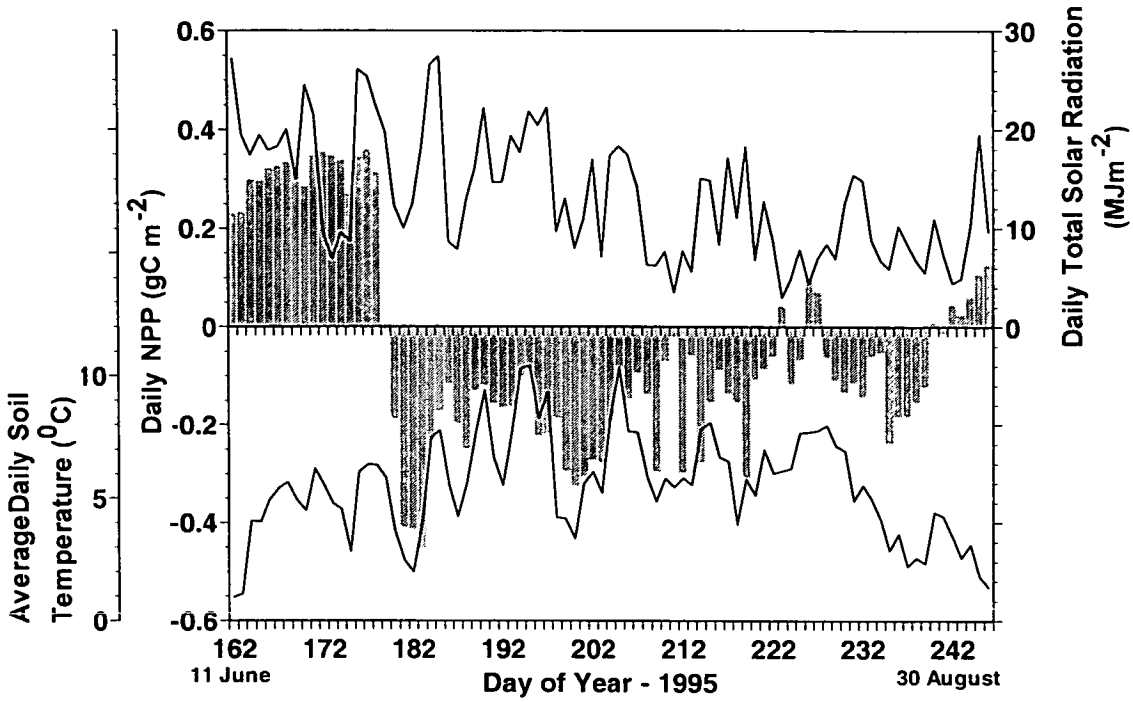

Figure 6-10 *Daily total solar radiation (upper trace) and average daily soil temperature (lower trace) superimposed on the modelled daily NEP (columns) for the period 11 June – 3 September 1995.*

6.4.7 Sensitivity analysis of model for 1995 period

The results from the sensitivity analysis of the new model parameters in the combined NEP model are shown in Table 6–6. The new model parameters have been split into two groups. Group 1 (Table 6–6(a)) consists of parameter values based on measurements either obtained at the field site or at other arctic sites. Varying these parameters, e.g. vegetation coverage, soil respiration rates, growth rate of moss as proportion of C_3 photosynthetic rate, is indicative of the effect of possible measurement error or the risk of applying nonlocal measurements.

Group 2 (Table 6–6(b)), consisting of parameters incorporated into the model to simulate moss/lichen effects on the control of the overall NEP, are either estimated from general considerations or evaluated during the optimization of the model. It is

Parameter	Default Value	-50% of Default Value‡	+50% of Default Value‡
a) Group 1 – Measured			
Soil Heat Flux as % of R_n	5	-3.802	-3.943
		-1.8%	1.9%
Respiration rate R_{10} for bare soil	0.103	-4.460	-3.270
		+15.2%	-15.5%
Respiration rate R_{10} for lichen cover	**0.6**	**-15.478**	**7.737**
		+299.8%	**-299.9%**
Respiration rate R_{10} for mixed bryophyte/vascular cover	**0.806**	**-6.896**	**-0.845**
		+78.1%	**-78.2%**
Light saturation level for moss	266	-2.741	-3.974
		-29.2%	+2.7%
Moss growth rate as proportion of C_3 rate	**0.15**	**-1.306**	**-6.436**
		-66.3%	**+66.3%**
Vegetation Cover: (Soil)(Moss-Lichen)(Vascular) (constrained by sum of cover =1: **[value]** is held at default value and other surfaces varied))	(0.2)(0.67)(0.13)		
	(0.1)**[0.67]**(0.23)	-22.27 (+475%)	
	(0.3)**[0.67]**(0.03)	14.528 (-475%)	
	(0.1)(0.77)**[0.13]**	-1.766 (-54%)	
	(0.3)(0.57)**[0.13]**	-5.975 (+54%)	
	[0.2](0.57)(0.23)	-24.374 (+530%)	
	[0.2](0.77)(0.03)	16.633 (-530%)	
b) Group 2 – Surmised and Optimised			
Wetting-up factor for moss in dew periods	0.2	-3.392	-4.015
		-12.4%	+3.7%
SoilT-DewpointT at which dew forms e.g. –1°C means dew forms when DewpointT is 1°C below soil temperature	0°C	*-1°C †*	***+1°C†***
		-2.220	**-6.749**
		-42.7%	**+74.3%**
Max. hourly evaporation for mosses	0.4	-2.075	-5.100
		-46.4%	+31.7%
No. of hrs after rain before photosynthesis can start	3	-3.657	-4.027
		-5.5%	+4.0%
Moss/Lichen Growth start day number	182	*172†*	*192†*
		-4.243	-3.274
		+9.6%	-15.4%
Moss/Lichen senescence start day number	233	*223†*	*243†*
		-3.731	No change
		-3.6%	0%
Vascular growth start day number	**182**	***172†***	***192†***
		-6.927	**2.188**
		+78.9%	**-156.5%**
Vascular senescence start day number	237	*227†*	*247†*
		-3.228	No change
		-16.6%	0%

Table 6-6 *Sensitivity analysis showing overall change in model output for variations of ±50% from the default value for each of the models' novel parameters † except for italised entries where 50% variation would have been unrealistic. For each parameter, upper figures are overall NEP for the period 11 June – 3 September 1995 (default overall NEP is 3.87 gC m^{-2}) and lower figures are percentage deviation from the default overall NEP. Parameters regarded as particularly sensitive are shown in bold type.*

within this latter group (e.g. wetting-up factor for moss in dew periods, start of growth, start of senescence) that the model must be seen to perform reasonably well, with sensible and realistic responses to perturbations.

It is evident from examining the sensitivity analysis for the measured variables that NEP is very sensitive to vegetation cover. Changing the proportion of surface covered by vascular plants by 10 per cent of the surface with no change in the proportion of the surface covered by mosses and lichens (i.e. the bare soil area increases or decreases inversely with vascular cover) produces nearly a 5-fold change in NEP. A similar change in surface cover occupied by mosses and lichens at the expense of bare soil coverage only produces a change of 54 per cent. Invasion of vascular plants into moss/lichen areas and vice-versa, with bare soil cover remaining the same, increases NEP by more than a factor of five. Climate change will alter the coverage and composition of the tundra vegetation and this result illustrates the large effect that relatively small changes in vegetation cover could have on the overall carbon dioxide budget at this site. Of the other measured parameters, the soil respiration rate, especially below the lichen cover, is also highly sensitive, indicating that a warming Arctic will increase soil respiration rates but not necessarily at rates sufficient to balance assimilation uptake.

Considering the surmised and optimised variables, it is apparent that the model is insensitive to the rate at which mosses and lichens wet up after desiccation, the length of the period following rain where liquid water on the surfaces of the leaves prevents photosynthetic activity, and the particular days on which mosses/lichens emerge from dormancy or start to senesce. However, while the timing of the start of senescence in the vascular plant community is little affected by varying the date, the model is highly sensitive to the start of vascular plant activity in the spring. This sensitivity may be explained by the effect of the near maximum radiation levels in June just after snowmelt, compared to the low light levels in early September.

6.4.8 *Model Confidence limits for 1995 period*

The driving variables and the important state parameters identified in the sensitivity analysis above were used to estimate confidence limits for the model output of the 1995 period. Simulated measurement errors of ± 5 per cent were applied to solar radiation, net radiation and relative humidity and ± 0.5°C were applied to air and soil temperature. The state parameters were varied by ± 10 per cent. Model outcomes from exploration of the variable and parameter space determined by the above error values were analysed. Model outputs ranged from -14.8 to 7.2 gC m^{-2}. The mean of the distribution of model outcomes was -4.08 gC m^{-2} (*c.f.* -3.9 gC m^{-2} for default model run) with a skewness of 0.009. By assuming normality the 1995 period had an NEP of -3.9 gC m^{-2} with a standard error of ± 3.7 gC m^{-2}.

6.4.9 *Active Season modelled NEP Budget – 1996*

To illustrate the effect that the timing of snowmelt has upon the subsequent active season NEP budget, the exact same period (days 162-246) was modelled in 1996 but extended to day 249 to include the measured fluxes on days 248 and 249. Similar variables were measured, and the same techniques as those used for the 1995 model runs were used to infill missing data and to provide evaporation rates. There was no optimisation performed on the model parameters except that the date for the final disappearance of snow and surface meltwater was set to 21 July (day 203) in accordance with the measurements of Harding and Lloyd (1998). The start date of senescence was exactly the same as for 1995 in line with evidence that the induction of autumn senescence occurs even when temperatures are favourable for growth (Shaver and Kummerow 1992). This implies some form of phenological action, possibly light intensity related, within the plant.

Figure 6–11 shows the outcome of the model simulation for 1996.

The snow covered period between 10 June and 11 July (days 162-193), when measured daily average soil temperatures at 25 mm increased from –2°C to 0°C, has a relatively constant soil respiration rate of 0.135 μmol m^{-2} s^{-1}. That soil respiration can occur at temperatures below freezing has been shown by Nakane (1978) whose results form part of the data set used by Lloyd and Taylor (1994) in the formation of

their soil respiration model. Heat penetration into the soil is sufficiently rapid that soil at 0.7m has become unfrozen by 24 July (day 206). The measurements at this time also show a consistent CO_2 source although the rate is highly variable. Measured emission rates are weakly linked to measured average daily windspeed (r^2=0.31) indicating that this variability may be the result of increased turbulence releasing stored CO_2 from within the snowpack, a process that the model is unable to simulate. From 12 July to 24 July (day 206), modelled soil respiration gradually rises as soil temperatures increase. The measurements also show a similar increase. 'Model' plant activity begins on 21 July and by 25 July has completely balanced the soil respiration. From then on, the measurements and model show the site to be a sink for carbon dioxide except for the period between 5 – 10 August when the site became a CO_2 source. This period was heavily overcast with low light levels (see solar radiation amounts on Figure 6–12) and with nearly continuous rain or drizzle. The rain maintained soil temperatures close to air temperature thus allowing soil respiration to be maintained at a relatively high level.

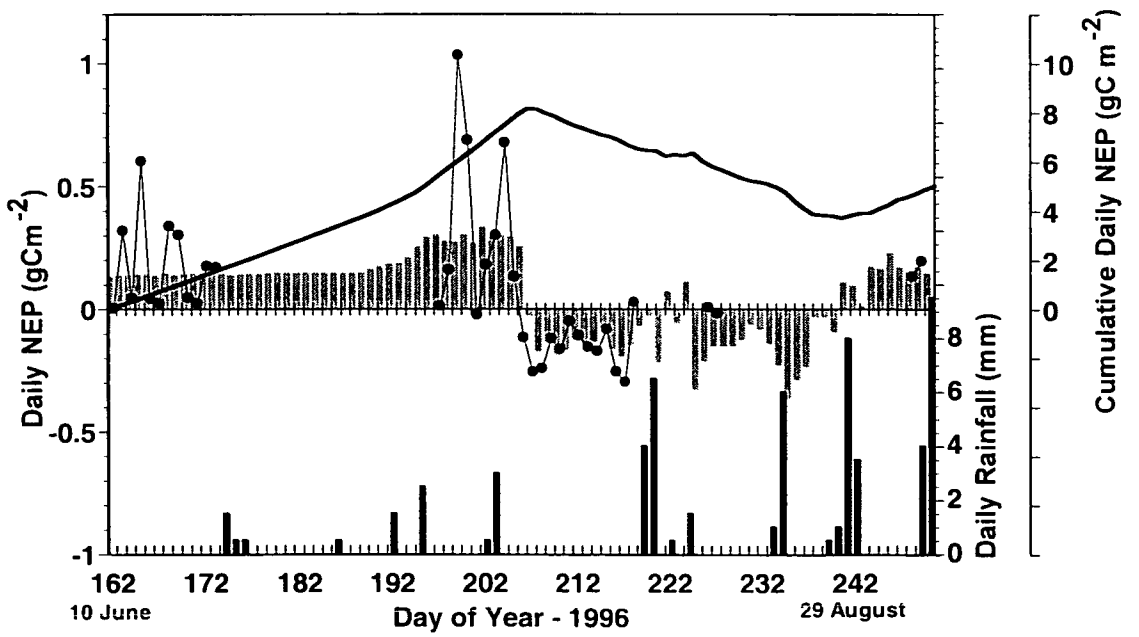

Figure 6-11 *Measured daily NEP (closed circles), modelled daily NEP (grey columns), daily rainfall (black columns) and cumulative modelled NEP (——) for the period 10 June – 6 September 1996.*

The necessity to either measure solar radiation at the vegetation surface or to record albedo for correct operation of this model is shown during the period 20 – 25 August (days 233-238). Snow fell and remained for these 5 days, as indicated by the change in albedo from bare surface values of about 10 per cent to around 70 per cent (see Figure 6–12). Soil temperatures at 25 mm also fell close to 0°C during this period. As the solar radiation was measured above the snow surface, the model produced strong daily CO_2 sinks. However, given reduced photosynthesis in the plants as a consequence of snow-cover, and reduced soil respiration at lower temperatures, it is likely that the overall carbon dioxide balance would be quite small and possibly even a source during this time.

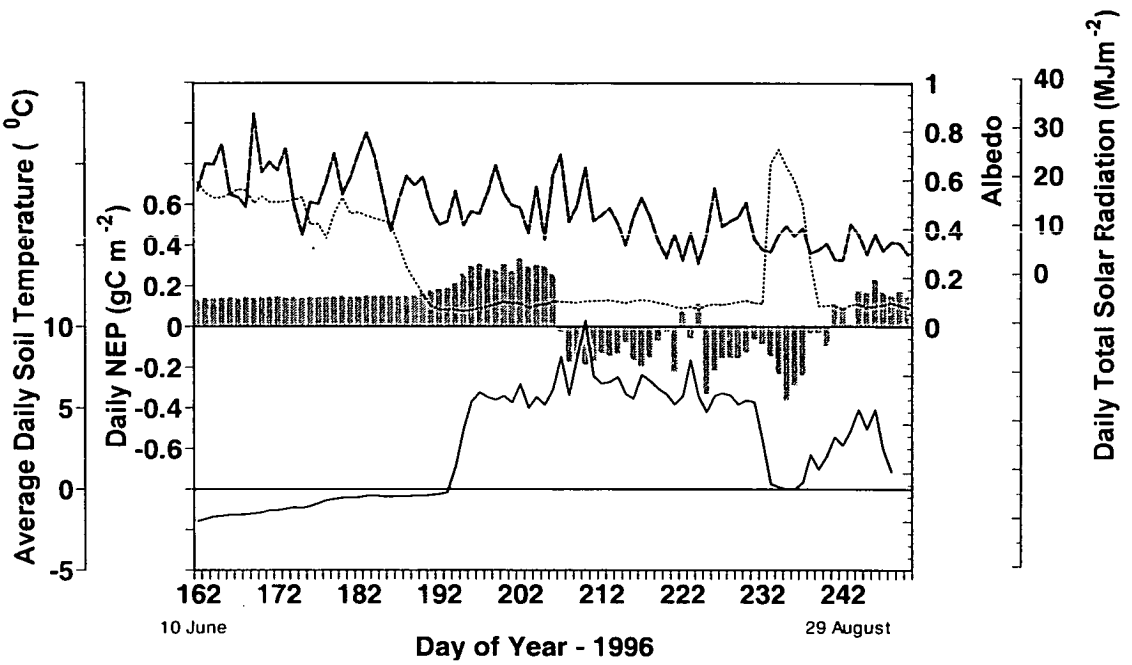

Figure 6-12 *Modelled daily NEP (grey columns), daily total solar radiation (dashed line), daily average albedo (dotted line) and daily average soil temperature at 25mm (solid line) for the period 10 June – 6 September 1996.*

A separation of modelled daily NEP in 1996 into daily NPP and soil respiration components (Figure 6-13) shows a different pattern to that shown for 1995 (Figure 6-9). In 1996, there appears to be a slight seasonality in the soil respiration values not obviously apparent in 1995. Daily NPP, due to the late disappearance of the snow cover has little opportunity to show any seasonality before the late summer

senescence begins. During this period, average daily soil respiration was 0.22 gC m^{-2} d^{-1} and NPP was 0.18 gC m^{-2} d^{-1}.

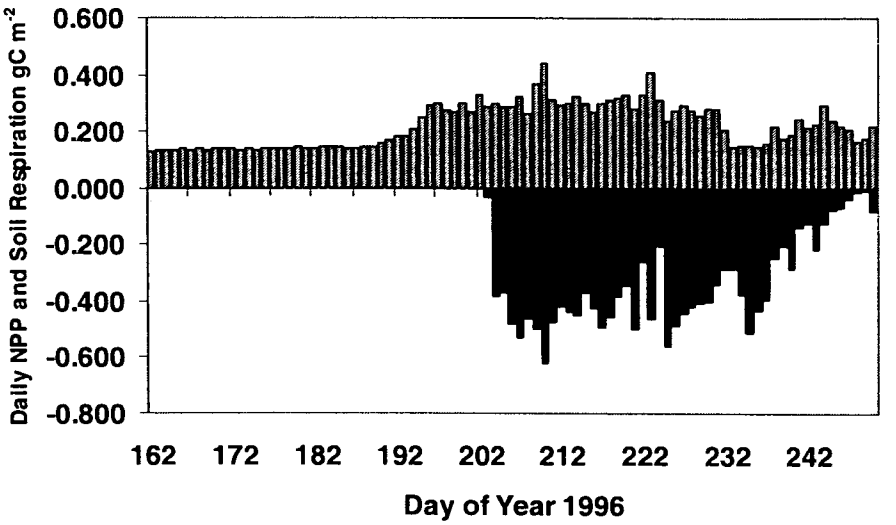

Figure 6-13 *Separation of the modelled daily NEP values into constituent NPP and soil respiration values for 1996*

The procedure used for the 1995 model run to obtain the overall standard error of the model output was applied to the model for the 1996 period. The cumulative daily NEP total depicted in Figure 6–11 shows that, in contrast to the same period in 1995, between 10 June and 6 September the site was a net source of carbon dioxide of 5.0 ± 3.3 gC m^{-2}. The active season in 1996 was much shorter (25 July – 27 August) and the surface assimilated –4.5 gC m^{-2}.

6.5 Discussion and Conclusions

The model has been shown to be capable of simulating the middle of the active season with a high degree of success. It was capable of simulating both the post snowmelt and senescent periods with reasonable success, despite the high level of heterogeneity in plant activity, snow cover and soil temperatures present at these times. Unlike other high arctic sites, the carbon dioxide balance at the polar semi-desert site during the summer is small but highly variable. The vascular plant community, with little or no water stress, appears from the model to maintain maximum photosynthetic activity throughout the active season providing light and

temperature conditions allow. The cryptogamic community are more sporadic, with photosynthetic activity only occurring after wetting of their surfaces with rain, dew or snow. Despite their much lower photosynthetic rate compared to vascular plants, the larger percentage cover of the cryptogams within the site increases their contribution to the overall assimilation rate. However, it is the variation in the soil respiration efflux, directly linked to soil temperature, which characterises the overall carbon dioxide balance during the summer season. The period between 11 June and 3 September 1995 was estimated to be a net carbon dioxide sink of 3.9 ± 3.7 gC m^{-2}.

The calibrated model was then used to simulate the active season at the site during 1996 and compared to the campaign measurements during that year. Both the end of the snowmelt and the start of senescence were prescribed, but otherwise the model was allowed to run with the parameter set for 1995. In general, the model simulates the periods when CO_2 fluxes were measured quite well. Both measurements and model indicate that the snow covered period has a net CO_2 efflux, although the model does not generate the variability seen in the measurements. This respiration may be a gradual release of CO_2 produced during the previous autumn although there is evidence that microbial production can occur in soils at temperatures below freezing. There is not the strong relationship in 1996 between soil temperature and overall CO_2 flux that was seen in 1995. This may be a consequence of the above average cloudiness in 1996, which may have limited the plant's photosynthetic activity. Wüthrich *et al.* (1998) observed that average PAR (sic) was as low as 325 µmol photons m^{-2} s^{-1}, well below the 400 µmol photons m^{-2} s^{-1} required for carbon fixation to exceed respiration in plant communities similar to those in this study. Despite this, the modelled average daily NEP during the 36 day active season period when NEP was negative (overall assimilation) was 0.139 gC m^{-2} compared to 0.161 gC m^{-2} for the same conditional 60 days in 1995.

The validation during 1996 highlighted the need to include the effects of summer snow showers on the plant photosynthetic activity. This could most easily be done by

using albedo measurements to signal snow events and modify the photosynthetic rate accordingly.

The modelling exercise was designed to provide a framework for future work. The minimal extension required to established models and simple optimisation provides the opportunity to modify parameters as data becomes available. The modelling exercise has shown that the timing of snowmelt, the frequency and duration of precipitation events during the summer and soil temperatures are the major parameters which define the overall carbon dioxide balance of this high arctic polar semi-desert site. Cloudiness and the timing of the autumn "freeze-up" are factors that may also have an important effect upon the CO2 balance but the limited data set does not provide conclusive evidence for this. The site switched from being a small sink of carbon into the vegetation during 1995 (-3.9 ± 3.3 gC m^{-2}) to a small source of carbon (5.0 ± 3.3 gC m^{-2}). from the vegetation/soil interface during the same period in 1996.

The results above are for an *active season* of only 83 days and do not represent the overall annual CO_2 budget that would need to include any possible winter time net CO_2 fluxes. Benoit *et al.* (1972) indicate that the minimum temperature for physiological activity in Arctic soils at Barrow, Alaska is –7°C, while Flanagan and Bunnnel (1980) found that litter decomposition ceased in similar soils at –7.5°C. Zimov *et al.* (1993) hypothesize that the action of permafrost formation would create a warm, dry and well-aerated microenvironment at the building front of the permafrost allowing microbial activity to continue. Such activity would also release further heat to maintain the conducive microenvironment, thus allowing biological activity to continue over much of the winter period

Figure 6-14(a) shows the progression of winter soil temperatures at the Ny-Ålesund site during 1996-97 and 1997-98 (Winter soil temperatures were not measured during 1995-1996). It is evident that biological activity and litter decomposition (on the above basis) would have been zero from February until at least the beginning of

June. From the 1997-98 data, excursions below -7°C may not be uncommon during the late autumn – early winter period.

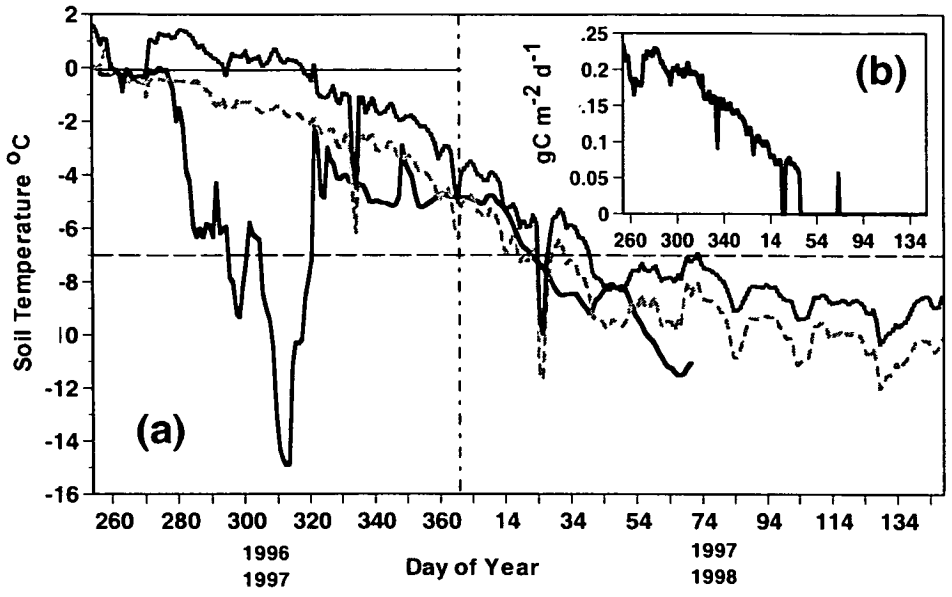

Figure 6-14 (a) *Wintertime progression of soil temperature.(——) is soil temperature at 25 mm depth during 1997-1998. (·····) and (-----) are soil temperatures at 20 and 200 mm depth respectively during 1996-1997.* **(b)** *Daily soil respiration for winter period 1996-1997, calculated from equation 6-2 and assuming R_{10} is equal to summertime value of 0.6 umol m^{-2} s^{-1}.*

Assuming that Equation 6.2 is applicable for estimating soil respiration at these temperatures, Figure 6-14(b) shows daily soil respiration amounts during the "winter" of 1996-97 above a threshold of -7°C. Total winter soil respiration through this analysis totals 23 gC m^{-2}. This must be viewed as highly speculative as the model respiration rate, R_{10} , is possibly inappropriate at these temperatures. Setting R_{10} to 0.103 μmol $_{co2}$ m^{-2} s^{-1} (the value found by Nakatsubo *et al.*(1998) for bare ground at Ny-Ålesund) reduces the winter total to 3.8 gC m^{-2}. Oechel *et al.*(1997) measured cold season CO_2 fluxes from moist Tussock tundra on the North Slope of Alaska of 0.3 gC m^{-2} d^{-1} but only 0.08 gC m^{-2} d^{-1} from Wet Sedge tundra. These are deep organic soils and probably represent upper limits to arctic wintertime soil respiration fluxes. Zimov *et al.* (1993) measured daily soil respiration rates of 0.15 gC m^{-2} d^{-1} from a site in N.E. Siberia between December and February, again in highly organic soils. These rates may not be appropriate for the polar semi-desert site

at Ny-Ålesund. However, wintertime CO_2 fluxes at the study site are probably not zero. Despite the difficulties, wintertime measurements should be attempted to establish annual total carbon balances and models should be improved in line with the measurements.

Chapter 7
Concluding Remarks

7 Concluding Remarks

The prognosis of Climate Models that the Arctic would experience a higher than average rise in temperature over the next fifty to one hundred years has focused attention on the fate of the northern organically rich soils. The possibility exists that warming of these soils will lead to increased greenhouse gas emission. The extent to which we believe this will happen is based on the forecasts from Climate models that have until now used measurements of land-atmosphere exchange from low to mid-arctic regions. The results from this thesis will hopefully broaden Climate models' prospectus to include the high Arctic. The Arctic is not all waterlogged deep organic soil bogs and fens, and a balance needs to be made between these and the extensive but organically poor high Arctic semi-deserts if climate models are to provide realistic forecasts for the effects of a warming Arctic on the world's weather. Of particular concern is whether the Arctic will become a source or sink for carbon dioxide. Several studies have indicated progression in both directions. This thesis has shown in the results from the modelling section that this site can be a source or a sink and that the fulcrum for this balance is probably the timing of snowmelt.

Eddy correlation equipment, with care and diligence, can be used in most environments and this thesis has shown that this now includes the high Arctic. Difficulties do still exist and field calibration is one of them in a climate that is often inclement even during the summer as explained in Chapter 4. Calibration is an important and necessary part of operating instruments but it is only of use if there is confidence in the calibration method and outcome. Calibration means to determine the true value (in this case measurement accuracy) of an instrument. Any process that falls short of this cannot be regarded as a calibration – it is then just a calibration procedure carried out that can effectively lead to less accurate results.

Meteorological and Climate models are driven by climate data and by surface characteristics that determine the rates of exchange of heat, water and trace gases

between the land and the atmosphere. Chapter 3, in describing the Ny-Ålesund site geographically and aerodynamically, has provided sufficient details concerning the important climate variables and resistance pathways to allow modellers to simulate this high arctic polar semi-desert. The high Arctic has a very short active season and the plants are adapted to deal with this by becoming active very quickly at the beginning of the season and maximising their growth potential over the short time available. It is therefore necessary to capture these effects by measurements at pivotal times of the active season. This thesis has focused on the snowmelt, mid summer and early autumn periods as being important phases of the Arctic summer. In Chapter 5, the partitioning of energy between evaporation, sensible heat and soil heating is explored. In contrast to temperate regions, heating of the soil is a major component of the energy balance especially during and just after snowmelt when it can consume most of the available energy. During the main summer period, evaporation is close to being equal to sensible heat, confirming other tundra study reports of evaporative ratios being close to 0.5. Evaporation in the active season in 1995 was over twice the summer rainfall – a situation that is potentially more serious for the dominant bryophyte plant community than for the vascular plants that have access to sufficient soil moisture. Despite being a shorter season, the summer of 1996 had a higher total of rainfall – not all of which was evaporated back into the atmosphere. Evaporation and sensible heat followed daily trends not unlike those at lower latitudes, if somewhat smaller. Evaporation and heating of the air continued throughout the 24-hour cycle as available energy remained positive throughout the summer until late July when net radiation, despite the polar day, began to be negative at night. The same cannot be said of the carbon dioxide fluxes, which at first sight show little pattern. There is little sign of the steady progression from dominant winter soil respiration to dominant summer assimilation observed at other lower latitude Arctic sites. The plant assimilation and soil respiration terms are of similar size at this site with the climate rather than any control by the plant community defining the overall balance. The three pivotal periods of the active season show highly different daily CO_2 fluxes with post snowmelt exhibiting somewhat chaotic values due to the inherent heterogeneity caused by snow patches and vegetation

emerging gradually from winter dormancy. The summer period shows a pattern during the day more akin to normal behaviour with assimilation fluxes dominating midday hours. The early autumn has very small fluxes with a balance between soil respiration and any remaining plant assimilation (probably mostly from the bryophytes) during midday with soil respiration dominating at night. On occasions when frost effectively stops any plant assimilation, the soil respiration probably approaches a maximum for that time of year.

Highly complicated photosynthetic models of plant assimilation have been created for C_3 and C_4 vascular plants. While the consensus was that bryophytes also assimilated carbon dioxide via the C_3 pathway, there had not been, to my knowledge, until this thesis any attempt to apply such a model to bryophyte-dominated landscapes. That there exists such a possibility is important for models as current models can then be run with little modification – just a different parameter set and driving data. By combining established soil respiration and C_3 plant assimilation models with an appreciation of the hydration strategy of bryophytes, this thesis has provided such a tool. Of particular note is the ability of the model to simulate the changes from dominant respiration to dominant assimilation especially at the pivotal times of the year. Inevitably there was some uncertainty in the value of some of the new parameters required to extend the model to a polar semi-desert. These parameters were calibrated with the 1995 active season data. The model then provided estimates of net ecosystem production for 1996 that were largely in accord with the measurements despite 1996 being, climatically, quite a different year to 1995. The model also highlighted the extent to which soil temperature and hence soil respiration rates control the overall CO_2 balance when light is not limited. While the overall net ecosystem productivity rates during mid-summer look similar, those in 1996 were lower overall than in 1995 indicating that possibly incoming radiation can often drop below plant photosynthesis saturation light levels even in mid-summer. Whether the high Arctic becomes warmer and wetter or warmer and drier, this thesis has, hopefully, provided a simple but effective model to explore the consequences.

As with all scientific experiments, there were measurements not taken, not taken seriously enough, or outside of this person's expertise. The size of the soil heat flux and the difficulty in obtaining measurement values that were sensible enough to be used in an energy closure exercise leads me to believe that greater effort must be placed in gaining a good estimate of areal soil heat flux. Single point measurements are of little benefit in heterogeneous terrain and development of instruments to measure net radiation and soil heat flux at the scale of eddy correlation flux measurements will help the energy closure problem.

According to the model, the site effectively either gained or lost about 5 gC m^{-2} over the prescribed 80 days of the active season. The combined litter and visible organic layer is typically some 25 mm thick. Such a thin layer could eventually disappear if the result of 1996 were to become the norm. The result in 1996 may be just an excursion from what has been largely a history of overall plant assimilation. Nevertheless, it would be interesting to assess the total carbon stock in what appears to be a largely mineral soil.

As with any micrometeorological experiment, results from two years data can never tell the whole picture. Fortuitously, 1995 and 1996 provided conditions which switched the site from a sink to a source of CO_2. Further research is needed to establish the frequency of the source-sink switch and the general pattern to which way it is heading. This was a micrometeorological experiment carried out by a non-expert in either plant physiology or soil physics. Future research must be geared to uniting the particular talents of all three communities

References

References

Addison, P.A., 1977. Studies on evapotranspiration and energy budgets on Truelove Lowland. In *Truelove Lowland, Devon Island, Canada: A high Arctic Ecosystem.* Ed. Bliss,L.C.,University of Alberta,Edmonton, 540pp.

Addison, P.A. & Bliss, L.C., 1980. Summer climate, microclimate, and energy budget of a polar semidesert on King Christian Island, N.W.T., Canada. *Arctic and Alpine Research* **12(2),** 161-170.

Ahrnsbrak, W.F. 1968. Summertime radiation balance and energy budget on the Canadian tundra. Technical Report No. 37, Task No. NR 387-022, ONR Contract No. 1202 (07), Madison, Department of Meteorology, University of Wisconsin.

Anderson, D.M. & Tice, A.R., 1970. Low-temperature phases of interfacial water in clay-water systems. *Soil Sci.Soc.Am.Proc.* **35,** 47-54.

Ångström, A., 1924. Om markbetäckningensinflytande på lyusklimatet. *Teknisk Tidskrift* **54,** 297.

Ångström, A. & Tryselius, O., 1934. Total radition from sun and sky in Abisko. *Geografiska Annaler* **16,** 53-69.

Balakov, S.A., Deryugin, B.A. & Sychev, K.A. and others., 1959. Radiatsonnyi teplovoi balans poverkhnosti sushi v Arktike (Radiation and heat balance on the Earth's surface in the arctic), *Trudy Glavnaya Geofizicheskaya Observatoriya* **92,** 102-126.

Barry, R.G., Courtin, G.M. & Labine, C., 1981. Tundra climate. In Bliss,L.C. *et al.*, Eds., *Tundra Ecosystems: A Comparative Analysis*, Intern. Biol. Program 25, Cambridge Univ. Press, 81.

Bellisario, L.M., Boudreau, L.D., Verseghy, D., Rouse, W.R. & Blanken, P.D., 2000. Comparing the performance of the Canadian Land Surface Scheme (CLASS) for two subarctic terrain types. *Atmosphere-Ocean* **38,** 181-204.

Benoit, R.E., Campbell, W.B. and Harris, R.W., 1972. Decomposition of organic matter in the Wet Meadow Tundra, Barrow. A revised word model. In *Proceedings of the 1972 Tundra Biome Symposium* J.Brown (Ed), Tundra Biome Center, University of Alaska, Fairbanks, pp 111-115.

Berlyand, T.G., 1967. Climatological research into the thermal balance. In Budyko,M.I., Ed. Voeikov Main Geophysical Observatory 1917-1967. *Trans. of the Main Geophys. Observatory.* No.218: 98-110

Billings, W.D., Luken, J.O., Mortensen, D.A., & Peterson, K.M. 1982. Arctic tundra: A source or sink for atmospheric carbon dioxide in a changing environment. *Oecologia*, **53**, 7-11.

Bliss, L.C. 1977. Truelove Lowland, Devon Island, Canada: A high Arctic Ecosystem. Edmonton, University of Alberta.707pp.

Bliss, L.C. & Matveyeva, N.V., 1992. Circumpolar Arctic Vegetation. *In* "Arctic Ecosystems in a Changing Climate - An Ecophysiological Perspective" (Chapin,F.S.,III, Jefferies,R.L., Reynolds,J.F., Shaver,G.R. & Svoboda,J. eds.), pp 59-89, Academic Press Inc., San Diego.

Bouyoucos, G.J., 1921. A new classification of soil moisture. *Soil Sci.* **11,** 33-47.

Brattbakk, I. (1981). *Vegetasjonskart S10 V28H60* (vegetation map) 1:10,000. Ny-Ålesund, Brøggerhalvøya, Svalbard. K.Norske Videnske. Selsk. Mus.Bot. avd. Trondheim.

Briggs, G.A., 1973. Diffusion estimates for small emissions. ATDL Contribution No.79 Atmospheric Turbulence and Diffusion Laboratory, Oak Ridge, Tenn.

Brown, R.J.E., 1965. Some observations on the influence of climatic and terrain features on permafrost at Norman Wells, N.W.T., Canada. *Can. J. Earth Sci.*, **2,** 15-31.

Bruland, O. & Maréchal, D. 1999. Energy and water balance of Active layer 1991-1994: Understanding Land Arctic Physical Processes 1996-1998. SINTEF Report No. STF22 A98417, Trondheim, Norway. ISBN 82-14-00835-2.

Brutsaert, W., 1979. Heat and mass transfer to and from surfaces with dense vegetation or similar permeable roughness. *Boundary-Layer Meteorol.* **16,** 365-388.

Brutsaert, W., 1984. *Evaporation into the Atmosphere*. D.Reidel, Dordrecht, Netherlands, 299pp.

Bryson, R.A., 1956. Preliminary estimates of the surface heat budget, summer, clear days at Point Barrow, Alaska. Department of Meteorology, Univ. of Wisconsin, Madison,Wisconsin.

Bryson, R.A. & Kuhn, P.M. 1962. Some regional heat budget values for northern Canada. *Geographical Bulletin*, **4 (17),** 57-65

Businger, J.A. & Yaglom, A.M., 1971. Introduction to Obukhov's paper on "Turbulence in an atmosphere with a non-uniform temperature", *Boundary-Layer Meteorol.* **2,** 3-6.

Calder, K.L., 1949. Eddy diffusion and evapoartion in flow over aerodynamically smooth and rough surfaces: A treatment based on laboratory laws of turbulent flow with special reference to conditions in the lower atmosphere. *Quart.J.Mech.Appl.Math.* **2,** 152-176.

Challinor, A., 1967: The structure of Brøggerhalvoya, Spitsbergen. *Geological Magazine* **104,** 322-336.

Chamberlain, A.C., 1966. Transport of gases to and from grass and grass-like surfaces. *Proc.Roy.Soc.London* **A290,** 236-265.

Chamberlain, A.C., 1968. Transport of gases to and from surfaces with bluff and wave-like roughness elements. *Quart.J.Roy.Meteorol.Soc.* **94,** 318-332.

Chapin, F.S., III, 1991. Integrated responses of plants to stress. *Bioscience* 41: 29-36.

Chapin, F.S., III, & Shaver,G.R., 1985. Individualistic growth response of tundra plant species to environmental manipulations in the field. *Ecology* **66**, 564-576.

Cheng, G., 1983. The mechanism of repeated-segregation for the formation of thick layered ground ice. *Cold Regions Science and Technology* **8,** 57-66.

Chernigovskii, N.T., 1961. Nekotorye kharakteristiki radiatsionnogo klimata Tsentral'noy Arktiki (Some characteristics of the radiation climate of the Arctic). Trudy Arktikiy I Antarktikiy Nauchno-Issledovatel'skiy Institut, Tom 253, Leningrad, Gidrometeoizdat.

Chernigovskii, N.T. & Marshunova, M.S., 1965. *Klimat Sovetskoy Arktiki, Radiatsionnyy rezhim (Climate of the Soviet Arctic, radiation regime)*, Leningrad, Gidrometeoizdat..

Christensen, T.R. 1991. Arctic and sub-arctic soil emission: possible implications for global climate change. *Polar Record* **27(162),** 205-210.

Christensen, T.R., 1993. Methane emission from Arctic tundra. *Biogeochem.* **21,** 117-139.

Christensen, T.R., Friborg, T., Sommerkorn, M., Kaplan, J., Illeris, L., Soegaard, H., Nordstroem, C. & Jonasson, S., 2000. Trace gas exchange in a high-arctic valley. 1. Variations in CO_2 and CH_4 flux between tundra vegetation types. *Global Biogeochemical Cycles* **14(3),** 701-714.

Church, J.E., 1941. Climate and evaporation in Alpine and Arctic Zones. Meteorological studies A. Reports of the Greenland Expeditions of the University of Michigan, *Part II Meteorology, Physiography and Botany,* Greenwood Press, New York

Collatz, G.J., Ball, J.T., Grivet, C. & Berry, J.A. 1991. Physiological and environmental regulation of stomatal conductance, photosynthesis and transpiration: a model that includes a laminar boundary layer. *Agric. and For. Meteorol.* **54,** 107-136.

Colman, E.A. & Hendrix,T.M., 1949. The fiberglas electrical soil-moisture instrument. *Soil Sci.* **67,** 425-438.

Courtin, G.M. & Labine,C.L., 1977. Microclimatological studies on Truelove Lowland. In *Truelove Lowland, Devon Island, Canada: A high Arctic Ecosystem.* Ed. Bliss,L.C.,University of Alberta,Edmonton, 540pp.

Cox, P.M., Huntingford, C. & Harding, R.J. 1998. A canopy conductance and photosynthesis model for use in a GCM land surface scheme. *J.Hydrol.* **212-213,** 79-94.

Cox, P.M., Betts, R.A., Bunton, C.B., Essery, R.L.H., Rowntree, P.R. & Smith, J. 1999. The impact of new land surface physics on the GCM simulation of climate and climate sensitivity. *Climate Dynamics* **15,** 183-203.

Coyne, P.I. & Kelley, J.J. 1975. CO_2 exchange over the Alaskan Arctic Tundra: Meteorological assessment by an aerodynamic method. *Journal of Applied Ecology*, **12,** 587-611.

Coyne, P.I. & Kelley, J.J. 1978. Meteorological Assessment of CO_2 Exchange over an Alaskan Arctic Tundra. In L.L. Tieszen (Ed.), *Vegetation and Production Ecology of an Alaskan Arctic Tundra.* New York: Springer-Verlag. pp. 300-321

Dahlgren,L. 1974. Solar radiation climate near sea level in the Canadian Arctic Archipelago, Meddelande Nr. 121, Uppsala, Meteorologiska Institutionen, Uppsala Universitet

De Bruin, H.A.R. & Moore, C.J., 1985. Zero plane displacement and roughness length for tall vegetation, derived from a simple mass conservation hypothesis. *Boundary-Layer Meteorol.***31,** 39-49.

Demidov, V.V., Ostroumov, V.Y., Nikitishena, I.A. & Lichko, V.I. 1995. Seasonal freezing and soil erosion during snowmelt. *Eurasian Soil Sci.*, **28,** 78-86.

Dolman, A.J., Lloyd, C.R. & Culf, A.D., 1992. Aerodynamic roughness of an area of natural open forest in the Sahel. *Ann. Geophys.* **10,** 930-934.

During, H.J., 1992. Ecological classifications of bryophytes and lichens. *In* "Bryophytes and Lichens in a Changing Environment" (Bates,J.W. and Farmer, A.M., eds.) pp. 1-31. Oxford Science Publications, Clarendon Press, Oxford.

Dyer, A.J., 1974. A review of flux-profile relationships. *Boundary-Layer Meteorol.* **7,** 363-372.

Dziadowiec,H. 1983. Preliminary studies on carbon dioxide evolution from tundra soils of Spitsbergen (Kaffiöyra, Oscar II Land, NW Spitsbergen). *Acta Universitatis Nicolai Copernici* **18,** 159-167.

Ershov, E.D., Cheverev, V.G., Lebedenko, Yu P. & Shevchenko, L.V., 1980. Water migration, formation of texture and ice segregation in freezing and thawing clayey soils. *Third International Conference on Permafrost, 10-13 July 1978, Edmonton, Alberta, Part 1: English translations of twenty-six of the Soviet papers.* National Research Council of Canada Publication 18119, Ottawa, Canada, pp. 159-175.

Fahnestock, J.T., Jones, M.H., Brooks, P.D., Walker, D.A. & Welker, J.M. 1998. Winter and early spring CO_2 efflux from tundra communities of northern Alaska. *Journal of Geophysical Research,* **103,** 29,023-29,027.

Fan, S.M., Wofsy, S.C., Bakwin, P.S., Jacob, D.J., Anderson, S.M., Kebabian, P.L., McManus, J.B., Kolb, C.E. & Fitzjarrald, D.R. 1992. Micrometeorological measurements of CH_4 and CO_2 exchange between the atmosphere and subarctic Tundra. *Journal of Geophysical Research,* **97 No. D15,** 16627-16643.

Flanagan, P.W. and Bunnell, F.L. 1980. Microflora activities and decomposition. In *An Arctic Ecosystem: The Coastal Tundra at Barrow, Alaska.* J.Brown, P.C.Miller, L.L.Tiezen and F.L.Bunnell (Eds), Van Nostrand Reinhold, New York, pp 291-334.

Fitzjarrald, D.R. & Moore, K.E., 1992. Turbulent transport over tundra. *J. Geophys. Res.* **97,** 16717-16729.

Fowler, D., Hargreaves, K.J., Skiba, U., Milne, R., Zahniser, M.S., Moncrieff, J.B., Beverland, I.J. & Gallagher, M.W., 1995. Measurements of CH_4 and N_2O fluxes at the landscape scale using micrometeorological methods. *Philosophical Transactions of the Royal Society of London,A* **351,** 339-356.

Funk, D.W., Pullman, E.R., Peterson, K.M., Crill, P.M. & Billings, W.D. 1994. Influence of water table on carbon dioxide, carbon monoxide, and methane fluxes from taiga bog microcosms. *Global Biogeochemical Cycles,* **8,** 271-278.

Gash, J.H.C. 1986. A note on estimating the effect of limiting fetch on micrometeorological evaporation measurements. *Boundary-Layer Meteorol.* **35,** 409-413.

Gash, J.H.C., Shuttleworth, W.J., LLoyd, C.R., André, J.-C., Goutorbe, J.-P. & Gelpe, J., 1989. Micrometeorological measurements in Les Landes Forest during HAPEX-Mobilhy. *Agric. and For. Meteorol.* **46,** 131-147.

Garratt, J.R. 1994. The Atmospheric Boundary Layer. Cambridge University Press, Cambridge, UK, 316pp.

Garratt, J.R. & Francey, R.J., 1978. Bulk characteristics of heat transfer in the unstable, baroclinic atmospheric boundary layer *Boundary-Layer Meteorol.* **15,** 399-421.

Gavrilova, M.K., 1963. Radiatsionnyi klimat arktiki. Leningrad, *Gidrometeorologicheskoe Izdatel'stvo.* (English translation: Radiation Climate of the Arctic. Jerusalem, *Israel Program for Scientific Translations*, 1966).

Gel'fan, A.N. 1989. Comparison of two methods of calculating soil freezing depth. *Meteorologiya i Gidrologiya* , **2,** 98-104.

Gimingham, C.H. & Smith, R.I.L. 1971. Growth form and water relations of mosses in the maritime Antarctic. *British Antarctic Survey Bulletin* **25,** 1-21.

Gorham, E., 1991. Northern peatlands: Rôle in the carbon cycle and probable responses to climatic warming. *Ecol. Applic.* **1,** 182-195.

Gregersen, O. & Eidsmoen, T., 1988. Permafrost conditions in the shore area at Svalbard. In *Permafrost, 5th International Conference on Permafrost*, 2-5 Aug 1988, Trondheim.

Grulke, N.E., Riechers, G.H., Oechel, W.C., Hjelm, U. & Jaeger, C. 1990. Carbon balance in tussock tundra under ambient and elevated atmospheric CO_2. *Oecologia*, **83**, 485-494.

Gryning, S.E., Hotslag, A.A.M., Irwin, J.S. & Sivertsen, B., 1987. Applied dispersion modelling based on meteorological scaling parameters. *Atmos. Environ.* **21,** 79-89.

Gusev, Y.M. & Yasitskiy, S.V. 1990. Effect of mulch on winter soil temperature conditions. *Pochvovedeniye*, 46-54.

Gusev, E.M., Busarova, O.Ye. & Yasinskii, S.V. 1997. A mesoscale model of soil freezing dynamics. *Meteorologiya i Gidrologiya*, **5,** 54-60.

Hagen, J.O., Korsen, O.M. & Vatne, G., 1991. Drainage pattern in a subpolar glacier: Brøggerbreen, Svalbard. *In*: Gjessing,Y., Hagen,J.O., Hassel,K.A., Sand,K. & Wold,B. (eds.): Arctic Hydrology, present and future tasks. *NHP-Report* 23, pp 121-131.

Hagen, J.O. & Lefauconnier, B., 1993. Reconstructed runoff from the high arctic basin Bayelva in Svalbard based on mass-balance measurements. *In*: Prowse,T.D., Ommanney,C.S.L. and Ulmer,K.E. (eds.) *Proceedings of the 9th international Northern Research Basin Symposium/Workshop, Canada 1992, NHRI-symposium* 10, pp 155-168.

Halldin, S. & Lindroth, A., 1992. Errors in net radiometry: Comparison and evaluation of six radiometer designs. *J.Atmos.Ocean.Tech* .**9,** 762-783.

Hamilton, J.D., Kelly, C.A., Rudd, J.W.M., Hesslein, R.H. & Roulet, N.T., 1994. Flux to the atmosphere of CH_4 and CO_2 from wetland ponds on the Hudson Bay lowlands (HBLs). *Journal of Geophysical Research* **99(D1),** 1495-1510.

Hand, I.F., 1941. A summary of total solar and sky radiation measurements in the United States. *Mon. Wea.Rev.*, **69,** 95-125.

Harding, R.J. & Lloyd, C.R. 1998. Fluxes of water and energy from three high latitude tundra sites in Svalbard. *Nordic Hydrology* **29,** 267-284.

Harding,R.J., Huntingford,C. & Cox,P.M. 2000. Modelling long-term transpiration measurements from grassland in southern England. *Agric. And For. Meteorol.* **100,** 309-322.

Harper, J.R. & Wiseman Jr., W.J., 1977. Temporal variation of surface roughness over a tundra surface. *J.Geophys.Res.* **82,** 3495-3497.

Harvey, L.D.D., 1988. On the role of high latitude ice, snow, and vegetation feedbacks in the climatic response to external forcing changes. *Clim.Change* **13,**191-224.

Hatfield, J.L., 1989. Aerodynamic properties of partial canopies. *Agric. and For. Meteorol.* **46,** 15-22.

Heathcote, N.H. & Armitage, A., 1959. The first International Polar Year. *Annals of the International Geophysical Year, Vol. 1:* 6-98. Pergamon Press, London.

Hicklenton, P.R. & Oechel, W.C. 1976. Physiological aspects of the ecology of *Dicranum fiscescens* in the subarctic. 1. Acclimation and acclimation potential of CO_2 exchange in relation to habitat, light, and temperature. *Can. J. Botany.* **54,** 1104-1119.

Hisdal, V., 1985. The Geography of Svalbard. Norsk PolarInstitutt, Oslo, 75pp.

Homén, Th., 1897. Der tägliche Wärmeumsatz im Boden und die Wärmestrahlung zwischen Himmel und Erde. *Acta Societatis Scientiarum Fenniae* **23 (3).**

Horst,T.W. 1999. The footprint for estimation of atmospheric-surface exchange fluxes by profile techniques. *Boundary-Layer Meteorol.* **90,** 171-188.

Huntingford,C., Cox,P.M. & Lenton,T.M. 2000. Contrasting responses of a simple terrestrial ecosystem model to global change. *Ecological Modelling* **134,** 41-58.

Husebye, S. 1994. Studies of Erosion and Sediment Transport at Svalbard. *In*: Sand,K. and Killingtveit,Å. (eds.) *Proceedings of the 10th International Northern Research Basins Symposium and Workshop, Spitsbergen, Norway, Aug 28 - Sep. 3 1994.*, pp 232-250.

IPCC. 1990.*Climate Change: The IPCC Scientific Assessment,* J.T.Houghton, G.J.Jenkins. and J.J.Ephraums (eds.), Cambridge University Press, Cambridge, UK, 365pp.

IPCC. 1996. *Climate Change: The Science of Climate Change,2nd Assessment report of the Intergovernmental Panel on Climate Change* J.T.Houghton, L.G.Meira Filho, B.A.Callander, N.Harris, A.Kattenberg, and K.Maskell, (eds.) Cambridge University Press, Cambridge, UK, 572pp.

Jarvis, P.G. 1976. The interpretation of the variances in leaf water potential and stomatal conductance found in canopies in the field. *Phil.Trans.Roy.Soc.* (Lond.) **B273,** 593-610.

Jones, H.G., 1992. Plants and Microclimate: a quantitative approach to environmental plant physiology. 2nd Ed. Cambridge University Press. 428pp.

Jones, M.H., Fahnestock, J.T., Walker, D.A., Walker, M.D. & Welker, J.M. 1998. Carbon dioxide fluxes in moist and dry arctic tundra during the snow-free season: Responses to increases in summer temperature and winter snow accumulation. *Arctic and Alpine Research, 30,* 373-380.

Jones, M.H., Fahnestock, J.T. & Welker, J.M. 1999. Early and late winter CO_2 efflux from Arctic tundra in the Kuparuk River watershed, Alaska, U.S.A. *Arctic, Antarctic and Alpine Research*, **31,** 187-190.

Kaimal, J.C. & Businger, J.A., 1963. A continuous-wave sonic anemometer-thermometer. *J.Appl. Meteorol.*, **2,** 156-164.

Kaimal, J.C. & Gaynor, J.E., 1991. Another look at sonic anemometry. *Boundary-Layer Meteorol.*, **56,** 401-410.

Kallio, P. & Heinonen, S. 1973. Ecology of *Rhacomitrium lanuginosum* (Hedw.) Brid. *Reports from the Kevo Subarctic Research Station.* **8,** 63-72.

Kallio, P. & Kärenlampi, L. 1975. Photosynthesis in mosses and lichens. In: *Photosynthesis and productivity in different environments.* IBP 3. J.P.Cooper (Ed), Cambridge: Cambridge University Press, pp.393-423.

Kane, D.L., Gieck, R.E. & Hinzman, L.D., 1990. Evapotranspiration from a small Alaskan Arctic watershed. *Nordic Hydrology* **21,** 253-272.

Kattenberg, A., Giorgi, F., Grassl, H., Meehl, G.A., Mitchell, F.B., Stouffer, R.J., Tokioka, T., Weaver, A.J. & Wigley, T.M.L. (1996). Climate models - Projections of future climate. In: *Climate Change 1995. The Science of Climate Change* (eds. J.T.Houghton, L.G. Meira Filho, B.A.Callander, N.Harris, A.Kattenberg & K.Maskell), pp. 285-357. Cambridge University Press, Cambridge.

Kershaw, K.A. 1975. Studies on lichen-dominated systems. XIV: The comparative ecology of *Alectoria nitidula* and *Cladina alpestris*. *Can. J. Botany* **53,** 2608-2613.

Kondratyev, K.Y.A., 1969. *Radiation in the Atmosphere*, Academic Press, New York, 912pp.

Korotkevich, Y.S. 1967. Polar Deserts. *Soviet Antarctic Exped. Inform. Bull.* **6(65),** 459-472. (Scripta Technica trans.; 6(65): 5-29 in original Russian)

Kustas, W.P., Prueger, J.H., Hipps, L.E., Hatfield, J.L. & Meek, D., 1998. Inconsistencies in net radiation estimates from use of several models of instruments in a desert environment. *Agric. and For. Meteorol.* **90,** 257-263.

Landsberg,J.J. 1977. Some useful equations for biological studies. *Experimental Agriculture* **13,** 273-286.

Lange, O.L., Tenhunen, J.D., Harley, P. & Walz, H. 1985. Methods for field measurements of CO_2 exchange: Diurnal courses of net photosynthesis capacity of lichens under Mediterranean climate conditions. In *Lichen Physiology and Cell Biology* ed. D.H.Brown, pp.23-39. Plenum, New York.

Larson, D.W. & Kershaw, K.A. 1975. Studies on lichen-dominated systems. XI: Lichen-heath and winter snow cover. *Can. J. Botany* **53,** 621-626.

Latimer, J.R. & Truhler, E.J. 1967. A survey of the measurement of solar and atmopheric radiation in Canada. Proceedings of the first Canadian conference on micrometeorology, part I, Toronto, Meteorological Branch, Department of Transport, p.116-135.

Leclerc, M.Y. and Thurtell, G.W. 1990. Footprint prediction of scalar fluxes using a Markovian Analysis. *Boundary-Layer Meteorol.* **52,** 247-258.

Lettau, H., 1969. Note on aerodynamic roughness-parameter estimation on the basis of roughness element description. *J.Appl. Meteorol.* **8,** 828-832.

Liestøl, O., 1977. Pingos,springs and permafrost in Spitsbergen. *Norsk Polarinstitutts Årbok 1975*, pp. 7-29.

Liestøl, O., 1980. Permafrost conditions in Spitsbergen. *Frost action in soils.*Oslo. Publication No.21.

Lloyd, C.R., Shuttleworth, W.J., Gash, J.H.C. & Turner, M., 1984. A microprocessor system for eddy correlation. *Agric. For. Meteorol.*, **33,** 67-80.

Lloyd, C.R., Gash, J.H.C. & Sivakumar,M.V.K., 1992. Derivation of the aerodynamic roughness parameters for a Sahelian savannah site using the eddy correlation technique. *Boundary-Layer Meteorol.* **58,** 261-271.

Lloyd, C.R., 1994. An investigation of an inhomogeneous surface in HAPEX-Sahel using a three-dimensional plume diffusion model. *Ann. Geophys.*, **12** (Suppl.2) : C336.

Lloyd, C.R., 1995. The effect of heterogeneous terrain on micrometeorological flux measurements. *Agric. and For. Meteorol.*, **73,** 209-216.

Lloyd, C.R., Harding, R.J. & Robinson, M. (1996). Preliminary results of energy and water balance from two tundra sites in Svalbard. *Proc. 10th International Northern Research basins Sym.,* Spitsbergen, 1994.

Lloyd, C.R., Bessemoulin, P., Cropley, F.D., Culf, A.D., Dolman, A.J., Elbers, J., Heusinkveld, B., Moncrieff, J.B., Monteny, B. & Verhoef, A., 1997. A comparison of surface fluxes at the HAPEX-Sahel fallow bush sites. *J.Hydrol.*, **188-189,** 400-425.

Lloyd, C.R. 1998. The application of an instrument for non-destructive measurements of soil temperature and resistance profiles at a high Arctic field site. *Hydrology and Earth System Sciences* **2,** 121-128.

Lloyd, C.R., Aurela, M., Hargreaves, K.J. & Nordstrøm, C. 1999a. Trace Gas Fluxes in European Arctic Regions. In *Greenhouse Gases and their role in Climate Change: the Status of research in Europe.* European Commission International Workshop (Eds. R.Valentini and C.Brüning), Orvieto, Italy, 10-13 November 1997.

Lloyd, C.R. Aurela, M., Bruland, O., Fowler, D., Friborg, T., Hansen, B.U., Harding, R.J., Hargreaves, K., Nordstroem, C., Laurila, T., Tuovinen, J.-P., Sand, K. & Vehvilainen, B., 1999b. Final Report of the Land Arctic Physical Processes (LAPP) Project. (Contract No. ENV4-CT95-0093). EC DG XII Climate and Environment, Brussels.

Lloyd, C.R. 2001. On the physical controls of the carbon dioxide balance at a high arctic site in Svalbard. *Theoretical and Applied Climatology* **70,** 167-182.

Lloyd, J. & Taylor, J.A. 1994. On the temperature dependence of soil respiration. *Funct. Ecol.* **8,** 315-323.

Longton, R.E. (1980). Physiological ecology of mosses. In *The Mosses of North America*, ed. R.J.Taylor & A.E.Leviton, pp. 77-113. San Fransisco, Pacific Division AAAS.

Longton, R.E. (1988). *The biology of polar bryophytes and lichens.* Cambridge: Cambridge University Press, 391pp.

Marshunova, M.S., 1961. Osnovnye zakomomernosti radiatsionnogo balansa postilayushchei poverkhnosti I atmosferi v Arktike. Trudy Arkticheskovo I Antarkticheskovo Nauchno-Issledovatel'skovo Instituta, Leningrad,

Radiotsionniy I Teplovoy Balans Arktiki **229,** 5-53. (Principal characteristics of the radiation balance of the underlying surface and of the atmosphere in the arctic. *Research Memorandum RM-5003-PR*, p.51-131, Santa Monica, Calif., Rand Corporation, 1996).

Marshunova, M.S. & Chernigovskii, N.T., 1966. Numerical characteristics of the radiationregime of the Soviet Arctic. Research Memoranmum RM-5233-NSF, Santa Monica, Calif., Rand Corporation: 279-297.

Marshunova, M.S. & Chernigovskii, N.T., 1971. Radiatsionnii Rezhim Zarubezhnoi arktiki (Radiation regime of foreign Arctic). Leningrad, *Gidromeorologicheskoe Izdatel'stvo.*, Leningrad. P.182.

Mather, J.R. & Thornthwaite, C.W., 1956. Microclimatic investigations at Point Barrow, Alaska, 1956. *Publications in Climatology,* **9,** Drexel Institute of Technology, Laboratory of Climatology, Centerton, N.J.

Mather, J.R. & Thornthwaite, C.W., 1958. Microclimatic investigations at Point Barrow, Alaska, 1957-1958. *Publications in Climatology,* **11,** Drexel Institute of Technology, Laboratory of Climatology, Centerton, N.J.

Maxwell, B., 1992. Arctic Climate: Potential for change under global warming. In Arctic Ecosystems in a Changing Climate. An ecophysiological perspective. Chapin III,F.S., Jefferies,R.L., Reynolds,J.F., Shaver,G.R. and Svoboda,J., (Eds.) Academic Press, San Diego, 469pp.

Mayo, J.M., Hartgerink, A.P., Despain, D.G., Thompson, R.G., van Zinderen Bakker, E.M.jr. & Nelson, S.D. 1977. Gas exchange studies of *Carex* and *Dryas*, Truelove Lowland. In Bliss,L.C.(Ed), *Truelove Lowland, Devon Island, Canada: A high Arctic Ecosystem.*1977, Edmonton, University of Alberta.707pp.

Maykut, G. & Church, P.E., 1973. Radiation climate of Barrow, Alaska, 1962-66. *J.Appl.Meteorol.* **12,** 620-628.

McKay, D.C. & Thurtell, G.W., 1978. Measurements of the energy fluxes involved in the energy budget of a snow cover. *J. Appl. Meteorol.* **17,** 339-349.

Miller, P.C., Oechel, W.C., Stoner, W.A. & Sveinbjörnsson, B. 1978. Simulation of CO_2 uptake and water relations of four Arctic bryophytes at Point Barrow, Alaska. *Photosynthetica* **12,** 7-20.

Miller, P.C., Kendall, R., and Oechel, W.C., 1983. Simulating carbon accumulation in northern ecosystems. *Simulation* **40,** 119-131.

Moncrieff, J.B., Massheder, J.M., de Bruin, H.A.R., Elbers, J., Friborg, T., Heusinkveld, B., Kabat, P., Scott, S., Soegaard, H. & Verhoef, A. 1997. A system to measure surface fluxes of momentum, sensible heat, water vapour and carbon dioxide. *J.Hydrol.,* **188-189,** 589-611.

Monin, A.S. & Obukhov, A.M., 1954. Basic laws of turbulent mixing in the ground layer of the atmosphere. *Trans, Geophys. Inst. Acad.,* Nauk USSR **151,** 163-187.

Monteith, J.L. 1965. Evaporation and the environment. *Symp.Soc.Expl.Biol.* **19,** 205-234.

Monteith, J.L., 1973. *Principles of Environmental Physics*. Edward Arnold, London, 241pp.

Monteith, J.L. & Unsworth, M.H., 1990. *Principles of Environmental Physics*. 2nd Ed. Edward Arnold, London. 291pp.

Molion, L.C.B. & Moore, C.J., 1983. Estimating zero-plane displacement for tall vegetation using a mass conservation method. *Boundary-Layer Meteorol.* **26,** 115-125.

Moon, P., 1940. Proposed standard radiation curve. *J.Franklin Inst.*, **230,** 583.

Moore, C.J., 1983. On the calibration and temperature behaviour of single-beam infra-red hygrometers. *Boundary-Layer Meteorol.*, **25,** 245-269.

Moore, C.J. 1986. Frequency response corrections for eddy correlation systems. *Boundary-Layer Meteorol.* **37,** 17-35.

Mortensen, N.G. & Larsen,S.E., 1994. Flow response characteristics and temperature sensitivity of the Solent sonic anemometer. *Ann. Geophys.*, **12(suppl II),** C539.

Muc, M., 1977. Ecology and primary production of Sedge-moss meadow communities, Truelove Lowland. In Bliss,L.C.(Ed), *Truelove Lowland, Devon Island, Canada: A high Arctic Ecosystem.*1977, Edmonton, University of Alberta.707pp.

Murray, F.W., 1967. On the computation of saturation vapor pressure. *J.Appl.Meteorol.*, **6,** 203-204.

Nakabayashi, H., Kodama, Y., Takeuchi, Y., Ozeki, T. & Ishikawa, N., 1996. Characteristics of heat balance during the snowmelt season in Ny-Ålesund, Spitsbergen Island. *Mem. Natl. Inst. Polar Res.*, Spec. Issue **51,** 255-266.

Nakano, K. 1980. Comparative studies of cycling of soil organic carbon in three primeval moist forests. *Japanese J.Ecology* **30,** 155-172.

Nakatsubo, T., Bekku, Y., Kume, A. & Koizumi, H. 1998. Respiration of the belowground parts of vascular plants: its contribution to total soil respiration on a successional glacier foreland in Ny-Ålesund, Svalbard. *Polar Research* **17,** 53 - 59.

Oberbauer, S.F., Sionit, N., Hastings, S.J. & Oechel, W.C., 1986. Effects of CO_2 enrichment and nutrition on growth, photosynthesis, and nutrient concentration of Alaskan tundra plant species. *Can.J.Bot.* **64,** 2993-2998.

Oberbauer, S.F., Gillespie, C.T., Cheng, W., Sala, A., Gebauer, R., & Tenhunen, J.D. 1996. Diurnal and seasonal patterns of ecosystem CO_2 efflux from upland tundra inthe foothills of the Brooks Range, Alaska, USA. *Arctic and Alpine Research,* **28,** 328-338.

Oberbauer, S.F., Starr, G., & Pop, E.W. 1998. Effects of extended growing season and soil warming on carbon dioxide and methane exchange of tussock tundra in Alaska. *Journal of Geophysical Research,* **103,** 29,075-29,082.

Obukhov, A.M., 1946. Turbulence in an atmosphere with non-uniform temperature. *Trudy Instit. Teoret. Geofiz.: AN-S.S.S.R.*, No.1 (English Translation: (1971), *Boundary-Layer Meteorol.* **2,** 7-29.

Oechel, W.C. 1976. Seasonal patterns of temperature response of CO_2 flux and acclimation in Arctic mosses growing *in Situ. Photosynthetica,* **10,** 447-456.

Oechel, W.C. & Collins, N.J. 1976. Comparative CO_2 exchange patterns in mosses from two tundra habitats at Barrow, Alaska. *Can.J.Bot.*, **54,** 1355-69.

Oechel, W.C. & Sveinbjörnsson, B. 1978. Primary production processes in Arctic bryophytes at Barrow, Alaska. In *Vegetation Production and Production Ecology of an Alaskan Arctic Tundra*, ed. L.L.Tieszen, pp 269-98. New York, Springer-Verlag.

Oechel, W.C. & Van Cleve, K., 1986. The rôle of bryophytes in nutrient cycling in the taiga. *In* "Forest Ecosystems in the Alaskan Taiga" (Van Cleve,K., Chapin,F.S.,III, Flanagan,P.W., Viereck,L.A., Dyrness,C.T., eds.) pp 121-137. Springer, New York.

Oechel, W.C. & Billings, W.D., 1992. Effects of Global Change on the Carbon Balance of Arctic Plants and Ecosystems. *In* "Arctic Ecosystems in a Changing Climate - An Ecophysiological Perspective" (Chapin III,F.S.,Jefferies,R.L., Reynolds,J.F., Shaver,G.R. and Svoboda,J. eds.), pp 139-168, Academic Press Inc., San Diego.

Oechel, W.C., Hastings, S.J., Vourlitis, G., Jenkins, M., Riechers, G. & Grulke, N. 1993. Recent change of Arctic tundra ecosystems from a net carbon dioxide sink to a source. *Nature* **361,** 520-523.

Oechel, W.C., Vourlitis, G. & Hastings, S.J. 1997. Cold season CO_2 emission from arctic soils. *Global Biochemical Cycles* **11,** 163-172.

Oechel, W.C., Vourlitis, G.L., Hastings, S.J., Zulueta, R.C., Hinzman, L. and Kane, D. 2000. Acclimation of ecosystem CO_2 exchange in the Alaskan Arctic in response to decadal climate warming. *Nature* **406,** 978-981.

Ohmura, A. 1972. Heat and water balance on Arctic tundra. In W.P.Adams. and F.M.Helleiner (Eds) International Geography 1972, Vol.1, Toronto, University of Toronto Press, pp 175-176.

Ohmura, A. 1981. Climate and Energy balance of Arctic tundra. *Zurcher Geographische Schriften,*3. ETH Zurich

Ohmura, A., 1982. A Historical review of studies on the energy balance of arctic tundra. *J.Clim.* **2,** 185-195.

Ohmura, A. & Müller, F. 1976. Heat balance measurement on Arctic tundra, Axel Heiberg Island, Canadian Arctic Archipelago. In I.P.Gerasinov (ed) *International Geography* ,1976, **Vol 2,** 80-84

Oke, T.R., 1987. *Boundary Layer Climates*, Methuen, London, 435pp.

Oliver, H.R. & Wright, I.R. 1990. Correction of errors associated with measurement of net all-wave radiation with double-domed radiometers. *Boundary-Layer Meteorol.* **53,** 401-407.

Orlov, D.S. & Biryukova, O.N. 1995. Organic carbon storage in the soils of the Russian Federation. *Eurasian Soil Sci.*, **28,** 1-19.

Ostendorf, B. 1996. Modeling the influence of hydrological processes on spatial and temporal patterns of CO_2 soil efflux from an Arctic tundra catchment. *Arctic and Alpine Research*, **28**, 318-327.

Orvin, A., 1934. Geology of the Kings Bay region, Spitsbergen. *Skrifter om Svalbard og Ishavet* **57,** 336 pp.

Panofsky, H.A. & Dutton, J.A. 1984. *Atmospheric Turbulence* John Wiley and Sons, New York, 397 pp.

Pasquill, F., 1949.Eddy diffusion of water vapour and heat near the ground. *Proc. Roy. Soc. London* **A198,** 116-140.

Perl, G., 1935. Zur Kenntnis der wahren Sonnenstrahlung in verschiedenen geographischen Breiten. *Meteorologische Zeitschrift* **52,** 85-89.

Planck, M., 1900. Zur Theorie des Gesetzes der Energieverteilung im Normalspektrum. *Verhandlung der Deutchen Physikalischen Gesellschaft* **2,** p.237-245.

Peterson, K.M., & Billings, W.D. 1975. Carbon dioxide flux from tundra soils and vegetation as related to temperature at Barrow, Alaska. *The American Midland Naturalist,* **94,** 88-98.

Peterson, K.M., Billings, W.D., & Reynolds, D.N. 1984. Influence of water table and atmospheric CO_2 concentration on the carbon balance of Arctic tundra. *Arctic and Alpine Research, 16,* 331-335.

Polubesova,T.A., Shirshova,L.T., Lefevre,M. & Romanenkov,V.A. 1996. Effect of freezing and thawing on the surface chemical properties of soils and clays. *Eurasian Soil Science* **28,** 104-114.

Poole, D.K., & Miller, P.C. 1982. Carbon dioxide flux from three Arctic tundra types in north-central Alaska, U.S.A. *Arctic and Alpine Research,* **14,** 27-32.

Post, W.M., Pastor, J., Zinke, P.J., & Strangenberger, A.G., 1985. Global patterns of soil nitrogen. *Nature* **317,** 613-616.

Post, W.M., ed., 1990. Report of a workshop on climate feedbacks and the rôle of peatlands, tundra, and boreal ecosystems in the global carbon cycle. ORNL/TM-11457. Natl. Tech. Info. Serv., Springfield, Virginia.

Rannik, Ü., Aubinet, M., Kurbanmuradov, O., Sabelfeld, K.K., Markkanen, T. and Vesala, T. 2000. Footprint analysis for measurements over a heterogeneous forest. *Boundary-Layer Meteorol.* **97,** 137-166.

Rastorfer, J.R. 1971. Effects of temperature on carbon dioxide compensation points of the moss *Drepanocladus uncinatus. Antarctic Journal of the United States* **6,** 162-163.

Reifsnyder, W.E., 1967. Radiation geometry in the measurement and interpretation of radiation balance. *Agric. Meteorol.*, **4,** 255-265.

Repp, K., 1979. Glacial hydrology, glacial erosion and sediment transport in a high Arctic environment. The Brøgger Glaciers, West Spirtbergen. Thesis. University of Oslo.

Repp, K., 1988. The hydrology of Baleyva, Northwest Spitsbergen. In: *The 7th Northern Research Basin Symposium/Workshop*, Ilulissat, Greenland, May 25-June 1, 1988, p. 105-115.

Romanova, E.N., 1971. *Mikkroklimat Tundr v Raione Taimyrskogo Statsionara, Biogeocenoses of Taimyr Tundra and their Productivity*, Nauka, Moscow, p.35 (English translation by P.Kuchar, *Microclimate in the vicinity of the Taimyr Field Station,* International Tundra Biome Translation 7, Tundra Biome Center, College, Alaska, 1972, p10.

Rönning, O.I., 1963. Phytographical problems in Svalbard. *North Atlantic Biota and their History* (A.Löve and D.Löve, eds.), Macmillan Co. and Pergamon Press (New York), pp 99-107.

Rott, H. & Obleitner, F., 1992. The energy balance of dry tundra in western Greenland. *Arctic and Alpine Res.* **24,** 352-362.

Rouse, W.R., 1984. Microclimate of Arctic tree line. 2. Soil microclimate of tundra and forest. *Water Resour.Res.* **20(1),** 67-73.

Sand, K., Hagen, J.O., Repp, K. & Berntsen, E., 1991. Climate related research in Svalbard. *Norw. Nat. Comm. Hydrol. Rep.*, **23,** 203-217.

Sand, K., & Bruland, O., 1999. Hydrology of the Svalbard LAPP Site. In *Final Report of the LAPP Project – European Commission Contract No. ENV4-CT95-0093* (C.R.Lloyd ed), Institute of Hydrology, Wallingford, 116pp.

Sartz, R.S., 1967. A test of three indirect methods of measuring depths of frost. *Soil Sci.* **104,** 273-278.

Saunders, I.R. & Bailey, W.G., 1994. Radiation and energy budgets of alpine tundra environments of North America. *Prog. Phys. Geog.* **18(4),** 517-538.

Scherer, D. 1992. Klimatologie und Fernerkundung: Erste Ergebnisse der Messkampagnen 1990/1991. *Stuttgarter Geograhische Studien*, **117,** 89-104.

Schmid, H.P. & Oke, T.R., 1990. A model to estimate the source area contributing to turbulent exchange in the surface layer over patchy terrain. *Quart.J.R.Meteorol.Soc.* **116,** 965-988.

Schmid, H.P. & Lloyd, C.R., 1999. Spatial representativeness and the location bias of flux footprints over inhomogeneous areas. *Agric. and For.Meteorol.* **93,** 195-209.

Schwerdtfeger, P. 1976. *Physical Principles of Micro-Meteorological Measurements* Developments in Atmospheric Science 6, Elsevier, Amsterdam.

Schotanus, P., Nieuwstadt, F.T.M. & de Bruin, H.A.R., 1983. Temperature measurement with a sonic anemometer and its application to heat and moisture fluxes. *Boundary-Layer Meteorol.*, **26,** 81-93.

Schuepp, P.H., Leclerc, M.Y., Macpherson, J.I. & Desjardins, R.L., 1990. Footprint prediction of scalar fluxes from analytical solutions of the diffusion equation. *Boundary-Layer Meteorol.* **50,** 355-373.

Schulze, E.D., Kelliher, F.M., Korner, C. & Lloyd, J. 1994. Relationships among maximum stomatal conductance, ecosystem surface conductance, carbon assimilation rate, and plant nitrogen nutrition: a global ecology scaling exercise. *Ann.Rev.Ecol.Sys.* **25,** 629-660.

Sendstad,E. 1981. Soil ecology of a lichen heath at Spitsbergen, Svalbard: Effects of artificial removal of the lichen plant cover. *J. Range Management* **34(6),** 442-445.

Seginer, I. 1974. Aerodynamic roughness of vegetated surfaces. *Boundary-Layer Meteorol.*, **5,** 383-393.

Shaver, G.R. & Kummerow, J. (1992). Phenology, Resource Allocation, and Growth of Arctic Vascular plants. In *Arctic Ecosystems in A Changing Climate: An Ecophysiological Perspective.* Eds. F.S.Chapin III, R.L.Jefferies, J.F.Reynolds, G.R.Shaver and J.Svoboda., pp. 193-211. San Diego, Academic Press Inc.

Shurpali, N.J., Verma, S.B., Kim, J. & Arkebauer, T.J. 1995. Carbon dioxide exchange in a peatland ecosystem. *J.Geophys.Res.* **100,** 14319-14326.

Shuttleworth, W.J., 1988. Corrections for the effect of background concentration change and sensor drift in real-time eddy correlation systems. *Boundary-Layer Meteorol.*, **42,** 167-180.

Shuttleworth, W.J., 1992. Evaporation. In Maidment,D.R. (Ed.) Handbook of Hydrology, pp 4.1-4.53, New York, McGraw-Hill.

Shuttleworth, W.J., McNeil, D.D. & Moore, C.J., 1982. A switched continuous wave sonic anemometer for measuring surface heat fluxes. *Boundary-Layer Meteorol.*, **23,** 425-448.

Shuttleworth, W.J.; Gash, J.H.C; Lloyd, C.R.; Moore, C.J.; Roberts, J.; Marques Filho, A.deO.; Fisch, G.; de Paula Silva Filho, V.; de Nazaré Góes Ribeiro, M.; Molion, L.C.B.; de Abreu Sá, L.D.; Nobre, J.C.A.; Cabral, O.M.R.; Patel, S.R.; & de Moraes, J.C. 1984. Eddy correlation measurements of energy partition for Amazonian forest. *Quart.J.R..Meteorol.Soc.* **110,** 1143-1162.

Shuttleworth, W.J., Gash, J.H.C., Lloyd, C.R., McNeil, D.D., Moore, C.J. & Wallace, J.S., 1988. An integrated micrometeorological system for evaporation measurement. *Agric. For. Meteorol.*, **43,** 295-317.

Skre, O., & Oechel, W.C. 1981. Moss functioning in different Taiga ecosystems in interior Alaska. I. Seasonal, phenotypic and drought effects on photosynthesis and response patterns. *Oecologia*, **48**, 50-59.

Smith, J. 1956. Some moving soils of Spitsbergen. *J.Soil Sci.* **7,** 10-21.

Soegaard,H. & Thorgeirsson,H. 1998. Carbon dioxide exchange at leaf and canopy scale for agricultural crops in the boreal environment. *J.Hydrol.* **213,** 51-61.

Soegaard, H. & Nordstroem, C. 1999. Carbon dioxide exchange in a high-arctic fen estimated by eddy covariance measurements and modelling. *Global Change Biology* **5,** 547-562.

Soegaard, H., Nordstroem, C., Friborg, T., Hansen, B.U., Christensen, T.R. & Bay, C., 2000. Trace gas exchange in a high-arctic valley. 3. Integrating and scaling CO_2 fluxes from canopy to landscape using flux data, footprint modeling, and remote sensing. *Global Biogeochemical Cycles* **14(3),** 725-744.

Stewart, J.B. & Verma, S.B. 1992. Comparison of surface fluxes and conductances at two contrasting sites within the FIFE area. *J.Geophys.Res.* **97 (D17),** 18623-18638.

Stull, R.B., 1988. An introduction to boundary-layer meteorology. *Kluwer Academic*, Dordrecht, 666pp.

Sveinbjörnsson, B. & Oechel, W.C. 1981a. Controls on CO_2 exchange in two Polytrichum moss species. 1. Field studies on the tundra near Barrow, Alaska. *Oikos*, **36**, 114-128.

Sveinbjörnsson, B. & Oechel, W.C. 1981b. Controls on CO_2 exchange in two Poyltrichum moss species. 2. The implications of belowground plant parts on the whole-plant carbon balance. *Oikos*, **36**, 348-354.

Sveinbjörnsson, B. & Oechel, W.C. 1983. The effect of temperature preconditioning on the temperature sensitivity of net CO_2 flux in geographically diverse populations of the moss *Polytrichum commune*. *Ecology*, **64**, 1100-1108.

Sverdrup, H.U. 1935. The ablation of Isachsen's Plateau and on the Fourteenth of July Glacier in relation to radiation and meteorological conditions. *Geografiska Annaler* **17,** 145-166.

Szerszén, L., 1968. Preliminary investigations of soil cover in the region of Hornsund, Vestspitsbergen. *Polish Spitsbergen Expeditions, 1957-1960,* Polish Acad. Sci. (Warsaw), **3,** 217-227.

Szilder, K., Henry, G.H.R., Lozowski, E.P. & Labine, C., 1996. Diagnosing the diurnal surface energy balance over the summer tundra at Princess Marie Bay from simple short-period measurements. *Theor. Appl. Climatol.* **54,** 201-211.

Tanner, C.B. & Pelton, W.L., 1960. Potential Evapotranspiration estimates by the approximate energy balance method of Penman. *J.Geophys.Res.* **65,** 3391-3413.

Tappeiner, U. & Cernusca, A. 1996. Microclimate and fluxes of water vapour, sensible heat and carbon dioxide in structurally differing subalpine plant communities in the central Caucasus. *Plant, Cell and Environment*, **19,** 403-417.

Tedrow, J.C.F. 1977. *Soils of the Polar Landscapes.*, New Jersey, Rutgers University Press.

Tetens, O., 1930. Über einige meteorologische Begriffe. *Z.Geophys.*, **6,** 297-309.

Thom,A.S. 1975. Momentum, mass and heat exchange of plant communities. In: *Vegetation and the Atmosphere. Volume 1. Priciples,* ed. Monteith,J.L., pp 57-109. Academic Press, London.

Tissue, D.T. & Oechel,W.C., 1987. Response of *Eriophorum vaginatum* to elevated CO_2 and temperature in the Alaskan arctic tundra. *Ecology* **68,** 401-410.

Valanne, N. 1984. Photosynthesis and photosynthetic products in mosses. In *The Experimental Biology of Bryophytes,* ed. A.F.Dyer and J.G.Duckett, pp. 257-273. London, Academic Press.

Vovinckel, E. 1966. The surface heat budgets at Ottawa and Resolute, N.W.T. Publication in Meteorology No.85, Montreal, Arctic Meteorological Research Group, McGill University.

Vowinckel, E. & Orvig, S., 1964. Energy balance of the Arctic, V, the heat budget over the Arctic Ocean. *Archiv für Meteorologie, Geophysik und Bioklimatologie*, Ser. B., Bd.14, Ht.3-4 : 303-325

Waelbroeck, C. & Louis, J.-F. 1995. Sensitivity analysis of a model of CO_2 exchange in tundra ecosystems by the adjoint method. *Journal of Geophysical Research*, **100,** 2801-2816.

Webb, E.K., Pearman, G.I. & Leuning, R., 1980. Correction of flux measurement for density effects due to heat and water vapour transfer. *Q.J.Roy.Meteorol.Soc.*, **106,** 85-100.

Weller, G. & Cubley,S. 1972. The microclimates of the arctic tundra. Pp 5-12. In: *Proc. 1972 Tundra Biome Symp.* S.Bowen (ed). CRREL. Hanover, N.H. 211 pp.

Weller, G. & Holmgren, B., 1974. The microclimates of the Arctic tundra. *J.Appl.Meteorol.*, **13,** 854-862.

Wendler, G. 1971. An estimate of the heat balance of avalley and hill station in central Alaska. *J.Appl.Meteorol.*, **10,** 684-693.

Whiting, G.J., Bartlett, D.S., Fan, S.M., Bakwin, P.S. & Wofsy, S.C. 1992. Biosphere/Atmosphere CO_2 exchange in Tundra ecosystems: Community

characteristics and relationships with multispectral surface reflectance. *Journal of Geophysical Research*, **97 No. D15**, 16671-16680.

Whiting, G.J., 1994. CO_2 exchange in the Hudson Bay lowlands: Community characteristics and multispectral reflectance properties. *Journal of Geophysical Research* **99(D1),** 1519-1528.

Wielgolaski, F.E. (1975). Primary Production in tundra. In *Photosynthesis and Productivity in Different Environments,* ed. J.P.Cooper, pp. 75-106. Cambridge, Cambridge University Press.

Wieringa, J., 1992. Updating the Davenport roughness classification. *J.Wind Eng.* **41-44,** 357-368.

Willmott,C.J. 1981. On the validation of models. *Physical Geography* **2,** 184-194.

Willmott,C.J. 1984. On the evaluation of model performance in physical geography. In: *Spatial Statistics and Models* G.L.Gaile anf C.J.Willmott (eds). Pp 443-460. Reidel, Dordrecht.

Wüthrich, Ch, Döbeli, C., Schaub, D. and Leser, H. 1994. The pattern of carbon-mineralisation in the high-arctic tundra (Western and Northern Spitsbergen) as an expression of landscape ecologic environment heterogeneity. *Z.Geomorph.N.F.*, **97,** 251-264.

Wüthrich, C., Möller,I. And Thannheiser, D. 1998. Soil carbon losses due to increased cloudiness in a high Arctic tundra watershed (Spitsbergen). Lewkowicz,A.G. and Allard,M. (eds.): *Proceedings: 7th International Conference on Permafrost*, Yellowknife, June 23-27, Nordicana, Université Laval, 1165-1172.

Wüthrich, Ch., Möller,I. And Thannheiser, D. 1999. CO_2-fluxes in different plant communities of a high-arctic tundra watershed (Western Spitsbergen). *J.Veg.Sci.* **10,** 413-420.

Young, K.L. and Woo, M.-K.1997. Modelling net radiation in a high arctic environment using summer field camp data. *Intl.J.Clim.* **17,** 1211-1229.

Zdunkowski, W.G. and Johnson, F.G. 1965. Infrared flux divergence calculations with newly constructed radiation tables. *J. Appl. Meteorol.* **4,** 371-377.

Zimov,S.A., Zimova,G.M., Daviodov,S.P., Daviodova,A.I., Voropaev,Y.V., Voropaeva,Z.V., Prosiannikov,S.F., Prosiannikova,O.V., Semiletova,I.V. and Semiletov.I.P., 1993. Winter biotic activity and production of CO_2 in Siberian soils: A factor in the Greenhouse Effect. *J.Geophys.Res.* **98 (D3),** 5017-5023.

Appendices

Appendices

1. A MathCad routine of the Collatz C_3 photosynthesis model as implemented in MOSES. It was used to check each stage of the writing of the software for the evaluation of CO_2 assimilation rates in Chapter 6. It is also a very good tool for investigating the effect of each of the parameters on the final photosynthetic rate. The figures down the right-hand side are the valuations at that stage of the equations to the left and above.

2. 4 papers which have been written with the data and methods contained in this thesis. Permission to reproduce these papers within this thesis has been given by the European Geophysical Society and Hydrology and Earth System Sciences (paper 1), Springer-Verlag, Vienna (papers 2 &3) and Blackwell Publishing (paper 4). These papers are protected by the publishers copyright and should not be reproduced without permission from the publishers.

Lloyd, C.R., 1998. The application of an instrument for non-destructive measurements of soil temperature and resistance profiles at a high Arctic field site. *Hydrology and Earth System Sciences* **2(1),** 121-128.

Lloyd, C.R., Harding, R.J., Friborg, T. and Aurela, M., 2001. Surface fluxes of heat and water vapour from sites in the European Arctic. *Theoretical and Applied Climatology* **70,** 19-33.

Lloyd, C.R., 2001. On the physical controls of the carbon dioxide balance at a high arctic field site in Svalbard. *Theoretical and Applied Climatology* **70,** 167-182.

Lloyd, C.R., 2001. The measurement and modelling of the carbon dioxide exchange at a high Arctic site in Svalbard. *Global Change Biology* **7,** 405-426.

MOSES Model: C3 Photosynthetic routine

Input Variables	$T_l := 283.2$	Leaf Temperature (K)
	$Sol := 500$	Solar Radiation (Wm^{-2})
	$P := 101300$	Pressure (Pa)
	$AH := 5.0$	Absolute Humidity (gm^{-3})
	$q := 3.0$	Specific Humidity at leaf surface
	$d_q := 0.0$	Canopy level Specific Humidity (kg H_2O/kg air)
Input Parameters	$r_s := 80$	Surface Resistance (sm^{-1})
	$r_a := 112$	Aerodynamic Resistance (sm^{-1})
	$d_{q.crit} := 0.15$	Critical Humidity Deficit (kg H_2O/kg Air)
	$O_a := 20900$	Atmospheric O_2 pressure (Pa)
	$f_o := 0.92$	$=c_i/c_a$ for $d_q=0$
	$F_d := 0.015$	Dark respiration Coeff.
	$CO2c := 4.9 \cdot 10^{-4}$	Canopy CO_2 concentration (kg CO_2 kg^{-1} air)
	$ep_{CO2} := 1.5196$	Mol.wt CO_2/Mol.wt dry air
	$\Omega := 0.15$	Leaf scattering coeff. for PAR
	$n_f := 0.0008$	Const. relating Vmax and Leaf N
	$V_{max} := 46.9 \cdot 10^{-6}$	Default value for Vmax (mol CO_2m^{-2} s^{-1})
	$\alpha := 0.04$	Quantum efficiency (mol CO_2/mol PAR photons)
	$n_l := 0.05$	Leaf Nitrogen concentration (kg N/kg C)
	$F_{smc} := 1$	Soil water factor (0-1)
	$Ratio := 1.6$	Ratio of leaf resistance for CO_2 to leaf resistance for H_2O
	$GL_{min} := 1.0 \cdot 10^{-6}$	Minimum leaf conductance for H_2O
	$R := 8.3144$	Gas Constant (J/K/mol)

COMMON CALCULATIONS FOR OPEN AND CLOSED STOMATA

S.V.P. from Monteith & Unsworth: valid from 273-293 K

$$e_s := 0.611 \cdot \exp\left(19.65 \cdot \frac{T_l - 273.13}{T_l}\right) \qquad e_s = 1.229$$

Vapour pressure from Abs.Hum:

$$e := \frac{AH \cdot T_l}{2165} \qquad e = 0.654$$

Specific Humidities: $q_s := \frac{0.622 \cdot e_s}{P \cdot 10^{-3}}$ $q := \frac{0.622 \cdot e}{P \cdot 10^{-3}}$ $q_s = 0.008$ $q = 0.004$

Maximum Specific Humidity deficit (kg H_2O kg^{-1} air): $A := [0.0 \quad (q_s - q)]$ $d_q := \max(A)$ $d_q = 0.004$

Canopy Level Specific Humidity Deficit (kg H_2O kg^{-1} air): $g_s := \frac{1}{r_s}$ $D_{qc} := \frac{d_q}{(1 + r_a \cdot g_s)}$ $D_{qc} = 0.001$

PAR absorbed by top leaf (Wm^{-2}): $I_{par} := 0.5 \cdot Sol$ $A_{par} := (1.0 - \Omega) \cdot I_{par}$ $A_{par} = 212.5$

Max. rate of carboxylation of Rubisco (without Temperature factor (mol CO_2 $m^{-2}s^{-1}$): $V_{max} := n_f n_l$ $V_{max} = 4 \cdot 10^{-5}$

Standard Q10 Temperature dependence: $T_{degc} := T_l - 273.13$

$$f_T(q_{10}) := q_{10}^{0.1 \cdot (T_{degc} - 25)}$$

Maximum rate of Carboxylation of Rubisco (mol CO_2 m^{-2} s^{-1}): $V_m := \frac{V_{max} \cdot f_T(2.0)}{\left[1 + \exp\left[0.3 \cdot (T_{degc} - 36)\right]\right]}$ $V_m = 1.42 \cdot 10^{-5}$

Dark Respiration (mol $CO_2 m^{-2}s^{-1}$): $R_D := F_d \cdot V_m$ $R_D = 2.131 \cdot 10^{-7}$

Canopy CO2 Pressure (Pa): $c_a := \frac{CO2c}{ep_{CO2}} \cdot P$ $c_a = 32.665$

CALCULATIONS FOR OPEN STOMATA

Photorespiration compensation point: $\tau := 2600 \cdot f_T(0.57)$ $\Gamma := \frac{O_a}{2 \cdot \tau}$ $\tau = 6.018 \cdot 10^3$ $\Gamma = 1.736$

τ = CO2/O2 Specificity ratio

Conversion factor: mol m^{-3} to Pa (J m^{-3}): $Conv := R \cdot T_l$ $Conv = 2.355 \cdot 10^3$

Calculate internal CO_2 Pressure: $c_i := (c_a - \Gamma) \cdot f_o \cdot \left(1 - \frac{D_{qc}}{d_{q.crit}}\right) + \Gamma$ $c_i = 29.911$

Convert absorbed PAR into mol PAR photons/m^2/s: $A_{cr} := \frac{A_{par}}{219000}$ $A_{cr} = 9.703 \cdot 10^{-4}$

Michaelis constants for CO_2 and O_2 (Pa): $K_c := 30.0 \cdot f_T(2.1)$ $K_c = 9.909$

$K_o := 30000 \cdot f_T(1.2)$ $K_o = 2.285 \cdot 10^4$

$p_i := P \cdot c_i$ $p_i = 3.03 \cdot 10^6$

Rate of Gross Photosynthesis: (Rubisco-limited)

$$W_c := V_m \cdot \frac{c_i - \Gamma}{c_i + K_c \cdot \left(1 + \frac{O_a}{K_o}\right)} \qquad W_c = 8.187 \cdot 10^{-6}$$

Rate of Gross Photosynthesis: (light limited)

$$W_l := \alpha \cdot A_{cr} \cdot \frac{c_i - \Gamma}{\left(c_i + 2 \cdot \Gamma\right)} \qquad W_l = 3.276 \cdot 10^{-5}$$

Rate of Gross Photosynthesis: Photosynthetic product Transport limited

$$W_e := 0.5 \cdot V_m \qquad W_e = 7.102 \cdot 10^{-6}$$

Calculate Quadratic Coeffs for solving minimum of W_c and W_l:

$$B_1 := 0.83 \qquad B_2 := -\left(W_c + W_l\right) \qquad B_3 := W_c \cdot W_l$$

Smoothed minimum of Carboxylation and Light-limited gross photosynthesis (mol $CO_2 m^{-2} s^{-1}$):

$$W_p := -\frac{B_2}{\left(2 \cdot B_1\right)} - \sqrt{\frac{B_2 \cdot B_2}{\left(4 \cdot B_1 \cdot B_1\right)} - \frac{B_3}{B_1}}$$

$B_1 = 0.83 \qquad B_2 = -4.094 \cdot 10^{-5} \qquad B_3 = 2.682 \cdot 10^{-10}$

$W_p = 7.776 \cdot 10^{-6}$

Calculate Quadratic Coeffs for solving minimum of W_c and W_l:

$$B_1 := 0.93 \qquad B_2 := -\left(W_p + W_e\right) \qquad B_3 := W_p \cdot W_e$$

Gross leaf photosynthesis (mol $CO_2 m^{-2} s^{-1}$):

$$W_L := -\frac{B_2}{\left(2 \cdot B_1\right)} - \sqrt{\frac{B_2 \cdot B_2}{\left(4 \cdot B_1 \cdot B_1\right)} - \frac{B_3}{B_1}}$$

$W_L = 5.854 \cdot 10^{-6}$

Calculate net rate of photosynthesis: $AL := \left(W_L - R_D\right) \cdot F_{smc} \qquad AL = 5.641 \cdot 10^{-6}$

Diagnose leaf conductance: $GL_{co2} := \frac{AL \cdot Conv}{\left(c_a - c_i\right)} \qquad GL_{co2} = 0.005$

$$GL := Ratio \cdot GL_{co2} \qquad GL = 0.008$$

Close stomata if net photosynthesis <=0 or leaf resistance < max. value:

$$GL := \begin{cases} GL_{min} & \text{if } \left(GL \le GL_{min}\right) + \left(AL \le 0.0\right) \\ GL & \text{otherwise} \end{cases} \qquad GL = 0.008$$

Top option are defined fluxes and conductances for closed stomata

$$GL_{co2} := \begin{cases} \frac{GL_{min}}{Ratio} & \text{if } \left(GL \le GL_{min}\right) + \left(AL \le 0.0\right) \\ GL_{co2} & \text{otherwise} \end{cases} \qquad GL_{co2} = 0.005$$

$$AL := \begin{cases} -R_D \cdot F_{smc} & \text{if } (GL \le GL_{min}) + (AL \le 0.0) \\ AL & \text{otherwise} \end{cases} \qquad AL = 5.641 \cdot 10^{-6}$$

$$c_i := \begin{cases} \dfrac{c_a - AL \cdot Conv}{GL \cdot \dfrac{1}{Ratio}} & \text{if } (GL \le GL_{min}) + (AL \le 0.0) \\ c_i & \text{otherwise} \end{cases} \qquad c_i = 29.911$$

Hydrology and Earth System Sciences, 2(1), *121–128* (1998) © EGS

Hydrology & Earth System Sciences

The application of an instrument for non-destructive measurements of soil temperature and resistance profiles at a high Arctic field site

C.R. Lloyd

Institute of Hydrology, Wallingford, OX10 8BB, UK.

Abstract

An easily constructed and installed instrument for measuring colocated soil temperature and resistance profiles is described. Minimum disturbance to the soil structure is achieved. The system indicates the melting front of permafrost at a high Arctic field site and shows the effect and extent of summer rainfall events upon the soil water profile. The system is capable of long-term recording of soil moisture profiles at a frequency commensurate with eddy correlation measurements of the surface fluxes of water vapour and carbon dioxide; it thus provides the information necessary for understanding the processes involved in the soil-atmosphere exchange of water and carbon dioxide.

Introduction

An investigation of the energy, water and carbon balance of an Arctic site, subject to seasonal permafrost, requires a measurement of the depth to which thawing of the permafrost has occurred during the summer. The effective exchange of heat, moisture and carbon dioxide during the short summer period occurs in this active soil and vegetation layer above the largely impermeable permafrost layer. In a biome where the soil is as important as the vegetation in providing sources and sinks for moisture and carbon dioxide, the thermal and moisture changes in the soil must be determined as often as the flux of moisture and carbon dioxide from the surface. Furthermore, in organic soils consisting of saturated and drying soil layers above an impermeable layer, be it rock or permafrost, knowledge of the depth of saturated and of unsaturated soil is essential to an understanding of the carbon dioxide and methane fluxes measured above the surface.

Current methods of measuring freezing depth and soil moisture profiles suffer from several disadvantages. The neutron probe method lacks the precision for near-surface measurements while capacitance probes are still largely unautomated. Time Domain Reflectometry (TDR) can provide measurements of freezing fronts and soil moisture but the method is expensive and can create large datasets with consequent time consuming analysis if complete waveforms (required for identification of the freezing front) are taken. There is also conflict between vertical positioning of the TDR probes for freezing front measurements and the preferred horizontal positioning of the TDR probes for soil moisture measurements which also creates some disruption to the soil structure. Gypsum blocks and glass fibre resistance units degrade, create disruption of the soil structure in their installation, and are not robust enough to withstand freezing.

Generally, any soil sensor installation, other than those near the surface, will involve some, often major, disturbance to the soil structure immediately surrounding the measurement position. Such disturbance, often involving trenching and subsequent back-filling, will affect both the thermal and moisture gradients. While some soil types and horizons may return to something approaching the original state after disturbance, clay soils and cold or perennially frozen soils, such as encountered in tundra regions, may take decades to return to their original state.

The measurement of freezing fronts in soils using soil temperature and soil resistivity is well known. However, the 0°C position in soil temperature profiles does not necessarily identify where the soil becomes frozen—as pointed out by Bouyoucos (1921), Post and Dreibelbis (1942), and Anderson and Tice (1970), who detected liquid water in soils at temperatures well below freezing point. There is a marked change in electrical resistivity of soil during freezing and thawing e.g. see Colman and Hendrix, (1949), and Sartz, (1967) who used glass fibre resistivity units to

measure the electrical resistance between two plates separated by a glass fibre cloth, the whole unit assumed to be in thermal and moisture equilibrium with the surrounding soil. However, installation of these units was achieved by Sartz (1967) only by augering 0.1 m holes, which were backfilled after installing the sensors. There was considerable soil disturbance and the glass fibre cloth also had a limited lifetime.

The measurement of temperature and resistivity in tundra soils requires an instrument capable of accurate and variable positioning and separation of sensor depths; of easy installation of sensor units in remote locations with little disturbance to a fragile soil structure; of long term operation and able to withstand the physical pressures of freezing soils and of measuring and recording data routinely at time averages from 10 minutes to 24 hours over periods of weeks, months or years.

Four types of soil temperature and soil resistivity profile units were described by Banner and van Everdingen, (1979), each successive type building on the lessons learnt in the previous ones. However, their final version still required power-augered holes of up to 0.23 m diameter, which were subsequently backfilled and they observed that poor backfilling produced poor electrical contact.

This paper describes the design, materials and fabrication details of an improved temperature and resistivity sensor unit together with data logging specifications and presents results from its use in an Arctic soil in Svalbard. The advantages and limitations of this device are discussed.

Instrument design

The instrument consists of a rigid hollow tube of circular cross-section of about 20mm, comprising narrow section brass rings separated by rigid plastic spacers. Each ring has an embedded thermocouple and a separate low-loss signal lead. The brass rings are held rigidly between the threaded plastic spacers. The whole unit is waterproof. Temperature at each brass ring position and resistance through the soil matrix situated between and around adjacent rings are measured via a multiplexer attached to a controlling datalogger.

THE PROFILE SENSOR ARRAY

Figure 1 shows a single disassembled measurement ring joint together with a plan view of the brass ring and a schematic of the profile assembly used in this paper for measurements in the surface 250 mm. The profile unit consists of 22mm outside diameter (o.d.). annular Naval brass (chosen for its good corrosion resistance, easy machinability and high thermal and electrical conductivities) rings (code BS 2874/CZ–112) separated by 21 mm o.d. PVC-U tubes of very low thermal and electrical conductivity, low linear expansion, and good weather resistance and tensile strength. The brass was chosen in preference to stainless steel because of its higher thermal and electrical conductivity, although it was recognised that tarnishing of the surface might lead to higher electrical resistance over time. Subsequent profile units had very thin chrome plating applied to the brass rings to overcome this tendency. The smaller diameter of the spacers eased installation in augered 22 mm holes and the larger diameter and annular form of the rings improved the chances of good contact between the soil surface and the rings once installed. At their ends, the tubes have male and female screw threads which, with silicone sealant, creates a waterproof joint between the tubes and the intervening brass ring. The PVC tubes can be of any required length above 25mm. Profile arrays of 1 m length have been installed successfully and probes of up to 2 m in length should present little difficulty in installation or operation The brass rings have two inside flanges which slot into the PVC tube and provide extra strength, and prevent twisting of the joint. They also provide the housing for a Teflon-sheathed 0.5 mm diameter Copper-Constantan thermocouple (part no. 5TC-TT-T–24–72, Omega Engineering, Broughton Astley, UK,) and, diametrically opposite, a brazed-in tag for soldered connection of the soil resistivity signal wire. The thermocouple is embedded and glued into a 1.6 mm hole using an epoxy resin capable of providing adhesion and strength at temperatures well below zero and with high thermal conductivity and low electrical conductivity (Part no. OB-CY20–2/–5, Newport Electronics, Broughton Astley,UK). When embedding the thermocouples, continuity checks were performed to ensure that no part of the exposed thermocouple bead was in contact with the brass ring. The thermocouple and the resistivity wire are therefore isolated electrically. A maximum of sixteen rings is limited by the the number of thermocouple and signal wires that can be accommodated within the PVC tube. The thermocouple and resistivity wires are fed through individual holes in sealing plates on either side of a 50 mm PVC-U head-unit, which is sealed by an O-ring onto the profile array. The size and mass of the head allows hand pressure, or judicious use of a soft hammer, for installation.

DATA LOGGING

The data were logged using an AM416 Multiplexer unit and a CR10 logger (Campbell Scientific, Shepshed, UK). In this paper the AM416 multiplexed two 8-level profile units to two differential analogue input pairs on the CR10 logger. Up to three multiplexer units can be accommodated by the CR10 logger, allowing six profile units to be logged. A 10CRT thermistor probe (Campbell Scientific, Shepshed, UK) in thermal contact with the AM416 provides the external reference temperature for the thermocouple measurements. The CR10 and AM416 are contained within a common insulated box to reduce the

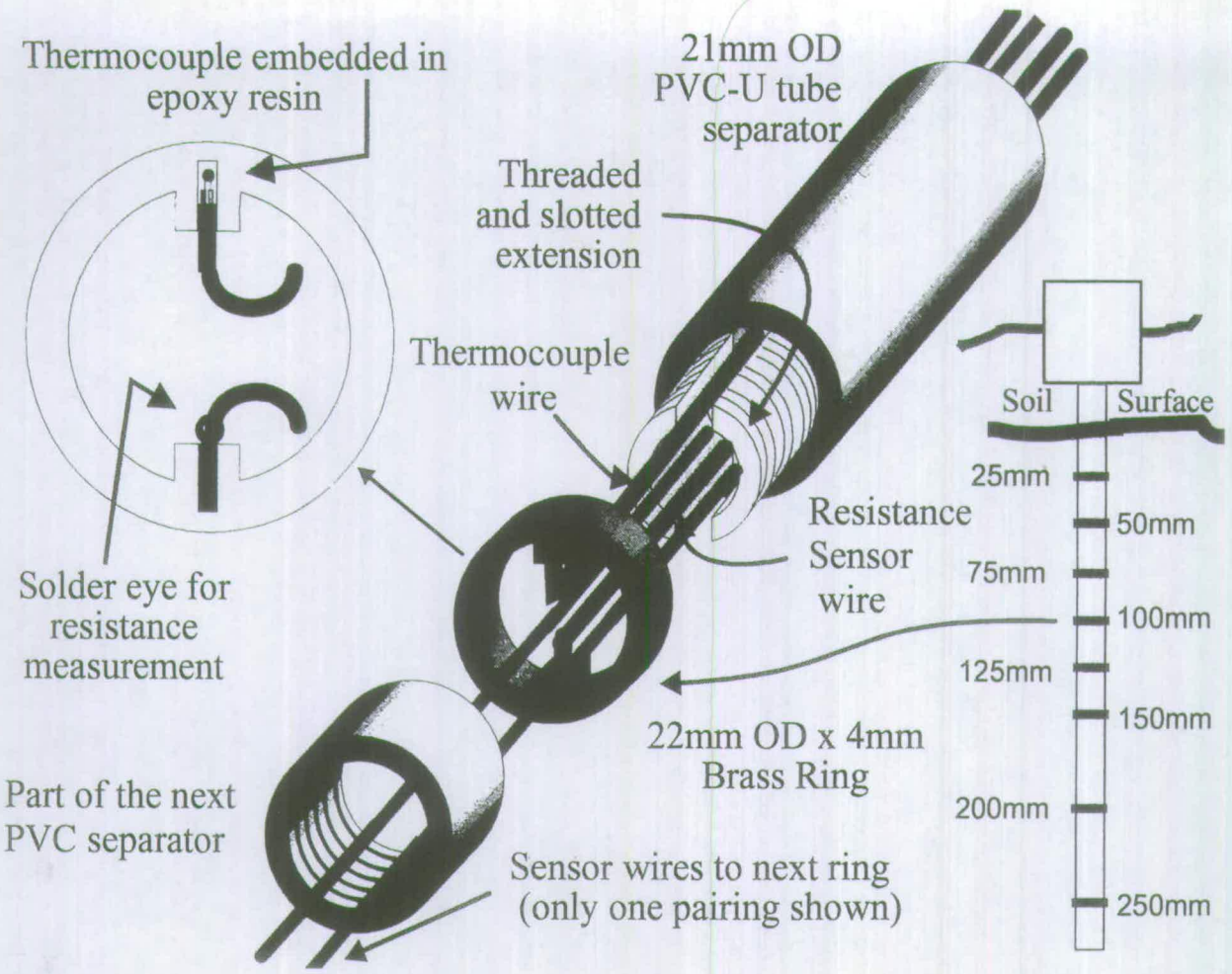

Fig. 1. *Schematic diagrams of the location of the thermocouple and resistance sensor wire within the brass ring, an exploded view of a single measurement joint and a complete profile sensor array within the soil.*

effects of external temperature gradients on the soil measurements. The soil resistivity measurements are made sequentially between adjacent rings, i.e. between ring 1 and 2, then between 2 and 3, etc. This is made possible by the isolating switching relays on the AM416. The CR10 uses an AC half bridge measurement instruction and a bridge transform instruction to convert the signal voltage measured across the soil matrix contained between adjacent rings to a soil resistance value. Rapid switching of this circuit limits polarisation of the rings. Although measurements can be taken automatically every 10 seconds (the time it takes for a complete cycle of measurements to go through the multiplexer), it was adequate for this application to take hourly measurements which were then stored, together with a daily average. The multiplexer and data logger were powered by a 12V sealed lead-acid battery with solar panel charging. Fig. 2 shows a complete prototype two profile unit assembly before installation. This assembly has 100mm and 25mm spacing on the profile units and chrome plated rings. The logger box would be placed in an insulated waterproof box for field operation.

Field application

INSTALLATION

The soil profile arrays were deployed as part of a larger experiment investigating the relationship between the water vapour, heat and carbon dioxide fluxes, and the heat and moisture gradients in the saturated and unsaturated soil layers above the permafrost. This experiment and site was in the glacier-fed Bayelva river valley close to Ny-Ålesund in Svalbard (78°56′N, 11°55′E). The area is on the border between the Middle Arctic Tundra Zone and the Northern Arctic Tundra Zone (Elvebakk, 1985) and has areas which are polar semi-desert. The site is typical northern Tundra and is described as 100–50% *Luzula* lichen heath (Brattbakk, 1981) on a clay silt soil with a 20 mm organic cover.

Ideally, soil profile units should be installed in the previous autumn to allow early spring measurement of the freezing depth. Unfortunately, the above-ground cables from the profile units installed in the autumn of 1994 were damaged by reindeer during the late autumn and it was necessary to reinstall a 0.25m profile unit on 13 June 1995.

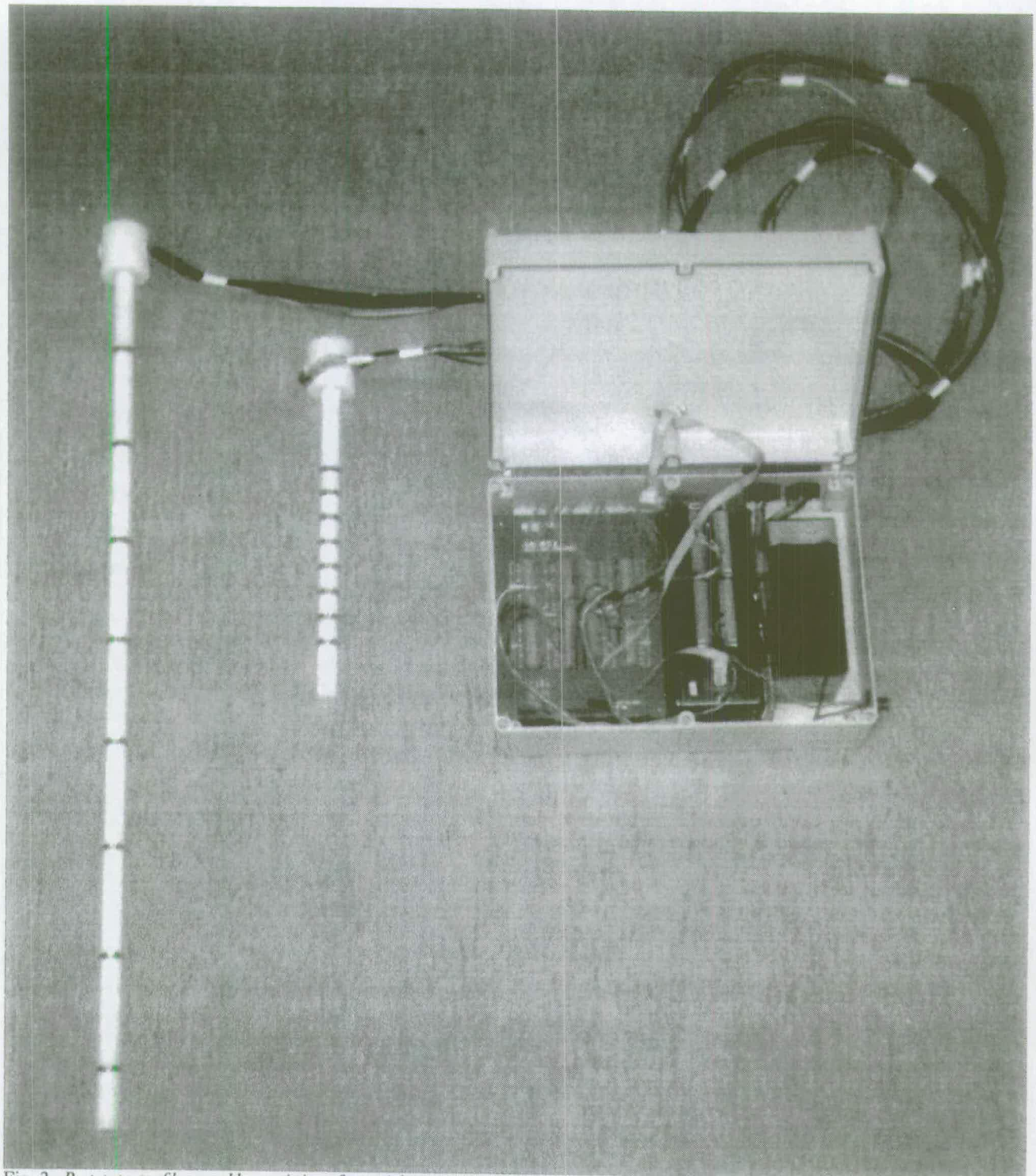

Fig. 2. *Prototype profile assembly consisting of two eight-position soil temperature and soil resistivity profile units with rings spaced at 100mm and 25mm. The logger box contains the AM416 Multiplexer, CR10 data logger and 12V battery.*

This shorter unit was used at this time because permafrost is difficult to auger. A hole was made using a 22 mm wood auger welded to a short length of 18mm rod. Drilling to greater depths involved screwing 0.5 m lengths of extension rod onto the wood drill. The hole was hand augered for better precision. The profile unit was then pushed carefully into the hole using hand pressure alone.

Results

Colman and Hendrix (1949) showed that resistance values were sensitive to temperature and soil water content. They also showed in the production of calibration curves of resistance values for varying soil water content and temperature that while absolute resistance values varied with

soil type, the slope of the lines relating temperature to resistance and soil moisture to resistance were very similar. Following this work, Seyfried (1993) used a simple linear temperature correction based on a single water content value, justifying this because the temperature fluctuations in his data were relatively small and the effect on the estimate of the soil water content was minimal. The resistance values in this paper have been corrected using the linear value of $-0.0154\ k\Omega\ K^{-1}$ found by Seyfried (1993). The temperature used was the mean of the two temperatures bracketing the resistance measurement. Figure 3 shows the diurnal change in the temperature and the soil resistivity profiles during the first few days after installation. Just after installation, at this late stage of the thaw, only the soil below 125 mm is at a temperature below 0°C. Temperature considerations alone imply that the soil is still frozen below 125mm on the 13 June, a conjecture confirmed by examining the diurnal resistances for these positions. The resistances are relatively high at the beginning of the trace, indicating frozen soil, but decrease rapidly to the unfrozen resistance values of about 2.5 $k\Omega$ as the temperature rises above the 0°C line. Note that the resistance values for the lowest two inter-ring distances are over an interval of 50 mm compared to 25 mm for the rest of the profile. The temperature profile also shows a gradient of nearly 10°C over a depth of 250 mm. Simple resistance graphs like Fig. 3 indicate the progression of thawing in the soil very effectively.

Once the soil has thawed, the soil resistance traces indicate soil moisture content over time and provide insight into ongoing soil processes. Figure 4 shows the temperature and soil resistance values for a week following the thawing events shown above, together with the 0.5 mm tips recorded by the raingauge attached to a nearby Automatic Weather Station (AWS). Three depths have been chosen from each of the profiles to show the following:

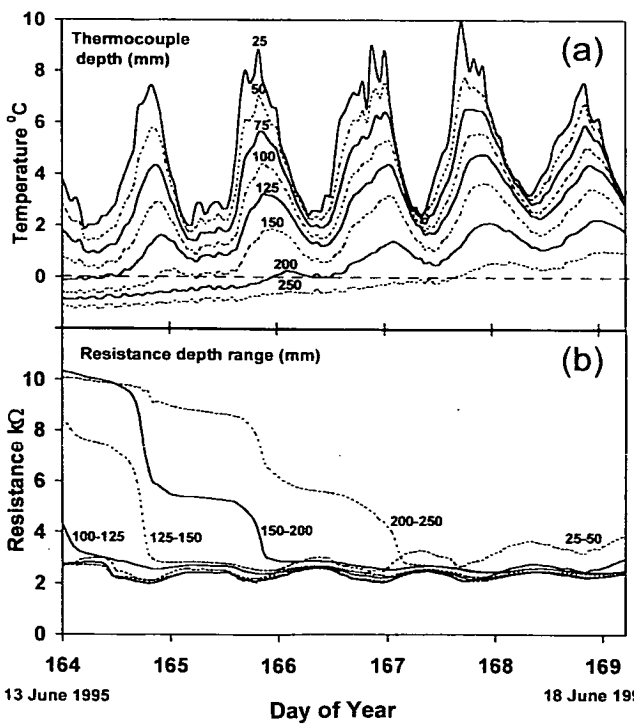

Fig. 3. *Diurnal changes in soil temperature (a) and soil resistance (b) for the period 13–18 June 1995.*

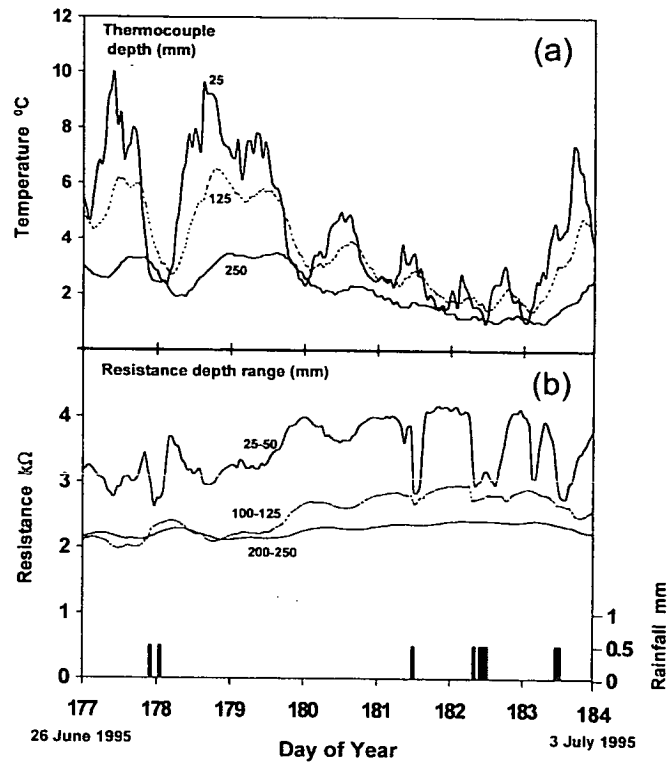

Fig. 4. *Diurnal changes in soil temperature (a) and soil resistance (b) following rainfall events for the period 26 June–2 July 1995.*

(i) the rainfall produced significant reductions in the soil resistance values from the surface down to 125 mm, the lowest point in the profile that could be regarded as responding to the rainfall events,
(ii) soil below this point did not change significantly in response to the rainfall events although it did respond gradually to the changing soil moisture,
(iii) the top 25 mm of soil dried very rapidly after cessation of rainfall.

The rainfall event apparently 'seen' by the 25–50mm soil resistance measurement on the night of 1–2 July (day numbers 182–183) is most probably real but was less than the 0.5 mm needed to cause the bucket to tip.

While Fig. 4 illustrates the way in which soil resistance values can indicate relative qualitative changes in soil moisture at different depths, water balance and process studies require absolute moisture values. The soil at this

site was therefore calibrated. A 0.8 kg sample from a soil monolith taken from an area adjacent to that in which the field sensors were installed was dried at 105°C for 24 hours. The sample was taken from the middle of the monolith approximately 100mm below the shallow organic layer. The sample was then crushed and any stones removed. The resultant soil had a dry bulk density of 1234.3 kg m^{-3}. A 100mm diameter open ended plastic drainage tube 100mm long was sealed onto a plastic chamber which had a sintered ceramic disc as the interface between the chamber and the soil sample tube. A 5mm layer of very fine washed and dried sand (dry bulk density of 1399 kg m^{-3}) was spread evenly across the ceramic disc to prevent clogging of the ceramic. The sand had a porosity of 0.48, close to that of 0.53 for the sample soil. Both materials therefore had similar moisture holding properties. A 15mm layer of the crushed clay soil was spread evenly on the sand. A resistance unit comprising 2 brass rings sealed to either end of a specially made solid 25mm profile separator was placed horizontally on the soil surface. Further clay soil was then spread around and over the resistance unit so that a further 15mm of soil covered the unit. The entire calibration rig was vibrated to ensure close packing of the soil particles. The wires from the resistance unit were attached to an AM416 Multiplexer and CR10 logger similar to that used in the field. A thermistor was installed in the outer edge of the soil layer at the depth of the middle of the resistance unit. Weights and volumes of soil, sand and resistance unit were recorded as was the weight of the entire calibration rig. The rig was supported on a balance which showed the change in weight due to changing moisture levels in the soil layer. The entire unit was then wet from the bottom up by applying a positive head of distilled water into the lower chamber. Distilled water was used as the field soil had a pH of 6.5. As soon as a film of water appeared on the surface of the soil, wetting up was terminated and water in the lower chamber was removed leaving an isolated soil layer close to saturation. The soil layer was allowed to dry naturally from the upper surface over a period of 2 weeks during which time soil temperature, soil resistance and calibration rig weight were recorded on a near daily basis. Figure 5 shows the calibration curve for this soil; logarithmic percentage gravimetric moisture content is plotted versus the logarithm of resistance. A similar relationship was found to apply to high clay-content soils by Reynolds *et al.* (1987) with some evidence of similar curvature. Bouyoucos and Mick, (1948) also found a non-linear relationship between the logarithm of resistance in glass fibre units and soil moisture across a wide range of soil types. Gupta and Hanks (1972) found a linear relationship between soil conductivity and moisture content in sandy and silty loam soils; this implies a non-linear relationship between soil resistance and soil moisture. It is interesting to speculate on the interpretation of the apparent increase in soil moisture values at constant resistances shown on the left hand side of the figure. The turning point may indicate the minimum surface moisture film on soil particles required to provide a continuous water path through the soil matrix. Under such a hypothesis additional soil moisture will not decrease this resistance.

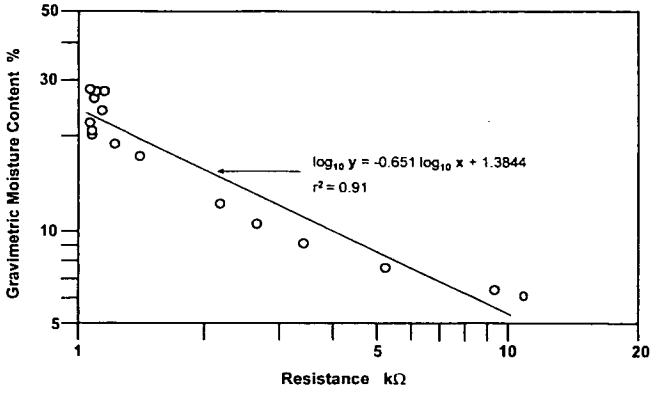

Fig. 5. *Soil resistance versus gravimetric soil moisture calibration curve and fitted equation for the soil at the Ny-Ålesund site.*

Using the linear regression equation for this calibration, values of resistance for the whole summer were converted to volumetric water content. The resistance values for the 50mm separation between 200–250mm was halved before applying the calibration. Figure 6 shows these moisture values and associated soil temperatures for specific depths, selected for clarity and to illustrate seasonal effects at important depths in the soil profile. The gap in the data was due to operator error in retrieving the data from the CR10 logger. The upper graph shows increasing and decreasing soil temperatures at the top and bottom of the profile associated with average diurnal ranges of approximately 6°C and 0.5°C respectively. The gradual rise in soil temperature during the post melt period is evident. This is followed by a period of generally constant temperature during the summer and then a gradual temperature drop as autumn approached. From this graph, the lowest level, at 250 mm, is expected to re-freeze on or about 5 September.

The lower graph, of seasonal variation in soil moisture, shows the effect of precipitation on the upper 125 mm of soil with only gradual and lagged response to this moisture addition being shown lower in the profile. The graph also shows the increasing gradient of soil moisture over the summer period with the lowest measurement staying relatively wet with increasing drying of the soil above this point. This drying of the soil profile confirms the results from the eddy correlation measurements during the same period, where evaporation from this site was nearly twice the rainfall. The evidence from both graphs indicates that refreezing of the entire profile during the year will probably occur in soil drier than that on average occurring during the summer.

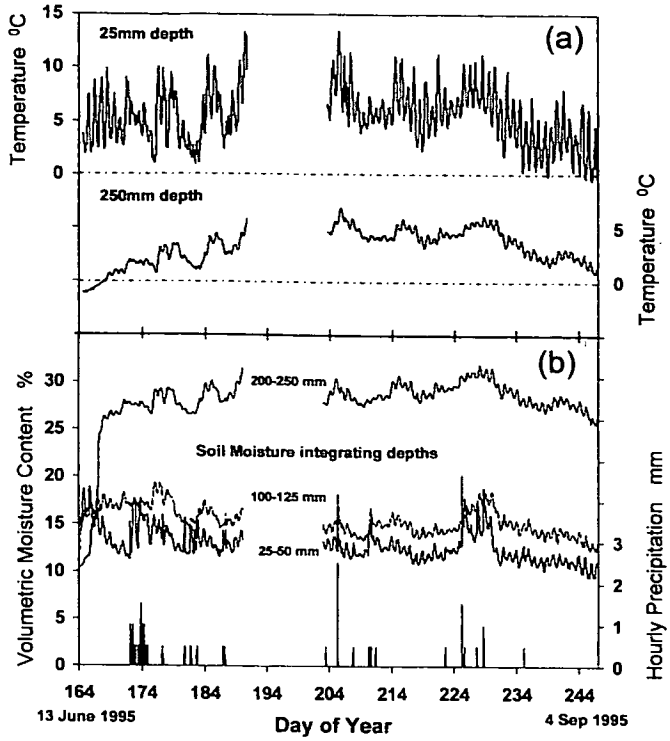

Fig. 6. *Soil temperatures (a) and soil moisture values (b) for selected depths in the soil and rainfall for the active summer period between the spring thaw and the autumn freeze.*

Discussion and conclusion

This method is inexpensive, robust, capable of operating unattended in harsh conditions and causes minimal physical change to the soil profile whose thermal and moisture properties are being investigated. The single narrow augered hole limits disturbance of the soil horizons in most soils, except those containing many stones or gravel, although these also present problems in measuring soil resistance and soil moisture by other methods. The robust profile system can be assembled and tested in the laboratory and rapidly and simply installed in the field. There is limited degradation of the soil profile units once installed, and the use of corrosion resistant naval brass and unpolarised resistance measurements allows their use in highly acidic soils. Current versions of the rings are plated with a thin chromium layer to limit corrosion even further with minimal increase in ring resistance. The use of oversize annular rings increases the possible contact area and provides contact points even in non-straight augered holes. As all the possible resistance paths between adjacent rings are in parallel, the overall resistance value is dominated by the lowest value—provided by the best ring-soil contact point.Criticism of measuring soil resistances between electrodes (as opposed to resistivity of material in potential equilibrium with the soil i.e. gypsum blocks and glass fibre units) centres mainly on the effect of ion concentration on the absolute value of soil resistivity (Schmugge *et al.*, 1980). This problem will limit the method where ionic concentration in the soil changes either in time or over the depth of the profile. Careful calibration is then required to ensure that real changes in soil moisture are not confounded with changes in the resistance due to ionic concentration changes.

For this reason, the use of soil resistance to measure soil moisture has lost favour in recent years, as neutron probe, gamma ray attenuation, soil capacitance and TDR methods have come to the fore. However, none of these methods permit inexpensive, frequent and long-term automatic measurements of combined and co-located soil temperature and soil moisture in the important surface soil layers, measurements of which are vital to the understanding of the soil-vegetation-atmosphere transfer of heat and moisture. The robustness of this application of the resistance method makes it especially suitable for unattended operation in harsh, remote field sites such as are encountered in the Arctic.

Acknowledgements

This work benefited immensely from the provision of the Arctic Research Station facilities at Ny-Ålesund by the UK Natural Environment Research Council. I would like to thank Nick Cox, the Arctic Research Station Base Manager for his help throughout this project and Alan Warwick, Institute of Hydrology Workshop Manager for help in the choice of materials and manufacturing design for the profile array.

References

Anderson, D.M. and Tice, A.R., 1970. Low-temperature phases of interfacial water in clay-water systems. *Soil Sci. Soc. Am. Proc.* 35: 47–54.

Banner, J.A. and van Everdingen, R.O., 1979. Frost gauges and freezing gauges. *NHRI Paper No.3. IWD Tech. Bull. No. 110., 18pp.*

Bouyoucos, G.J., 1921. A new classification of soil moisture. *Soil Sci.* 11: 33–47.

Bouyoucos, G.J. and Mick, A.H., 1948. A fabric absorption unit for continuous measurement of soil moisture in the field. *Soil Sci.* 66: 217–232.

Brattbakk, I., 1981. *Broggerhalvoya, Svalbard, vegtasjonskart 1:10, 000.* Oslo: Norsk Polarinstitutt.

Colman, E.A. and Hendrix, T.M., 1949. The fiberglas electrical soil-moisture instrument. *Soil Sci.* 67: 425–438.

Elvebakk, A., 1985. Higher phytosociological syntaxa on Svalbard and their use in subdivision of the Arctic. *Nordic J. Botany* 5: 273–284.

Gupta, S.C. and Hanks, R.J., 1972. Influence of water content on electrical conductivity of the soil. *Soil Sci. Soc. Am. Proc.* 36: 855–857.

Post, F.A. and Dreibelbis, F.R., 1942. Some influences of frost penetration and microclimate on the water relationships of woodland, pasture, and cultivated soils. *Soil Sci. Soc. Am. Proc.* 7: 95–104.

Reynolds, T.D., Shepard, R.B., Laundré, J.W. and Winter, C.L., 1987. Calibrating resistance-type soil moisture units in a high-clay-content soil. *Soil Sci.* **144**: 237–241.

Seyfried, M.S., 1993. Field calibration and monitoring of soil-water content with fiberglass electrical resistance sensors. *Soil Sci. Soc. Am. J.* **57**: 1432–1436.

Sartz, R.S., 1967. A test of three indirect methods of measuring depth of frost. *Soil Sci.* **104**: 273–278.

Schmugge, T.J., Jackson, T.J. and McKim, H.L., 1980. Survey of methods for soil moisture determination. *Wat. Resour. Res.* **16**: 961–979.

Theor. Appl. Climatol. 70, 19–33 (2001)

Theoretical and Applied Climatology

[1] Centre for Ecology and Hydrology, Wallingford, UK
[2] Institute of Geography, University of Copenhagen, Denmark
[3] Finnish Meteorological Institute, Helsinki, Finland

Surface fluxes of heat and water vapour from sites in the European Arctic

C. R. Lloyd[1], R. J. Harding[1], T. Friborg[2], and M. Aurela[3]

With 10 Figures

Received November 1, 1999
Revised April 17, 2000

Summary

Measurements of the surface fluxes of heat and water vapour were taken at four sites across the European Arctic as part of the EU funded LAPP project. The sites cover a range of latitudinal, altitudinal and climatic conditions. The most northerly site is near Ny-Ålesund, Svalbard, a polar semi-desert with continuous permafrost. A second permafrost site is a fen area in the Zackenberg valley, East Greenland. Finally two sites in northern Finland, Skalluvaara and Kaamanen are on the southern boundary of the region affected by permafrost. At all sites measurements were made of the turbulent fluxes of heat and water vapour using eddy correlation equipment for at least one active season.

The net radiation totals for July and August are similar at all sites. At the sites with permafrost a substantial proportion (over 20%) of the net radiation goes into soil heat flux, to thaw the soil moisture in the top metre. Of the remaining energy just over half is used for evaporation. At the Finnish sites the vegetation is largely deciduous and this is seen in the record with higher evaporative ratios in July and August, after the vegetation becomes green. The Finnish sites tend to have higher surface resistance to evaporation; however, the evaporative demand is greater leading to slightly higher evaporation rates.

The two Finnish sites have a similar seasonal pattern determined by the water table and seasonality of the vegetation. The two northern sites show a pattern that is determined primarily by the variation of water table only. It is concluded that the water balance through the active season is influenced primarily by the history of snow cover. The seasonality of the vegetation, the permafrost and the depth of water table are also important influences.

1. Introduction

The Arctic is a region that experiences considerable climate change. Overpeck et al. (1997) document increases of temperature in the Arctic starting in the mid 19th century, based on proxy data. The observational record also shows general increases in temperature in the last three decades, as large as 1 °C per decade, over central Siberia and Alaska; other areas, such as Greenland and northern Canada, have experienced cooling. These changes are consistent with the predictions from global climate model simulations with rising CO_2 levels, which show large changes in temperature at high latitudes, primarily concentrated in continental regions (IPCC, 1996).

The Arctic is a fragile environment. Temperature is often a limiting factor in plant and animal development. In all areas development is limited by the shortness of the snow-free period, when plant growth is possible, although low summer and autumn temperature can also limit plant growth and soil decomposition. Changes in the vegetation patterns in response to climate changes have already been observed, notably by Myneni et al. (1997), who observed an earlier greening of the Arctic by two weeks associated with the earlier disappearance of the spring snow cover. There are

large stores of soil carbon in the tundra and boreal regions (Christensen et al., 1999; Post et al., 1982). With global warming increased decomposition could release considerable quantities of CO_2 or CH_4. The rate of release of these gases, and in particular the partition between them, will be dependent on the climate and hydrology.

The arctic land surface is highly heterogeneous. It contains unique assemblages of vascular plants, mosses, lichens and bare soil – the proportions of these vary considerably, often over quite small distances, and are strongly influenced by the climate and hydrology. As well as the local variability there is also a considerable variation across the Arctic. In the European Arctic the mean July temperatures range from under 5 °C in the far north to approaching 15 °C near the Arctic Circle in Finland. The diurnal range also doubles across the region, leading to a contrast of over 15 °C in the average daytime temperatures. Obviously in a region limited by temperature these contrasts might be expected to have a considerable impact on the patterns of plant growth and the evaporation.

The annual totals of evaporation are low in the Arctic, but the evaporation is concentrated in the summer months, when the total energy levels can be as high as in lower latitudes. Precipitation is also low and, although a considerable amount of water is made available by the spring snow melt, there is the potential for summer water stress, particularly in freely drained areas. However permafrost can impede infiltration leading to extensive areas of waterlogged ground. To assess the impact of both man-made and natural changes in the arctic there is a need for models to accurately describe the energy, water and carbon fluxes in the arctic.

Measurements of surface fluxes and hydrology were made in the European Commission funded 'Land Arctic Physical Processes' (LAPP) programme with an aim to characterise typical tundra surfaces, in terms of energy, CO_2 and water fluxes. Measurements were made at four sites: Ny-Ålesund, in Svalbard, Zackenberg in Greenland and at two sites in Northern Finland. The measurements thus extend from a high Arctic tundra surface in Svalbard to mire sites in subarctic Finland. All the sites are wetlands to different degrees and appear to be well supplied with water throughout the active season. This paper aims to identify the important processes which determine the fluxes of heat and water vapour in the arctic and provide some of the essential parameters (albedo, roughness, surface resistance) on which land surface models of arctic regions may be based, along with a measure of the variability of these parameters. The measured active season energy and evaporative fluxes from all the four sites are presented along with the partition of the incoming radiation and typical evaporative parameters for each site. The measurements of fluxes of carbon dioxide and methane fluxes from the sites are presented in companion papers in this issue (Aurela et al. (this issue); Hargreaves et al. (this issue); Laurila et al. (this issue); Lloyd (this issue) and Nordstroem et al. (this issue)).

2. Site descriptions

The basic site characteristics are summarised in Table 1. The greatest contrast between the sites is in the summer temperatures, which range in July from 2.6 °C in Zackenberg to 12.3 °C in Northern Finland. In addition the two northern sites are underlain by permafrost whereas in northern Finland the soil is only frozen for part of the year.

2.1 Ny-Ålesund, Svalbard site: Leirhaugen

Ny-Ålesund is situated at 79°56′N, 11°55′E on a peninsular on the southern edge of Kongsfjorden (King's Bay) on the west coast of Spitsbergen island, Svalbard, Fig. 1. The area has recent glacial moraines, strandflats (a coastal lowland plain, partly covered with marine deposits) and postglacial terraces and raised beaches fronting steep flanked mountains which have intervening glaciers and permanent snowfields. Only the uppermost decimetres of the ground thaw during the summer. Below this, the ground remains permanently frozen to depths of 100 to 400 m (Liestøl, 1977 and 1980). The flux measurements were made on a site in the floodplain of the braided Bayelva river.

The mean July temperature at Ny-Ålesund is 5 °C with temperatures outside the range 1–10 °C being uncommon (Harding and Lloyd, 1998). The west coast of Spitsbergen normally has less than 400 mm of precipitation a year, with a maximum in the autumn. Rain can occur even in the middle of winter, as can snow in the summer. The period of the midnight sun begins on 18 April and ends on 24 August, a period of 129 nights.

Table 1. Site characteristics

	Ny-Ålesund	Zackenberg	Kaamanen	Skalluvaara
Lat.	79°56′ N	74°28′ N	69°08′ N	69°49′ N
Long.	11°55′ E	20°34′ W	27°17′ E	27°12′ E
Altitude	20 m	50 m	155 m	280 m
Veg. Type	Luzula lichen heath	Arctic fen	Aapa mire	Palsa mire
Soil type	River gravel/clay with thin peat cover	Peat	Peat	Peat
Typical snow free season	Late June to August	July to August	mid May to October	mid May to October
Total rainfall mm	337[3]	214[1]	468[2]	See Kaamanen
Mean annual temperature	− 5.5 °C	− 10 °C[1]	2.6 °C[2]	See Kaamanen
Mean July temperature	4.7 °C	3.8 °C[1]	12.3 °C[2]	See Kaamanen
Permafrost (Y/N)	Y	Y	N	N

[1]Averages from Daneborg, Greenland, 20 km SE of Zackenberg
[2]Averages from Kevo Sub-Arctic Research Station
[3]Isfjord Radio

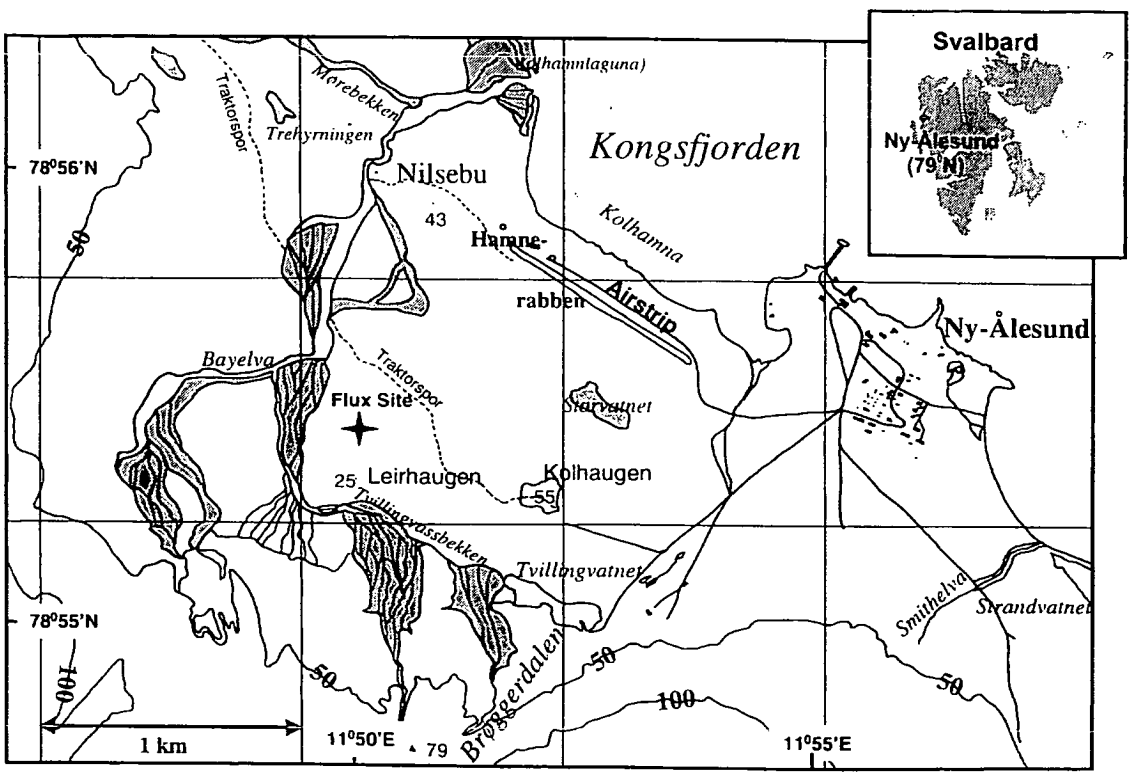

Fig. 1. Location of Leirhaugen measurement site close to Ny-Ålesund, Svalbard

The vegetation at the site consisted of three main plant communities designated by Brattbakk (1981) as 100–50% luzula sedge heath (Norw. Vardefrytle lavhei), 100–50% saxifraga heath (Norw. Rødsildre lavhei) and 100–50% Deschampsia grass tundra mire (Norw. Fjellbunke snøleie). These percentage figures relate to vegetation type within the overall vegetation cover and not to the percentage areal vegetation cover. The vegetation cover at the measurement site was

estimated to be approximately 60%, the remainder being bare soil with a small proportion of stones. The first spring plants do not flower before mid-June and the growing period is generally over around mid-August.

Flux measurements were taken at Ny-Ålesund during the active seasons of 1995 and 1996 (Harding and Lloyd, 1998). The snow melt was anomalously late in 1996, extending into July, leading to a very short active season. For this reason only the 1995 observations are presented here.

2.2 *Zackenberg, Greenland sites: Rylekærene*

The Greenland site is in the locality of the Zackenberg Ecological Research Station (74°28′ N 20°34′ W) in North-east Greenland within an area classified as High Arctic (see Fig. 2). The Zackenberg area is characterised by continuous permafrost, with a maximum thickness of the active layer of between 0.2 and 0.8 m under most surface types, depending on underlying material.

In 1996, the first full calendar year of climate data at Zackenberg, the mean air temperature at 2 m was −9.2 °C, the maximum temperature was 16.6 °C (mid July) and the minimum temperature was −33.7 °C (mid January). The period with frequent temperatures above 0 °C began at the end of May and lasted until the beginning of September. The total precipitation was 223 mm water equivalent with most precipitation occurring during the period January–April (Meltofte and Rasch, 1998). During 1997 the valley remained

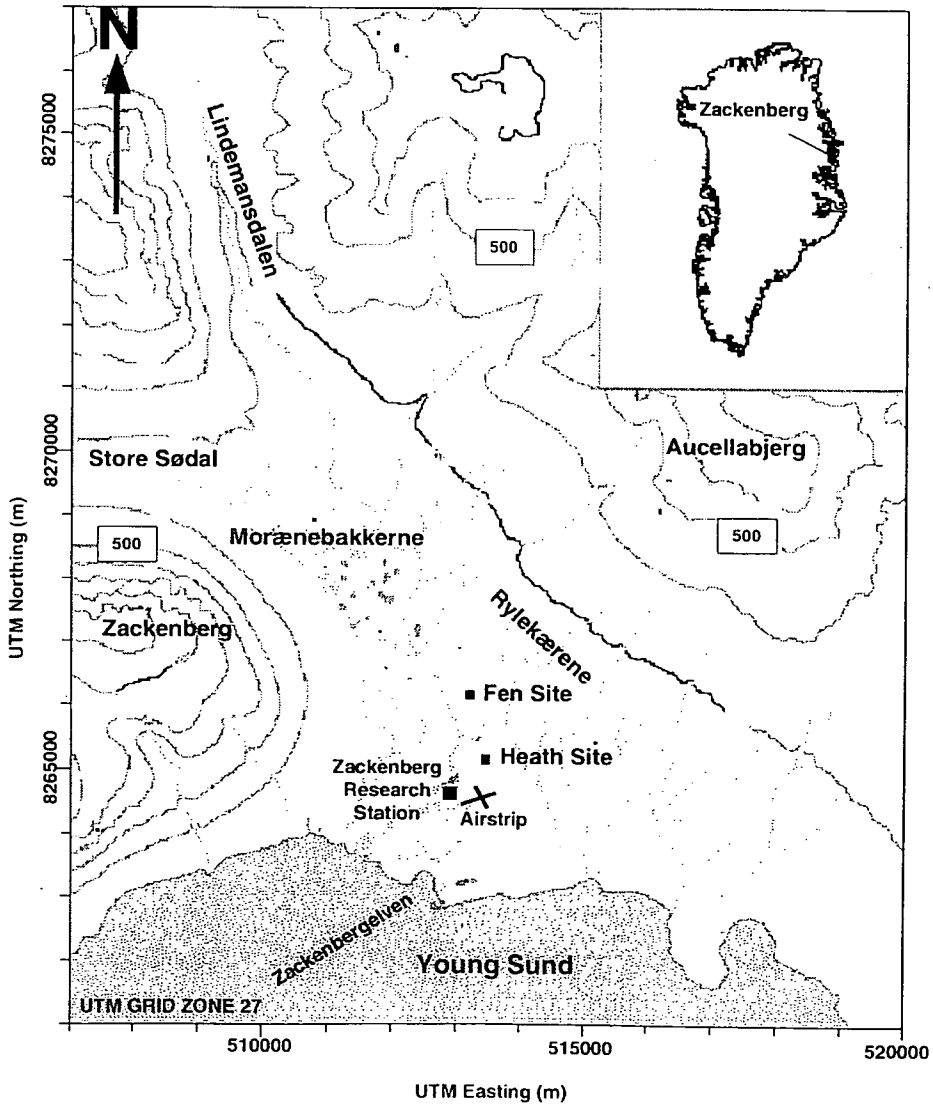

Fig. 2. The location of the Fen and heath sites at Rylekærene, Zackenberg, Greenland

snow covered until the third week of June and the development of the active layer reached its maximum depth in the first week of August.

The study site was established near the centre of an extensive fen area covering approximately 1 × 1.5 km of which all hollow parts were water covered through most of the summer. The most important species found in the fen are: *Eriophorum scheuchzeri* (Arctic cotton grass), *E. triste*, *Dupontia psilosantha* and *Arctagrostis latifolia* (Polar grass), with hummocks and more elevated parts dominated by *Salix arctica* (Arctic willow) and mosses.

The measurements were taken during 1996 and 1997. The measurements during 1997 are more complete and this year is emphasised below, although some measurements are presented from 1996.

2.3 Skalluvaara and Kaamanen Sites, northern Finland

The northern Finland sites are at Skalluvaara (69°49′ N, 27°12′ E) and Kaamanen (69°08′ N, 27°17′ E), 90 km to the south, Fig. 3. The nearest long-term climate station is at the Kevo Sub-Arctic Research Station where the mean annual precipitation is 468 mm, with between 30 and 40 per cent falling as summer rainfall (Hämet-Ahti, 1963). The average winter snow cover tends to reach a maximum at the end of March, then snowmelt begins and average snow cover has usually disappeared by the end of May. The first autumn snowfalls begin in September but permanent snow cover does not commence until the beginning of October. The growing season lasts from 110 to 120 days. The sun is continually in the sky for 64 days in summer, from mid-May until the end of July, and does not rise above the horizon for 54 days in winter from late November to mid-January. As well as the mean summer temperatures the diurnal variations are larger at the northern Finnish sites, compared with the two high latitude sites, with the result that the summer daytime temperature can be in excess of 20 °C, compared with 5–10 °C in Zackenberg and Ny-Ålesund.

The Skalluvaara field site is an elevated mire situated like a saucer between surrounding gentle slope fjelds at an altitude of 280 m a.m.s.l. At the field site there are hummocks surrounding the sphagnum pools – typically 0.5 m high. The hummocks support dwarf birch (*Betula nana*), juniper (*Juniperus communis*) and dwarf shrubs such as crowberry (*Empetrum hermaphroditum*) and *Vaccinium* species. The pools were dominated by *Sphagnum lindbergii*, *S. riparium* and *S. jensenii*.

The Kaamanen site is an aapa mire (altitude 155 m a.m.s.l.). It is dominated by a hummock-hollow structure with typical horizontal scale of a few meters, with the hummocks ranging between 0.3 and 0.8 m in height. The ratio of the area covered by hummocks and hollows is approximately 2:1. The peat depth in the fen is approximately 1 m, quite typical of a northern aapa mire. To the west of the measurement site there is a Scots pine forest approximately 6 m in height.

The vegetation varies significantly on different parts of the fen. The vegetation of the hollows is typical of mesotrophic fens. The hummocks have more oligotrophic or even ombrotrophic vegetation. The higher hummocks were dominated by *Dicranum fuscescens* (dusky fork moss), whereas the wetter parts were more vegetated by *Sphagnum rubellum* (red dwarf peat moss). *Pleurozium schreberi* (red-stemmed feather moss) was the third common moss species on the fen. The hollows were partially covered by different sedges (*Carex*).

The measurements at Skalluvaara were made in 1997. The measurements at Kaamanen were made in 1997 and are continuing, only the data from 1997 are presented below.

3. Measurements

The instruments deployed at each site are outlined in Table 2. At each site direct measurements were made of the turbulent fluxes of sensible and latent heat, using eddy correlation, for the late snow melt period and the majority of the active season (at least until the end of August). Supporting measurements of the radiation components (solar, reflected solar and net-allwave), air temperature, air humidity and wind speed were made at all sites. Soil variables, such as temperature, soil moisture and water table heights were made when appropriate. Soil heat flux was measured at two sites, although it is difficult to interpret these measurements, probably due to the heterogeneous

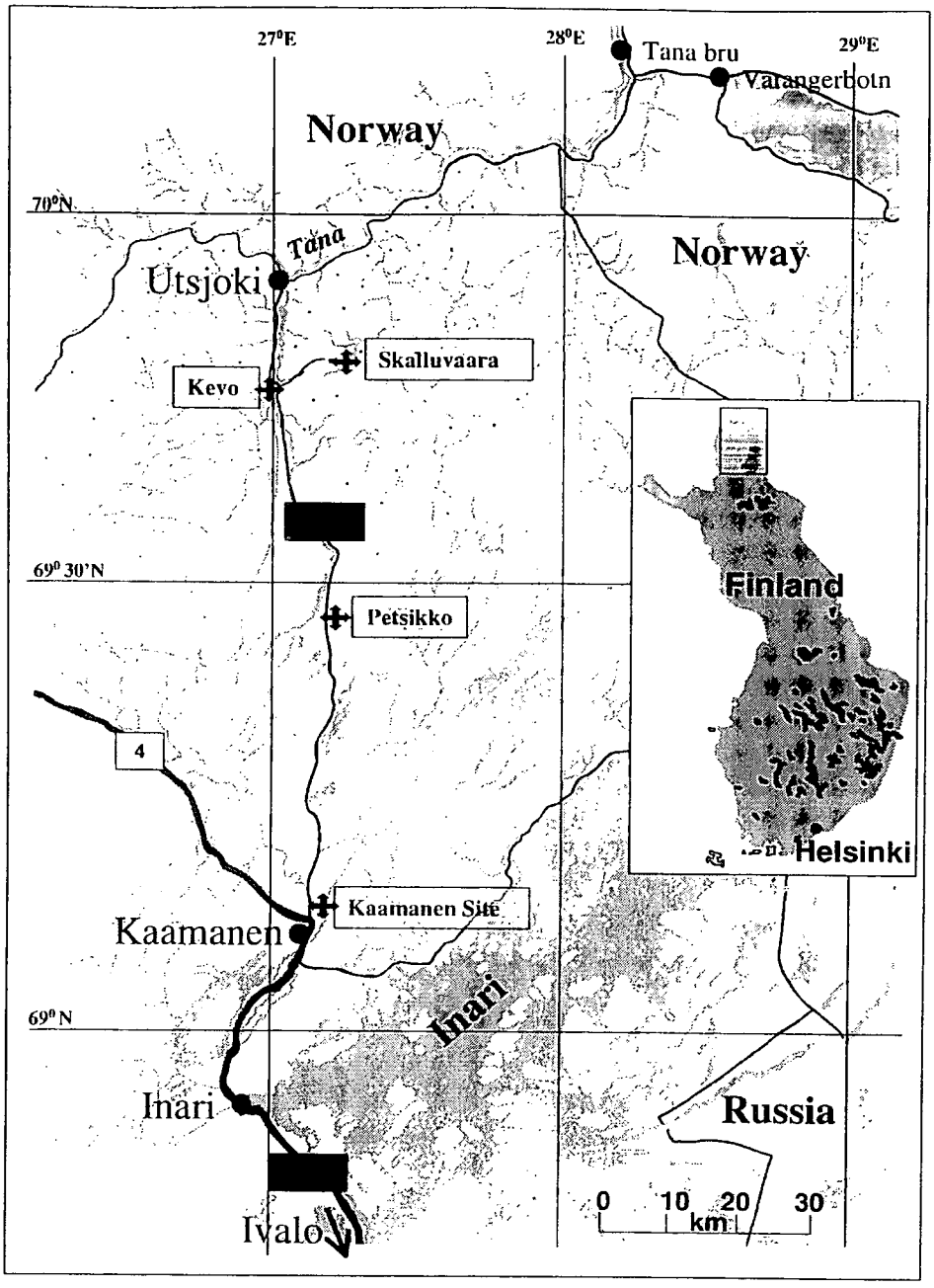

Fig. 3. Map showing Skalluvaara and Kaamanen sites in northern Finland

and often water logged soils, and these are not presented here.

At all sites measurements of turbulent fluxes were made with a Solent/Li-Cor closed path system. At two sites, Ny-Ålesund and Skalluvaara the turbulent fluxes were also measured using the Hydra Mk II. This latter system is a portable, open-path eddy correlation device described in detail by Shuttleworth et al. (1988). It comprises a one-dimensional ultrasonic anemometer, a light-weight cup anemometer, a fine thermocouple and an infrared hygrometer coupled to an on-line computer for the calculation of surface fluxes. The measurement heights were chosen to be well above the surface roughness sub-layer (see Table 3). In addition to the measurement of the fluxes of heat and water vapour the system also provides measurements of momentum flux, net radiation, air temperature, humidity and wind speed. The Solent/Li-Cor system is a combination of a Solent 3D ultrasonic anemometer with a Li-Cor closed path infrared gas analyser (Moncrieff et al., 1997).

Table 2. Details of equipment deployed at each site

Site Year		Ny-Ålesund Leirhaugen 1995	Zackenberg Heath/Fen 1996/7	Kevo Skalluvaara 1997	Kaamanen 1997
Eddy-correlation parameters	u,v,w	Hydra	Solent	Hydra, Solent 1012R2	Solent
	T	Cr-Co T/C: Sonic	Solent Sonic derived	Fine wire T/C; Sonic	ATI SWS-211
	CO_2	Li-Cor 6262	Li-Cor 6262	Li-Cor 6262	Li-Cor 6262
	H_2O	Hydra	Li-Cor 6262	Li-Cor 6262	Li-Cor 6262
Height of flux instruments		3 m	2.7 m	3.5 m	5.4 m
Climate Parameters	Net radiation	REBS Q*6	REBS Q*6	REBS Q*	REBS Q*7
	Solar	Kipp & Zonen CM5	Kipp and Zonen CM7	Kipp & Zonen CM5	Kipp & Zonen CM7B
	Reflected	Kipp & Zonen CM5	Kipp and Zonen CM7	Kipp & Zone CM5	Kipp & Zonen CM7B
	PAR	–	Li-Cor Li-190 SA	Skye SKP 215	Licor LI-190 SZ
	Longwave, in	Eppley PIR	Eppley PIR	Eppley PIR	–
	Longwave, out	Everest 4000.4GL	Heinmann KT-17	Everest 4000.4GL	Everest 4000.4GL
	Air temperature	Rotronic MP 100A	Rotronic MP100A	Vaisala HMP35AC	Campbell 107and/ or Vaisala HMP233
	Relative Humidity	Rotronic MP 100A	Rotronic MP100A	Vaisala HMP35AC	Vaisala HMP233
	Wind speed	Campbell A100L2	Solent Sonic derived	Campbell A100L2	Campbell A100L2
	Wind direction	Didcot DWD	Solent Sonic derived	Campbell W200P	Campbell W200P
	Water depth	–	Campbell PDCR 1830	Campbell PDCR 10	Campbell PDCR 1830
	Soil temperature	Cu-Co Thermocouple	Co-Cu Thermocouple	Omega T/C	Campbell 107
	Soil Heat Flux	Thornthwaite plates	–	REBS HFT-3 plates	–
	Precipitation	RIMCO Tipping bucket	(Belfort with Nipher)	(Belfort with Nipher)	Casella

While the sensible heat fluxes from these two systems agreed very well, there were systematic discrepancies between the latent heat fluxes in the Ny-Ålesund measurements. Consideration of these differences leads to the conclusion that the open path measurements were probably more accurate. In the analysis presented below the fluxes of heat and water vapour are taken from the Hydra systems at the Ny-Ålesund and Skalluvaara sites and the Solent/Li-Cor systems at the other sites. The momentum fluxes are known to be underestimated by the Hydra system and those from the Solent systems were used at all sites.

4. Estimates of albedo and roughness

The seasonal pattern of short wave albedo, σ_{SW}, was similar at all sites and is illustrated by the trace from Skalluvaara in Fig. 4a and b. The major feature of the σ_{SW} was associated with the melting of the snow, with a rapid decline from between 0.6 and 0.7 to 0.1 within a few days. Following snow melt there was a steady increase as the soil dried out and the vegetation developed. At Skalluvaara, at least, there was a final small decrease after day 220, which may have been associated with the senescence of the vegetation. The development of the vegetation is further indicated by albedo of the Photosynthetically Active Radiation (PAR), Fig. 4b, which shows increasing radiation absorption in these wavebands between days 160 and 200, with approximately constant values after this. Ny-Ålesund had the lowest albedo of all the sites (Table 3), less than 10% directly after snowmelt. This was because of the large proportion of bare, organic soil.

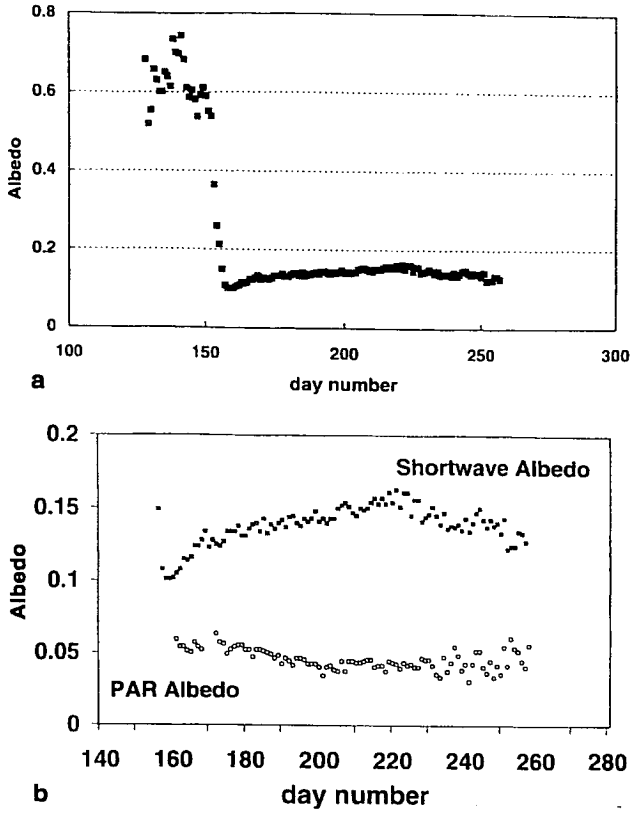

Fig. 4. (a) Seasonal variation of daily mean shortwave albedo at Skalluvaara, for 1997. (b) Seasonal variation of daily mean albedo for shortwave and photosynthetically active radiation at Skalluvaara, for 1997

The roughness lengths for momentum were calculated at all sites from the measurement of momentum exchange by inverting the equation:

$$u = u* \left[\ln\left(\frac{z-d}{z_0}\right) - \Psi \right]$$

where:

u is the wind speed ($m\,s^{-1}$),
$u*$ is the friction velocity ($m\,s^{-1}$),
z is the height of measurement (m),
d is the displacement height (assumed here to be = 0.1 m),
z_0 is the roughness length (m) and
Ψ is a stability correction for unstable conditions (see for example Paulson, 1970).

To avoid large errors calculations were only made when the wind speed exceeded $1\,m\,s^{-1}$ and $u*$ exceeded $0.1\,m\,s^{-1}$. Only neutral and unstable conditions were considered. Despite these filters, the scatter of the hourly values was considerable (see e.g., Fig. 5 for Skalluvaara) and Table 3 presents median values over the entire season for all the sites. The lowest value was at Ny-Ålesund, this is consistent with the low vegetation at this site. The two mire sites had comparatively high values of measured roughness, again consistent with the observed vegetation and the hummocky nature of the surface.

5. Energy and water fluxes

Figure 6 shows the mean cumulative fluxes of net radiation (Rn), latent heat (L.E), sensible heat (H) and the residual (Rn-L.E-H) for day numbers 160 to 240 recorded at the four sites. These diagrams were constructed from the daily totals. In all cases the net radiation record was complete. There were some gaps in the record of the turbulent fluxes, however these were less than 5% of the total, and

Table 3. Mean measured parameters, days 180–240 and seasonal variation of albedo

	Ny-Ålesund	Zackenberg 1997 (1996)	Kaamanen	Skalluvaara
Mean measured parameters, days 180–240				
Albedo	0.107	0.172	0.129	0.14
Roughness length (m)[†]	0.003	0.013 (0.010)	0.034	0.025
Surface resistance ($s\,m^{-1}$)	106	76 (115)	163	136
Seasonal variation of albedo				
Days 160–180	–	–	0.109	0.123
Days 180–200	0.098	0.142	0.131	0.139
Days 200–220	0.109	0.171	0.139	0.150
Days 220–240	0.115	0.204	0.137	0.147

[†] median values

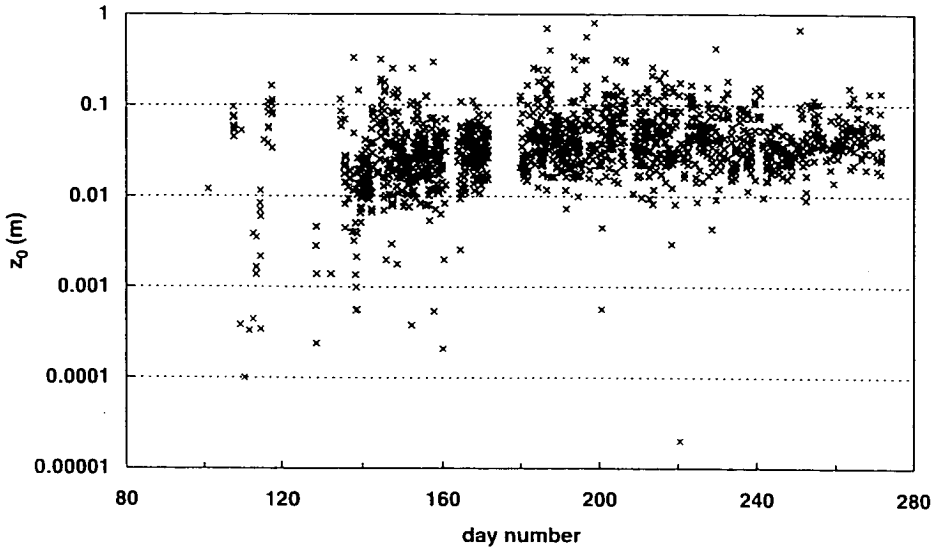

Fig. 5. Hourly roughness lengths z_0 (m) from Skalluvaara site calculated from the momentum flux measurements

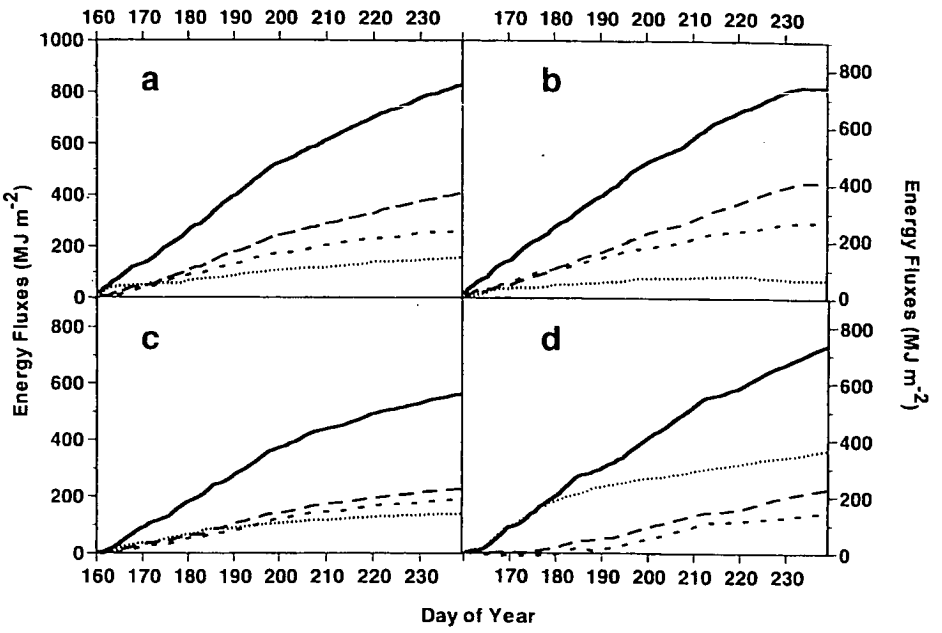

Fig. 6. Mean cumulative fluxes of net radiation (—), latent heat (– –), and sensible heat (---), and the residual of the energy balance (. . . . .) from the four LAPP sites: (a) Kaamanen, (b) Skalluvaara, (c) Ny-Ålesund and (d) Zackenberg

for this diagram these missing data have been infilled using the mean evaporative ratio (L.E/Rn) from that site. This period was snow free at all sites except Zackenberg Fen, where snow persisted until day 176 (see Table 4).

At first sight the patterns of cumulative fluxes appear similar at all sites. The cumulative net radiation varied from just under 600 MJ m^{-2} at Ny-Ålesund to just over 800 MJ m^{-2} at Kaamanen. Overall more energy went into evaporation than sensible heat flux. In the early part of the year the partition into sensible and latent heat was about equal but the latent heat tended to be greater in the second part of the season. At the southern sites (Kaamanen and Skalluvaara) the latent heat began to diverge from the sensible heat at about day 180 (the end of June), at Zackenberg the divergence was not noticeable until day 210 (the beginning of August) and at Ny-Ålesund there was hardly any change. This relative increase of evaporation was probably the result of the greening of the vegetation after

Table 4. Mean meteorological conditions and fluxes for the month of July

	Ny-Ålesund	Zackenberg	Kaamanen	Skalluvaara, Kevo
Year	1995	1997	1997	1997
Date of complete snow melt*	153	176	143	153
Mean temperature (°C)	5.2	3.6	14.3	11.8
Total evaporation, mm	16.6	17.3	26.9	27.7
(latent heat, MJ m^{-2})	(41.6)	(43.2)	(67.3)	(69.4)
Total net radiation (MJ m^{-2})	95.0	120.8	132	108.7
Total sensible heat (MJ m^{-2})	34.5	38.3	45	38.9
Evaporative ratio	0.44	0.36	0.51	0.64
Bowen ratio	0.83	0.87	0.67	0.56
Priestley–Taylor Coefficient†	0.87	0.76	0.82	0.99

* determined by albedo measurements for year in question
† median values

it has emerged from the snow pack. The lack of seasonality at Ny-Ålesund was probably a result of the type of vegetation at this site, which is predominantly evergreen, with a large proportion of bare soil.

The residual trace is a measure of the energy going into the ground, possibly exaggerated by any flux loss in the measurement of the turbulent fluxes. The Zackenberg trace was also affected by the presence of snow in the first 16 days, at this time the turbulent fluxes were small (and in the case of the sensible heat was negative) and the radiant energy went into snow melt. Apart from the first 15 days (when snow was affecting Zackenberg) the traces from Ny-Ålesund and Zackenberg were similar with between 150 and 200 MJ m^{-2} (between one quarter and one third of the radiant energy) entering the ground heat store. These two sites have permafrost and so it is to be expected that a considerable amount of energy entered the soil to melt the soil water in its upper layers throughout the active season. It is noticeable that the residual was greatest in the early part of the active season. The soil was only seasonally frozen at Skalluvarra and Kaamanen and was observed to be unfrozen by the end of June. At Skalluvarra the residual reached approximately 50 MJ m^{-2} in the early part of the season, consistent with melting of ice in the top half metre of soil. At Kaamanen the accumulated residual continued to increase throughout the summer, up to a maximum value of 150 MJ m^{-2}, this may be the result of either a systematic flux loss in the eddy correlation measurements or problems with the representivity of the radiation measurements at this fairly inhomogeneous site.

The daily evaporative ratios (L.E/Rn) calculated for the four sites demonstrate further the picture described above (Fig. 7). The ratio was zero, or negative, during snow cover and rose once the snow has melted to approximately one half. There was then a further rise towards the end of the season. The July averages (Table 4) show higher values at the two southerly sites. There is some evidence that the evaporative ratio increased immediately after rainfall, see Harding and Lloyd (1998).

The Priestley–Taylor coefficient, α, (Priestley and Taylor, 1972) is frequently used to describe the evaporation from arctic surface (e.g., Young and Woo, 1999; Stewart and Rouse, 1976; Rouse et al., 1987). The coefficient is calculated from the equation:

$$L.E = \alpha \frac{\Delta}{\Delta + \gamma} A$$

where:

L is the latent heat of vaporisation (J kg^{-1}),
E is the evaporation (kg s^{-1} m^{-2}),
Δ is the slope of the saturated vapour pressure curve (Pa K^{-1}),
γ is the psychrometric constant (Pa K^{-1}) and
A is the available energy (W m^{-2}), in the calculations below this is approximated by the net radiation.

McNaughton and Spriggs (1989) showed that α takes a fairly constant value of between $1.26 \pm 10\%$ for a mid-latitude site when the atmospheric

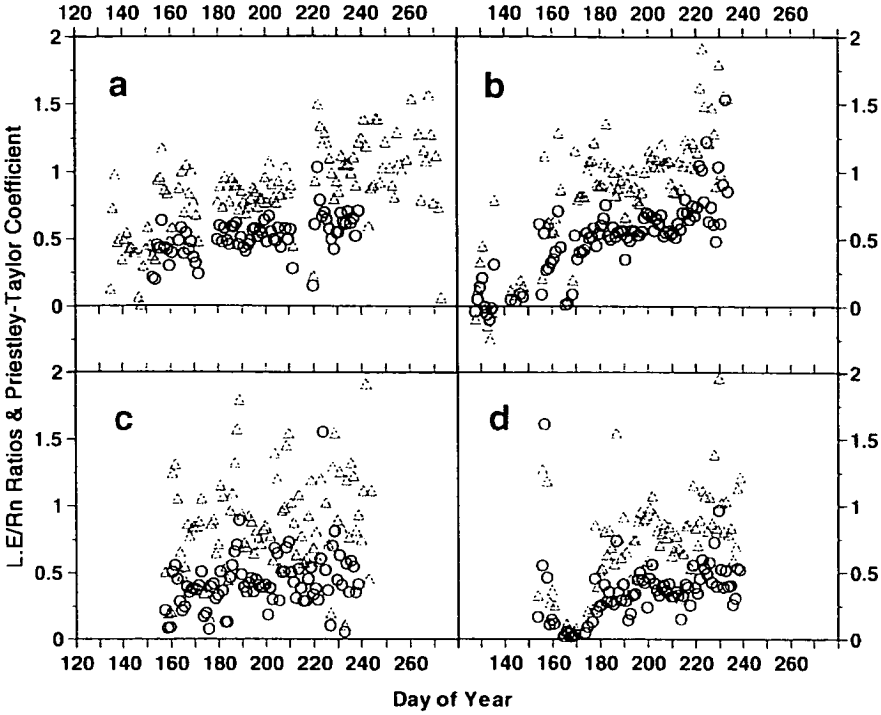

Fig. 7. Daily values for evaporative ratio (o) and Priestley-Taylor coefficient (Δ) for the four LAPP sites: (a) Kaamanen, (b) Skalluvaara, (c) Ny-Ålesund, (d) Zackenberg

boundary layer is in equilibrium with a surface well supplied with water (when the surface resistance is less than $100\,s\,m^{-1}$). The concept of Priestley and Taylor is probably not strictly applicable to the Ny-Ålesund and Zackenberg sites, whose climates are dominated by the proximity of the sea (in particular at Ny-Ålesund the air temperatures are remarkably constant, Harding and Lloyd, 1998). Not-with-standing these latter reservations the calculated daily values of α were fairly consistent at just under one for the snow free periods at all sites (Fig. 7). This value is also consistent with the values quoted by other workers in the Arctic (e.g., Young and Woo, 1999; Stewart and Rouse, 1976) and with the range of values quoted by Baldocchi and Vogel (1997) for a variety of mid-latitude sites. The low values of α are probably a result of the high surface resistance values (see next section), although Huntingford and Monteith (1998) show that α would be expected to be dependent on the temperature in the lower atmosphere, with a lower α at lower temperature.

6. Estimates of surface resistance for evaporation

In order to compare the behaviour of the surface in terms of its evaporative characteristics the effective surface resistance, r_s ($s\,m^{-1}$) was calculated by inverting the Penman–Monteith equation (Monteith, 1965):

$$LE = \frac{\Delta A + \rho C_P \dfrac{(e_s - e_a)}{r_{ah}}}{\Delta + \gamma\left(1 + \dfrac{r_s}{r_{ah}}\right)}$$

where:

C_p is the specific heat of air ($J\,kg^{-1}\,K^{-1}$),

e_a is the vapour pressure (Pa),

e_s is the saturated vapour pressure at the air temperature (Pa) and

r_{ah} the aerodynamic resistance for heat and water vapour ($s\,m^{-1}$), which was estimated:

$$r_{ah} = \frac{\left(\ln \dfrac{z-d}{z_{0h}}\right)^2}{k^2 u}$$

where k is the von Karman's constant. The roughness length, z_{0h}, was estimated from the eddy correlation measurements of momentum, the roughness length appropriate for heat and water vapour transport was assumed to be one tenth that for momentum (see e.g., Garratt, 1992). The absolute available energy, A, is unknown because of uncertainties in the ground heat flux. However, in this analysis A is equated to the sum of the

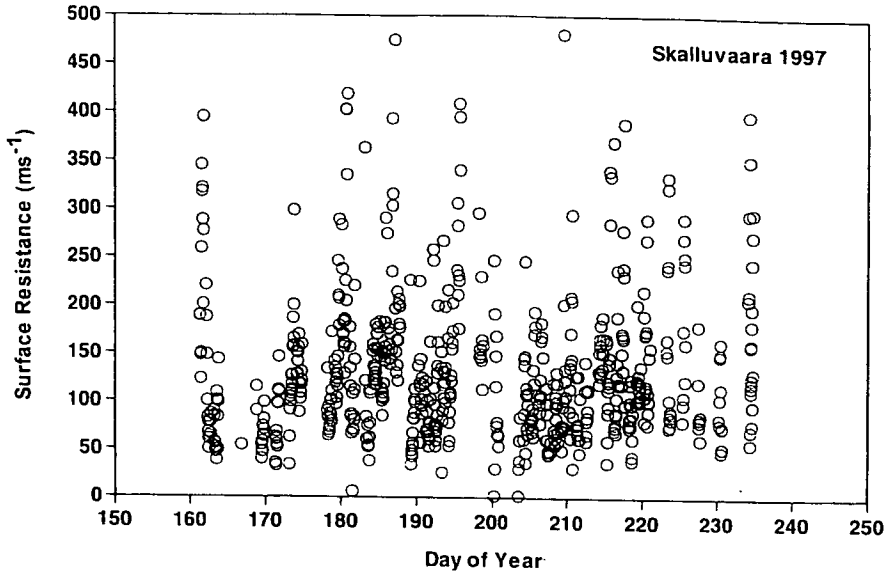

Fig. 8. Hourly estimates of surface resistance R_s (ms^{-1}) for the Skalluvaara site

measured latent and sensible heat fluxes. The calculation was made hourly in order to determine the diurnal and environmental responses. The scatter on the hourly estimates was considerable (see e.g., Fig. 8), a result of real variability and also inevitable errors in the hourly flux measurements. Calculations were only made on days on which no rain was recorded, the introduction of this filter made a small (2%) increase in the mean value.

The mean values for the active season (day 180 to 240) range from 76 to 163 $s\,m^{-1}$, Table 3. The lowest values were at Zackenberg and Ny-Ålesund, which seem to show a clear difference to the sites in northern Finland. There was a considerable seasonal variation in the resistance values, Fig. 9. Although the hour to hour variation is considerable the standard errors on the period means (standard deviation/number of observations) are typically 5% of the mean value, suggesting that the seasonal variations are significant. The processes are probably best illustrated at Kaamanen, which has the longest run of data during the snow free period. The water table measurements at this site showed a high water table directly after melt, which decreased steadily through June and reached a stable summer value at the end of June. The resistance was initially low (days 160–180),

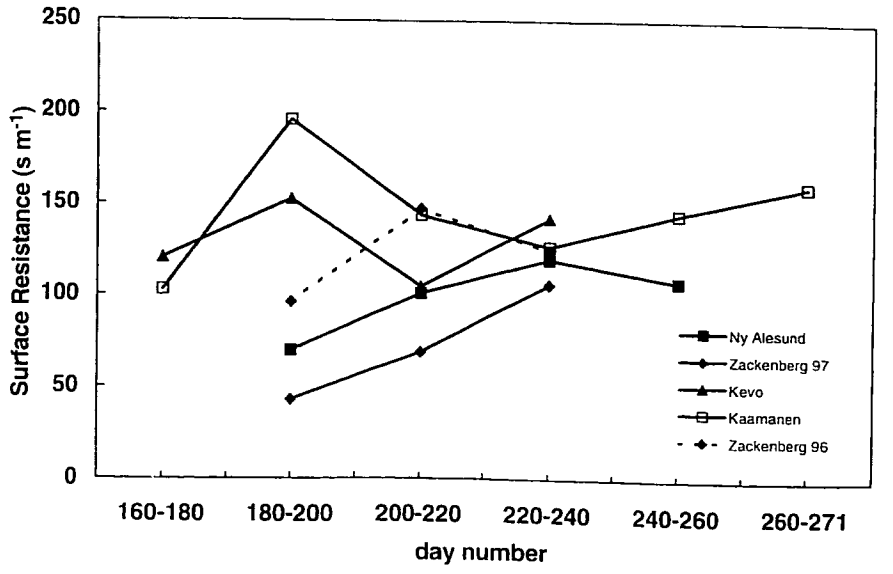

Fig. 9. Seasonal variation of surface resistance R_s (ms^{-1}) for the four sites

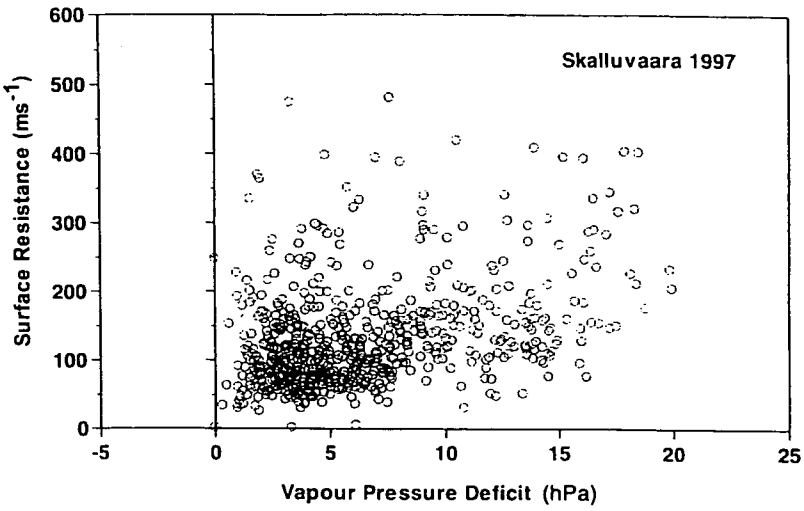

Fig. 10. Dependence of surface resistance R_s (ms^{-1}) on the vapour pressure deficit for Skalluvaara

presumably the effect of the high water table directly after snowmelt (the snow disappeared at day 143). The resistance remained high for the next 20 day period, and then dropped. Finally the resistance rose after day 240. The NDVI (Normalised Difference Vegetation Index) and CO_2 flux measurements at Kaamanen (not shown but see Laurila et al., this issue) suggest that the vegetation did not green up until day 180 and may not have peaked until after day 200. Thus the low resistance between days 200 and 240 corresponded to the period of maximum greenness (see Laurila et al., this issue). The vegetation died rapidly after the first frosts in early September and this probably explains the increase of resistance in the latter part of the year.

The surface resistance values calculated for Skalluvaara showed a similar seasonal pattern during June, July and August (days 160–240), unfortunately the measurements did not extend far enough into September to see the effect of the Autumn dieback. At the more northerly sites the resistance started at a very low value in June, directly after snowmelt, and increased through July and August, presumably as the surface dried out.

No consistent diurnal variations were shown at the sites but all sites showed some increase of resistance with increasing vapour pressure deficit (see for example Fig. 10 for Skalluvaara). This was not so marked at the more northerly sites, due to the smaller range and lower values of the deficits observed at these sites.

7. Conclusions

The direct measurements of the active season energy and water fluxes from four high latitude wetland sites are presented. The cumulative totals show many similarities, with similar total radiative energy inputs and similar energy partition into latent and sensible heat flux; with an approximately equal balance of sensible and latent heat in the early part of the season and greater latent heat in the second half. The two northerly sites have permafrost and at these sites a substantial proportion of the radiant energy goes into melting the soil water in the active layer during the summer. One result of this substantial 'loss' of energy is that the total latent heat flux for the active season is about 200 $MJ\,m^{-2}$ (equivalent to just under 100 mm evaporation) at the more northerly sites and over 400 $MJ\,m^{-2}$ (near to 200 mm evaporation) at the Finnish sites.

A number of other studies have shown that the evaporative ratio is approximately one half (see e.g., Rott and Obleitner, 1992; Ohmura, 1982; Fitzjarrald and Moore, 1992). However Harding and Lloyd (1998) showed that, while this value was typical for a well-vegetated surface, over a surface with sparse vegetation, typical of polar deserts, a lower ratio was more likely. Also Rouse et al. (1987) found higher bowen ratios (lower evaporative ratios) at low temperatures. This study found values for the Priestley–Taylor coefficient of less than one, a value consistent with the observed, high surface resistances (Baldocchi and Vogel, 1997). In

contrast Stewart and Rouse (1976) found values near to 1.26 (the commonly quoted value for lower latitudes) for a sedge meadow in the Hudson Bay area (although they did find lower values for a lichen dominated raised beach).

The calculation of effective surface resistance by the inversion of the Penman–Monteith equation provides a means of separating the ability of the surface to evaporate from the atmospheric demand. The pattern of the hourly calculated values of r_s show large variations but many patterns can be discerned and again the two northerly sites show a different behaviour to the sites in northern Finland. The mean values of r_s are approximately 50% higher at the Finnish sites and this may be related to the more deciduous nature of the vegetation at the Finnish sites. At these sites there is little green vegetation at the beginning and end of the season whereas at the higher latitude sites evergreen vascular plants and mosses dominate the vegetation. The vapour pressure deficits are also larger at the southern sites, which will tend to lead to larger resistance values. The Finnish sites show a characteristic seasonal behaviour with low values of r_s directly after snowmelt, r_s then rises as the snowmelt flooding drops. By July the resistance drops again as the vegetation develops and then finally rises in September as the vegetation dies back. At the northerly sites the pattern is simpler with the resistance rising steadily throughout the season, as the surface gradually dries out. Rouse et al. (1987) found similar values for canopy resistance for sedge grass in the Hudson Bay area (typically about $140\,s\,m^{-1}$). However this latter study describes a rapid increase in surface resistance below 12 °C, a feature not found in these measurements.

In conclusion we see that the overriding control on the seasonal energy balance is by the presence of snow, which determines both the start of the active season and also the initial soil moisture conditions. There is also a strong seasonal variation in the surface resistance, which is related to both the initial flooding following the snowmelt and the subsequent vegetation growth (a feature itself controlled by final disappearance of the snow cover). The final increase in surface resistance is due to the senescence of the vegetation, which is probably a phenologically driven process, but may be related to the first autumn frosts. Harding and Lloyd (1998) demonstrated a considerable year to year variability in the overall energy balance at the Svalbard site. This variability was again related to the occurrence of a snow cover. In this case the crucial factor was the depth of the snow cover in the spring. The surface resistance values at the two northern sites appear to be much less than those further south. It is not clear whether this is a climatic influence (for example due to low vapour pressure deficits) or a feature of the vegetation (an increased dominance of mosses and bare soil). However it is likely that climate warming might lead to change in the makeup of the vegetation, probably with increased dominance of vascular plants, and an increased dryness of the air, both these processes will lead to a increase in the effective surface resistance of the vegetation community. This study points to the considerable sensitivity of the energy and vegetation cycles to the physical climate and suggests a large potential for feedbacks between changes in climate and the surface energy balance.

Acknowledgements

The authors would like to thank the numerous field workers from the three Institutes who assisted with the measurements, often in very difficult conditions. The measurements were partly funded through the EU funded LAPP programme (contract number ENV4-CT95-0093).

References

Baldocchi DD, Vogel A (1997) Seasonal variation of energy and water vapor exchange rates above and below a boreal jack pine canopy. J Geophys Res 102: 28939–28951

Bay C (1998) Vegetation mapping of Zackenberg valley, Northeast Greenland. Danish Polar Center and Botanical Museum, University of Copenhagen, 29 pp

Brattbakk I (1981) Vegetasjonskart S10 V28H60 (vegetation map) 1:10,000. Ny-Ålesund, Brøggerhalvøya, Svalbard. K norske Videnskap Selsk Mus Bot avd Trondheim

Christensen TR, Jonasson S, Callaghan TV, Havström M (1999) On the potential CO_2 release from tundra soils in a changing climate. Applied Soil Ecol 11: 127–134

Fitzjarrald DR, Moore KE (1992) Turbulent transports over tundra. J Geo Res 97: 16717–16729

Garratt JR (1992) The atmospheric boundary layer. Cambridge: Cambridge University Press, 316 pp

Hämet-Ahti L (1963) Zonation of the mountain birch forests in northernmost Fennoscandia. Ann Bot Soc "Vanamo" 34(4): 1–127

Harding RJ, Lloyd CR (1998) Fluxes of water and energy from three high latitude tundra sites in Svalbard. Nordic Hydrol 29: 267–284

Huntingford C, Monteith JL (1998) The behaviour of a mixed-layer model of the convective boundary layer coupled to a big leaf model of surface energy partitioning. Bound-Layer Meteorol 88: 87–101

IPCC (1996) Climate change 1995 – the science of climate change. Cambridge: Cambridge University Press

Laurila T et al (2000) Seasonal variations of net CO_2 exchange in European Arctic ecosystems 70: 183–201

Liestøl O (1977) Pingos, springs and permafrost in Spitsbergen. Norsk Polarinstitutts Årbok 1975: pp 7–29

Liestøl O (1980) Permafrost conditions in Spitsbergen. Frost action in soils. Oslo. Publication No 21

Lloyd CR (1998) The application of an instrument for non-distructive measurements of soil temperature and resistance profiles at a high Arctic field site. Hydrol and Earth Sys Sci 2: 121–128

Meltofte H, Rasch M (eds) (1998) Zackenberg Ecological Research Operations, 3rd Annual Report, 1997. Danish Polar Center, Ministry of Research and Information Technology

McNaughton KG, Spriggs TW (1989) A mixed layer model for regional evaporation. Bound-Layer Meteorol 34: 243–262

Moncrieff JB, Massheder JM, de Bruin H, Elbers J, Friborg T, Heusinkveld B, Kabat P, Scott S, Soegaard H, Verhoef A (1997) A system to measure surface fluxes of momentum, sensible heat, water vapour and carbon dioxide. J Hydrol 188–189: 589–611

Monteith JL (1965) Evaporation and environment. Proceedings of Symposium on Experimental Biology 19: 205–234

Myneni RB, Keeling CD, Tucker CJ, Asrar G, Nemani RR (1997) Increased plant growth in northern high latitudes from 1981 to 1991. Nature 386: 698–702

Ohmura A (1982) Evaporation from the surface of the arctic tundra on Axel Heiberg Island. Wat Res Res 18: 291–300

Overpeck J, Hughen K, Hardy D, Bradley R, Case R, Douglas M, Finney B, Gajewski K, Jacoby G, Jennings A, Lamoureux S, Lasca A, MacDonald G, Moore J, Retelle M, Smith S, Wolfe A, Zielinski G (1997) Arctic environmental change of the last four centuries. Science 278(5341): 1251–1256

Paulson CA (1970) The mathematical representation of wind speed and temperature profiles in the unstable atmospheric surface layer. J Appl Meteorol 9: 857–861

Post WM, Emanuel WR, Zinke PJ, Stangenberger AJ (1982) Soil carbon pools and world life zones. Nature 298: 156–159

Priestley CHB, Taylor RJ (1972) On assessment of surface heat flux and evaporation using large-sale parameters. Mon Wea Rev 100: 81–92

Rott H, Obleitner F (1992) The energy balance of dry tundra in western Greenland. Arctic and Alpine Res 24: 352–362

Rouse WR, Hardill SG, Lafleur P (1987) The energy balance in the coastal environment of James Bay and Hudson Bay during the growing season. J Climatol 7: 165–179

Shuttleworth WT, Gash JHC, Lloyd CR, McNeil DD, Moore CJ, Wallace JS (1988) An integrated micrometerological system for evaporation measurement. Agric Meteor 43: 295–317

Stewart RB, Rouse WR (1976) Simple models for calculating evaporation from dry and wet tundra surface. Arctic and Alpine Res 8: 263–274

Young KL, Woo M (1999) Hydrological response of a patchy high arctic wetland. Proc of 12th Symposium of Northern Research Basins, Iceland 1999: 385–409

Authors' addresses: C. R. Lloyd, R. J. Harding, Institute of Hydrology-Wallingford, McLean Building, Crowmarsh Gifford, Wallingford, Oxfordshire OX 10 8BB, UK; T. Friborg, Institute of Geography, University of Copenhagen, Denmark; M. Aurela, Finnish Meteorological Institute, Helsinki, Finland.

Theor. Appl. Climatol. 70, 167–182 (2001)

Theoretical and Applied Climatology

Institute of Hydrology, Wallingford, United Kingdom

On the physical controls of the carbon dioxide balance at a high Arctic site in Svalbard

C. R. Lloyd

With 8 Figures

Received November 1, 1999
Revised April 17, 2000

Summary

Current predictions of the effects of climate change indicate that the Arctic may experience a larger than average increase in temperature with consequent changes to the length of the snow-free active summer period, winter snow depth and amount and frequency of summer precipitation being highly probable. This paper reports on measurements of carbon dioxide flux at a high arctic site at Ny-Ålesund (78° 56′ N, 11° 55′ E), Svalbard and the physical climate variables that largely control this flux. It is shown that during three important precipitation-free periods of the active summer period, namely post snowmelt, high summer, and early autumn, the net balance between CO_2 flux from the soil (due to respiration of roots and soil organisms) and CO_2 assimilation by the vegetation is controlled largely by soil temperature and solar radiation. A simple combined photosynthetic assimilation-soil respiration model is shown to be capable of simulating the net CO_2 flux during mid-summer, but is less proficient in the post snowmelt period and in early autumn when the simple models' inability to simulate the effects of emergent growth and ponding during the former and senescence, freezing temperatures and dew during the latter indicates the need for a more complex descriptive model. The net CO_2 flux during the measurement periods progresses from a net CO_2 source of $0.3\,gC\,m^{-2}\,d^{-1}$ during late snowmelt to a mid summer net CO_2 sink of $-0.39\,gC\,m^{-2}\,d^{-1}$, returning to a net CO_2 source of $0.1\,gC\,m^{-2}\,d^{-1}$ in the early autumn. Simple extrapolation of the data indicates that, during the active summer season in 1995, this site was a net sink of CO_2 of approximately $-9\,gC\,m^{-2}$.

1. Introduction

Global Climate Model (GCM) sensitivity experiments indicate that atmospheric warming due to increased greenhouse gases will be greatest in the Arctic (e.g., Kattenberg et al., 1996). The implied effect of this warming is to increase the release of carbon dioxide and methane from the deep organic soils of the tundra – a conjecture somewhat supported by experimental evidence (e.g., Billings et al., 1982; Oechel et al., 1993). However, Post et al. (1982) indicated that while the tundra "life-zone group" contains the highest amount of soil carbon there is a steep gradient in soil carbon densities across the tundra "life-zones" of the order of a factor of 5 between moist tundra and rain tundra – a factor difference which would be increased if the polar semi-desert tundra of the high arctic were included. Arctic tundra lands devoid of ice cover $5.6 \times 10^6\,km^2$, 20 per cent of which is high arctic polar semidesert, typical of Svalbard. Net annual plant production of vascular plants (above and below ground), mosses and lichens range from $1\,g\,m^{-2}$ in the polar deserts to $1000\,g\,m^{-2}$ in the low Arctic (Bliss and Matveyeva, 1992). Pertinently, currently unpublished evidence is beginning to indicate that the

descriptions of the terrestrial-atmosphere exchange of water vapour, heat and carbon dioxide may be deficient in some tundra regions where mosses and lichens exist alongside vascular plants and the soil is subject to not only surface freezing but also permafrost. In consequence, the Arctic cannot be treated as a single biome, and consequently the underlying processes governing the energy, water and carbon exchange over the different surfaces need further research.

In particular, for the high Arctic, while the predictions for temperature increase are thought to be relatively secure, those for precipitation and active season length are less so. Precipitation change predictions for Svalbard are from +2 mm to −1 mm per day (Mitchell et al., 1990). Higher winter temperatures may initially create increased winter snowfall (Warrick and Oerlemans, 1990; Miller and de Vernal, 1992), which may both increase the winter snowpack depth and shorten the length of the active season. While the overall physiological responses of mosses, lichens and flowering plants to light, temperature and CO_2 concentration are essentially similar (Proctor, 1982; Kershaw, 1985) the ability of vascular plants to limit their water loss through stomatal control will allow them to flourish (if nutrients are available) in a future warmer, drier polar region at the expense of the moss and lichen communities, which because of their thin cell walls and low internal resistance, rapidly lose water and consequent photosynthetic activity (Tenhunen et al., 1992). However, any change to the precipitation frequency and length of the active season will impact initially upon the radiation balance of the surface and its impact upon the photosynthetic activity of the vegetation and respiration from the soil.

In the high Arctic carbon dioxide assimilation by vegetation and respiration of carbon dioxide by plants and soil are often of similar magnitude and occur at the same time in the constant daylight of the active summer season. Despite this, the effect of physical processes such as vegetation and soil temperature, vegetation type and cover, light intensity and water content upon carbon dioxide exchange has been widely investigated but usually through artificial control of the environment, either in the laboratory or in the field and mostly, but not entirely, in Alaska and northern Canada (e.g., Peterson and Billings, 1975; Oechel and Collins, 1976; Bliss, 1977; Oberbauer et al., 1991; Whiting et al., 1992; Oechel et al., 1993; Verville et al., 1998; Christensen et al., 1998). Only the work reported by Richardson and Finegan (1977), Svoboda (1977) and Vitt and Pakarinen (1977) in Bliss (1977) from the polar semi-desert site at Truelove Lowland on Devon Island, Canada are from a surface similar to that surrounding Ny-Ålesund, Svalbard. On Svalbard itself, only chamber and cuvette measurements of CO_2 exchange have been reported (Dziadowiec, 1983; Schipperges, 1992).

The effect of the harsh conditions and remote nature of the Arctic upon instruments and their deployment has meant that research into larger scale CO_2 exchange using micrometeorological methods has been relatively recent, again in Alaska, Canada and Greenland (see Coyne and Kelley, 1975; Fan et al., 1992; Vourlitis and Oechel, 1997; Soegaard and Nordström, 1999). Of these, only the work of Soegaard and Nordström could be classified as high Arctic, and their measurements were taken over surfaces with relatively high primary productivity in contrast to the high Arctic semi-desert site investigated in this paper.

This paper has two aims:

- To catalogue the field scale net CO_2 flux from a typical high Arctic polar semi-desert site.
- To show the extent to which a solar radiation and soil temperature driven model can adequately describe the measured net CO_2 flux.

2. Methods and materials

2.1 Modelling considerations

The aim of this paper are to show the magnitude and temporal variation of the net CO_2 balance and to indicate to what extent the CO_2 flux is a function of solar radiation and soil temperature. Consequently, models of carbon assimilation and soil respiration having solar radiation and soil temperature as driving data were chosen.

The carbon dioxide flux measured above a vegetated surface (A) is the net balance between the net assimilation of CO_2 from the atmosphere by vegetation photosynthesis (W) minus the net input of CO_2 into the atmosphere via plant (R_d) and soil respiration (R_s) where soil respiration is

the sum of heterotrophic microbial decomposition and root respiration viz.,

$$A = (W - R_d) - R_s \quad (1)$$

A micrometeorological convention is used in this paper whereby photosynthesis produces a negative CO_2 flux (extracting CO_2 from the atmosphere) and respiration a positive flux (adding CO_2 to the atmosphere). For convenience, the model used in this paper to evaluate Eq. 1 will be designated as the Net Ecosystem Exchange (NEE) model.

2.1.1 The soil respiration module

Soil respiration is influenced by soil temperature and to a lesser extent by soil moisture. Soil moisture at this site was not regarded as limiting soil respiration rates thereby enabling the soil respiration model of Lloyd and Taylor (1994) to be used. From a comprehensive survey of soil respiration results, they derived an empirical exponential equation relating soil respiration to soil temperature, which was an unbiased estimator over a wide range of temperatures, given by:

$$R_s = R_{10} e^{308.56\left(\frac{1}{56.02} - \frac{1}{T_s - 227.13}\right)} \quad (2)$$

where R_s is soil respiration, R_{10} is the soil respiration rate at 10 °C, T_s is soil temperature. This model has been successfully applied at a high Arctic fen site in Greenland by Soegaard and Nordstroem (1999).

2.1.2 The photosynthetic module

Several studies have indicated that cryptogams (mosses and lichens) probably fix CO_2 by the C_3 pathway as in most temperate and polar flowering plants (Rastorfer, 1971; Valanne, 1984). Although comprehensive models of photosynthetic behaviour in C_3 plants have been developed (e.g., Collatz et al. (1991)), the simple empirical Michaelis-Menten enzyme kinetic model which can simulate the functional response of leaf-level photosynthesis to light (if not the biochemistry) was chosen to investigate the importance of solar radiation on the net CO_2 exchange. The basic form of the Michaelis-Menten kinetic model as used by Hollinger et al., 1994 is described by:

$$P = \frac{P_{\max} I}{K_m + I} - R_d \quad (3)$$

where $P_{\max}$ is a maximum rate of photosynthesis, I is light intensity measured as the photosynthetically active photon flux density (PPFD), K_m is the Michaelis constant (the PPFD at which P is half of $P_{\max}$) and R_d is a respiratory term.

2.1.3 Emergence and senescence factors

The soil respiration has little seasonality other than through the change in soil temperature and moisture that occurs during the active summer season. In contrast, the arctic vegetation rapidly changes from inactivity under the snowpack to full photosynthetic activity once the snow has disappeared (Shaver and Kummerow, 1992). Although not as rapid, the vascular vegetation begins to senesce during the late summer, even though light amounts are still sufficient for growth. However, the cryptogams will continue to photosynthesise, providing light and moisture are sufficient, until stopped by continuous freezing temperatures (Longton, 1988a). These two processes of emergence and senescence moderate the overall photosynthetic rate given by Eq. 3. A symmetric sigmoid model (Landsberg, 1977), used to simulate these processes, has the general form:

$$y = \frac{y_{\max}}{1 + e^{-(b+kx)}} \quad (4)$$

where $y_{\max}$ is an asymptotic value and b and k are shape factors. By setting $y_{\max} = 1$ and using y as a multiplicative factor to the photosynthesis model, photosynthesis during emergence and senescence were constrained between zero and the maximum photosynthetic activity.

2.1.4 Model performance and parameter evaluation

The performance of the model was assessed using the method recommended by Willmott (1984). He argued that the usual means of reporting the quantitative correlation between measured or observed (O) and modeled or predicted (P) values, namely Pearson's product-moment correlation coefficient (r) or the coefficient of determination (r^2), are insensitive to a wide range of additive and proportional differences that can exist between O and P. In this paper, Willmott's statistic designated as the degree of agreement (d) is used. The statistic d varies between 0 (complete

disagreement) and 1 (perfect agreement) and is given by:

$$d = 1 - \frac{N.RMSE^2}{\sum_{i=1}^{n}[(P_i - \overline{O}) + (O_i - \overline{O})]^2} \quad (5)$$

where N is the number of observations and $\overline{O}$ is the mean observed value. *RMSE* is the root mean square error given by:

$$RMSE = \left[N^{-1}\sum_{i=1}^{N}(P_i - O_i)^2\right]^{\frac{1}{2}} \quad (6)$$

which can be separated into systematic ($RMSE_s$) and unsystematic ($RMSE_u$) parts (Willmott, 1981) through the expression:

$$RMSE^2 = RMSE_s^2 + RMSE_u^2 \quad (7)$$

In assessing whether a model is acceptable, not only should *RMSE* be low, but $RMSE_s$ should be relatively small, i.e., the model explains most of the systematic variation and $RMSE_u$ should approach *RMSE*.

To assess the effect of solar radiation and soil temperature upon the overall CO_2 balance of this site, the four parameters of the NEE model, namely R_{10}, P_{max}, K_m and R_d and the two emergence/senescence factors (b and k) were optimised for each of the individual periods. The optimisation was a simple maximisation of d through examination of the entire parameter space occupied by the six parameters within selected but appropriate ranges.

2.2 The Ny-Ålesund site

The measurement site was located within the Bayelva floodplain to the west of Ny-Ålesund, Svalbard (79° 56′ N, 11° 55′ E). A full description of the site is given in Lloyd et al. (1996) and Lloyd et al. (This Issue) but pertinent details are repeated here. Climate measurements were sited on a 5° north facing slope of approximately 200 m in length which terminated in a floodplain area approximately 250 m both in length and width where the flux measurements were made.

The vegetation around Ny-Ålesund, as in the rest of Svalbard, has a mosaic character, where over a few square metres, it may alternate between communities of plant species typical of mounds and ridges and those typical of wetland depressions. The large differences in the distribution of plant communities are more a consequence of soil moisture and snow cover rather than the underlying geology. Despite the availability of 24 hour daylight from 18 April, the first spring vascular plants do not flower before mid-June and the growing period is generally over around mid-August, coincident with the end of the midnight sun period. Mosses and lichens, however, will continue to photosynthesise from first emergence from the snowpack in the spring through the summer and autumn, providing temperature, moisture and light levels allow it (Longton, 1988a). The vegetation at the study site consists of three main plant communities. These are designated (Brattbakk, 1981) as 100–50% *Luzula confusa* lichen heath (Norw. Vardefrytle lavhei), 100–50% *Saxifraga oppositifolia* lichen heath (Norw. Rødsildre lavhei) and 100–50% *Deschampsia alpina* snow-bed community (Norw. Fjellbunke snøleie). There is also a small strip of < 10% *saxifraga* heath close to the Bayelva river. The percentages refer to the proportion of total *vegetation* cover not the proportion of ground area that the vegetation covers. In particular, the major species at the site were *Saxifraga oppositifolia, Cetraria delisei, Drepanocladus* spp. and *Luzula confusa*. A simple vegetation mapping of the flux measurement site indicated that 48 per cent was lichen or moss, 20 per cent of the surface was vascular plants, 28 per cent was bare soil and 4 per cent was stone-covered.

The soil on the slope is a thin (0.02 m) organic soil overlying clay silt with stone stripes formed by permafrost action. The flat floodplain has a similar thin organic soil overlying schist and psammite gravels interspersed with a clay fraction.

2.3 Climate and soil measurements

For completeness, although not all used in this paper, the following climate and soil variables were measured. An Automatic Weather Station (AWS) was situated halfway up the slope and measured the separate components of incoming shortwave (CM5, Kipp and Zonen, NL) and longwave radiation (PIR, Eppley Lab, Rhode Island, USA), reflected shortwave radiation (CM5, Kipp and Zonen, NL), net radiation (Didcot Instruments, Abingdon, UK), relative humidity and air temperature (MP100A, Rotronic AG, Switzerland),

windspeed and wind direction (both Didcot Instruments, Abingdon, UK), rainfall (Rimco 0.5 mm, Australia) and snowdepth using an ultrasonic distance sensor (UDG01, Campbell Scientific, Shepshed, UK). Adjacent to the AWS were soil temperature and resistance profile units, initially used to indicate the thawing front, but also the soil temperature and soil moisture during the active season as described in Lloyd (1998). Two of these profile units measured soil temperatures using thermocouples and surrogate soil moisture from soil resistance values at 25 mm depth intervals from the surface down to 250 mm and 100 mm depth intervals from the surface down to 0.8 m.

2.4 Carbon dioxide and water vapour flux measurements

Towards the middle of the adjoining floodplain, fluxes of sensible and latent heat, momentum and carbon dioxide were measured using the eddy correlation technique (e.g., Shuttleworth et al., 1988; Moncrieff et al., 1997). A thin mast supported at 2.7 m a three dimensional sonic anemometer (Gill Solent, Lymington, UK) and an inlet tube through which air was conveyed to an infrared gas analyser (IRGA, 6262, Licor Inc, Lincoln, Nebraska, USA) situated 0.5 m above the surface which measured the concentrations of water vapour and carbon dioxide. The inlet tube consisted of a specially formed stainless steel tube of 5 mm ID and 0.5 m length which drew air from a position adjacent to the measurement volume centre of the sonic transducer array. The inlet had a cover which prevented any rainfall from entering and also minimised air being drawn from within the sonic anemometer measurement volume. The stainless steel tube was coupled to a length of silicone rubber tube (Masterflex C-FLEX Tubing, Barnant Co., Illinois) of the same diameter chosen for its impermeability to water vapour and carbon dioxide. Air was sucked down this tube through the IRGA using a membrane pump (Charles Austen, Byfleet, UK) on the outflow side of the IRGA at a flowrate of 12.5 $lmin^{-1}$. This flowrate minimised lagtimes and maintained the turbulent structure within the sample tube but is above the maximum flow for the IRGA. The flow was therefore split with 3.5 $lmin^{-1}$ passing through the sample cell of the IRGA. The IRGA was operated in absolute mode, in which the air in the sample cell is compared to air flowing in a closed loop through an adjacent reference cell. This reference air had all water vapour and carbon dioxide removed from it using chemicals.

2.5 Eddy correlation data logging

The analogue outputs from the IRGA were transmitted to the anemometer, digitised and then logged together with the anemometer outputs by a laptop computer at a frequency of 21 Hz. The raw data, amounting to 24 Mb per day, were also logged on removable hard disks connected to the laptop. Various corrections to the fluxes for co-ordinate rotation, sensor separation, damping of fluctuations and high frequency loss (see Moore, 1986; Moncrieff et al., 1997) were included either within the logging or in post-processing software. The fluxes were calculated on-line and output as 20-min averages. In order to compare fluxes with the other data from the AWS and the soil sensors, the period fluxes were combined to produce hourly values.

2.6 IRGA calibration

From time to time the IRGA requires calibration for drift in both zero offset and gain. The IRGA used in this study had been serviced and calibrated by the manufacturer prior to the 1995 field season. The standard practice of calibrating the span (gain) of the IRGA at regular intervals using dew-point hygrometers and span gases was not carried out. In the high arctic summer, where air temperatures are typically about 5 °C and relative humidities are usually above 80 per cent, dew-points are often very close to zero, if not negative and span gas bottles left in the field can be subject to settling which could lead to erroneous concentration values. The possibility of calibrating the IRGA wrongly was therefore a possibility. Experience of other researchers with this instrument has shown that if the zero calibration does not drift substantially, then the gain will also not have drifted. Zero calibrations, involving chemical removal of CO_2 and H_2O, were performed every week with this in mind and the IRGA was serviced and calibrated by the manufacturer at the start of each season and calibrated at the Institute of Hydrology at the end of each season before being returned to the manufacturer for

servicing. While drift in the zero offset has no effect upon the flux value, there is a nearly linear relationship between gain drift and flux error. The seasonal drift in gain was less than 5 per cent and fluxes were adjusted by this amount assuming a constant drift in time.

2.7 Measurement campaigns

The AWS was installed at the site in June 1994 and provided nearly continuous hourly data to July 1999. The soil temperature and soil resistance profile units were installed on 13 June 1995 and have again provided nearly continuous data to July 1999.

The flux measurement system was operated during three campaigns in 1995 (26 June–6 July, 25 July–11 Aug, 29 Aug–5 Sep.). The neccessity to service the flux system every 2–3 days meant that data could only be taken when staff were present at Ny-Ålesund. Periods within these campaigns have been chosen to illustrate the major physical controls on the carbon dioxide balance at this high arctic field site.

3. Results

3.1 Overall carbon dioxide balance

Figure 1 shows the daily and cumulative net carbon exchange together with the precipitation events during the 1995 active season. Also shown are the particular periods within those campaigns that have been chosen for further investigation of the relationship between net carbon exchange and soil temperature and solar radiation. Summer period rainfall was lower than average during 1995 at 59 mm (mean precipitation in 1971–80 during the period June–Aug was 88 mm – Steffensen, 1982). Rainfall events at Ny-Ålesund during the summer are usually light drizzles with rainfall rates of 0.5 mm per hour being typical and with only occasional heavier events. It is not unusual for some of these precipitation events to be either snow or sleet. Analysis periods chosen are rainfall-free (as measured by the raingauge) but not necessarily precipitation-free, as will be shown below. The periods chosen for this analysis illustrate three important times during the active summer season: post snowmelt, with only isolated patches of snow lying on the ground; the major growth phase of mid-summer; and the vascular plant senescence and general atmospheric and soil cooling that occurs at the end of the summer and early autumn.

3.2 Physical processes

Soil temperature and soil moisture typically control the soil respiration of CO_2. Because of the location of this site within the floodplain of the Bayelva river, the site experiences lateral groundwater flow above the permafrost horizon from the adjacent braided streams, which maintains soil moisture at a fairly constant level, and except during the major

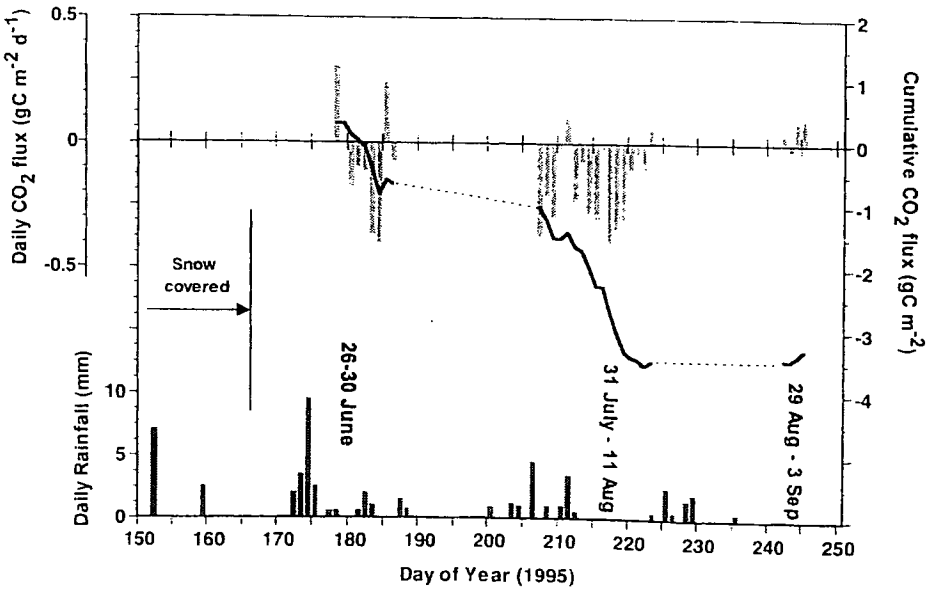

Fig. 1. Daily net CO_2 and cumulative net CO_2 flux, daily rainfall and the investigated periods during the three measurement campaigns in 1995

snowmelt period and during rainfall events, did not saturate the organic soil layer. Even in response to a rainfall event, Lloyd (1998) showed that soil moisture at this site did not markedly change below 20 cm and the moisture levels above this position returned quite rapidly to pre-rainfall event levels after cessation of rainfall as evaporation from the soil took place. The soil moisture effect upon carbon dioxide flux from the soil is therefore assumed constant and not investigated.

3.2.1 26–30 June 1995: the post-snowmelt period

At this time of year, not all the vegetation has begun its summer growth – only those moss hummocks that had appeared first through the disappearing snow cover. Photosynthesis will be dependent upon solar radiation but with 40 per cent of the ground being completely or partially bare, soil temperature (and hence soil respiration) is also heavily coupled to solar radiation. A regression of soil temperature against solar radiation during this period indicated a good linear relationship with an $r^2 = 0.75$. Figure 2 shows the hourly measurements of solar radiation, soil temperature at 25 mm (i.e., at the easily visible horizon between the organic and mineral soil layers) and CO_2 flux for the period between the two precipitation events bracketing this precipitation free period.

Figure 3 compares the measured and modelled net CO_2 flux. The optimisation process for the model parameters for this period produced the values for P_{max}, K_m, R_d and R_{10} shown in Table 1. $P_{max} = 1.39\,\mu mol\,m^{-2}\,s^{-1}$ is within the range of cryptogamic photosynthesis rates (0.3–1.8 $\mu mol\,m^{-2}\,s^{-1}$) reported by Kallio and Kärenlampi (1975). The estimate for the Michaelis constant, $K_m = 340\,\mu mol\,m^{-2}\,s^{-1}$ is acceptable in a mixed vascular and cryptogamic vegetation. Longton (1988b) indicates that mosses saturate at 0.5–0.7 $J\,cm^{-2}\,min^{-1}$ PAR (equivalent to 360–510 $\mu mol\,m^{-2}\,s^{-1}$ PPFD), which is approximately 30 per cent of the level typical for local angiosperms. Dark respiration $R_d = 0.024\,\mu mol\,m^{-2}\,s^{-1}$ is 0.017 of P_{max} – a proportion similar to that of 0.015 reported to occur between dark respiration and and the maximum rate of carboxylation of Rubisco in C_3 plants (Cox et al., 1999). The soil respiration rate at 10 °C, $R_{10} = 0.97\,\mu mol\,m^{-2}\,s^{-1}$ is between the value ($1.6\,\mu mol\,m^{-2}\,s^{-1}$) used by Soegaard and Nordstroem (1999) at their Zackenberg site in Greenland and a value of soil respiration = $0.6\,\mu mol\,m^{-2}\,s^{-1}$ obtained at 6.9 °C by Nakatsubo et al. (1998) at Ny-Ålesund.

Figure 3a shows the measured and modelled hourly average CO_2 flux and illustrates the high variability in measured fluxes compared to the modelled output. This difference in variability may be indicative of factors (e.g., heterogeneity) other than solar radiation and soil temperature contributing to the variability of the overall CO_2 flux. The post snowmelt period was characterised by high surface heterogeneity, due to snow patches,

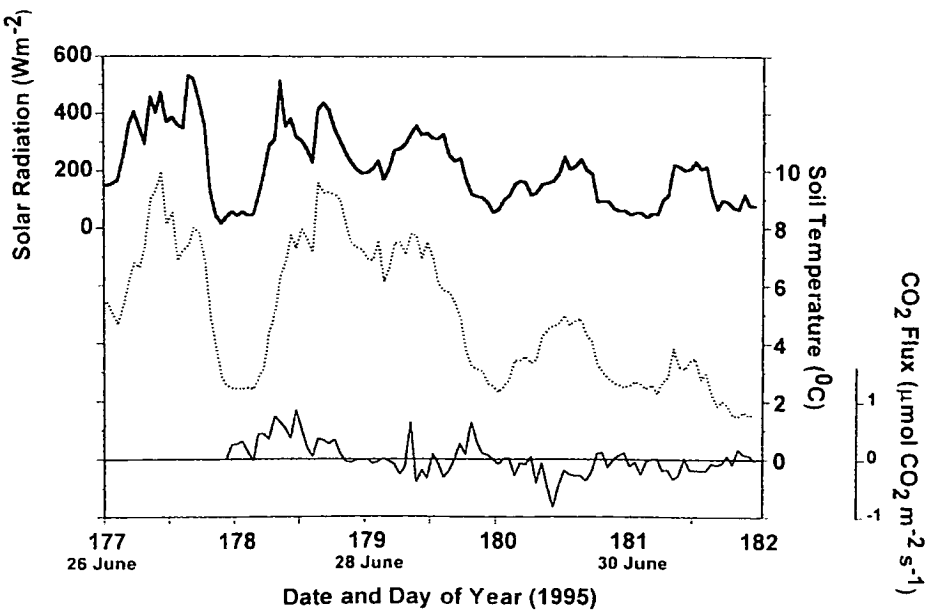

Fig. 2. Hourly average values during the period 26–30 June 1995 of Solar radiation (—), Soil temperature at 25 mm depth (.....) and net CO_2 flux (—)

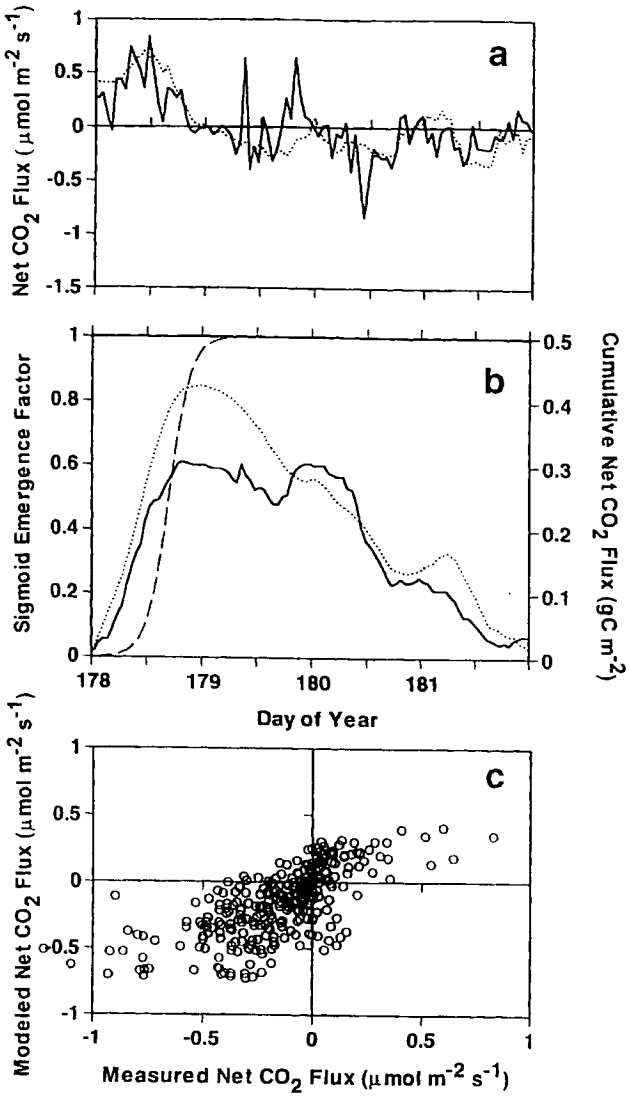

Fig. 3. Net CO_2 flux during the period 26–30 June 1995. (a) Hourly average values of measured (—) and modelled (.....) flux, (b) Cumulative measured (—) and modelled (.....) flux and the vegetation "emergence" factor (– – –), (c) Scatter plot of hourly modelled versus hourly measured flux

water pools and mixed dormant and active vegetation, a heterogeneity which is incapable of being simulated by a simple model of solar radiation and soil temperature from measurements at a single point. This difficulty of combining or comparing areal flux measurements with point measurements has been investigated by Lloyd (1995).

The cumulative CO_2 balances shown in Fig. 3b indicates an initial period of overall CO_2 flux into the atmosphere of $0.32\,gC\,m^{-2}$ followed by a period of overall CO_2 uptake with the total combined period being a slight CO_2 source of $0.07\,gC\,m^{-2}$. Also shown in Fig. 3b is the optimised form of the sigmoid "emergence factor" curve. Figure 3c shows the reasonable agreement between the measured and modelled CO_2 flux values. During this period the degree of agreement d between the hourly measured and modelled CO_2 flux values was 0.811 indicating good agreement. *RMSE* overall was low at 0.223 with $RMSE_u$ = 0.2029 approaching *RMSE* and $RMSE_s$ = 0.0198 equal to 9 per cent of *RMSE* indicating a reasonable model – see Table 1.

3.2.2 31 July–11 August 1995: high summer

Figure 4 shows the measured solar radiation, soil temperature and net CO_2 flux for this period of 12 days without rain. The vascular and cryptogamic vegetation should now be photosynthesising at rates controlled largely by available energy and plant moisture status. During such an extended period without apparent precipitation, there is a high probability of the mosses and lichens desiccating and reducing, if not entirely stopping, their photosynthesis. Despite having relatively clear skies, solar radiation levels during this period were lower as a result of the sun's lower elevation. The soil temperature at 25 mm depth again clearly follows solar radiation levels although the relationship is not as good as for the period 26–30 June. Only 53 per cent of the variation in soil temperature is explained by solar radiation – possibly indicating the effect of insulation of the drying bryophytes on the underlying soil surface during this time. This period of twelve days produced a net assimilation of $-2.06\,gC\,m^{-2}$, an average of $-0.17\,gC\,m^{-2}\,d^{-1}$. Figure 5, in a similar fashion to Fig. 3, compares the hourly and cumulative measured and model values for net CO_2 flux. The model's parameters were again optimised to produce a maximum in d for this period. The model parameter values are shown in Table 1. P_{max} has increased by 25 per cent, qualitatively in agreement with the observations that maximum photosynthetic rates in bryophytes are higher in summer than in the spring (Oechel, 1976). The Michaelis constant, K_m, has not substantially changed (−10%) and the dark respiration value, R_d has increased from 0.024 to 0.072 in line with the increased maximum photosynthetic rate and increased photosynthetic activity. The vegetation is assumed to be fully

Table 1. Optimised values for the six parameters in the combined Net Ecosystem Exchange model together with the statistics describing the performance of the model for the three investigated periods

Parameter		26–30 June	31 Jul.–11 Aug	29 Aug–3 Sep
Maximum rate of photosynthesis	P_{max}	1.39	1.75	1.58
The Michaelis-Menten constant	K_m	340	310	250
Dark respiration	R_d	0.024	0.072	0.042
Rate of soil respiration at 10 °C	R_{10}	0.97	0.68	0.61
Emergence/Senescence factor	Sigmoid b	−7.4	–	−0.2
Emergence/Senescence factor	Sigmoid k	0.43	–	0.006
Degree of agreement	d	0.811	0.819	0.4736
Root Mean Square Error	RMSE	0.2227	0.2107	0.1976
Unsystematic RMSE	$RMSE_u$	0.2029	0.1895	0.1584
Systematic RMSE	$RMSE_s$	0.0198	0.0211	0.0392

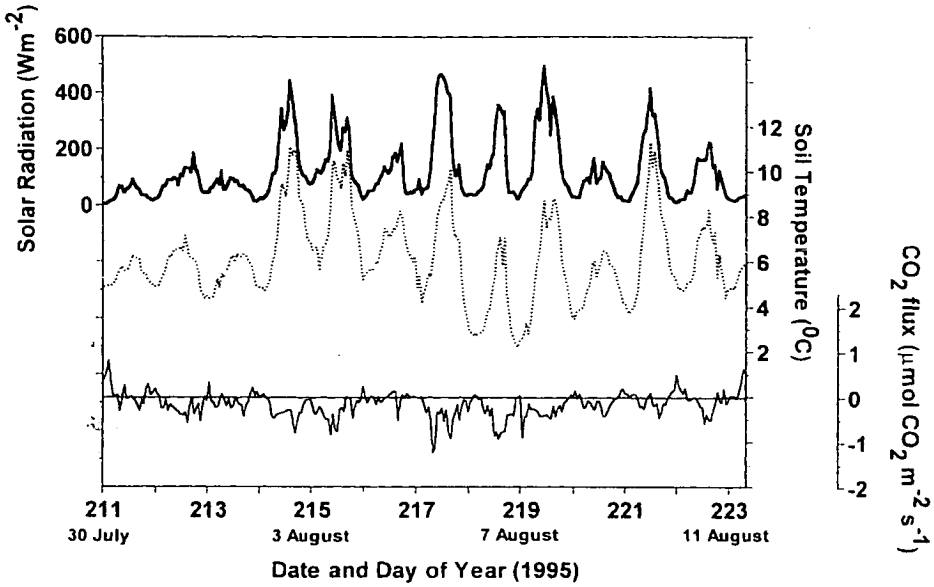

Fig. 4. Hourly average values during the period 31 July–11 August 1995 of Solar radiation (—), Soil temperature at 25 mm depth (.....) and net CO_2 flux (—)

"emergent" by this time and the "emergence factor" employed for the post snowmelt period has been set to 1 in the model. The soil respiration rate, R_{10} has decreased to 0.68, possibly indicating a more sustainable rate in contrast to the high rate obtained for the period following snowmelt. The high rate in the post snowmelt period modelling exercise may indicate the possible build-up of CO_2 in the soil horizon during the winter and early spring period before the soil becomes fully unfrozen. The degree of agreement d, $RMSE$, $RMSE_s$ and $RMSE_u$ are not substantially different to those within the post snowmelt period – these are shown in Table 1. Both the hourly and cumulative plots of measured and modelled net CO_2 (Fig. 5a and 5b) agree very well, with the model able to simulate the hourly values in contrast to the post snowmelt period. During the summer period, the heterogeneity due to snow patches, waterlogged areas and dormant vegatation has largely disappeared and the simple model appears adequate. In both the hourly and cumulative comparisons, the model appears to underestimate plant assimilation at the beginning and overestimate it towards the end of the period. While in the first instance, this is a consequence of the optimisation procedure in minimising the differences, it also indicates that the overall rate of plant assimilation may be reducing towards the end of the period as the cryptogams desiccate and reduce their photosynthetic contribution to the total plant assimilation. A plot of residual (Observed – Model)

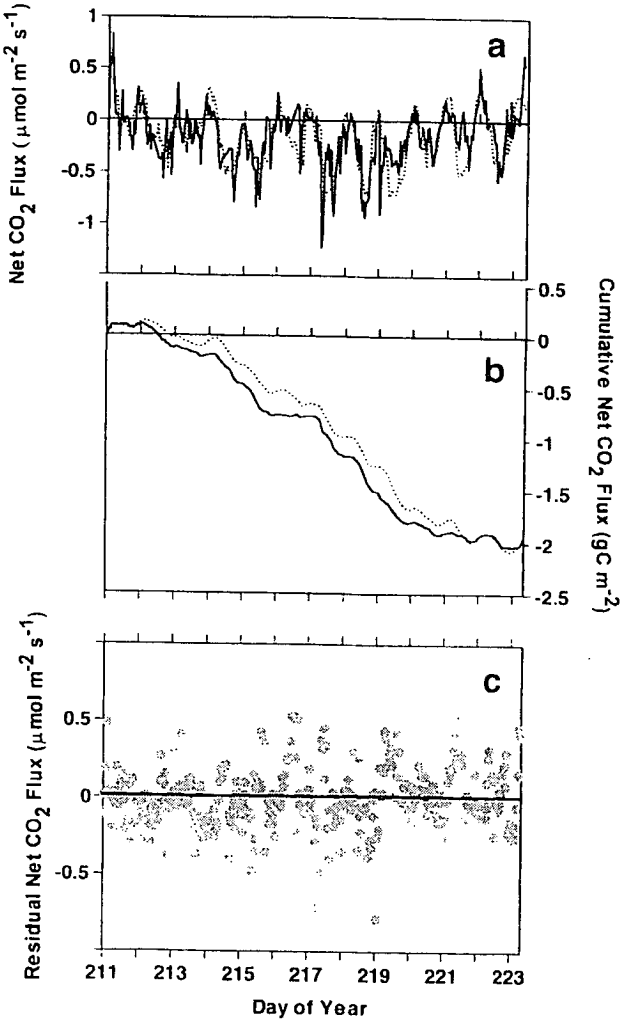

Fig. 5. Net CO_2 flux during the period 31 July – 11 August 1995. (**a**) Hourly average values of measured (—) and modelled (.....) flux, (**b**) Cumulative measured (—) and modelled (.....) flux and the vegetation "emergence" factor (– – – –), (**c**) Residual plot of hourly measured minus hourly modelled flux

values (Fig. 5c) shows the general adequacy of the model in that the residuals show constant variance and independence. The only real information that can be gained is the slight upward trend in the residuals with time which may be explained by the inadequacy of the model to simulate the dessicating cryptogams.

The cumulative plots in Fig. 5b also indicate another possible factor that is currently missing from the model but is important in cryptogam dominated surfaces. There are occasions when the model appears to indicate a net respiration when the measurements are showing either a neutral or even an overall assimilation. In reality this may be caused by re-wetting of the cryptogamic vegetation by dew, mist or fog. Figure 6 projects the difference between soil temperature and the dewpoint calculated from the sonic anemometer temperature and the AWS relative humidity measurements at 2.7 m onto the cumulative CO_2 flux measurements. As Monteith and Unsworth (1990) point out, any negative differences between the soil and dewpoint temperature over surfaces whose water content contains dissolved salts or water is held by capillary forces in a porous medium (i.e., both soil and bryophytes at this site) implies a strong possibility of dew formation at the surface. There are several occasions shown by the arrowed lines where the measured CO_2 trace (in contrast to the modelled output) turns from a carbon source to a carbon sink following a time of implied dew formation. Dew formation (and mist and fog) would appear to be important for this surface's carbon balance and its effects should probably be included in a more complex model.

3.2.3 29 August–3 September 1995: early autumn

The sun is much lower in the sky during this period which is reflected in the much lower solar radiation levels shown in Fig. 7. However the final three days have clear skies. Once again soil temperature at 25 mm closely follows solar radiation. This period's carbon dioxide flux balance is now characterised by soil respiration outweighing plant assimilation. The vascular plants visibly senesced during late August but the mosses and lichens would be capable of photosynthesis while moisture levels in their plant cells were sufficiently high. This photosynthetic period would have been extended as dew and frost formation replenished the cell moisture levels.

The measured hourly CO_2 flux and cumulative CO_2 flux are again compared in Fig. 8a and 8b respectively. The sigmoid "emergence factor" shown in Fig. 8b has now been reversed to model the senescence of the vascular plants. The model parameters were again optimised to maximise d and are shown in Table 1. P_{max} in the optimisation has fallen to 1.58, again consistent with both the gradual senescence of the vascular vegetation and observations that maximum photosynthetic activity in arctic vegetation reduces in the early autumn (Oechel, 1976). The Michaelis constant K_m has

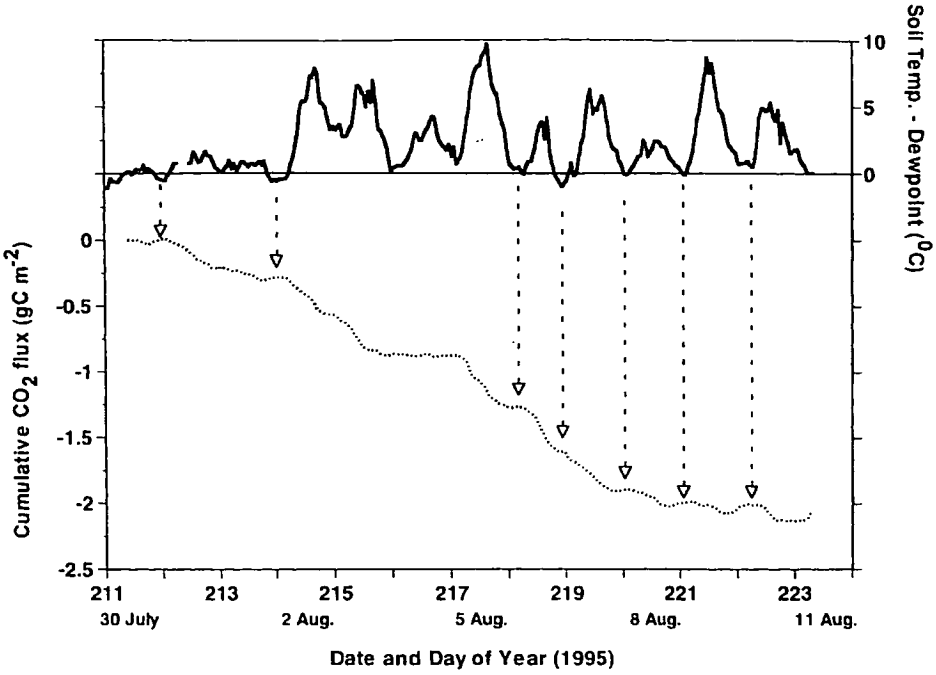

Fig. 6. Hourly average values during the period 31 July–11 August 1995 of the difference between soil temperature at 25 mm depth and dewpoint at 2.7 m (—); and the cumulative net CO_2 flux (.....)

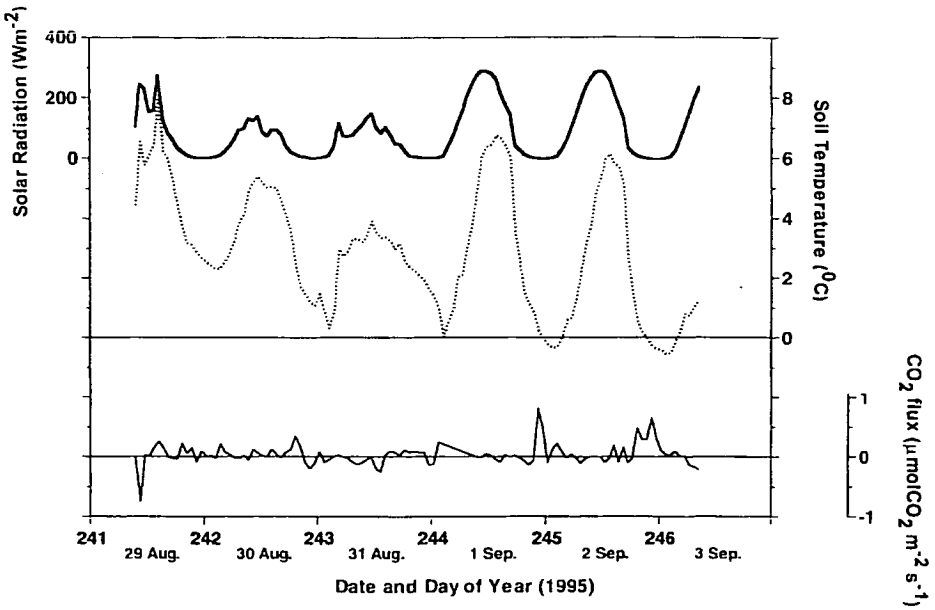

Fig. 7. Hourly average values during the period 29 August–3 September 1995 of Solar radiation (—), Soil temperature at 25 mm depth (.....) and net CO_2 flux (—)

dropped to 250 possibly reflecting the reduction in radiation levels. Both the dark respiration factor R_d and the soil respiration rate R_{10} have fallen to 0.042 and 0.61 respectively, consistent with a general slowing down of the CO_2 exchange process. The model is able to simulate the general trend of a net CO_2 source during the period but does not simulate the hour by hour variability in the measured flux. This is reflected in the low value for d and the other statistical parameter, *RMSE*. $RMSE_s$ is now 20 per cent of *RMSE* indicating that the model is worse at explaining the systematic variation in the observations than during the spring and summer periods where $RMSE_s$ were 9 and 10 per cent respectively. A plot of residual (Observed-Model) values (Fig. 8c)

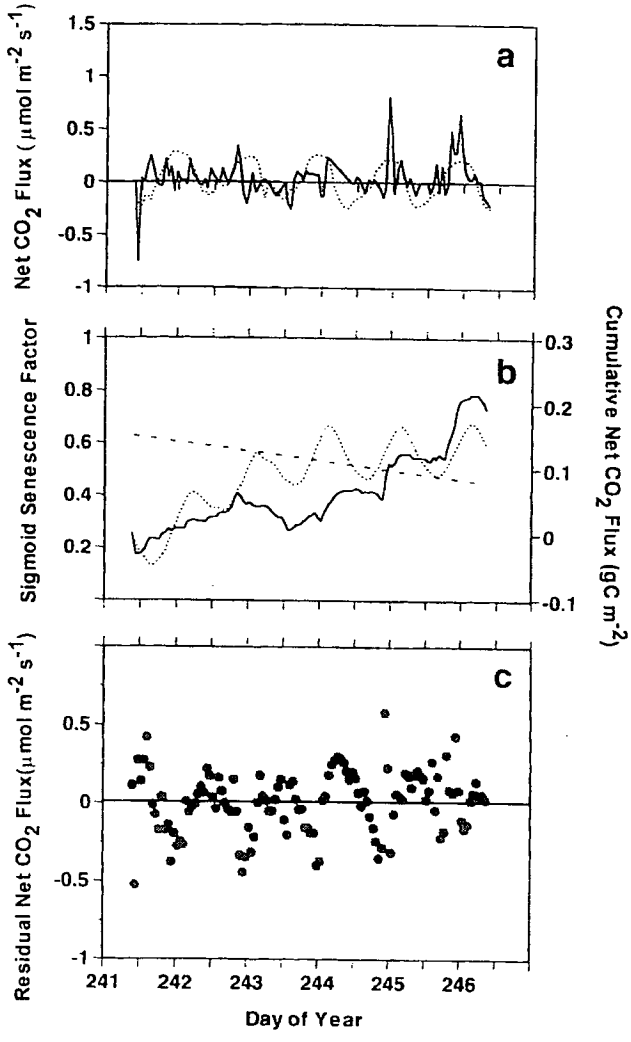

Fig. 8. Net CO_2 flux during the period 29 August–3 September 1995. (**a**) Hourly average values of measured (—) and modelled (.....) flux, (**b**) Cumulative measured (—) and modelled (.....) flux and the vegetation "senescence" factor (– – – –), (**c**) Residual plot of hourly measured minus hourly modelled flux

shows little divergence or trend over time but exhibits several sequences of serial correlation particularly during day 244.

4. Discussion

4.1 Overall CO_2 balance

The results presented here indicate that in general this high Arctic polar semidesert site follows the pattern of other high Arctic sites with a pattern of early season net CO_2 efflux followed by summer net CO_2 assimilation followed by a return to net CO_2 efflux in the autumn. However there is evidence that the surface can switch between being a sink or a source of CO_2 on a day to day basis depending upon the solar radiation level, near surface soil temperature and frequency/duration of precipitation, whether it be rain, snow, dew or frost. In responding to climate change, high Arctic polar semideserts may initially become a source of CO_2 if the region becomes warmer and drier, because soil respiration will exceed the assimilation by the mixture of vascular plants and dessicating bryophytes. This period of CO_2 efflux may be short-lived as not only is the current amount of organic matter available for soil respiration limited in these high Arctic semidesert soils, but the vascular plants in a milder climate would be expected to increase their growth rate and percentage cover thus increasing net assimilation *if nutrients were available*. This is an important point because the poor soil nutrient status of high Arctic polar semideserts may confer a degree of resilience to rapid change in these ecosystems in response to climate change (Wookey and Robinson, 1997; Robinson et al., 1998). If the climate at these sites becomes warmer and wetter, then the expected increase in vascular and mosses and lichen cover will again be constrained by the nutrient availability.

Net CO_2 production is difficult to compare with previous data, in which net plant production and net soil respiration were rarely measured at the same time at the same site. At the polar desert raised beach site at Truelove Lowland, Devon Island, Svoboda (1977) measured net above and below ground vascular plant production of 18 g m^{-2}, with bryophyte production of 2 g m^{-2} and lichen production of 3 g m^{-2} for areal ground coverage of 41.2, 10.4 and 9.5 per cent respectively. More generally in the high Arctic, Miller et al. (1983) estimated that Polar semi-desert was accumulating carbon at a rate of 4 gC m^{-2} yr^{-1} or 8 per cent of the total Arctic tundra accumulation, a figure comparable to that extrapolated from the measurements shown in Fig. 1.

The campaign based measurements presented here do not allow easy extrapolation to a net seasonal CO_2 balance. A maximum daily net CO_2 efflux of 0.3 gC m^{-2} was recorded at the beginning of the post snowmelt period possibly due to the release of soil CO_2 as the ground became unfrozen.

The maximum daily net CO_2 assimilation was $-0.39\,gC\,m^{-2}$. Average CO_2 balance during the post snowmelt period was $-0.14\,gC\,m^{-2}\,d^{-1}$ while during the period 31 July–11 August, the average CO_2 balance was $-0.19\,gC\,m^{-2}\,d^{-1}$ – a value comparable to the mean value obtained by Dziadowiec (1983) at a similar site on Svalbard. The early autumn period was characterised by predominantly net CO_2 efflux with an average period value of $0.04\,gC\,m^{-2}\,d^{-1}$ but occasionally days still produced uptakes of $-0.02\,gC\,m^{-2}$ but overall the trend was towards efflux of the order of $0.095\,gC\,m^{-2}\,d^{-1}$. With assumptions about the generality of the measurements and when senescence began in the vascular vegetation these values, if interpolated through the summer period, indicate that the site at Ny-Ålesund was a sink for CO_2 of approximately $-9\,gC\,m^{-2}$ although this value should be treated with caution. This amount can be contrasted with the high Arctic site at Zackenberg, N.E.Greenland (74° N), where Soegaard and Nordstroem (1999) using eddy correlation measured a growing season net ecosystem CO_2 exchange of $-96.3\,gC\,m^{-2}$ of which $-157.6\,gC\,m^{-2}$ was net carbon assimilation and $61.2\,gC\,m^{-2}$ was soil emission. Their site had almost total vegetation cover dominated by vascular plants demonstrating the wide range in CO_2 exchange that is present even in the high Arctic. At lower arctic latitudes, at the heavily researched sites in Alaska (68–72° N), carbon balances ranged from an accumulation rate of $-109\,gC\,m^{-2}\,yr^{-1}$ reported by Chapin et al. (1980) to carbon losses of $180–360\,gC\,m^{-2}\,yr^{-1}$ reported by Oechel and Riechers (1987).

Hence the "Arctic" as a whole has a wide range in the size of the carbon balance which needs to be considered when predicting the effect of climate change on the Arctic and the likely size of any resultant emission of CO_2 into the atmosphere.

4.2 Process responses

4.2.1 Solar radiation and temperature

Polar environments are often considered light-limited because maximum irradiance is lower than elsewhere, and NAR in flowering plants rises with increasing irradiance to levels approaching full sunlight (Tieszen, 1978). However, bryophytes reach light saturation at approximately 30 per cent of the level typical for adjacent vascular plants (Longton, 1988b) and midsummer solar radiation is often continuously above the moss compensation level. Net assimilation can therefore continue 24 hours per day at the highest latitude (other conditions being favourable). This may explain the success of the simple radiation driven photosynthetic model in simulating the summer CO_2 uptake. Schipperges (1992) in comparing CO_2 gas exchange in *Cetraria nivalis* and *C. delisei* at a field site near Ny-Ålesund found flatter light response curves for *C.delisei* with a light compensation point at $100\,\mu mol\,m^{-2}\,s^{-1}$ and light saturation at about $200\,\mu mol\,m^{-2}\,s^{-1}$. At this study field site during the period 31 July–11 August 1995, radiation amounts were above the light compensation point and saturation point for 75 and 48 per cent of the time respectively.

4.2.2 Soil respiration

Rates of carbon dioxide efflux (respiration) from the soil have been linked to thaw depth, water table depth, soil temperature and soil moisture (e.g., Funk et al., 1994; Oberbauer et al., 1996; Christensen et al., 1998). At the Ny-Ålesund site the water table depth and soil moisture varied little. Thaw depth is important for deep organic soils but probably has less effect upon shallow organic soils as found in polar semi-deserts. The use of a soil respiration model driven solely by soil temperature is therefore justified.

Sendstad (1981), at a lichen heath close to Ny-Ålesund dominated by *Cetraria delisei*, measured respiration from soil samples of between $40–96\,mg\,CO_2\,m^{-2}\,hr^{-1}$ (equivalent to 0.25–0.61 $\mu mol\,m^{-2}\,s^{-1}$) at 5 °C and 32 per cent H_2O during the summer of 1978. At a coastal strandflat located in Kaffiöyra, NW Spitsbergen, Dziadowiec (1983) using open chambers measured nearly $50\,g\,CO_2\,m^{-2}$ over a 48 day period with maximum and minimum hourly values of 56.8 and 31.7 $mg\,CO_2\,m^{-2}\,hr^{-1}$ (0.36 and 0.2 $\mu mol\,m^{-2}\,s^{-1}$ respectively) at a site described as a poorly developed arctic brown soil whose profile appears to closely resemble the site described in this paper. These figures compare well with the modelled soil respiration rates during the period 31 July–11 August where the average rate was 0.46 $\mu mol\,m^{-2}\,s^{-1}$ with maximum and minimum rates of 0.77 and 0.28 $\mu mol\,m^{-2}\,s^{-1}$ respectively.

4.2.3 Carbon assimilation

Identification of the processes responsible for above-ground uptake of CO_2 by the plant community is complicated by the different physiology of the vascular and cryptogam plant communities. Oechel and Sveinbjörnsson (1978) stated that net assimulation rates (NAR) in mosses at a site near Barrow, Alaska were only 8–9 per cent of that in vascular plant leaves. Of equal importance is the vascular plants' ability and cryptogamic plants' inability to utilise soil moisture for growth – the photosynthetic rate of the latter controlled by cell moisture levels filled by atmospheric wetting of its leaf surfaces and emptied by evaporation. The descriptive model used in this paper did not differentiate between vascular and cryptogamic vegetation but a predictive model would probably have to incorporate these important factors if the effects of climate change were to be fully investigated.

4.2.4 Modeling considerations

The modelling exercise in this paper demonstrated the ability of simple soil respiration and photosynthetic models using near surface soil temperature and solar radiation to describe the observed CO_2 fluxes during precipitation-free periods. For predictive purposes, this may not be sufficient as factors such as precipitation, percentage of vegetation cover, organic layer depth, soil moisture and the differing photosynthetic response of the vegetation cover may also change in response to climate change. The effect of some of these factors on the net CO_2 flux and the inadequacy of the simple model to fully simulate them have been hinted at through the comparison between the measurements and modelled results. There is therefore a need to improve the description of vegetation and soil processes within land surface models in order to account for these important factors affecting the heterogeneous moss/lichen/bare soil surfaces subject to soil freezing and permafrost which are typical of the high Arctic polar semi-desert.

5. Conclusions

The seasonal change in the net CO_2 flux at a high Arctic polar semi-desert site is examined for three important and different times of the arctic active season, namely the post-snowmelt, summer and early autumn periods. The observed net CO_2 flux, comprising respiration by soil and vegetation and assimilation by vegetation is shown, through the use of a simple combined soil respiration and photosynthetic model, to be largely controlled by the climate factors of near surface soil temperature and solar radiation. The periods were chosen to be free of precipitation but the results show that precipitation events, including dew formation, fogs and frosts are also important factors in maintaining bryophyte photosynthetic activity. The change from winter dormancy to full photosynthetic activity in the post snowmelt period and the gradual senescence of the vascular plants in the late summer and early autumn are also of importance. The heterogeneity of the post snow melt period due to both the vegetation emergence and the patchy snow cover and waterlogged ground creates particular problems in modelling this surface at a critical time of the active season when the surface changes from a general CO_2 source to a sink.

Extrapolation of the short period measurements to the whole active summer season, together with certain assumptions, indicate that the site at Ny-Ålesund during 1995 was a sink for CO_2 of approximately $-9\,gC\,m^{-2}$.

Acknowledgements

The author would like to thank Richard Harding, Tim Kyte and Mike Stroud of the Institute of Hydrology who assisted in the collection of the data and Nick Cox, Station manager of the NERC Arctic Station at Ny-Ålesund who helped in many ways with the logistics of operating at this site. The funding of this work was shared between NERC and the EU supported LAPP programme (Contract No. ENV4-CT95-0093).

References

Billings WD, Luken JO, Mortensen DA, Petersen KM (1982) Arctic tundra: a sink or source for atmospheric carbon dioxide in a changing environment? Oecologia 53: 7–11

Bliss LC (1977) Truelove Lowland, Devon Island, Canada: a High Arctic Ecosystem. Edmonton: University of Alberta Press, 533 pp

Bliss LC, Matveyeva NV (1992) Circumpolar Arctic vegetation. In: Chapin III FS, Jefferies RL, Reynolds JF, Shaver GR, Svoboda J (eds) Arctic ecosystems in a changing climate – an ecophysiological perspective. San Diego: Academic Press, pp 59–89

Brattbakk I (1981) Vegetasjonskart S10 V28H60 (vegetation map) 1:10,000. Ny-Ålesund, Brøggerhalvøya, Svalbard K norske Videnske Selsk Mus Bot avd Trondheim

Chapin III FS, Miller PC, Billings WD, Coyne PI (1980) Carbon and nutrient budgets and their control in coastal tundra. In: Brown J, Miller PC, Tieszen LL, Bunnell FL (eds) An arctic ecosystem: the coastal tundra at Barrow, Alaska. Stroudsburg, Pennsylvania: Dowden, Hutchinson & Ross, pp 458–482

Christensen TR, Jonasson S, Michelsen A, Callaghan TV, Havström M (1998) Environmental controls on soil respiration in the Eurasian and Greenlandic Arctic. J Geophys Res 103(D22): 29,015–29,021

Collatz GJ, Ball JT, Grivet C, Berry JA (1991) Physiological and environmental regulation of stomatal conductance, photosynthesis and transpiration: a model that includes a laminar boundary layer. Agric Forest Meteor 54: 107–136

Cox PM, Betts RA, Bunton CB, Essery RLH, Rowntree PR, Smith J (1999) The impact of new land surface physics on the GCM simulation of climate and climate sensitivity. Climate Dynamics 15: 183–203

Coyne PI, Kelley JJ (1975) CO_2 exchange over the Alaskan Arctic Tundra: Meteorological assessment by an aerodynamic method. J Appl Ecol 12: 587–611

Dziadowiec H (1983) Preliminary studies on carbon dioxide evolution from tundra soils of Spitsbergen (Kaffiöyra, Oscar II Land, NW Spitsbergen). Acta Universitatis Nicolai Copernici 18: 159–167

Fan SM, Wofsy SC, Bakwin PS, Jacob DJ, Anderson SM, Kebabian PL, McManus JB, Kolb CE, Fitzjarrald DR (1992) Micrometeorological measurements of CH_4 and CO_2 exchange between the atmosphere and subarctic Tundra. J Geophys Res 97(D15): 16627–16643

Funk DW, Pullman ER, Peterson KM, Crill PM, Billings WD (1994) Influence of water table on carbon dioxide, carbon monoxide, and methane fluxes from taiga bog microcosms. Global Biogeochem Cycles 8: 271–278

Hollinger DY, Kelliher FM, Byers JN, Hunt JE, McSeveny TM, Weir PL (1994) Carbon dioxide exchange between an undisturbed old-growth temperate forest and the atmosphere. Ecology 75: 134–150

Kallio P, Kärenlampi L (1975) Photosynthesis in mosses and lichens. In: Cooper JP (ed) Photosynthesis and productivity in different environments. IBP 3. Cambridge: Cambridge University Press, pp 393–423

Kattenberg A, Giorgi F, Grassl H, Meehl GA, Mitchell JFB, Stouffer RJ, Tokioka T, Weaver AJ, Wigley TML (1996) Climate models – projections of future climates. In: Climate Change 1995, the Science of Climate Change, IPCC, Cambridge: Cambridge University Press, pp 285–357

Kershaw KA (1985) Physiological ecology of lichens. Cambridge Studies in Ecology. Cambridge: Cambridge University Press, 273 pp

Landsberg JJ (1977) Some useful equations for biological studies. Expl Agric 13: 273–286

Longton RE (1988a) Adaptations and strategies of polar bryophytes. Bot J Linn Soc 98: 253–268

Longton RE (1988b) The Biology of polar bryophytes and lichens. Cambridge: Cambridge University Press, 391 pp

Lloyd CR (1995) The effect of heterogeneous terrain on micrometerological flux measurements: a case study from HAPEX-Sahel. Agric Forest Meteor 73: 209–216

Lloyd CR (1998) The application of an instrument for non-destructive measurements of soil temperature and resistance profiles at a high Arctic field site. Hydrology and Earth System Sciences 2(1): 121–128

Lloyd CR, Harding RJ, Robinson M (1996) Preliminary results of energy and water balance from two tundra sites in Svalbard. Proc 10th International Northern Research Basins Sym, Spitzsbergen, 1994, pp 609–630

Lloyd CR, Harding RJ, Friborg T, Aurela M (2001) Surfaces fluxes of heat and water vapour from sites in the European Arctic. Theor Appl Climatol 70: 19–33

Lloyd J, Taylor JA (1994) On the temperature dependence of soil respiration. Funct Ecol 8: 315–323

Miller GH, de Vernal A (1992) Will greenhouse warming lead to Northern Hemisphere icesheet growth? Nature 355: 244–246

Miller PC, Kendall R, Oechel WC (1983) Simulating carbon accumulation in northern ecosystems. Simulation 40: 119–131

Mitchell JFB, Manabe S, Tokioka T, Meleshko V (1990) Equilibrium climate change. In: Houghton JT, Jenkins GJ, Ephraums JJ (eds) Climate change, the IPCC scientific assessment. Cambridge: Cambridge University Press, pp 131–172

Moncrieff JB, Massheder JM, de Bruin HAR, Elbers J, Friborg T, Heusinkveld B, Kabat P, Scott S, Sögaard H, Verhoef A (1997) A system to measure surface fluxes of momentum, sensible heat, water vapour and carbon dioxide. J Hydrol 188–189: 589–611

Monteith JL, Unsworth M (1990) Principles of environmental physics, 2nd edn. London: Arnold, 291 pp

Moore CJ (1986) Frequency response corrections for eddy correlation systems. Bound-Layer Meteor 37: 17–35

Nakatsubo T, Bekku Y, Kume A, Koizumi H (1998) Respiration of the below ground parts of vascular plants: its contribution to total soil respiration on a successional glacier foreland in Ny-Ålesund, Svalbard. Polar Research 17(1): 53–59

Oberbauer SF, Tenhunen JD, Reynolds JF (1991) Environmental effects on CO_2 efflux from water track and tussock tundra in Arctic Alaska, USA Arctic and Alpine Research 23: 162–169

Oberbauer SF, Cheng W, Gillespie CT, Ostendorf B, Sala A, Gebauer R, Virginia RA, Tenhunen JD (1996) Landscape patterns of carbon dioxide exchange in tundra ecosystems. In: Reynolds JF, Tenhunen JD (eds) Landscape function and disturbance in Arctic Tundra. New York: Springer, pp 223–256

Oechel (1976) Seasonal patterns of temperature response of CO_2 flux and acclimation in arctic mosses growing in situ. Photosynthetica 10: 447–456

Oechel WC, Collins NJ (1976) Comparative CO_2 exchange patterns in mosses from two tundra habitats at Barrow, Alaska. Can J Bot 54: 1355–1369

Oechel WC, Riechers GH (1987) Response of a tundra ecosystem to elevated atmospheric carbon dioxide. In: Response of Vegetation to Carbon dioxide 037 US Dept

of Energy, Carbon dioxide Research Division, Washington, DC

Oechel WC, Sveinbjörnsson B (1978) Primary production processes in Arctic bryophytes at Barrow, Alaska. In: Tieszen LL (ed) Vegetation production and production ecology of an Alaskan Arctic Tundra. New York: Springer, pp 269–298

Oechel WC, Hastings SJ, Vourlitis G, Jenkins M, Riechers G, Grulke N (1993) Recent change of Arctic Tundra ecosystems from a net carbon dioxide sink to a source. Nature 361: 520–523

Peterson KM, Billings WD (1975) Carbon dioxide flux from tundra soils and vegetation as related to temperature at Barrow, Alaska. The American Midland Naturalist 94: 88–98

Post WM, Emanuel WR, Zinke PJ, Stangenberger AG (1982) Soil carbon pools and world life zones. Nature 298: 156–159

Proctor MCF (1982) Physisological ecology: water relations, light and temperature responses, carbon balance. In: Smith AJE (ed) Bryophyte ecology. London: Chapman and Hall, pp 333–381

Rastorfer JR (1971) Effects of temperature on carbon dioxide compensation points of the moss Drepanocladus uncinatus. Antarctic Journal of the United States 6: 162–3

Richardson DHS, Finegan E (1977) Studies on the lichens of Truelove Lowland. In: Bliss LC (ed) Truelove Lowland, Devon Island, Canada: a High Arctic Ecosystem. Edmonton: University of Alberta Press, pp 245–262

Robinson CH, Wookey PA, Lee JA, Callaghan TV, Press MC (1998) Plant community responses to simulated environmental change at a high arctic polar semi-desert. Ecology 79(3): 856–866

Schipperges B (1992) Patterns of CO_2 gas-exchange and thallus water content in Arctic lichens along a ridge profile near Ny-Ålesund, Svalbard. Polar Research 11: 47–68

Sendstad E (1981) Soil ecology of a lichen heath at Spitsbergen, Svalbard: Effects of artificial removal of the lichen plant cover. J Range Management 34: 442–445

Shaver GR, Kummerow J (1992) Phenology, resource allocation, growth od arctic vascular plants. In: Chapin III FS, Jefferies RL, Reynolds JF, Shaver GR, Svoboda J, Chu EW (eds) Arctic ecosystems in a changing climate: an ecophysiological perspective. San Diego: Academic Press, pp 193–211

Shuttleworth WJ, Gash JHC, Lloyd CR, McNeil DD, Moore CJ, Wallace JS (1988) An integrated micrometeorological system for evaporation measurement. Agric Forest Meteor 43: 295–317

Soegaard H, Nordstroem C (1999) Carbon dioxide exchange in a high-arctic fen estimated by eddy covariance measurements and modelling. Global Change Biology 5: 547–562

Steffensen EL (1982) The climate at Norwegian arctic stations. Klima 5, Norske Meteorologiske Institutt, Oslo, 1–44

Svoboda J (1977) Ecology and primary production of raised beach communities, Truelove Lowland. In: Bliss LC (ed) Truelove Lowland, Devon Island, Canada: a high arctic ecosystem. Edmonton: University of Alberta Press, pp 185–216

Tenhunen P, Lange OL, Hahn S, Siegwolf R, Oberbauer SF (1992) The ecosystem role of poikilohydric tundra plants. In: Chapin III FS, Jefferies RL, Reynolds JF, Shaver GR, Svoboda J, Chu EW (eds) Arctic ecosystems in a changing climate: an ecophysiological perspective. San Diego: Academic Press, pp 213–256

Tieszen LL (ed) (1978) Vegetation and production ecology of an Alaskan Arctic Tundra. New York: Springer

Valanne N (1984) Photosynthesis and photosynthetic products in mosses. In: Dyer AF, Duckett JG (eds) The experimental biology of bryophytes. London: Academic Press, pp 257–273

Verville JH, Hobbie SE, Chapin III FS, Hooper DU (1998) Response of tundra CH_4 and CO_2 flux to manipulation of temperature and vegetation. Biogeochemistry 41: 215–235

Vitt DH, Pakarinen P (1977) The bryophyte vegetation, production, organic compounds of Truelove Lowland. In: Bliss LC (ed) Truelove Lowland, Devon Island, Canada: a High Arctic Ecosystem. Edmonton: University of Alberta Press, pp 225–244

Vourlitis GL, Oechel WC (1997) Landscape-scale CO_2, H_2O vapour and energy flux of moist-wet coastal tundra ecosystems over two growing seasons. J Ecol 85: 575–590

Warrick RA, Oerlemans J (1990) Sea level rise. In: Houghton JT, Jenkins GJ, Ephraums JJ (eds) Climate change, the IPCC scientific assessment. Cambridge: Cambridge University Press, pp 257–282

Whiting GJ, Bartlett DS, Fan SM, Bakwin PS, Wofsy SC (1992) Biosphere/Atmosphere CO_2 exchange in Tundra ecosystems: Community characteristics and relationships with multispectral surface reflectance. J Geophys Res 97(D15): 16671–16680

Willmott CJ (1981) On the validation of models. Physical Geography 2: 184–194

Willmott CJ (1984) On the evaulation of model performance in physical geography. In: Gaille GL, Willmott CJ (eds) Spatial statistics and models. Dordrecht: D. Reidel Publishing Co, pp 443–460

Wookey PA, Robinson CH (1997) Responsiveness and resilience of high Arctic ecosystems to environmental change. Opera Botanica 132: 215–232

Author's address: C. R. Lloyd, Centre for Ecology and Hydrology – Wallingford, Maclean Building, Crowmarsh Gifford, Wallingford, Oxfordshire OX10 8BB, United Kingdom.

Global Change Biology (2001) 7, 405–426

The measurement and modelling of the carbon dioxide exchange at a high Arctic site in Svalbard

COLIN R. LLOYD
Centre for Ecology and Hydrology, Wallingford, (formerly the Institute of Hydrology), Crowmarsh Gifford, Wallingford OX10 8BB, UK

Abstract

Well-documented models of soil respiration and C_3 photosynthesis are combined to investigate the overall carbon dioxide balance of a high arctic polar semidesert site near Ny-Ålesund, Svalbard. Measurements of carbon dioxide fluxes from an eddy correlation system and climate variables are used to calibrate this combined model for the snowmelt–summer period in 1995. Particular emphasis was put on modelling effectively the separate soil respiration and net photosynthesis of the moss/lichen, vascular plant and bare soil areas within the heterogeneous site, and ascertaining whether moss/lichen communities could be effectively modelled using a C_3 photosynthetic model. The calibrated model of 1995 data was subsequently tested in predictive mode against eddy correlation flux measurements recorded in 1996. The model is shown to simulate effectively both years and highlights the important role that the timing of snowmelt, summer precipitation and soil temperature has upon the overall carbon dioxide balance of this site. A previous conjecture by the author from the limited flux measurements that the investigated period in 1995 was an overall sink for carbon dioxide and that the same period in 1996 was an overall source of carbon dioxide is borne out by the model runs with 3.9 ± 3.7 gC m^{-2} being assimilated into the vegetation during the 1995 period and 5.0 ± 3.3 gC m^{-2} being returned to the atmosphere during the same period in 1996.

Keywords: Arctic, carbon dioxide, Svalbard, net ecosystem productivity, eddy correlation, model

Received 7 June 2000; revised version received 8 December and accepted 21 December 2000

Introduction

The Arctic is a fragile environment and is one of the most sensitive areas of the world to future global warming. Sensitivity studies with Global Climate Models have suggested that atmospheric warming resulting from increasing CO_2 levels will be greatest at high latitudes (e.g. Kattenberg *et al.* 1996), and that this is primarily through the strong feedback between air temperature, ice and snow cover at these latitudes. Other studies have focused on the possible feedbacks involving the carbon stores contained in the above-ground vegetation and below-ground soil, and whether these will lead to the arctic continuing to be a carbon sink (as in the past) or becoming a future carbon source (and therefore a positive feedback on greenhouse gases). Oechel *et al.* (1993, 1997) show changes from carbon sink to carbon source at sites in Alaska but this and other studies have been conducted primarily in the low Arctic. This was pointed out by Soegaard & Nordstroem (1999) who hypothesized that this might not be typical of the high Arctic; their measurements showed that a study site at Zackenberg, Greenland was a carbon sink in 1996. However, they did point out that Shurpali *et al.* (1995) had found that a dry year producing a net carbon source was followed by a wet year producing a carbon sink. From their modelling exercise and recorded temperature changes over the past 30 years Soegaard & Nordstroem (1999) predicted that their site had not yet changed from a net carbon sink to a net carbon source. At Ny-Ålesund, Lloyd *et al.* (1999) had indicated from campaign flux measurements taken throughout the active summer seasons of 1995 and 1996 that the surface switched from

Correspondence: tel +44/ (0)1491 692330, fax +44/ (0)1491 692424, e-mail crl@ceh.ac.uk

a net carbon sink in 1995 to a net carbon source in 1996. At Eidembukta, 50 km to the south of Ny-Ålesund, Wüthrich *et al.* (1999) also found 1996 to be a net source of carbon during 1996 and attributed this to the cold and cloudy summer in that year.

In the absence of separately determined soil respiration and net photosynthesis measurements, eddy correlation flux measurements of carbon dioxide have been used in this paper to 'tune' a combined model consisting of classic soil respiration and Net Primary Productivity (NPP) uptake modules [NPP equals Gross Primary Productivity (GPP) – plant respiration]. The model was calibrated for the carbon sink year of 1995 and then run without further modification to test the ability of the model to predict the overall carbon dioxide balance during 1996.

The model of photosynthesis used in this paper is that developed by Cox *et al.* (1998, 1999), which is based upon the work of Collatz *et al.* (1991) for C_3 plants. Cox *et al.* (1998, 1999) developed the model for inclusion in the Meteorological Office (UK) Surface Exchange Scheme (MOSES) which serves as the land surface scheme in the Hadley Centre Global Climate Model (GCM). Although this paper does not directly use the MOSES model, in separating the NPP module from the overall MOSES model the author has maintained the integrity of the MOSES model by using its defined state variables, model structure and C_3 parameter values.

Method and materials

The Ny-Ålesund, Svalbard Site

The measurement site is situated at Leirhaugen, 2 km west of Ny-Ålesund (79°56'N, 11°55'E) on the Brøggerhalvøya Peninsula on the southern edge of Kongsfjorden on the west coast of Spitsbergen, Svalbard. Fuller descriptions of the area surrounding Ny-Ålesund, the general climate of the region and details of the measurement site are contained in Lloyd *et al.* (1996, 1999) and Lloyd (2001) but details relating to this paper are repeated here. The site is in the middle of the floodplain of the braided glacial river Bayelva in an area designated as Subpolar desert (Tedrow 1977) which equates to the Tundra–Moss–Lichen zonation of Korotkevich (1967). The whole area is underlain by continuous permafrost to depths of 100–400 m of which only the uppermost metre thaws during the summer. The braiding creates streams that are typically shallow with little energy to substantially alter the soil horizon with the settled soil probably more mixed by solifluction action than by streamflow motion (Smith 1956). The underlying rock at the study site is a red sandstone with a thickness of about 200 m overlain with glacial schist and psammite gravels and carboniferous limestone boulders in a silty clay and sand gley soil that has a thin (0.02 m) organic soil cover. The climate of Svalbard in general, and Ny-Ålesund in particular, is warmer than its northerly position would suggest, with the coldest months of February and March experiencing a mean monthly temperature of between –8 °C and –16 °C with temperatures below –30 °C being uncommon. During the summer, the area experiences mean July temperatures of 5 °C with temperatures outside the range 1–10 °C being uncommon. Although the absolute humidity of the air is only 4 or 5 g m^{-3}, the water vapour content of the air is very often close to saturation, which leads to frequent fogs during the summer and the possibility of dew formation. The area normally has less than 400 mm of precipitation a year, with a maximum in the autumn. Rain can occur in the middle of winter as can snow during the summer. The period of the year when the entire solar disc remains above the horizon (the period of the 'midnight sun') is 129 days long beginning on 18 April and ending on 24 August.

The vegetation at the field site is characterized by communities of plant species typical of mounds, ridges and wetland depressions, as in the rest of Svalbard. The communities form a mosaic over a few square metres whose distribution is more a consequence of soil moisture and snow cover rather than the underlying geology. The first spring vascular plants do not flower before mid-June despite the availability of constant daylight from 18 April and the growing period is generally over around mid-August, coincident with the end of the midnight sun period. Cryptogams (mosses and lichens), however, will continue to photosynthesize from first emergence from the snowpack in the spring through the summer and autumn providing temperature, moisture and light levels allow it (Longton, pers comm.). The vegetation at the study site consists of three main plant communities. These are designated (Brattbakk 1981) as 100–50% Luzula confusa lichen heath (Norw. Vardefrytle lavhei), 100–50% *Saxifraga oppositifolia* lichen heath (Norw. Rødsildre lavhei) and 100–50% *Deschampsia alpina* snow-bed community (Norw. Fjellbunke snøleie). There is also a small strip of < 10% Saxifraga heath close to the Bayelva river. The percentage cover values relate to the total *vegetation* present and not the proportion of ground area that the individual vegetation type covers. In particular, the major species at the site were Saxifraga oppositifolia, *Drepanocladus* spp. and *Luzula confusa*. The vascular plants, including *Saxifraga oppositifolia* and *Luzula confusa* typically exist both on formerly bare ground and coexist either within or on top of the open and highly branched *Cetraria delisei* lichen; the mosses tend to form isolated hummocky mounds. The vegetation height was typically 5 cm, with

moss mounds up to 10 cm in height. A simple mapping of the flux measurement site indicated that 48% of the vegetation was lichen or moss, 20% of the surface was vascular plants, 28% was bare soil and 4% was stone (Lloyd, 2001).

Measurements

CO_2 and energy fluxes. Fluxes of CO_2, H_2O, sensible heat and momentum were measured towards the middle of a 250 m × 250 m area of the floodplain. The measurements were made on top of a thin mast at a height of 2.7 m above the surface using the eddy correlation technique. The vector components of the wind were measured using a 3D sonic anemometer (Solent R2, Gill Instruments, Lymington, UK). The atmospheric concentrations of CO_2 and H_2O were measured using a Li-Cor 6262 (Li-Cor Inc., Lincoln, NB) InfraRed Gas Analyser (IRGA). The IRGA was fitted with a pressure transducer to allow on-line pressure corrections to be made. A pump (Model CAPEX V2X, Charles Austin, Byfleet, UK) on the outlet side of the IRGA cell pumped sample air at 13 L min^{-1} down a 2.5-m long tube from an inlet at the same height as the middle of the anemometer array but approximately 30 mm to one side. The tube inlet was shielded to prevent rain from entering the tube and also to minimize flow distortion through the anemometer caused by the flow of air down the tube. The tube, made of silicon rubber (Masterflex 6424–25, Masterflex, IL), chosen for its impermeability to carbon dioxide and water vapour, had an internal diameter of 5 mm. In 1995, the time lag between the measurement of the vertical windspeed and the measurement of the gas concentration in the IRGA cell was set at 0.5 s, as determined by calculating the flow time from the dimensions, distances and flow rate of the air through the tube. In 1996, time lags were determined on-line using the data logging software, by maximizing the covariances between vertical windspeed and the two gases, CO_2 and H_2O.

Raw data output from the IRGA and Solent anemometer were logged continuously at 21 Hz on a laptop computer into 20-min (1995) or 30-min periods (1996). The laptop computer also calculated on-line period average fluxes. In 1995, the controlling software package was developed at the Institute of Hydrology; in 1996, the EdiSol software package (Moncrieff *et al.* 1997) was used. In 1995 the inability to leave the system running unattended for more than 3 days meant that CO_2 and H_2O flux data from the Li-Cor system was only taken during the short field expeditions during the summer. In 1996, field campaigns began well before snowmelt but a waterlogged laptop computer at the end of snowmelt again limited flux measurements from the IRGA system. In 1995, an Institute of Hydrology Hydra eddy correlation system (Shuttleworth *et al.* 1988) measuring sensible and latent heat fluxes and net radiation (Q*5, REBS, Seattle, WA) operated continuously at the same South Site from 30 May to 3 September. In 1996, the Hydra operated continuously alongside the Solent-Licor system from 17 July to 6 September.

Flux measurement errors. The Solent is normally stable in its calibration provided that the geometry of the sensor head is not altered. However, the Li-Cor 6262 IRGA requires calibration from time to time for drift in both zero offset and gain. There is no standard interval between calibrations of the span of the Li-Cor 6262 IRGA. Goulden *et al.* (1996) at a site with easy access, climate controlled hut and mains electricity automatically recalibrated every 5 h while at a field site in Italy Valentini *et al.* (1996) calibrated the IRGA manually every 2 weeks. The calibration is typically performed using dew-point hygrometers and CO_2 span gases. In the high arctic summer, air temperatures are typically 5 °C and relative humidities are usually above 80% resulting in dewpoint temperatures often close to or below 0 °C. Span gas bottles left at a remote field site are subject to settling in cold conditions, which could lead to erroneous concentration values. The possibility of calibrating the IRGA wrongly was therefore a possibility. The experience of other researchers with this instrument has shown that the gain is unlikely to have changed substantially if the zero calibration has also not drifted substantially. Zero calibrations involving the chemical removal of CO_2 and H_2O were performed every week. The IRGA was also serviced and calibrated by the manufacturer at the beginning and end of both the 1995 and 1996 field seasons. While drift in the zero offset has no effect upon the flux value, there is a nearly linear relationship between gain drift and flux error. The seasonal drift in span was less than 5% and the fluxes were adjusted by this amount assuming a constant drift in time using the procedure recommended by Li-Cor (Li-Cor Technical Note 123).

Previous measurements of photosynthesis and soil respiration in high arctic polar semidesert sites (Mayo *et al.* 1977; Dziadowiec 1983) indicated that the overall long-term net CO_2 flux would probably be small. The net flux is the sum of individual instantaneous flux measurements, summed over hourly and daily periods. The instantaneous measurements, as well as the hourly and daily summations, have associated error terms. Soegaard *et al.* (2000) evaluated the standard error from individual error terms within a similar Solent/Li-Cor 6262 flux system at a high arctic site in Greenland, as ± 7%. Thus, for typical active-season daytime hourly fluxes at the Ny-Ålesund site of –40 mg CO_2 m^{-2} h^{-1}, the standard error is 2.8 mg CO_2 m^{-2} h^{-1}. During an extended period during the thaw, Soegaard *et al.* (2000) also measured a very low

and stable CO_2 flux which gave a standard error of 1.4 mg CO_2 $m^{-2} h^{-1}$, and concluded that the detection limit for the flux system could be considered as equal or smaller than this amount. Consideration of the hourly standard error leads to an estimate of 13.8 mg m^{-2} d^{-1} for the daily net flux standard error at the Ny-Ålesund site. However, as Soegaard *et al.* (2000) indicate, the hourly samples of flux measurements are highly autocorrelated and thus not independent. Salas (1993) provides a method for obtaining an unbiased estimate of the daily standard error by reducing the sample size to the equivalent number of independent observations. This procedure was applied to all measured data for complete days in 1995 and 1996.

Micrometeorological, radiation and soil measurements. An Automatic Weather Station (AWS) was installed in June 1994 on a 5°-N-facing slope of approximately 200 m in length that terminated in the floodplain area where the flux measurements were made. The AWS operated continuously until August 1999. Pertinent to this paper, the AWS measured incoming shortwave radiation (CM5, Kipp and Zonen, Delft, Netherlands) and net allwave radiation (Didcot Instruments, Abingdon, UK), relative humidity and air temperature in an unaspirated radiation shield (MP100A, Rotronic AG, Switzerland), windspeed (DWR, Didcot Instruments, Abingdon, UK) and wind direction (DWD, Didcot Instruments, Abingdon, UK) and rainfall (0.5 mm tipping bucket, Rimco, Australia). Soil temperature and electrical resistance profile units described in Lloyd (1998) were installed in August 1994 but were not fully operational until June 1995. They operated nearly continuously until August 1999.

Model components

The CO_2 flux (μmol $m^{-2} s^{-1}$) measured above a vegetated surface, often called the Net Ecosystem Productivity (NEP), is the balance between the uptake from the atmosphere of CO_2 by vegetation photosynthesis (W) minus the input of CO_2 into the atmosphere via plant (R_d) (equivalent to GPP), and soil respiration (R_S), where soil respiration is the sum of heterotrophic microbial decomposition and root respiration namely,

$$NEP = (W - R_d) - R_S. \quad (1)$$

A micrometeorological convention is used in this paper whereby photosynthesis produces a negative CO_2 flux (extracting CO_2 from the atmosphere) and respiration a positive flux (adding CO_2 to the atmosphere).

Because the surface of the tundra site is characterized by a mixture of predominantly cryptogamic vegetation with isolated dwarf vascular plants and bare soil or stone patches, the model contains separate evaluations of bare soil/stony surface soil respiration, vascular net CO_2 uptake and its underlying soil respiration, and cryptogamic net CO_2 uptake and its underlying soil respiration.

Soil respiration. Soil respiration is influenced by soil temperature and to a lesser extent by soil moisture. Soil moisture at this site was not regarded as limiting soil respiration rates thus enabling the soil respiration model of Lloyd & Taylor (1994) to be used, given by:

$$R_s = R_{10} e^{308.56\left(\frac{1}{56.02} - \frac{1}{T_S - 227.13}\right)} \quad (2)$$

where R_S (μmol $m^{-2} s^{-1}$) is soil respiration, R_{10} is the soil respiration rate at 10 °C and T_S (K) is soil temperature. Soegaard & Nordstroem (1999) have successfully applied this model at a high-arctic fen site in Greenland.

Each surface type within the model had a different R_{10} value and the model's area average soil respiration value was obtained from the individual soil respiration rates adjusted by their proportional cover.

The photosynthesis model. Several studies have indicated that cryptogams probably fix CO_2 by the C_3 pathway as in most temperate and polar flowering plants (Rastorfer 1971; Valanne 1984). The photosynthesis model used for both cryptogams and vascular plants in this study is the C3 model of Collatz *et al.* (1991) as used by Cox *et al.* (1999), wherein the specific functional forms can be found. In the nomenclature of Cox *et al.* (1999), the gross leaf photosynthetic rate (W) approaches the minimum or most limiting of the three potentially limiting rates; W_{CARB}, the rate of gross photosynthesis controlled by the mid-day Rubisco capacity (V_m); W_{LITE}, the potential photosynthetic rate dependent upon light and CO_2 availability; and W_{EXPT}, the potential photosynthetic rate dependent upon the transport of photosynthetic products within the leaf. The rate of dark respiration in C_3 plants is assumed to be a constant fraction (0.015) of the maximum rate of carboxylation of Rubisco.

Moisture control on photosynthesis. Cryptogamic plants differ from vascular plants in their response to soil and atmospheric moisture. Mosses and lichens typically are uncoupled from soil moisture, as they have no water-carrying root systems. However, soil moisture can diffuse through the cryptogamic mat as water vapour and, under suitable conditions, condense on the outer surfaces.

There is therefore a need to differentiate between the photosynthetic responses of cryptogams and vascular plants to changes in their moisture status. In vascular plants, this was achieved in the model of Cox *et al.* (1998) through direct dependence of the net photosynthetic rate

on the soil moisture status which had a functional form described by Stewart & Verma (1992) for the 'Jarvis' model (Jarvis 1976. The resultant soil moisture-adjusted net rate of photosynthesis in this paper is described by:

$$A_L = (W - R_d)\beta_S, \quad (3)$$

where A_L is net rate of photosynthesis and β_S is the soil moisture factor which ranges between 0 (soil moisture concentration below the 'wilting point', when transpiration ceases) and 1 (soil moisture concentration above the 'critical point', above which plants are not water limited). At the Ny-Ålesund site, the volumetric soil moisture concentration at the lower root level was observed to be above an assumed critical point for these plants (Lloyd 1998) and β_S was set to 1 throughout.

For the cryptogamic community, transpiration and photosynthesis are not limited by variation in the soil moisture concentration. However, photosynthesis in cryptogams reduces as moisture is lost by diffusion through the cell walls. There is also evidence of reduced photosynthetic rates above a certain water content (Oechel & Collins 1976). The exact response curve and rate varies from species to species and with temperature and latitude and no account of these differences were made in the model. Instead an evaporative loss factor, operating in place of β_S in (3) above was used to limit transpiration and hence photosynthesis at the cryptogamic leaf level. This evaporative loss factor, β_E, was composed of a surface evaporation rate and an initial cryptogam moisture content value. The surface evaporation rate was evaluated from the Penman–Monteith equation (Monteith 1965) using data from the AWS and with the saturation vapour pressure e_{sat} and vapour pressure e calculated at the leaf temperature. Hourly mean values of surface resistance, r_s, were evaluated by inverting and solving the Penman–Monteith equation for r_s using measurements of sensible and latent heat, air temperature and aerodynamic resistance from the eddy correlation sensors between 25 July and 10 August 1995. The frequency histogram of the hourly mean values of r_s was skewed and a square-root transform was applied before the seasonal mean was estimated as 80 s m^{-1} with a standard deviation of 20 s m^{-1}.

Lange *et al.* (1985) showed decreases of water content in two lichen species in Alaska from 200% of dry weight (dwt) to 25% of dwt in 12 h, during which period, after an initial respiration burst, net photosynthesis reached a peak after 9 h and then rapidly fell away and ceased after 12 h. Gimingham & Smith (1971) showed in *Calliergon sarmentosum* (a similar moss species to *Drepanocladus* at the Ny-Ålesund) a progression from 100% water content to 15% water content in 10 h. While laboratory measurements of water absorption by mosses may typically show uptakes of >1000% of dwt, water contents under field conditions seldom exceed 300% of dwt (Hicklenton & Oechel 1976). In the model, the initial cryptogam moisture content value was used as a free variable to characterize the simulation output but was adjusted, within limits, to provide desiccation times comparable to the above observations.

There is little evidence of cryptogams being able to extract water vapour from the air to replenish cell water concentrations. Although some mosses have specialized root-like structures for transport of moisture from the soil, the mosses at this site do not, and the only way that moisture levels within the cryptogamic cells can increase is through precipitation events, i.e. rain, fog, dew or snow (Longton 1980). The photosynthetic process within cryptogams is thus controlled by the opposing actions of evaporation leading to desiccation and halting of the photosynthetic process and wetting through precipitation leading to resumption of the photosynthetic process.

The process of refilling the moisture store within the cryptogamic community is achieved by allowing the evaporative loss factor, β_E, to increase after a precipitation event. For periods during precipitation and for some hours afterwards the surfaces of the cryptogamic leaves would have been covered with a liquid water layer and been incapable of photosynthesis. There do not appear to be any published results describing the amount of liquid water that cryptogamic canopies can support or how long this water takes to drain or evaporate away allowing photosynthesis to resume. The model therefore includes a variable time delay, which was optimized during the formation of the model's parameter set.

Lloyd (2001) observed that there appeared to be instances during the period 30 July – 11 August when possible dew formation was effectively allowing the cryptogams to resume photosynthetic activity (as observed in the measured net CO_2 flux) many days after the last precipitation event.

Lange *et al.* (1985) showed that dew formation raised water content from desiccation to 50% water content (by dwt) and led to a burst of photosynthetic activity which had a rate and duration similar in extent to that occurring after rainfall. Dew formation was adjudged to have occurred if soil temperature was less than the dew-point of the overlying air, i.e. (see Monteith & Unsworth 1990) if:

$$T_s - \frac{T_a}{\left(\frac{1-\ln\left(\frac{e}{e_{sat}}\right)}{B}\right)} < 0 \quad (4)$$

where T_S is assumed leaf temperature given by the surface soil temperature, T_a is air temperature as measured at 2.7 m by the sonic anemometer and e and

e_{sat} are the vapour pressure and saturated vapour pressure at the leaf temperature as estimated from measurements of relative humidity recorded by the AWS. The factor $B = \lambda M_w/RT$, where λ is the latent heat of vaporization, M_w is the molecular weight of water, R is the gas constant and T is a standard temperature = 293 K; B is set at 19.65, which according to Monteith & Unsworth (1990) provides more exact estimates of e_{sat} over the temperature range 273–293 K.

Where dew was assumed to have occurred, β_E was allowed to increase but at a slower rate than that following a rainfall precipitation event. Figure 1 shows the flowchart for deciding the size, rate and direction of β_E in response to wetting and drying periods.

Leaf Area Index (LAI). LAI is used in many models of plant growth and in MOSES to regulate the seasonal increase or decrease in photosynthetic activity. Soegaard & Nordstroem (1999), at Zackenberg, NE Greenland, found a linear rise of LAI from 0 to 1.2 over 20 days during spring and a similar degree of decrease from 1.2 to 0 over 24 days during the late summer. However, their site was predominantly sedges and grasses, which initiate new growth each year. The change in LAI that accompanies the increasing utilization of CO_2 in emerging deciduous plants is not appropriate at the Ny-Ålesund site where little change is observed in LAI despite increasing photosynthetic activity. Leaf Area Index (LAI) of the predominantly evergreen vascular plant and cryptogam community was not measured at the Ny-Ålesund site. However, the maximum LAI was estimated to be much lower than at the Zackenberg site. Nevertheless, the plant community at Ny-Ålesund does increase its photosynthetic activity after snowmelt and decrease its photosynthetic activity at the end of summer. A surrogate replacement for LAI was used to model the change from zero to full photosynthetic activity in the spring (the Growth Factor, GF) and from full activity to dormancy in the autumn (the Senescence Factor, SF). These factors were applied to the separate vascular and cryptogamic surfaces using individual percentage surface cover values (Lloyd, 2001). It is recognized that the two plant communities have different photosynthetic activity strategies not only in the spring but also in the autumn when cryptogams will continue to photosynthesize through late summer and autumn providing that temperature, moisture and light levels allow it (Hicklenton & Oechel 1976; Oechel & Sveinbjörnsson 1978). However, in the absence of data on this aspect and a desire to keep the model as simple as possible meant that the same GF rates were applied to both the vascular

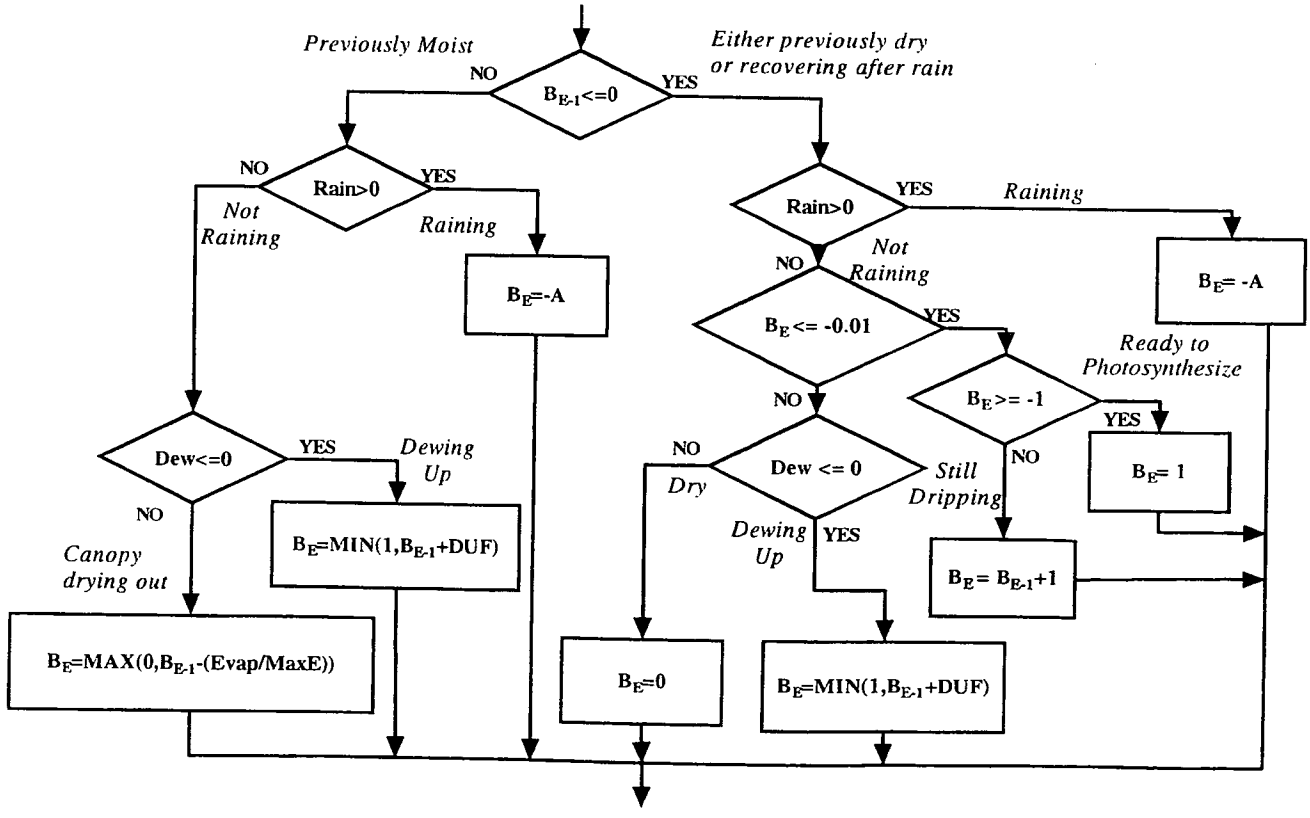

Fig. 1 Decision flowchart for water content status of cryptogams. DUF, maxE and A are described in Table 3.

and cryptogamic plant communities. After the spring increase in activity, full potential photosynthetic activity was assumed to occur until late summer. A symmetrical growth equation, identified by Landsberg (1977) was used for the GF (and the SF) model. This is given by:

$$GF = SF = \frac{1}{1 + e^{-(b+kt)}} \quad (5)$$

where b and k are different shape factors for the GF and SF models and t is an hourly time step. The rate at which GF increased (in spring) or SF decreased (in the autumn) were, in the absence of any defining work, given a free parameter status in a simple optimization scheme which explored the total parameter space for the shape factors b and k.

Assimilation rates. Maximum net assimilation rates (NAR) in cryptogams are considerably lower on a dry weight basis than in angiosperm leaves (Longton 1988). Wielgolaski (1975) found that maxima in the foliage of tundra angiosperms were 7–33 mg CO_2 g^{-1} h^{-1} compared to less than 5 mg CO_2 g^{-1} h^{-1} in the green parts of associated mosses and lichens. Similarly, Oechel & Sveinbjörnsson 1978) at a site near Barrow, Alaska, considered that NAR in mosses were only 8–9% of that of vascular plant leaves. Kallio & Kärenlampi (1975) indicated that C_3 plants have maximum net photosynthetic rates of 20–45 mg CO_2 dm^{-2} h^{-1} compared to 0.5–2.0 mg CO_2 dm^{-2} h^{-1} in lichens and less than 3.0 mg CO_2 dm^{-2} h^{-1} in mosses.

The cryptogamic NAR was found to simulate the measured flux when set to 15% of the vascular rate (comparable to the maximum difference between rates in Wielgolaski 1975).

Light saturation limits in cryptogams. Miller *et al.* (1978) show that all four investigated moss species at Barrow, Alaska, were radiant energy saturated at 300 J m^{-2} s^{-1} PAR. Longton (1988) states that in polar species, light compensation points for both mosses and vascular plants in open tundra at Barrow are commonly 5–12 J m^{-2} s^{-1} PAR but that mosses saturate at 80–120 J m^{-2} s^{-1} PAR, approximately 30% of the level typical for local angiosperms. During the period 30 July – 11 August 1995, 11% and 15% of the measured hourly average incoming solar radiation values were above 300 and 233 W m^{-2}, respectively, but that including these cutoffs reduced overall light availability by only 7% and 14%, respectively. Nevertheless, a light saturation limit of 266 W m^{-2} was applied to the cryptogamic photosynthetic process. No such limitation was applied to the vascular plant photosynthetic process.

Sensitivity analysis. No deviation from the parameter set routinely used within MOSES (and the Hadley Centre GCM) for the C_3 photosynthetic module has been applied in the modelling aspects of this paper (see Table 1). Sensitivity analyses of this part of the model have been performed previously in Harding *et al.* (2000) and Huntingford *et al.* (2000). However, the additional parameters required to create the NEP model, i.e. the integration of the moss/lichen community into the MOSES C_3 photosynthetic routine and the addition of the soil respiration model, were subjected to a sensitivity analysis. Each parameter in turn was varied by ± 50% around its estimated or optimized value and the resultant estimates of NEP were compared to the NEP estimate given by the default parameter set for the 1995 modelling period.

Evaluation of the model's performance. The method recommended by Willmott (1984) was used to assess the overall performance of the model. He reported that his degree of agreement statistic d was a better measure of the quantitative correlation between observations (O) and modelled values (M) than the usual Pearson product-moment correlation coefficient (r) or coefficient of determination (r^2) which are insensitive to a wide range of additive and proportional differences that can exist between O and M. The statistic d varies between 0 (complete disagreement) and 1 (complete agreement) and is given by:

$$d = 1 - \frac{N \cdot RMSE^2}{\sum_{i=1}^{n} \left[(M_i - \overline{O}) + (O_i - \overline{O}) \right]^2} \quad (6)$$

where N is the number of observations, $\overline{O}$ is the mean observed value and $RMSE$ is the standard root mean square error. In order to gain further insight into the model's performance, Willmott (1981) separates $RMSE$ into systematic ($RMSE_s$) and unsystematic ($RMSE_u$) parts. An acceptable model would not only have a high d, but the $RMSE$ should be low with relatively small $RMSE_s$ (i.e. the model explains most of the systematic variation) and with $RMSE_u$ approaching $RMSE$. In assessing the degree to which solar radiation and soil temperature control CO_2 flux, Lloyd (2001) used this method to optimize (and to evaluate the performance of) a simple model by minimizing the differences between measured hourly average values of CO_2 flux and modelled hourly values of NEP. In this study, where the aim is to model the active season CO_2 balance, the model's performance (and optimization of its free parameters) were assessed by minimizing the differences between the cumulative values of measured CO_2 flux and modelled values of NEP at hourly intervals. There is also evidence of increased confidence in period totals when estimating fluxes in heterogeneous terrain (Lloyd

et al. 1997). Evaluations of constants defined above and their units are shown in the results section below.

Results

The measurements during the three periods in 1995 investigated in Lloyd (2001) were chosen to optimize the free parameters within the model. These periods: 26–30 June, 30 July – 11 August and 29 August – 3 September represented three pivotal phases of the active season in 1995; the post snowmelt initial growth, full summer growth and late summer senescence, respectively.

Post snowmelt growth periods are characterized by patchy snow cover, waterlogged areas and increasing but variable growth, factors that lead to heterogeneity in both the soil respiration and the photosynthetic activity within the emerging vegetation. Similarly, late summer and early autumn are characterized by heterogeneous plant senescence coupled with frosts. In conditions like these, it can be difficult to interpret model results based on point measurements of radiation and soil temperature with flux measurements that are integrations over a considerable area.

These heterogeneities, although not fully absent, are minimized during the main summer period. Therefore the full summer growth period (31 July – 11 August) was used to investigate the performance and reaction of the model to variation in the free parameters. Despite the inherent difficulty, the early and late periods were then used to parameterize the GF/SF factors in order to incorporate plant growth and plant senescence into the model. Soil respiration was assumed to be without seasonal variability other than that provided by temperature.

Soil respiration

Nakatsubo *et al.* (1998) in their study of soil respiration rates at Ny-Ålesund had a site (Site III) at the top of the slope where the AWS was situated. Their results are shown verbatim in Table 2. The soil respiration model of Lloyd & Taylor (1994) requires values for R_{10} in $\mu mol\, CO_2\, m^{-2} s^{-1}$. Equation (2) was therefore solved for R_{10} using the results of Nakatsubo and converted to the required units. These values (linearly averaged where there are two solutions) are also shown in Table 2. Soegaard & Nordstroem (1999) set $R_{10} = 1.6\, \mu mol\, CO_2\, m^{-2} s^{-1}$ for their Zackenberg, Greenland site based on a study in a boreal part of Sweden by Soegaard & Thorgeirsson (1998). The author's

Table 1 Parameter values for the C3 photosynthetic model – these are the same as the default values within the standard MOSES model

Parameter	Name	Units	Value	MOSES Default value
Pressure	Press	Pa	101300	101300
Surface resistance	rs	sm^{-1}	80	
Aerodynamic resistance	ra	sm^{-1}	112	
Critical humidity deficit	dqcrit	$Kg_{H20}\ kg_{air}^{-1}$	0.15	0.15
Atmospheric Oxygen pressure	Oa	Pa	20900	20900
C_i/C_a for $dq = 0$	fo	–	0.92	0.92
Dark respiration coefficient	Fd	–	0.015	0.015
Canopy CO_2 concentration		$Kg_{CO2}\ kg_{air}^{-1}$	4.90E-04	4.90E-4
Mol wt. O_2/Mol wt. Dry air	Epo2		1.106	1.106
Mol wt CO_2/Mol wt. Dry air	EpCO2		1.5196	1.5196
Atmospheric Oxygen concentration	O2	$Kg_{O2}\ kg_{air}^{-1}$	0.23	0.23
CO_2 mixing ratio	CO2	$Kg_{CO2}\ kg_{air}^{-1}$	0.00049	0.00049
Leaf scattering coefficient for PAR	Omega	–	0.15	0.15
Const. Relating Vmax and Leaf Nitrogen	nf	–	0.0008	0.0008
Default value for Vmax	Vmax	$Mol_{CO2}\ m^{-2} s^{-1}$	4.69E-05	4.69E-05
Quantum efficiency	ALPHA	$Mol_{CO2}\ mol_{PAR}^{-1}$ photons	0.04	0.04
Leaf nitrogen concentration	nl	$Kg_N\ kg_C^{-1}$	0.05	0.05
Leaf resistance for CO_2/Leaf resistance for H_2O	ratio		1.6	1.6
Minimum leaf conductance for H_2O	Glmin		1.00E-06	1.00E-06
Gas constant		$JK^{-1}\ mol^{-1}$	8.3144	8.3144
Coupling coeffs for colimitation	BETA1		0.83	0.83
Coupling coeffs for colimitation	BETA2		0.93	0.93
Soil Water factor for vascular plants	fsmc		1	0–1

Table 2 Soil respiration results (after Nakatsubo *et al.* 1998) and calculated R_{10} values based on these results as used initially in the model

Surface	Soil temperature (°C)	Total respiration rate (mg $_{CO2}$ $m^{-2}h^{-1}$)	Calculated R_{10} (μmol $_{CO2}$ $m^{-2}s^{-1}$)
Bare ground	7.6	12.8	0.103
Crust: cyanobacteria and lichens	7.3	54.8	0.389
	7.6	39.5	
Mixed: bryophytes and vascular plants	6.2	81.2	0.806
	6.9	96.4	

Table 3. General and cryptogamic-specific parameter values used in the combined soil respiration and photosynthetic model. The variable names are used in Fig. 1

Parameters	Units	Value
General		
Soil Heat Flux as percentage of Net Radiation	%	5
Bare Soil cover	%	20
Cryptogamic plant cover	%	67
Vascular plant cover	%	13
Number of hours after rain before plant photosynthesis can start (A)	h	3
Cryptogamic		
Light Saturation point for cryptogams	Wm^{-2}	266
Cryptogamic growth rate as proportion of vascular plant growth		0.15
Maximum evaporation rate from cryptogamic surfaces (maxE)	$mm\,h^{-1}$	0.5
Rate at which cryptogams can absorb precipitation (DUF)	$mm\,h^{-1}$	0.2

own observation of the site used by Nakatsubo *et al.* (1998) and their fig. 2 showing the surface at Site III indicates that while the bare ground and mixed bryophyte and vascular plant surfaces are very similar to those referred to in this paper, the crust surface of cyanobacteria and lichens was much sparser and closer to bare ground cover when compared to the more highly vegetated moss/lichen surface at the flux site. The lichen cover value for R_{10} was left free to assume some value between 0.389 and 0.806 (see Table 2) during the creation of the model parameter set and was subsequently set to 0.6.

The difference in respiration rates is a compound effect of the difference in carbon amount in the soil underlying the vegetation, the difference in soil temperature caused by the effect of overlying vegetation and also any uptake of CO_2 by the vegetation as the CO_2 diffuses through it. Figure 2 shows the resultant modelled soil respiration values for the individual surfaces (per unit area) and the overall average soil respiration, R_S equal to the linear sum of the individual respiration rates scaled by their percentage surface cover for the period 30 July – 11 August 1995.

Wüthrich *et al.* (1994), using soda-lime absorption techniques at undefined sites around Ny-Ålesund, found respiration rates that were three times higher (up to 6 g CO_2 m^{-2} d^{-1}) than those of Nakatsubo *et al.* (1998). In a later study, Wüthrich *et al.* (1999), using a Li-Cor 6252 infrared gas analyser to take *in-situ* measurements at a field site 50 km south of Ny-Ålesund, found soil respiration rates in *Cetraria delisei* sites that were approx. 1 g CO_2 m^{-2} d^{-1} and 4 g CO_2 m^{-2} d^{-1} at a mixed *Cetraria–Salix* site. Both these sites were ungrazed by reindeer (Wüthrich, pers. comm.), unlike the site in this study, and no data on soil temperature was given.

Net ecosystem production: 30 July – 11 August 1995

Cryptogamic water availabilities. Rainfall amounting to 3.5 mm during the early hours of 30 July followed by an isolated 0.5 mm during the early morning of 31 July was the only recorded precipitation during this period (see Fig. 3b). However, as shown by Lloyd (2001), there were instances during the whole period when calculated leaf temperatures dropped below the dewpoint leading to the likely deposition of dew onto the cryptogamic leaf

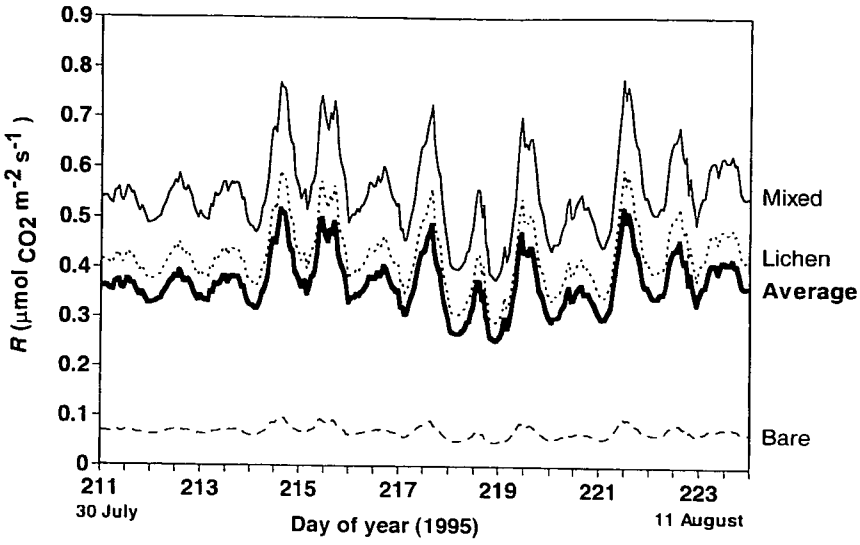

Fig. 2 Modelled soil respiration from bare soil, lichen covered soil, mixed vascular/bryophyte soil and area cover average soil respiration for the period 30 July – 11 August 1995.

surfaces. While the vascular plants were assumed not to be significantly affected by either rainfall or dewfall, both situations would tend to affect the photosynthetic rate of the cryptogams; after initially inhibiting photosynthesis because of the deposition of a liquid film onto the leaf surfaces photosynthetic rates would then increase as the moisture is absorbed and the liquid water film disappears as a result of absorption, drainage and evaporation. The dewfall rate and amount was assumed not to cause significant surface liquid water. Figure 3(b) shows the progression of the β_E factor (controlling the occurrence of cryptogamic photosynthesis) in the model as it responds initially to rainfall and then to dewfall. The cryptogamic leaf surfaces in the model can only photosynthesize when $\beta_E > 0$; maximum rates are achieved when $\beta_E = 1$. β_E becomes negative during rain and begins to approach zero after cessation of rainfall as the surface liquid water disappears. Rainfall is assumed to fully replenish the water concentration in the leaves allowing the full photosynthetic rate to be potentially achieved.

Gross Primary Production (GPP). Figure 4(a) shows the modelled progression of unit area GPP during the period for the individual cryptogamic and vascular plant communities and the overall GPP produced by combining area-cover weighted values. It can be seen that during this period the model simulates only seven periods of cryptogamic photosynthetic activity in response to the rain and dew events, but that these are still significant in the overall GPP values, despite the lower photosynthetic rate of cryptogams, because of the large surface area covered by such vegetation. The model also shows that, despite the continuous daylight, there is a marked diurnal variation in the photosynthetic rate.

The summation of net GPP and net soil respiration produces the net carbon dioxide flux into the atmosphere, i.e. NEP as defined in (1). Comparison between the hourly measured and modelled NEP and the cumulative measured and modelled NEP is shown in Fig. 4(b). The model generally follows the hourly measurements but without the measurement variability. This is because the measurements are subject to spatial heterogeneity as the wind direction and atmospheric stability changes — heterogeneity that is not built into the model. Lloyd *et al.* (1997) showed that the effects of heterogeneity are smoothed out when fluxes are summed over periods and the cumulative plots shown in Fig. 4(b) provide a better gauge of the performance of the model. The fit between model and measurements is generally good although the model misses the large photosynthetic uptake on days 215 and 217. Day 215 was characterized by high air temperature but relatively low soil temperature, while Day 217 was characterized by clear skies, high solar radiation and high air and soil temperatures. Statistically, as shown in Table 4, the model performed well overall, with a high Willmott *d* statistic of 0.989. However, RMSE was relatively high and $RMSE_s$ and $RMSE_u$ were comparable in size, indicating a systematic error in the difference between the measurements and the model. Examination of Fig. 4(b) indicates that the pivotal point was the large measured assimilation rates on Day 217, which the model failed to simulate.

Net ecosystem production: 27–30 June 1995

Harding & Lloyd (1998) showed that snow cover had virtually disappeared by 15 June in 1995. Figure 5(a)

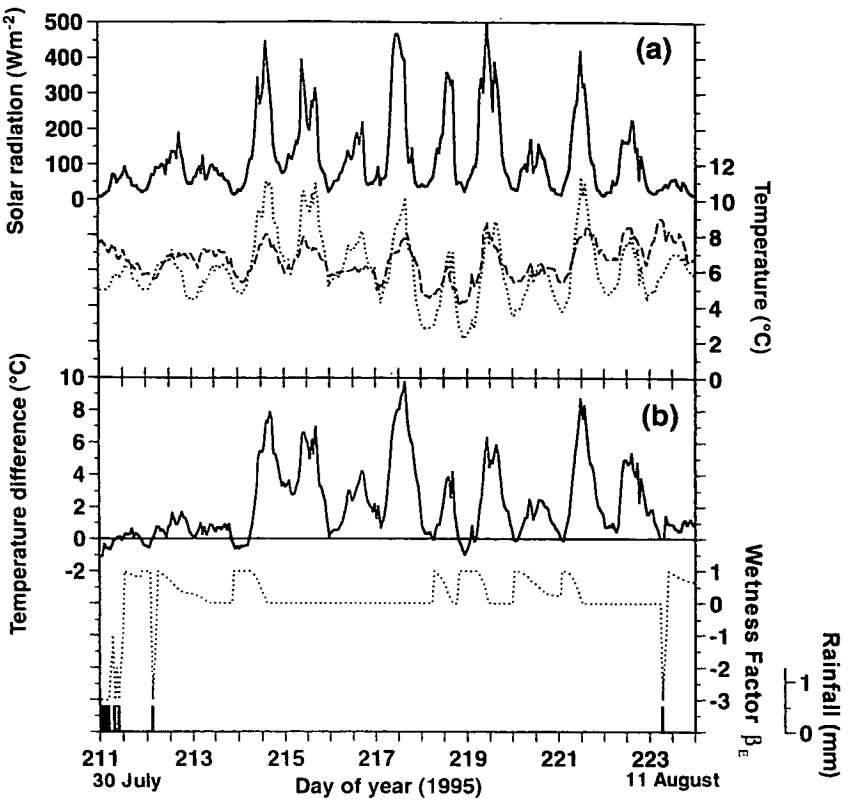

Fig. 3 (a) Solar radiation (solid line), air temperature (dashed line), soil temperature at 25 mm (dotted line) and rainfall (columns) for the period 30 July to 11 August 1995. (b) The expected occurrence of dew as indicated by the difference between leaf and dewpoint temperature (upper line); the rainfall (lower columns) and the effect these two conditions have upon the wetness factor (dotted line) controlling the photosynthesis of the cryptogams for the period 30 July – 11 August 1995.

shows the solar radiation, air and near-surface soil temperatures for the period 27–30 June (days 178–181) together with the isolated precipitation events that bracket this period. While near-surface soil temperature is closely coupled to solar radiation, air temperature is probably influenced by the disappearance of the last snow patches and eventually begins to exceed the soil temperature. This post snowmelt period of 4 days was characterized by very cold and windy weather on 28 June (Day 179) followed by intermittent light snow showers during the early hours and afternoon of Day 180, and again during the early hours of Day 181, and with intermittent but strong snow showers during the afternoon of Day 181. These snow showers were mostly light but did settle and may have inhibited photosynthetic activity by partially shading the vegetation.

The comparison between individual hourly average modelled and measured NEP and their cumulative totals during 27–30 June 1995 (days 178–181) is shown in Fig. 5(b) in an analogous way to Fig. 4(b). Also shown is the optimized Growth Factor (GF) used to simulate vegetation emerging from dormancy. The defining shape factors, b and k for GF are shown in Table 4. The model fails to simulate the spiky nature of the measurements, which is probably a consequence of the heterogeneity caused by patchy snow cover and soil moisture, and the different rates of photosynthetic activity from the emergent vegetation, effects that are lacking in the model. The cumulative modelled NEP follows the cumulative measured CO_2 flux in general with the early period indicating a net source of CO_2 followed by the period of net uptake of CO_2. The model however, fails to simulate the net uptake during the early part of Day 179 or the net source periods during the latter hours of the same day. The divergence between model and measurements during the latter half of Day 181 is easier to explain, as intermittent but strong snow showers would have inhibited plant assimilation, as evident from the measurements – a factor that the model is unable at present to simulate. The model in this period performed reasonably well, with a Willmott d of 0.947 (see Table 4), and with low RMSE, most of which was accounted for by unsystematic error indicating that the model's parameters have been efficiently optimized for this period.

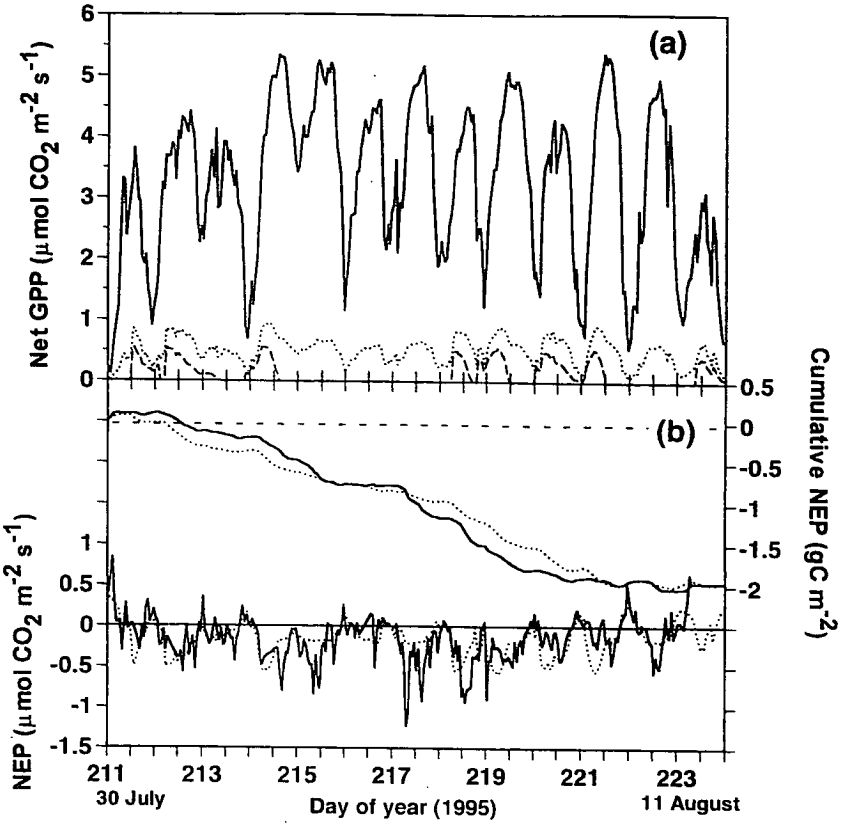

Fig. 4 (a) Gross Primary Production (GPP) per unit area for vascular plants (solid line), cryptogams (dashed line) and overall area weighted GPP for the surface (dotted line) for period 30 July – 11 August 1995. (b) Comparison between measured (solid lines) and modelled (dotted lines) Net Ecosystem Production (NEP) for the summer period 30 July – 11 August 1995: Lower plots are individual hourly average NEP and upper plots are cumulative NEP.

Table 4 Growth Emergence Factor (GF) and Senescence Factor (SF) parameter values and statistical measures of model performance for the three model calibration periods in 1995

	Period		
Parameter	**26–30 June**	30 Jul – 11 Aug	29 Aug – 3 Sep
GF (or SF) factor *b*	−5.1	N/A	(−0.4)
GF (or SF) factor *k*	0.16	N/A	(−0.01)
Willmott *d* statistic	0.947	0.989	0.973
RMSE	0.055	0.1483	0.022
$RMSE_u$	0.048	0.1078	0.020
$RMSE_s$	0.026	0.1018	0.008
r^2	0.877	0.974	0.92

Net ecosystem production: 29 August – 3 September 1995

Figure 6 shows a similar comparison to previous periods (Figs 3,4 and 5) of the major driving factors of solar radiation and soil temperature and air temperature (Fig. 6a) and the measured CO_2 fluxes and modelled NEP (hourly and cumulative; Fig. 6b). Figure 6(a) shows that this period (days 241–246), at the beginning of the autumn, began with overcast skies and low maximum radiation levels of less than 150 Wm^{-2}, but had clear skies on 1 and 2 September (days 244, 245) with maximum solar radiation levels of 290 Wm^{-2} at solar noon on both days. Overnight soil temperatures at 25 mm dropped

Table 5 Mean and SEM for each of the complete measurement days in 1995

Date (1995)	Day number	Mean daily NEP (gCm^{-2})	Unbiased daily SE ($gC\,m^{-2}$)	Unbiased daily SE (% of mean)
27 June	178	0.300	0.017	6
28 June	179	0.004	0.013	361
29 June	180	−0.177	0.014	8
30 June	181	−0.093	0.010	11
30 July	211	0.102	0.015	15
31 July	212	−0.228	0.014	6
01 August	213	−0.065	0.011	17
02 August	214	−0.276	0.024	9
03 August	215	−0.295	0.016	5
04 August	216	−0.012	0.009	75
05 August	217	−0.392	0.019	5
06 August	218	−0.338	0.021	6
07 August	219	−0.298	0.017	6
08 August	220	−0.097	0.017	18
09 August	221	−0.038	0.017	44
10 August	222	−0.097	0.015	15
30 August	242	0.037	0.009	24
31 August	243	−0.018	0.008	46
01 September	244	0.082	0.012	15
02 September	245	0.095	0.012	13

below zero from Day 244 to the end of the period (Day 246). There was no rainfall during this period, the last rainfall having occurred on Day 235. The vascular vegetation was assumed to be into a senescent state while the cryptogamic vegetation would be expected to continue to photosynthesis providing moisture, temperature and light levels allowed it. The Senescent Factor, SF, used to reduce the overall effective area of active vegetation is plotted in Fig. 6(b) and the shape factors, b and k, for SF are tabulated in Table 4. In contrast to the trend from dormancy to full activity seen during the post snowmelt period, the optimization of the SF factor (see Fig. 6b) produced a very gradual descent into vegetative dormancy during the late summer and autumn. The general trend in both measurement and modelled NEP, shown in Fig. 6(b), is for the period to be an overall source of CO_2 as soil respiration, although diminishing, is reducing at a slower rate than the photosynthetic uptake from the senescing vegetation. The model, however, shows much larger diurnal cycles than seen in the measurements and there is evidence of a photosynthetic lag in the measurements with peak photosynthetic uptake occurring later in the diurnal cycle than the model predicts. The model statistically performs well, with a Willmott d statistic of 0.973, and with very low *RMSE* of 0.022, most of which, again, is accounted for by unsystematic error indicating good model parameter estimation (see Table 4).

Flux measurement errors in 1995

Table 5 shows the mean daily value of NEP and the Standard Error of the mean for complete days during the three periods examined above. Two-thirds of the individual standard errors are less than or equal to 15% of the mean and those measurement errors above this figure are for very small overall daily NEP values. The size of standard errors found at this site are comparable to those evaluated by Soegaard *et al.* (2000) at their Greenland site. They estimated daily standard errors to be of the order of ± 15%.

Modelled NEP budget: 11 June – 3 September 1995

Hourly measurements of the driving variables of the model – incoming solar radiation, air temperature, near surface soil temperature and rainfall – were measured from 11 June to 3 September (days 162–246). Incoming solar radiation and rainfall measurements were missing from 10 to 24 July. Auxiliary hourly measurements of net radiation, relative humidity, wind direction and replicates of air and soil temperature were also measured over this period and used to evaluate evaporation rates for the cryptogamic vegetation and for infilling missing data in the driving variables.

The date for the final disappearance of snow was prescribed so that the growth factor value at the

Table 6. Sensitivity analysis showing overall change in model output for variations of ± 50% from the default value for each of the models' novel parameters †except for italized entries where 50% variation would have been unrealistic. For each parameter, upper figures are overall NEP for the period 11 June – 3 September 1995 (default overall NEP is 3.871 $gC\,m^{-2}$) and lower figures are percentage deviation from the default overall NEP. Parameters regarded as particularly sensitive are shown in bold type

Parameter	Default Value	−50% of default value†	+50% of default value
(a) Group 1 – Measured			
Soil Heat Flux as percentage of R_n	5	−3.802	−3.943
		−1.8%	1.9%
Respiration rate R_{10} for bare soil	0.103	−4.460	−3.270
		+15.2%	−15.5%
Respiration rate R_{10} for lichen cover	**0.6**	**−15.478**	7.737
		+299.8%	−299.9%
Respiration rate R_{10} for mixed bryophyte/ vascular cover	**0.806**	**−6.896**	−0.845
		+78.1%	−78.2%
Light saturation level for moss	266	−2.741	−3.974
		−29.2%	+2.7%
Moss growth rate as proportion of C3 rate	**0.15**	−1.306	−6.436
		−66.3%	+66.3%
Vegetation cover: (Soil)(Moss–Lichen)(Vascular)	(0.2)(0.67)(0.13)		
(constrained by sum of cover = 1: (0.1)**[0.67]**(0.23)	−22.27 (+475%)		
[value] is held at default value and other surfaces varied)	(0.3)**[0.67]**(0.03)	14.528 (−475%)	
	(0.1)(0.77)**[0.13]**	−1.766 (−54%)	
	(0.3)(0.57)**[0.13]**	−5.975 (+54%)	
	[0.2](0.57)(0.23)	−24.374 (+530%)	
	[0.2](0.77)(0.03)	16.633 (−530%)	
(b) Group 2 – Surmised and optimized			
Wetting-up factor for moss in dew periods	0.2	−3.392	−4.015
		−12.4%	+3.7%
Soil *T*–Dewpoint *T* at which dew forms,	0 °C	*−1* °C †	***+1 °C†***
e.g. −1 °C means dew forms when Dewpoint *T*		−2.220	**−6.749**
is 1 °C below soil temperature		−42.7%	**+74.3%**
Max. hourly evaporation for mosses	0.4	−2.075	−5.100
		−46.4%	+31.7%
No. of h after rain before photosynthesis can start	3	−3.657	−4.027
		−5.5%	+4.0%
Moss/lichen growth start day number	182	*172†*	192†
		−4.243	−3.274
		+9.6%	−15.4%
Moss/lichen senescence start day number	233	*223†*	243†
		−3.731	No change
		−3.6%	0%
Vascular growth start day number	182	***172 †***	***192†***
		−6.927	2.188
		+78.9%	−156.5%
Vascular senescence start day number	237	227 †	247†
		−3.228	No change
		−16.6%	0%

beginning of the first intensive CO_2 measurement (model calibration) period (i.e. days) and in the full summer season model run were identical in value. Similarly the Senescence Factor during the late summer and autumn was prescribed to be identical in both the calibration period (days 241–246) and the same period in the full summer model run. The Senescence Factor was also extrapolated backwards in time until SF equalled 1(i.e. full activity) in the full summer season model run. The model thus suggested that the transition from full growth into senescence began around 21 August, close to the end of the period of the midnight sun.

Figure 7 shows the modelled estimates of individual and cumulative daily NEP from 11 June to 3 September 1995 with the measured daily CO_2 flux superimposed together with the daily rainfall. The end of snowmelt is prescribed as occurring on 27 June (Day 178). Before that date, GF is zero for both vascular and cryptogamic

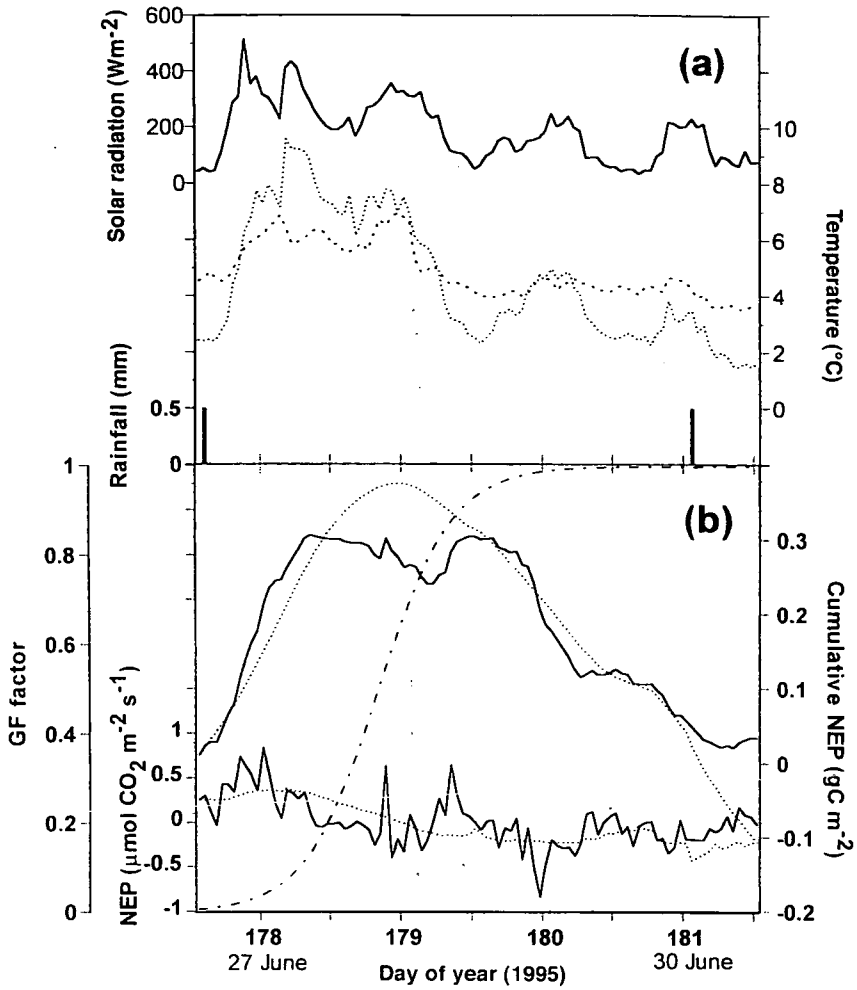

Fig. 5 (a) Solar radiation (solid line), air temperature (dashed line), soil temperature at 25 mm (dotted line) and rainfall (columns) for the period 27 June to 30 June 1995. (b) Comparison between measured and modelled NEP for the post snowmelt period 27 June – 30 June 1995. Legend is same as for Fig. 5. The post snowmelt increase in vegetation photosynthetic activity is shown by the model Growth Factor (GF) – (dot and dash line).

vegetation, the outcome of the calibration of GF for the period 27–30 June. A consequence of this is a rapid and large switch from CO_2 source to CO_2 sink as the vegetation is 'switched on' at the start of the first intensive measurement period. Rapid transition from CO_2 source to CO_2 sink is a characteristic of the high arctic summer (Soegaard & Nordstroem 1999). However, the size of the switch is probably not realistic as there is evidence that cryptogamic vegetation can begin to photosynthesize under snow providing that light levels are sufficiently high (Kershaw 1975; Larson & Kershaw 1975), a process missing from the model that would have reduced the size of the overall CO_2 source. The possibility that the Day 178 had an anomalously high CO_2 source also cannot be discounted.

The model shows little evidence of a steady increase to a summer maximum (negative within this paper's sign convention) in gross daily NEP in contrast to the results of Soegaard & Nordstroem (1999) which displayed a sinusoidal summer pattern with an evident maximum around 21 July in 1996. The model indicates that, while the overall daily carbon dioxide balance is a sink, the day-to-day variation is high and the model effectively predicts the response of the vegetation to periods with and without rainfall. For the period 9–24 July, when rainfall measurements were missing at the site, measurements of rainfall at Ny-Ålesund (Bruland & Maréchal 1999) of 0.7, 0.1, 0.1 and 0.9 mm on 7, 11, 18 and 19 July, respectively, were substituted.

Overall, as shown by the modelled cumulative daily NEP curve, the period between 11 June and 3 September 1995 had an overall NEP of $-3.9\,gC\,m^{-2}$ and was characterized by a period of carbon dioxide release to the atmosphere up to 28 June (Day 179) followed by

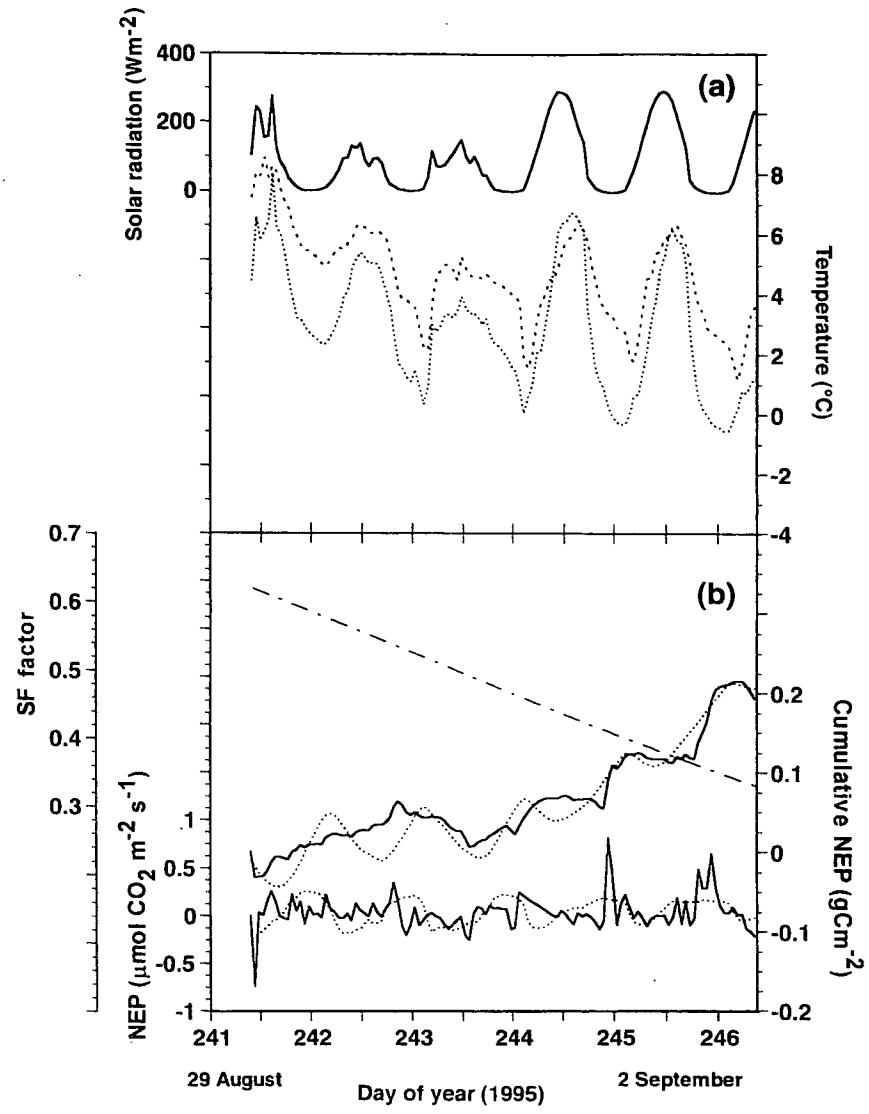

Fig. 6 (a) Solar radiation (solid line), air temperature (dashed line), soil temperature at 25 mm (dotted line) and rainfall (columns) for the period 29 August to 3 September 1995.(b) Comparison between measured and modelled NEP for the early autumn period 29 August – 3 September 1995. Legend is the same as for Fig. 6 except that the change in the vegetation photosynthetic activity is now modelled by the Senescence Factor (SF) (dot and dash line).

carbon dioxide uptake throughout the summer with the autumn becoming a carbon dioxide source. The active season in 1995 (28 June – 29 August), arbitrarily defined as the start and finish of prolonged daily CO_2 assimilation, produced a CO_2 assimilation of -9.7 gC m^{-2}. Confidence in these figures is examined in the sensitivity and confidence analysis below. The importance of soil respiration to the overall carbon balance of this high arctic site can be seen in Fig. 8 where daily average soil temperature at 25 mm and daily total solar radiation are overlaid on the daily NEP amounts. It is evident that the NEP balance follows closely the soil temperature, which is itself dependent in these relatively bare soils upon solar radiation. Such a result implies that plant assimilation is near optimal with soil respiration providing the control on the overall carbon dioxide balance.

Sensitivity analysis of model for 1995 period

The results from the sensitivity analysis of the novel model parameters in the combined NEP model are shown in Table 6. The new model parameters have been split into two groups. Group 1 (Table 6a) consists of parameter values based on measurements either obtained at the field site or at other arctic sites. Varying these parameters, e.g. vegetation coverage, soil respiration rates, growth rate of moss as proportion of C_3 photosynthetic rate is indicative of the effect of possible

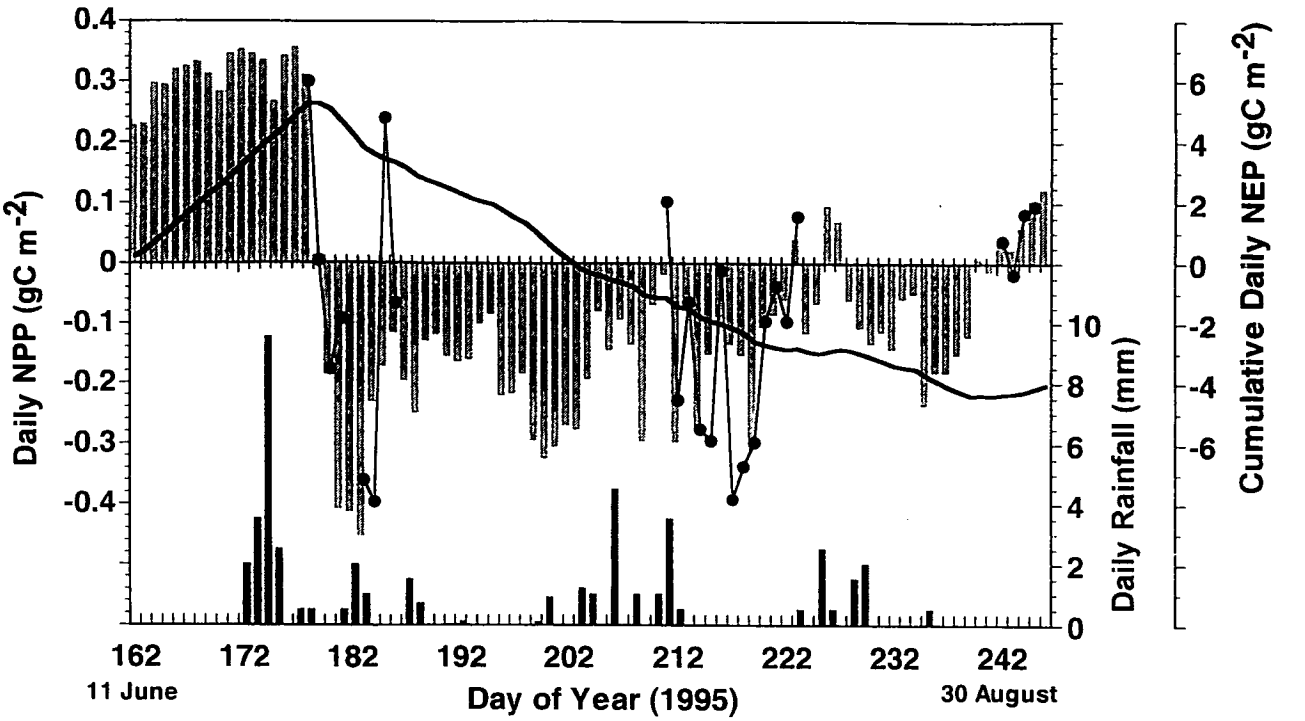

Fig. 7 Measured daily NEP (closed circles), modelled daily NEP (grey columns), daily rainfall (black columns) and cumulative modelled NEP (—) for the period 11 June – 3 September 1995.

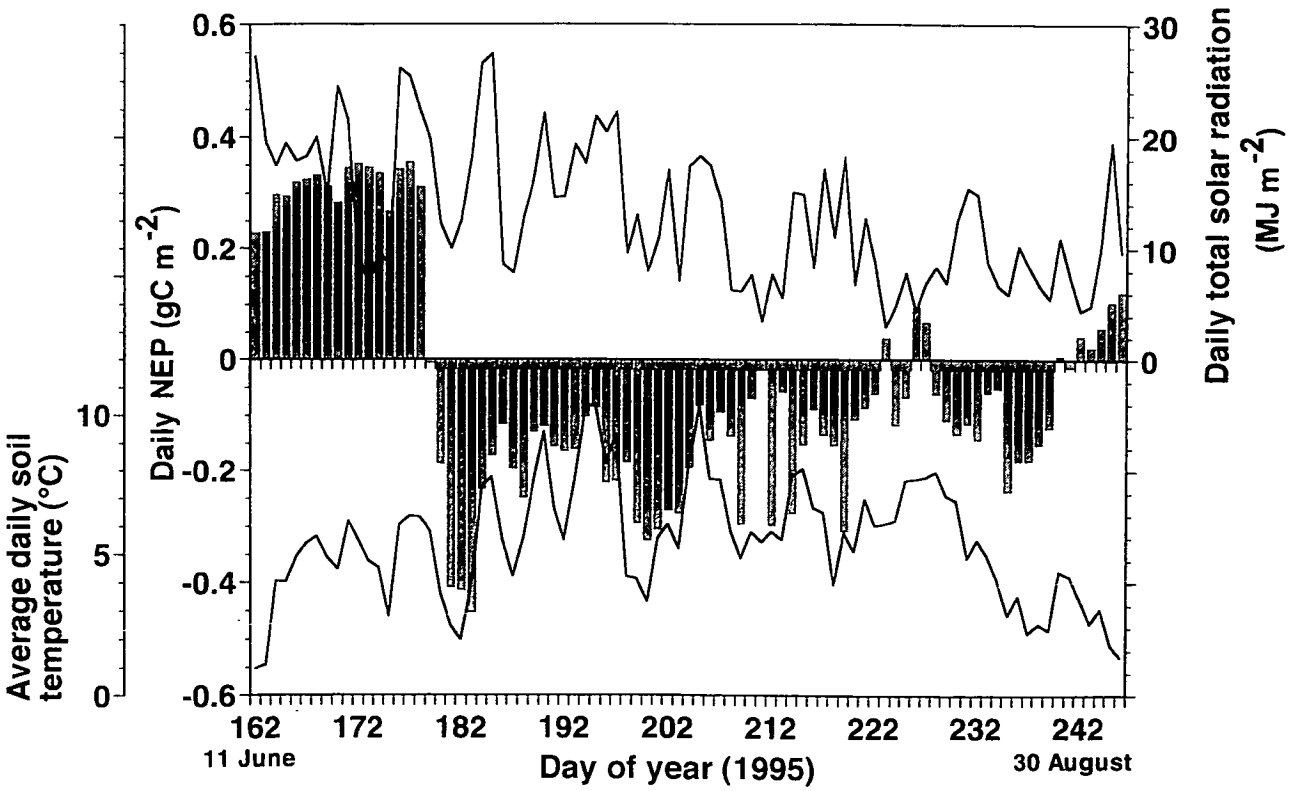

Fig. 8 Daily total solar radiation (upper trace) and average daily soil temperature (lower trace) superimposed on the modelled daily NEP (columns) for the period 11 June – 3 September 1995.

measurement error or the risk of applying nonlocal measurements. Group 2 (Table 6b), consisting of parameters incorporated into the model to simulate moss/lichen effects on the control of the overall NEP, are either estimated from general considerations or evaluated during the optimization of the model. It is within this latter group (e.g. wetting-up factor for moss in dew periods, start of growth, start of senescence) that the model must be seen to perform reasonably well, with sensible and realistic responses to pertubations.

It is evident from examining the sensitivity analysis for the measured variables that NEP is very sensitive to vegetation cover. Changing the proportion of surface covered by vascular plants by 10% of the surface with no change in the proportion of the surface covered by mosses and lichens (i.e. the bare soil area increases or decreases inversely with vascular cover) produces a 475% change in NEP. A similar change in surface cover occupied by mosses and lichens at the expense of bare soil coverage only produces a change of 54%. Invasion of vascular plants into moss/lichen areas and *vice versa*, with bare soil cover remaining the same, produces a 530% change in NEP. Climate change will alter the coverage and composition of the tundra vegetation and this result illustrates the large effect that relatively small changes in vegetation cover could have on the overall carbon dioxide budget at this site. Of the other measured parameters, the soil respiration rate, especially that below the lichen cover, is also highly sensitive indicating that a warming Arctic will increase soil respiration rates but not necessarily at rates sufficient to balance assimilation uptake.

Within the surmised and optimized variables, it is apparent that the model is insensitive to the rate at which mosses and lichens wet up after dessication, the length of the period following rain where liquid water on the surfaces of the leaves prevents photosynthetic activity, and the particular days on which mosses/lichens emerge from dormancy or start to senesce. However, while the timing of the start of senescence in the vascular plant community is little affected by varying the date, the model is highly sensitive to the start of vascular plant activity in the spring. This sensitivity may be explained by the effect of the near maximum radiation levels in June just after snowmelt, compared to the low light levels in early September.

Model confidence limits for 1995 period

The driving variables and the important state parameters identified in the sensitivity analysis above were used to estimate confidence limits for the model output of the 1995 period. Measurement errors of ± 5% were applied to solar radiation, net radiation and relative humidity and ± 0.5 °C were applied to air and soil temperature. The state parameters were varied by ± 10%. Model outcomes from exploration of the variable and parameter space determined by the above error values were analysed. Model outputs ranged from −14.8–7.2 $gC\,m^{-2}$. The mean of the distribution of model outcomes was $-4.08\ gC\,m^{-2}$ (cf. $-3.9\ gC\,m^{-2}$ for default model run) with a skewness of 0.009. By assuming normality the 1995 period had an NEP of $-3.9\ gC\,m^{-2}$ with an SE of $\pm 3.7\ gC\,m^{-2}$.

Modelled NEP budget: 10 June – 6 September 1996

In order to illustrate the effect that the timing of snowmelt has upon the subsequent active season NEP budget, exactly the same period (days 162–246) was modelled in 1996 but extended to Day 249 to include the measured fluxes on days 248 and 249. Similar variables were measured, and the same techniques as those used for the 1995 model runs were used to infill missing data and to provide evaporation rates. There was no optimization performed on the model parameters except that the date for the final disappearance of snow and surface meltwater was set to 21 July (Day 203) in accordance with the measurements of Harding & Lloyd (1998) and the start date of senescence was exactly the same as for 1995 in line with evidence that the induction of autumn senescence occurs even when temperatures are favourable for growth (Shaver & Kummerow 1992). This implies some form of phenological action, possibly light intensity related, within the plant.

Figure 9 shows the outcome of the model simulation for 1996. The snow covered period between 10 June and 11 July (days 162–193), when measured daily average near surface soil temperatures increased from −2 °C to 0 °C, has a relatively constant soil respiration rate of $0.135\ \mu mol_{CO2}\ m^{-2}\,s^{-1}$. That soil respiration can occur at temperatures below freezing is shown by Nakane (1980), whose results form part of the dataset used by Lloyd & Taylor (1994) in the formation of their soil respiration model. Heat penetration into the soil is sufficiently rapid that soil at 0.7 m has become unfrozen by 24 July (Day 206). The measurements at this time also show a consistent CO_2 source although the rate is highly variable. Measured emission rates are weakly linked to measured average daily windspeed ($r^2 = 0.31$) indicating that this variability may be the result of increased turbulence releasing stored CO_2 from within the snowpack, a process that the model is unable to simulate. From 12 July to 24 July (Day 206), modelled soil respiration gradually rises as soil temperatures increase. The measurements once again show a similar increase. Model plant activity begins on 21 July and by the 25 July has completely balanced the soil respiration. From then

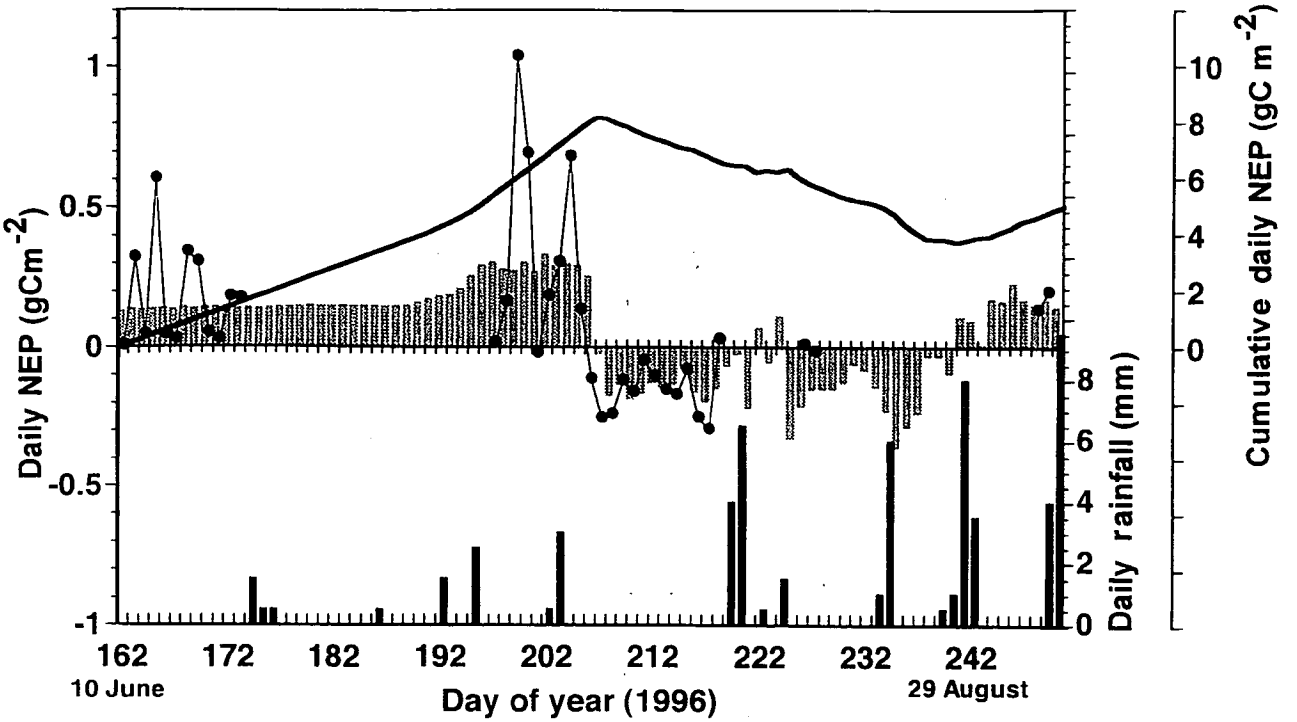

Fig. 9 Measured daily NEP (closed circles), modelled daily NEP (grey columns), daily rainfall (black columns) and cumulative modelled NEP (—) for the period 10 June – 6 September 1996.

on, the measurements and model show the site to be a sink for carbon dioxide except for the period between 5 and 10 August, when the site became a CO_2 source. This period was heavily overcast, giving low light levels (see solar radiation amounts in Fig. 10), with nearly continuous rain or drizzle. The rain maintained soil temperatures close to air temperature thus allowing soil respiration to be maintained at a relatively high level.

The necessity to either measure solar radiation at the vegetation surface or to record albedo for correct operation of this model is shown during the period 20–25 August (days 233–238) when snow fell and remained for these 5 days, as indicated by the change in albedo from bare surface values of about 10% to around 70% (see Fig. 10). Surface soil temperatures also fell close to 0 °C during this period. As the solar radiation was measured above the snow surface, the model produced strong daily CO_2 sinks; however, given reduced photosynthetic activity in the plants as a consequence of snow-cover, and reduced soil respiration at lower temperatures, it is likely that the overall carbon dioxide balance would be quite small and possibly even a source during this time.

The procedure used for the 1995 model run to obtain the overall standard error of the model output was applied to the model for the 1996 period. The cumulative daily NEP total depicted in Fig. 9 shows that, in contrast to the same period in 1995, between 10 June and 6 September the site was a net source of carbon dioxide of 5.0 ± 3.3 gC m^{-2}. The active season in 1996 was much shorter (25 July–27 August) and the surface assimilated -4.5 gC m^{-2}.

Discussion and conclusions

Results from the calibration and verification of a composite carbon dioxide balance model are presented. The soil respiration model of Lloyd & Taylor (1994) has been linked to the C_3 photosynthetic model of Collatz *et al.* (1991) and used to simulate carbon dioxide flux measurements from a surface consisting of mosses, lichens, dwarf vascular plants and bare soil at a polar semidesert site on Svalbard. The short but continuous periods of data taken during the summer of 1995 were used to parameterize the photosynthetic model as implemented within the Hadley Centre MOSES model. The cryptogamic and vascular plant communities were modelled separately and then combined with the soil respiration model. For the cryptogams, this process entailed converting a soil moisture factor, used in MOSES to regulate photosynthetic activity in vascular plants, to simulate the direct linkage between cell

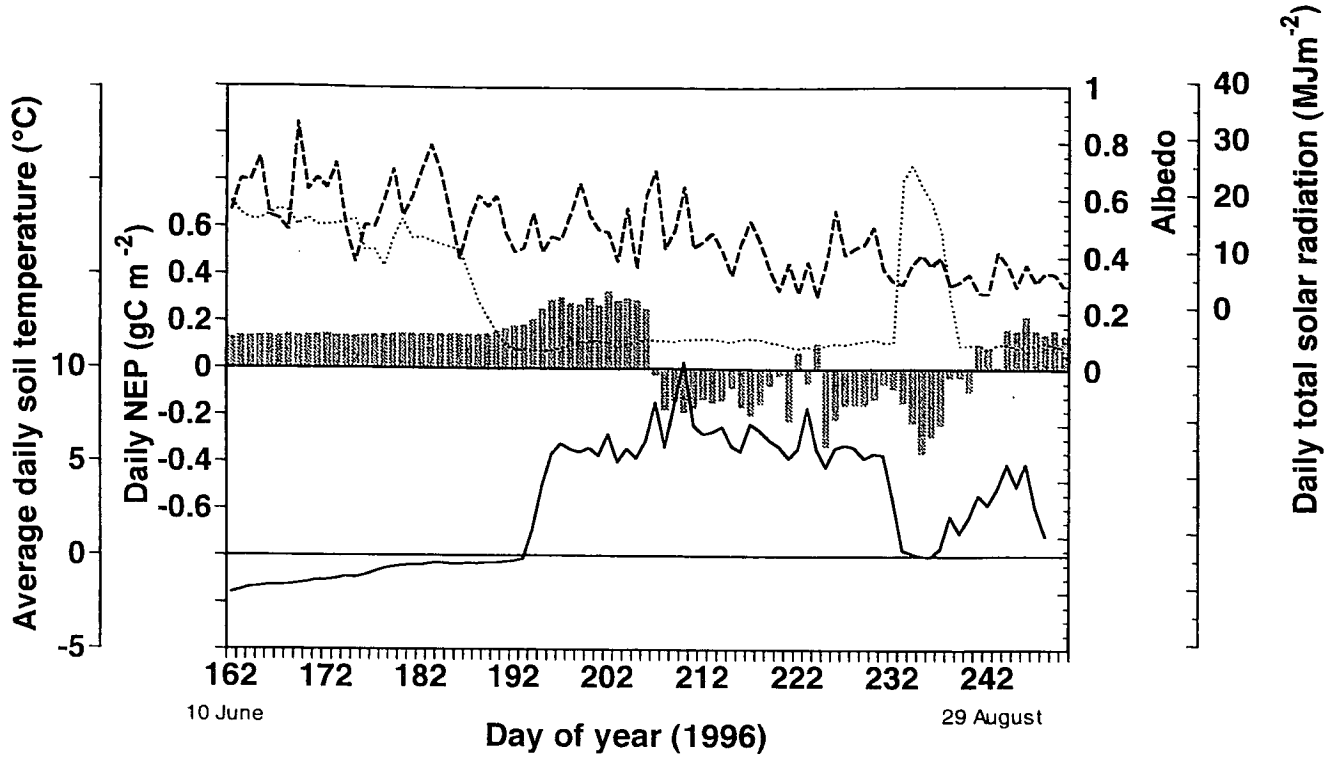

Fig. 10 Modelled daily NEP (grey columns), daily total solar radiation (dashed line), daily average albedo (dotted line) and daily average soil temperature at 25 mm (solid line) for the period 10 June – 6 September 1996.

moisture levels and carbon dioxide assimilation that is peculiar to cryptogams. This was achieved by a process of wetting up through precipitation and drying out through evaporation. Increasing photosynthetic activity as the winter snow cover melts and decreasing photosynthetic activity as senescence progresses at the end of the summer, are modelled using Growth Factor (GF) and allied Senescence Factor (SF) analogous to the use elsewhere of LAI for predominantly deciduous sites.

The model was shown to be capable of simulating the middle of the active season with a high degree of success and was capable of simulating both the post snowmelt and senescent periods with reasonable success despite the high level of heterogeneity in plant activity, snow cover and soil temperatures present at these times. Unlike other high arctic sites, the carbon dioxide balance at the polar semidesert site during the summer is small but highly variable. The vascular plant community, with little or no water stress, appears from the model to maintain maximum photosynthetic activity throughout the active season, depending on light and temperature conditions. The cryptogamic communities are more sporadic, with photosynthetic activity only occurring after wetting of their surfaces with rain, dew or snow. Despite their much lower photosynthetic rate compared to vascular plants, the larger percentage cover of the cryptogams within the site increases their contribution to the overall assimilation rate. However, it is the variation in the soil respiration efflux, directly linked to soil temperature, which characterizes the overall carbon dioxide balance during the summer season. The period between 11 June and 3 September 1995 was estimated to be a net carbon dioxide sink of 3.9 ± 3.7 gC m^{-2}.

The calibrated model was then used to simulate the active season at the site during 1996 and compared to the campaign measurements during that year. Both the end of the snowmelt and the start of senescence were prescribed, but otherwise the model was allowed to run with the parameters set for 1995. In general, the model simulates the periods when CO_2 fluxes were measured quite well. Both measurements and model indicate that the snow-covered period has a net CO_2 efflux although the model does not generate the variability seen in the measurements. This respiration may be a gradual release of CO_2 produced during the previous autumn although there is evidence that microbial production can occur in soils at temperatures below freezing. There is not the strong relationship in 1996 between soil temperature and overall CO_2 flux that was seen in 1995. This may be a consequence of the above-average cloudiness in 1996, which may have limited the plants photosynthetic activity. Wüthrich *et al.* (1998) observed that average PAR was as low as 325 µmol photons $m^{-2} s^{-1}$, well below the 400 µmol photons $m^{-2} s^{-1}$

required for carbon fixation to exceed respiration in plant communities similar to those examined in this study.

The validation during 1996 highlighted the need to include the effects of summer snow showers on plant photosynthetic activity. This could be done most easily by using albedo measurements to signal snow events and modifying the photosynthetic rate accordingly.

The modelling exercise has shown that the timing of snowmelt, the frequency and duration of precipitation events during the summer and soil temperatures are the major parameters which define the overall carbon dioxide balance of this high arctic polar semidesert site. Cloudiness and the timing of the autumn 'freeze-up' are factors that also may have an important effect upon the CO_2 balance but the limited dataset does not provide conclusive evidence for this. The site switched from being a small sink of carbon into the vegetation during the snowmelt-summer period in 1995 ($-3.9 \pm 3.7\,gC\,m^{-2}$) to a small source of carbon ($5.0 \pm 3.3\,gC\,m^{-2}$) from the vegetation/soil interface during the same period in 1996.

Acknowledgements

The author would like to thank Richard Harding, Tim Kyte and Mike Stroud of the Institute of Hydrology who assisted in the collection of the data and Nick Cox, Station Manager of the NERC Arctic Research Station at Ny-Ålesund who helped in so many ways. The funding of this work was shared between NERC and the EU supported LAPP Programme (Contract No. ENV4-CT95-0093).

References

Brattbakk I (1981) *Vegetasjonskart S10, V28H60* (vegetation map) *Ny-Ålesund, Brøggerhalvøya, Svalbard. K. Norske Videnske*, scale 1: 10,000. Selsk. Mus. Bot. avd, Trondheim, Norsk Polar Institutt.

Bruland O, Maréchal D (1999) *Energy and water balance of Active layer 1991-1994: Understanding Land Arctic Physical Processes 1996-1998.* SINTEF Report no. STF22 A98417. SINTEF, Trondheim.

Collatz GJ, Ball JT, Grivet C, Berry JA (1991) Physiological and environmental regulation of stomatal conductance, photosynthesis and transpiration: a model that includes a laminar boundary layer. *Agricultural and Forest Meteorology*, **54**, 107–136.

Cox PM, Huntingford C, Harding RJ (1998) A canopy conductance and photosynthesis model for use in a GCM land surface scheme. *Journal of Hydrology*, **212–213**, 79–94.

Cox PM, Betts RA, Bunton CB, Essery RLH, Rowntree PR, Smith J (1999) The impact of new land surface physics on the GCM simulation of climate and climate sensitivity. *Climate Dynamics*, **15**, 183–203.

Dziadowiec H (1983) Preliminary studies on carbon dioxide evolution from tundra soils of Spitsbergen (Kaffiöyra, Oscar II Land, NW Spitsbergen). *Acta Universitatis Nicolai Copernici*, **18**, 159–167.

Gimingham CH, Smith RIL (1971) Growth form and water relations of mosses in the maritime Antarctic. *British Antarctic Survey Bulletin*, **25**, 1–21.

Goulden ML, Munger JW, Fan S-M, Daube BC, Wofsy SC (1996) Measurements of carbon sequestration by long-term eddy covariance: methods and a critical evaluation of accuracy. *Global Change Biology*, **2**, 169–182.

Harding RJ, Lloyd CR (1998) Fluxes of water and energy from three high latitude tundra sites in Svalbard. *Nordic Hydrology*, **29**, 267–284.

Harding RJ, Huntingford C, Cox PM (2000) Modelling long-term transpiration measurements from grassland in southern England. *Agricultural and Forest Meteorology*, **100**, 309–322.

Hicklenton PR, Oechel WC (1976) Physiological aspects of the ecology of *Dicranum fiscescens* in the subarctic. 1. Acclimation and acclimation potential of CO_2 exchange in relation to habitat, light, and temperature. *Canadian Journal of Botany*, **54**, 1104–1119.

Huntingford C, Cox PM, Lenton TM (2000) Contrasting responses of a simple terrestrial ecosystem model to global change. *Ecological Modelling*, **134**, 41–58.

LI-COR Inc. (1998) *Implementing a span adjustment and/or the Band broadening correction on measured data.* Application Note 123. LI-COR Inc, Lincoln, NB.

Jarvis PG (1976) The interpretation of the variances in leaf water potential and stomatal conductance found in canopies in the field. *Philosophical Transactions of the Royal Society of London*, **B273**, 593–610.

Kallio P, Kärenlampi L (1975) Photosynthesis in mosses and lichens. In: *Photosynthesis and Productivity in Different Environments* (ed. Cooper JP), IBP 3, pp. 393–423. Cambridge University Press, Cambridge.

Kattenberg A, Giorgi F, Grassl H *et al.* (1996) Climate models – Projections of future climate. In: *Climate Change 1995. The Science of Climate Change* (eds Houghton JT *et al.*), pp. 285–357. Cambridge University Press, Cambridge.

Kershaw KA (1975) Studies on lichen-dominated systems. XIV: The comparative ecology of *Alectoria nitidula* and *Cladina alpestris*. *Canadian Journal of Botany*, **53**, 2608–2613.

Korotkevich YS (1967) Polar Deserts. *Soviet Antarctic Expedition Information Bulletin*, **6** (65), 459–472. [Scripta Technica (transl.), **6** (65), 5–29, in original Russian.]

Landsberg JJ (1977) Some useful equations for biological studies. *Experimental Agriculture*, **13**, 273–286.

Lange OL, Tenhunen JD, Harley P, Walz H (1985) Methods for field measurements of CO_2 exchange: Diurnal courses of net photosynthesis capacity of lichens under Mediterranean climate conditions. In: *Lichen Physiology and Cell Biology* (ed. Brown DH), pp. 23–39. Plenum, New York.

Larson DW, Kershaw KA (1975) Studies on lichen-dominated systems. XI: Lichen-heath and winter snow cover. *Canadian Journal of Botany*, **53**, 621–626.

Lloyd CR (1998) The application of an instrument for non-destructive measurements of soil temperature and resistance profiles at a high Arctic field site. *Hydrology and Earth System Sciences*, **2**, 121–128.

Lloyd CR (2001) On the physical controls of the carbon dioxide balance at a high arctic site in Svalbard. *Theoretical and Applied Climatology*, in press.

Lloyd J, Taylor JA (1994) On the temperature dependence of soil respiration. *Functional Ecology*, **8**, 315–323.

Lloyd CR, Harding RJ, Robinson M (1996) Preliminary results of

energy and water balance from two tundra sites in Svalbard. In: *Proceedings of the 10th International Northern Research Basins Symposium, Spitsbergen, 1994.*

Lloyd CR, Bessemoulin P, Cropley FD *et al.* (1997) A comparison of surface fluxes at the HAPEX-Sahel fallow bush sites. *Journal of Hydrology*, **188–189**, 400–425.

Lloyd CR, Aurela M, Hargreaves KJ, Nordstrøm C (1999) Trace Gas Fluxes in European Arctic Regions. In: *Greenhouse Gases and Their Role in Climate Change: the Status of Research in Europe European Commission International Workshop, Orvieto, Italy, 10–13. November, 1997* (eds Valentini R, Brüning C).

Longton RE (1980) Physiological ecology of mosses. in the. *Mosses of North America* (eds Taylor RJ, Leviton AE), pp. 77–113. Pacific Division AAAS, San Francisco, CA.

Longton RE (1988) *The Biology of Polar Bryophytes and Lichens.* Cambridge University Press, Cambridge, 391pp.

Mayo JM, Hartgerink AP, Despain DG, Thompson RG, van Zinderen Bakker jr EM, Nelson SD (1977) Gas exchange studies of *Carex* and *Dryas*, Truelove Lowland. In: *Truelove Lowland, Devon Island, Canada: a High Arctic Ecosystem* (ed. Bliss LC), pp. 265–280. University of Alberta Press, Edmonton

Miller PC, Oechel WC, Stoner WA, Sveinbjörnsson B (1978) Simulation of CO_2 uptake and water relations of four Arctic bryophytes at Point Barrow, Alaska. *Photosynthetica*, **12**, 7–20.

Moncrieff JB, Massheder JM, de Bruin HAR *et al.* (1997) A system to measure surface fluxes of momentum, sensible heat, water vapour and carbon dioxide. *Journal of Hydrology*, **188–189**, 589–611.

Monteith JL (1965) Evaporation and Environment. In: The State and Movement of Water in living Organisms. Proc. 19th Symposium of the Society for Experimental Biology, Swansea 1964. Cambridge University Press, Cambridge, pp. 205–234.

Monteith JL, Unsworth M (1990) *Principles of Environmental Physics.* Arnold, London, 291pp.

Nakane K (1980) Comparative studies of cycling of soil organic carbon in three primeval moist forests. *Japanese Journal of Ecology*, **30**, 155–172.

Nakatsubo T, Bekku Y, Kume A, Koizumi H (1998) Respiration of the belowground parts of vascular plants: its contribution to total soil respiration on a successional glacier foreland in Ny-Ålesund, Svalbard. *Polar Research*, **17**, 53–59.

Oechel WC, Collins NJ (1976) Comparative CO_2 exchange patterns in mosses from two tundra habitats at Barrow, Alaska. *Canadian Journal of Botany*, **54**, 1355–1369.

Oechel WC, Sveinbjörnsson B (1978) Primary production processes in Arctic bryophytes at Barrow, Alaska. In: *Vegetation Production and Production Ecology of an Alaskan Arctic Tundra* (ed. Tieszen LL), pp. 269–298. Springer, New York.

Oechel WC, Hastings SJ, Vourlitis G, Jenkins M, Riechers G, Grulke N (1993) Recent change of Arctic tundra ecosystems from a net carbon dioxide sink to a source. *Nature*, **361**, 520–523.

Oechel WC, Vourlitis G, Hastings SJ (1997) Cold season CO_2 emission from arctic soils. *Global Biochemical Cycles*, **11**, 163–172.

Rastorfer JR (1971) Effects of temperature on carbon dioxide compensation points of the moss *Drepanocladus uncinatus*. *Antarctic Journal of the United States*, **6**, 162–163.

Salas JD (1993) Analysis and modeling of hydrological time series. In: *Handbook of Hydrology* (ed. Maidment DR), pp. 19.1–19.72. McGraw-Hill, New York.

Shaver GR, Kummerow J (1992) Phenology, Resource Allocation, and Growth of Arctic Vascular plants. In: *Arctic Ecosystems in a Changing Climate: an Ecophysiological Perspective* (eds. Chapin III FS *et al.*), pp. 193–211. . Academic Press, San Diego, CA.

Shurpali NJ, Verma SB, Kim J, Arkebauer TJ (1995) Carbon dioxide exchange in a peatland ecosystem. *Journal of Geophysics Research*, **100**, 14,319–14,326.

Shuttleworth WJ, Gash JHC, Lloyd CR, McNeil DD, Moore CJ, Wallace JS (1988) An integrated micrometeorological system for evaporation measurement. *Agricultural Meteorology*, **43**, 295–317.

Smith J (1956) Some moving soils of Spitsbergen. *Journal of Soil Science*, **7**, 10–21.

Soegaard H, Nordstroem C (1999) Carbon dioxide exchange in a high-arctic fen estimated by eddy covariance measurements and modelling. *Global Change Biology*, **5**, 547–562.

Soegaard H, Thorgeirsson H (1998) Carbon dioxide exchange at leaf and canopy scale for agricultural crops in the boreal environment. *Journal of Hydrology*, **213**, 51–61.

Soegaard H, Nordstroem C, Friborg T, Hansen BU, Christensen TR (2000) Trace gas exchange in a high-arctic valley. 3. Integrating and scaling CO_2 fluxes from canopy to landscape using flux data, footprint modeling, and remote sensing. *Global Biogeochemistry and Cycles*, **14** (3), 725–744.

Stewart JB, Verma SB (1992) Comparison of surface fluxes and conductances at two contrasting sites within the FIFE area. *Journal of Geophysics Research*, **97** (D17), 18,623–18,638.

Tedrow JCF (1977) *Soils of the Polar Landscapes.* Rutgers University Press, New Jersey, NY.

Valanne N (1984) Photosynthesis and photosynthetic products in mosses. In: *The Experimental Biology of Bryophytes* (eds Dyer AF, Duckett JG), pp. 257–273. Academic Press, London.

Valentini R, de Angelis P, Matteucci G, Monaco R, Dore S, Scarascia Mugnozza GE (1996) Seasonal net carbon dioxide exchange of a beech forest with the atmosphere. *Global Change Biology*, **2**, 199–207.

Wielgolaski FE (1975) Primary Production in tundra. In: *Photosynthesis and Productivity in Different Environments* (ed. Cooper JP), pp. 75–106. Cambridge University Press, Cambridge.

Willmott CJ (1981) On the validation of models. *Physical Geography*, **2**, 184–194.

Willmott CJ (1984) On the evaluation of model performance in physical geography. In: *Spatial Statistics and Models* (eds. Gaile GL, Willmott CJ), pp. 443–460. Reidel, Dordrecht.

Wüthrich Ch, Döbeli C, Schaub D, Leser H (1994) The pattern of carbon-mineralisation in the high-arctic tundra (Western and Northern Spitsbergen) as an expression of landscape ecologic environment heterogeneity. *Zeitscrift für Geomorphologie N F*, **97**, 251–264.

Wüthrich C, Möller I, Thannheiser D (1998). Soil carbon losses due to increased cloudiness in a high arctic tundra watershed (Spitsbergen). In: *Proceedings of the 7th International Conference on Permafrost, June 23–27, Yellowknife* (eds Lewkowicz A G, Allard M), pp. 1165–1172. Université Laval, Nordicana

Wüthrich Ch, Möller I, Thannheiser D (1999) CO_2-fluxes in different plant communities of a high-arctic tundra watershed (Western Spitsbergen). *Journal of Vegetation Science*, **10**, 413–420.